

Development of Poly(ethylene oxide)-*block*-poly(ϵ -caprolactone) based Micelles for Tumor Targeted Drug and siRNA Delivery

by

Shyam Madhusudan Garg

A thesis submitted in partial fulfillment of the requirements for the degree of

Doctor of Philosophy

in

Pharmaceutical Sciences

Faculty of Pharmacy and Pharmaceutical Sciences
University of Alberta

© Shyam Madhusudan Garg, 2015

Abstract

The use of nanotechnology has made significant advancements in cancer diagnosis and treatment. Polymeric micelles are a relatively new generation of nanocarriers mostly intended for the delivery of hydrophobic drugs. In this thesis, our objective was to develop an optimized polymeric micellar platform based on functionalized poly(ethylene oxide)-*block*-poly(ϵ -caprolactone) (PEO-*b*-PCL) block copolymers for tumor targeted drug and/or siRNA delivery. Accordingly, modification of the core and shell structure in this platform was pursued to maximize the delivery of incorporated cargo to malignant tissue, while avoiding its nonspecific distribution to healthy organs. In this context, modification of the core in PEO-*b*-PCL micelles with a hydrophobic side-group i.e. benzyl carboxylate (PEO-*b*-PBCL), was shown to increase the stability of micelles. The improved stability of micelles led to enhanced accumulation of nanocarriers into orthotopic breast tumors in mice, which was evidenced through optical imaging of a near infrared (NIR) cy5.5, tagged micelles. Modification of the micellar shell with a breast cancer targeting peptide, i.e. P18-4, on the other hand, resulted in a more rapid homing of the nanocarriers in breast tumors. In the next step, crosslinking of the alkyne modified core of PEO-*b*-PCL micelles by diazide poly(ethylene glycol) by click chemistry, was shown to further enhance micellar stability. This approach was not able to sustain the release of encapsulated paclitaxel (PTX) or JSI-124 from micelles, however. JSI-124 was then chemically conjugated to the core of PEO-*b*-PCL micelles. The developed nanocarrier sustained the release of JSI-124 and maintained its STAT3 inhibitory activity in B16 melanoma at lower potency. Interestingly, the JSI-124 polymeric micellar conjugate have shown better potency than the free drug in modulation of immune response in tumor induced immunosuppressed dendritic cells (DCs). We have

finally pursued modification of PEO-*b*-PCL micelles with grafted polyamines to improve the efficacy of these nanocarriers in tumor targeted siRNA delivery. For this purpose, cholesteryl groups were conjugated to the core of PEO-*b*-P(CL-*graft*-spermine) (PEO-*b*-P(CL-*g*-SP) micelles. The modification improved transfection efficiency of siRNA in breast cancer cells *in vitro*, but had no significant effect in their *in vivo* activity in tumor gene silencing following intratumoral or intravenous administration of siRNA delivery system. Modification of the PEO shell with an integrin targeting peptide i.e. RGD4C, led to better siRNA silencing activity in tumor after systemic administration, however. In conclusion, our results show that modification of the core and/or shell of polymeric micelles can be used to fine-tune relevant properties of these nanocarriers leading to their potential use as versatile pharmaceutical excipients for tumor targeted drug/siRNA delivery.

Preface

Section 1.2 of Chapter one of this thesis has been published as Xiong X-B, Falamarzian A, Garg SM, Lavasanifar A, Engineering of amphiphilic block copolymers for polymeric micellar drug and gene delivery, *Journal of Controlled Release*, 155,247-261 (2011). Xiong X-B was responsible for the manuscript composition. Both Falamarzian A and I, contributed to two sections of the manuscript and also contributed to manuscript edits. Lavasanifar A was the supervisory author and was involved with the manuscript composition.

Chapter two of this thesis has been published as Garg SM, Vakili MR, Lavasanifar A, Polymeric micelles based on poly(ethylene oxide) and α -carbon substituted poly(ϵ -caprolactone): an *in vitro* study on the effect of core forming block on polymeric micellar stability, biocompatibility, and immunogenicity, *Colloids and Surfaces B: Biointerfaces*, 132, 161-170 (2015). I was responsible for the data collection and analysis as well as the manuscript composition. Vakili MR assisted with some of the data collection and contributed to manuscript edits. Lavasanifar A was the supervisory author and was involved with concept formation and manuscript composition.

Chapter four of this thesis has been published as Garg SM, Xiong X-B, Lu C, Lavasanifar A, Application of click chemistry in the preparation of poly(ethylene oxide)-*block*-poly(ϵ -caprolactone) with hydrolysable crosslinks in the micellar core, *Macromolecules*, 44, 2058-2066 (2011). I was responsible for the data collection and analysis as well as the manuscript composition. Xiong X-B assisted with some of the data collection and contributed to manuscript edits. Lu C assisted with some of the data collection. Lavasanifar A was the supervisory author and was involved with concept formation and manuscript composition.

Dedication

I dedicate this thesis:

To my beloved father, *Madhusudan Garg*, for making me the person I am today. You have been my biggest critic which has always pushed me to reach new heights. Thank you *Papa* for all the guidance and support throughout every moment of my life.

To my beloved mother, *Shashi Garg*, for her support throughout my entire life. It was your unconditional love and belief in my capabilities that motivated me to set higher targets. Thanks *Mummy* for the love and blessings you have showered upon me every moment of my life.

To my beautiful wife, *Raina Bellani*, who has always held my hand and supported me through the good and bad times. It was your unconditional love and support during my thesis that kept me motivated throughout the course of my PhD. Thanks *Raina* for being there for me every step of the way.

In memory of my late grandfather, *Ramratan Garg*, for his unconditional love and support early in my life. I know you are still watching over me from high up in the sky. Thanks *Dadaji* for your blessings throughout my life. I will miss you.

To my supervisor, *Dr. Afsaneh Lavasanifar*, for her constant support and guidance throughout my PhD Program. You were there to teach, guide, mentor, critic, inspire, and support me, which has always motivated me to work harder. Thanks *Dr. Lavasanifar* for being my *Guru* and instilling in me the passion for research.

Acknowledgements

- I sincerely thank my supervisor, Dr. Afsaneh Lavasanifar, for her continued support and guidance throughout my PhD Program. Over the course of my PhD, she trained me to develop from a young inquisitive student into a well-trained independent researcher.
- I sincerely thank my supervisory committee members, Dr. Kamaljit Kaur, for her advice during committee meetings and for providing me with the peptide to use for my formulations; and Dr. Raimar Löbenberg, for his advice and support during committee meetings and during my tenure as a teaching assistant.
- I sincerely thank my examining committee members, Dr. Hasan Uludağ, for serving on my candidacy and defense committee, for providing me access to his lab and materials, and for his expert advice when I was working with siRNA delivery; and Dr. Carlos Velázquez-Martínez, for serving on my candidacy and defense committee, and for his expert advice and feedback during my seminars.
- I sincerely thank Dr. Xiao-Bing Xiong and Dr. Mohammad Reza Vakili for training me in polymer chemistry; Dr. Samar Hamdy and Dr. Ommoleila Molavi for training me in culturing of dendritic cells and T-cells; Dr. Arash Falamarzian for assistance with siRNA delivery; and Dr. Mostafa Shahin for training me with the HPLC.
- I sincerely thank Dr. Hamidreza Montazeri Aliabadi and Kate Agopsowicz for training me in *in vivo* studies; Dr. Mary Hitt for her expertise in breast cancer tumor models; Dr. Rania Soudy for assisting me with the peptides for my formulations; Dan McGinn for assistance with intravenous injections; and Igor Paiva and Amir Soleimani for assistance with *in vivo* studies.
- I sincerely thank Dr. Vishwanatha Somayaji for assistance with LC-MS and NMR analysis; Jingzhou Huang (George) for assistance with flow cytometry; Geraldine Barron (Gerry) for assistance with confocal microscopy; Dr. Nick Nation for assistance with histopathological examination; Suellen Lamb for assistance with tissue processing; and Arlene Oatway for assistance with transmission electron microscopy.
- I sincerely thank Drew Price and James Chaulk for maintaining the lab instruments which made sure I finished my work on time; Stacey Engel and Bobbie McDonald

for their help and expertise while working in the animal facility; and Nicole Favis for her help and expertise while working in the AIVI animal facility.

- I sincerely thank my present and previous lab-mates for creating a friendly environment in the lab. Their feedback and suggestions have helped me greatly during my research.
- I sincerely thank my family and friends who have stood by me at every point in my life. Their continued love and support is what motivates me to keep aiming higher.
- Lastly, I sincerely thank the Alberta Cancer Foundation and the Alberta Innovates Health Solutions for providing me with financial support during my PhD program. Their support for cancer research instilled the passion in me for cancer research. I also thank the J.N. Tata Endowment trust for providing the initial support for me to come to Canada and join this PhD Program; the Golden Key International Honor Society for providing me with financial support during my PhD; the CIHR Institute of Cancer Research for financial support for traveling to two conferences; and finally the Faculty of Pharmacy and Pharmaceutical Sciences and the University of Alberta for accepting me into this PhD Program and for supporting me during the course of my PhD program.

Table of Contents

Chapter One: Introduction	1
1.1 Nanotechnology in Cancer therapy	2
1.2 Polymeric micelles: Advantages and Challenges.....	5
1.2.1 Engineering of Micellar Core for Improved Properties in Drug Delivery.....	8
1.2.2 Engineering of the Micellar Shell for Improved Properties in Drug Delivery.....	27
1.2.3 Simultaneous Engineering of Core and Shell.....	35
1.3 Immune System and Cancer	39
1.4 Cancer Immunotherapy	40
1.5 Cancer Immunosuppression.....	42
1.6 STAT3 in Cancer	43
1.6.1 Introduction to STAT3	43
1.6.2 Role of STAT3 in tumor growth	46
1.6.3 Role of STAT3 in tumor-induced immunosuppression	46
1.6.4 Targeting STAT3 for cancer immunotherapy	47
1.7 Role of Myeloid Cell Leukemia-1 (MCL-1) in Cancer.....	52
1.7.1 Targeting MCL-1.....	53
1.8 Research Proposal.....	58
1.8.1 Central Hypothesis	58
1.8.2 Rationale.....	58
1.8.3 Working Hypotheses	61
1.8.4 Specific Objectives	63
 Chapter Two: Polymeric Micelles based on Poly(ethylene oxide) and α- carbon Substituted Poly(ϵ-caprolactone): An <i>In Vitro</i> Study on the Effect of Core Forming Block on Polymeric Micellar Stability, Biocompatibility, and Immunogenicity	65

2.1 Introduction.....	66
2.2 Experimental Section.....	69
2.2.1 Materials	69
2.2.2 Mice	69
2.2.3 Synthesis of Block Copolymers	70
2.2.4 Characterization of Synthesized Block Copolymers and Preparation of Micelles.....	71
2.2.5 Assessing the Physicochemical Stability of Polymeric Micelles	73
2.2.6 Evaluation of Protein Adsorption from Serum on Polymeric Micelles.....	74
2.2.7 Assessing the <i>in vitro</i> immunogenicity of polymeric micelles against BMDCs	75
2.2.8 Statistical Analysis	76
2.3 Results	76
2.3.1 Synthesis and Characterization of Block Copolymers	76
2.3.2 Micellization of Block Copolymers	77
2.3.3 The Effect of Pendent Group on PCL on the Physical Stability of Polymeric Micelles.....	81
2.3.4 The Effect of Pendent Group Chemistry on the Hydrolytic Degradation of Polymeric Micelles	87
2.3.5 The Effect of Micellar Core Structure on Serum Protein Adsorption.....	93
2.3.6 Assessing the <i>In Vitro</i> BMDC Mediated Immunogenicity of Polymeric Micelles.....	95
2.4 Discussion.....	97
2.5 Conclusion	102
2.6 Acknowledgements.....	103
 Chapter Three: Traceable Polymeric Micelles for Breast Cancer	
Targeting	104
3.1 Introduction.....	105
3.2 Experimental Section.....	107
3.2.1 Materials	107
3.2.2 Cell line.....	107

3.2.3 Synthesis of Cy5.5 Conjugated Block Copolymers	108
3.2.4 Synthesis of P18-4 Modified Block Copolymers	109
3.2.5 Characterization of Synthesized Block Copolymers	110
3.2.6 Preparation and Characterization of Block Copolymer Micelles	110
3.2.7 <i>In Vitro</i> Cell Uptake Study using Flow Cytometry	113
3.2.8 <i>In Vitro</i> Cell Uptake Study using Confocal Microscopy	113
3.2.9 Animal Models	114
3.2.10 <i>In Vivo</i> Imaging and Tissue Biodistribution	115
3.2.11 Statistics	116
3.3 Results	116
3.3.1 Labeling of PEO- <i>b</i> -PCL and PEO- <i>b</i> -PBCL with NIR dye	116
3.3.2 Preparation of NIR labeled micelles	122
3.3.3 <i>In Vitro</i> Cell uptake Study	127
3.3.4 <i>In vivo</i> body distribution and tumor-targeting ability of polymeric micelles in orthotopic breast cancer model	133
3.3.5 <i>Ex vivo</i> distribution and tumor-targeting ability of polymeric micelles in orthotopic breast cancer model	138
3.4 Discussion	142
3.5 Conclusion	147
3.6 Acknowledgements	148

Chapter Four: Application of Click Chemistry in the Preparation of Poly(ethylene oxide)-<i>block</i>-poly(ϵ-caprolactone) with Hydrolysable Crosslinks in the Micellar Core	149
4.1 Introduction	150
4.2 Experimental Section	153
4.2.1 Materials	153
4.2.2 Synthesis of α -Propargyl Carboxylate- ϵ -Caprolactone	153
4.2.3 Synthesis of PEO- <i>block</i> -Poly(α -Propargyl Carboxylate- ϵ - Caprolactone) (PEO- <i>b</i> -PPCL)	155
4.2.4 Micelle Formation and Core-Crosslinking	156

4.2.5 Characterization of Micelles.....	156
4.2.6 Evaluation of Protein Adsorption on Micelles.	158
4.2.7 Preparation of PTX loaded Micelles.	158
4.2.8 Release of PTX from Polymeric Micelles.	159
4.3 Results and Discussion.....	160
4.3.1 Synthesis and Characterization of Block Copolymers.	160
4.3.2 Micellization of Block Copolymers and Core-Crosslinking.	166
4.3.3 Protein Adsorption on Micelles.	172
4.3.4 Preparation and Characterization of Polymeric Micelles Containing Physically Encapsulated PTX.	175
4.4 Conclusion.....	177
4.5 Acknowledgement.....	178
 Chapter Five: Self-associating Poly(ethylene oxide)-<i>block</i>-poly(ϵ-caprolactone (PEO-<i>b</i>-PCL) Drug Conjugates for the Delivery of STAT3 Inhibitor JSI-124: Application in Cancer Immunotherapy.....	
5.1 Introduction.....	179
5.2 Experimental Section.....	181
5.2.1 Materials.....	181
5.2.2 Mice.....	182
5.2.3 Cell line.....	183
5.2.4 Synthesis of PEO- <i>b</i> -poly(α -JSI-124-carboxylate- ϵ -caprolactone) (PEO- <i>b</i> -P(CL-JSI-124)).....	183
5.2.5 Characterization of PEO- <i>b</i> -P(CL-JSI-124).....	185
5.2.6 Self Assembly of PEO- <i>b</i> -P(CL-JSI-124) and characterization of assembled structures.....	186
5.2.7 Release of JSI-124 from PEO- <i>b</i> -P(CL-JSI-124).....	187
5.2.8 Generation of bone marrow derived dendritic cells (BMDCs).....	188
5.2.9 Cell viability studies.....	189
5.2.10 Cell cycle analysis.....	190
5.2.11 Generation of tumor-induced immunosuppressed DCs.....	191

5.2.12 Analysis of p-STAT3 level by flow cytometry	191
5.2.13 Assessment of the functional characteristics of DCs by flow cytometry and ELISA	193
5.2.14 Assessment of the functional characteristics of DCs by MLR.....	194
5.3 Results	195
5.3.1 Synthesis and characterization of PEO- <i>b</i> -P(CL-JSI-124) block copolymer.....	195
5.3.2 Characterization of PEO- <i>b</i> -P(CL-JSI-124) micelles	198
5.3.3 Release of JSI-124 from PEO- <i>b</i> -P(CL-JSI-124)	199
5.3.4 Cell viability studies	201
5.3.5 Cell cycle analysis	205
5.3.6 STAT3 inhibitory activity	207
5.3.7 Immunomodulatory effects of JSI-124 and its polymer conjugate on B16 tumor induced immune-suppressed BMDCs.....	210
5.4 Discussion.....	215
5.5 Conclusion	220
5.6 Acknowledgements.....	221
Chapter Six: Modification of the Core/Shell Structure in Poly(ethylene oxide)-<i>block</i>-poly(ϵ-caprolactone-<i>graft</i>-spermine) Micellar siRNA for MCL-1 Gene Silencing in Tumor Xenografts	222
6.1 Introduction.....	223
6.2 Experimental Section.....	226
6.2.1 Materials	226
6.2.2 Cell lines	227
6.2.3 Synthesis of Cholesteryl Substituted PEO- <i>b</i> -P(CL-g-SP) Block Copolymers	228
6.2.4 Synthesis of RGD4C-PEO- <i>b</i> -PCCL with pendant N,N- dimethyldipropylene-triamine (DP) (RGD4C-PEO- <i>b</i> -P(CL-g-DP)).....	229
6.2.5 Preparation of polymeric micellar siRNA complexes for <i>in vivo</i> study.....	230
6.2.6 Animal models.....	230

6.2.7 <i>In vivo</i> activity of MCL-1 siRNA micelles after intratumoral and intravenous injection	231
6.2.8 Statistics.....	232
6.3 Results	233
6.3.1 Synthesis and Characterization of PEO- <i>b</i> -P(CL- <i>g</i> -SP-Chol).....	233
6.3.2 <i>In vivo</i> activity of MCL-1 siRNA micelles following intratumoral injection.....	235
6.3.3 <i>In vivo</i> activity of RGD4C-functionalized versus plain MCL-1 siRNA micelles after intravenous injection	237
6.4 Discussion.....	241
6.5 Conclusion	244
6.6 Acknowledgements.....	245
Chapter Seven: General Discussion, Conclusion, and Future Directions	247
7.1 General Discussion.....	248
7.2 Conclusion	254
7.3 Future Studies	256
References.....	258
Appendix A.....	287
Appendix B.....	291
Appendix C.....	301

List of Tables

Table 1.1 Polymeric micellar delivery systems in clinical trials. ²³⁻³²	7
Table 1.2 Agents used for STAT3 targeting. ^{228, 231, 239}	49
Table 2.1 Characteristics of prepared block copolymers and block copolymer micelles	79
Table 3.1 Characteristics of prepared block copolymers.....	118
Table 3.2 Characteristics of prepared block copolymer micelles.....	125
Table 4.1 Elemental analysis by XPS giving atomic and mass concentrations (%) of the following elements.....	171
Table 4.2 Characteristics of PTX loaded copolymer micelles when DMF was used as the solvent for micellization ($n = 3$)	175
Table 5.1 Characteristics of prepared block copolymers and block copolymer micelles	199
Table 6.1 Characteristics of polymers used in the study	234
Table 6.2 Polymer compositions for the preparation of siRNA micellar complexes for <i>in vivo</i> study.....	234

List of Figures

Figure 1.1 Schematic illustration of established nanotherapeutic platforms.....	4
Figure 1.2 Schematic illustration of polymer structures and assembled RGD-functionalized micelles containing NIRF imaging probes.	19
Figure 1.3 Synthesis of PEO- <i>b</i> -P(CL-PTX) block copolymer; <i>in vitro</i> release profile of physically loaded PTX	20
Figure 1.4 PEO- <i>b</i> -P(CL-polyamine) micelles for siRNA delivery.....	26
Figure 1.5 Chemical structure of P18-4 peptide.....	35
Figure 1.6 STATs pathway in cancer cells.....	45
Figure 1.7 Chemical structure of JSI-124.....	51
Figure 2.1 TEM picture of PEO- <i>b</i> -PCL, PEO- <i>b</i> -PBCL, and PEO- <i>b</i> -PCCL block copolymer micelles (110,000X).	80
Figure 2.2 Average size (<i>Z</i> -average) and polydispersity index (PDI) changes of micelles as a function of time	83
Figure 2.3 Intensity size distributions of micelles as a function of incubation time	84
Figure 2.4 Percentage intensity and polydispersity index (PDI) of micelles as a function of time.....	86
Figure 2.5 ¹ H NMR spectrum of PEO ₁₁₄ - <i>b</i> -PCL ₄₂ block copolymer in CDCl ₃ and peak assignments.....	89
Figure 2.6 ¹ H NMR spectrum of PEO ₁₁₄ - <i>b</i> -PBCL ₁₉ block copolymer in CDCl ₃ and peak assignments.	90
Figure 2.7 ¹ H NMR spectrum of PEO ₁₁₄ - <i>b</i> -PCCL ₁₉ block copolymer in CDCl ₃ and peak assignments.	91

Figure 2.8 Degradation of the core of micelles as a function of time by ¹ H NMR.	92
Figure 2.9 Percentage of total protein adsorbed on PEO- <i>b</i> -PCL, PEO- <i>b</i> -PBCL, and PEO- <i>b</i> -PCCL micelles after incubation in FBS for 4 hrs.	94
Figure 2.10 Immunogenicity of micelles measured in terms of promoting the phenotype maturation and cytokine secretion by DCs.	96
Figure 3.1 ¹ H NMR spectrum of (A) PEO- <i>b</i> -PCL, (B) PEO- <i>b</i> -PBCL, (C) PEO- <i>b</i> -PCL-PCC, and (D) PEO- <i>b</i> -PBCL-PCC in CDCl ₃ and peak assignments.	120
Figure 3.2 TEM picture of block copolymer micelles (110,000X).	126
Figure 3.3 Percentage intensity of micelles as a function of time in the presence of SDS.	127
Figure 3.4 Cellular uptake of cy5.5-loaded micelles (MFI) by A) MDA-MB-231-luc-D3H2LN and B) MCF10A cells.	129
Figure 3.5 Cellular uptake of cy5.5-loaded micelles (% positive cells) by A) MDA-MB-231-luc-D3H2LN and B) MCF10A cells.	130
Figure 3.6 Cellular uptake of cy5.5-loaded micelles by MDA-MB-231-luc-D3H2LN cells with (+) or without (-) pre-treatment with excess of free P18-4 peptide.	131
Figure 3.7 Cellular distribution of cy5.5-loaded micelles by confocal microscopy.	132
Figure 3.8 Evaluation of orthotopic breast tumor model.	134
Figure 3.9 <i>In vivo</i> biodistribution and tumor accumulation of cy5.5-loaded micelles.	135
Figure 3.10 Average radiant efficiency in tumor of plain and P18-4 modified A) PEO- <i>b</i> -PCL, and B) PEO- <i>b</i> -PBCL micelles at 4 h, 24 h, 48 h, and 72 h after intravenous administration of cy5.5-loaded micelles.	137
Figure 3.11 <i>In vivo</i> biodistribution and tumor accumulation of cy5.5-loaded micelles.	140

Figure 3.12 <i>In vivo</i> biodistribution and tumor accumulation of cy5.5-loaded micelles.	141
Figure 4.1 ¹ H NMR and IR spectrum of α -propargyl carboxylate- ϵ -caprolactone.....	162
Figure 4.2 ¹³ C NMR spectrum of α -propargyl carboxylate- ϵ -caprolactone	163
Figure 4.3 ¹ H NMR and IR spectrum of PEO- <i>b</i> -PPCL.....	165
Figure 4.4 TEM picture of A) non-crosslinked micelles and B) crosslinked micelles. Particle size distribution of C) non-crosslinked micelles and D) crosslinked micelles by DLS in water and in acetone.....	168
Figure 4.5 ¹ H NMR spectrum and peak assignments of (A) non-crosslinked micelles and (B) crosslinked micelles in CDCl ₃	169
Figure 4.6 IR spectrum of (A) crosslinked micelles and (B) non-crosslinked micelles.....	170
Figure 4.7 XPS spectrum of nitrogen (N 1s) in core-crosslinked micellar sample.	171
Figure 4.8 A) Gel permeation chromatogram of a) BSA solution, b) crosslinked micelles, and c) mixture of crosslinked micelles and BSA; B) Protein adsorption of crosslinked and non-crosslinked micelles	174
Figure 4.9 <i>In vitro</i> release profile of physically encapsulated PTX from different micellar formulations.....	177
Figure 5.1 Characterization of PEO- <i>b</i> -P(CL-JSI-124).....	197
Figure 5.2 <i>In vitro</i> release profile of JSI-124 from PEO- <i>b</i> -PCCL or PEO- <i>b</i> -P(CL-JSI- 124) micelles.....	200
Figure 5.3 Assessment of the anticancer activity of PEO- <i>b</i> -P(CL-JSI-124) micelles against B16 melanoma cell line.....	202
Figure 5.4 Assessment of the cytotoxicity of PEO- <i>b</i> -P(CL-JSI-124) micelles to BMDCs.....	203

Figure 5.5 Selectivity index (SI) of free JSI-124 and PEO- <i>b</i> -P(CL-JSI-124) micelles by B16-F10 cells vs. BMDCs.....	204
Figure 5.6 Representative cell cycle analysis of B16 cells exposed to free or conjugated JSI-124.	206
Figure 5.7 Assessment of the p-STAT3 inhibitory activity of PEO- <i>b</i> -P(CL-JSI-124) in B16 melanoma cells.....	208
Figure 5.8 Assessment of the p-STAT3 inhibitory activity of PEO- <i>b</i> -P(CL-JSI-124) in BMDCs.	209
Figure 5.9 The effects of JSI-124 and PEO- <i>b</i> -P(CL-JSI-124) on the maturation and activation of B16 tumor induced immune-suppressed BMDCs.	211
Figure 5.10 The effects of JSI-124 and PEO- <i>b</i> -P(CL-JSI-124) on the function of B16 tumor induced immune-suppressed BMDCs in activating T-cells.....	214
Figure 6.1 <i>In vivo</i> MCL-1 siRNA activity in nude mice bearing MDA-MB-435 WT xenograft treated with three intratumoral injections of polymer/siRNA formulations or HEPES.....	236
Figure 6.2 <i>In vivo</i> MCL-1 siRNA activity in nude mice bearing MDA-MB-435 WT xenograft treated with three intravenous injections of polymer/siRNA formulations or dextrose.....	240

List of Schemes

Scheme 1.1 The developed library of functionalized PEO-PCL polymers.....	61
Scheme 2.1 General synthesis scheme for the preparation of PEO- <i>b</i> -PCL, PEO- <i>b</i> -PBCL, and PEO- <i>b</i> -PCCL block copolymers.....	78
Scheme 3.1 Synthetic scheme for the preparation of PEO- <i>b</i> -PCL-PCC-cy5.5 and PEO- <i>b</i> -PBCL-PCC-cy5.5.....	119
Scheme 3.2 Synthetic Scheme for the preparation of P18-4 modified PEO- <i>b</i> -PCL and PEO- <i>b</i> -PBCL block copolymers.....	121
Scheme 3.3 Synthetic Scheme for the preparation of cy5.5 loaded (A) PEO- <i>b</i> -PCL, (B) P18-4 decorated PEO- <i>b</i> -PCL, (C) PEO- <i>b</i> -PBCL, and (D) P18-4 decorated PEO- <i>b</i> -PBCL micelles.....	124
Scheme 4.1 Synthetic scheme for the preparation of core-crosslinked micelles.....	154
Scheme 5.1 Synthetic scheme for the preparation of PEO- <i>b</i> -P(CL-JSI-124) block copolymer micelles.....	196

List of Abbreviations

4AB; 4-acetyl benzoic acid

ABCs; Amphiphilic block copolymers

ABL; Abelson leukaemia

Abz; 4-aminobenzoate

Acetal-PEO-*b*-PBCL; Acetal-PEO-poly-(α -benzyl carboxylate- ϵ -caprolactone)

Acetal-PEO-*b*-PCCL; Acetal-PEO-poly(α -carboxyl- ϵ -caprolactone)

AmB; Amphotericin B

APC; antigen presenting cell

ATRP; atom transfer radical polymerization

BCL-2; B-cell CLL/lymphoma 2

BCR; breakpoint-cluster region

BIEE; 1,2-bis(2-iodoethoxy)ethane

bis-MPA; 2,2-bis(methylol)propionic acid

BMDC; bone-marrow derived dendritic cells

BSA; bovine serum albumin

Bu-Li; butyllithium

CCC; cationic comb type copolymers

cDNA; complementary deoxyribonucleic acid

CMC; Critical micelle concentration

CP; cyclophosphamide

cRGDfK; cyc(Arginine-Glycine-Aspartic acid-D-Phenylalanine-Lysine)

CT; computed tomography

DC; Dendritic cells

DCC; N,N-dicyclohexyl carbodiimide

DCPM; disulfide crosslinked polyion micelles

DEA; diethylamino

DiR; (1,1'-dioctadecyltetramethyl indotricarbocyanine iodide)

DLS; Dynamic light scattering

DMA; dimethylamino

DMF; dimethyl formamide

DMSO; dimethyl sulfoxide

DNA; deoxyribonucleic acid

DOPE; dioleoylphosphatidyl ethanolamine

DOX; Doxorubicin

DP; N,N-dimethyldipropylenetriamine

EDTA; ethylenediamine tetracetate

EGFP; Enhanced green fluorescence protein

FAM; 5-carboxyfluorescein

FBP; folate-binding protein

FDA; Food and Drug Administration

FITC; fluorescein isothiocyanate

FRET; fluorescence resonance energy transfer

Gal; galactosamine

GAPDH; Glyceraldehyde phosphate dehydrogenase

GFP; Green fluorescence protein

Gly; glycine

GM-CSF; granulocyte macrophage - colony stimulating factor

GPC; gel permeation chromatography

GRGDS; Glycine-Arginine-Glycine-Aspartic acid-Serine

HNSCC; Head and neck squamous cell carcinoma

I.V.; Intravenous

IC₅₀; 50 % inhibitory concentration

ICG; indocyanine green

IFN; Interferon

IL; interleukin

JAK; janus kinase

LEV; levulinic acid

LHRH; luteinizing hormone releasing hormone

LPS; lipopolysaccharide

mAb; monoclonal antibody

MAL; maleimide

MAL-PEO-PCL; Maleimide-terminated PEO-PCL

MCL-1; Myeloid cell leukemia sequence 1

MDR; Multi drug resistant

MHC; major histocompatibility complex

MMP2; Matrix metalloproteinase 2

MPS; mononuclear phagocyte system

MR; magnetic resonance

MRI; magnetic resonance imaging

mRNA; messenger RNA

MW; molecular weight

N/P; Nitrogen to phosphate

NHS; N-hydroxy succinimide

NIR; near infra-red

NIRF; near infra-red fluorophore

NKT; natural killer T-cell

NON; plain

ODN; oligonucleotides

P(NIPAAm-*co*-MAAc)-*g*-PLA; poly(*N*-isopropyl acrylamide-*co*-methacryl acid)-*g*-PLA

P2VP; PEO-*b*-poly(2-vinylpyridinium)

PAA; poly(acrylic acid)

PAA-*b*-PS; poly(acrylic acid)-*b*-poly(styrene)

PCL; Poly(ϵ -caprolactone)

PCMA; poly(2-cinnamoyl ethyl methacrylate)

PDMA-*b*-P(NIPAM-*co*-AzPAM); poly(N,N-dimethylacrylamide)-*b*-poly(N-isopropylacrylamide-*co*-3-azidopropylacrylamide)

PE; Phosphothioethanol

PE; Phosphatidyl ethanolamine

PEG; Poly(ethylene glycol)

PEI; Polyethyleneimine

PEI-LA; Polyethyleneimine-linoleic acid

PEO; Poly(ethylene oxide)

PEO-*b*-P(Asp); PEO-*b*-poly(L-aspartic acid)

PEO-*b*-P(CL-*g*-SP); poly(ethylene oxide)-*block*-poly(ϵ -caprolactone-*g*-spermine)

PEO-*b*-P(CL-*g*-SP-Chol); poly(ethylene oxide)-*block*-poly(ϵ -caprolactone-*g*-spermine-cholesteryl carboxylate)

PEO-*b*-P(CL-*g*-TP); poly(ethylene oxide)-*block*-poly(ϵ -caprolactone-*g*-tetraethylenepentamine)

PEO-*b*-P(CL-Hyd-DOX); poly(ethylene oxide)-*block*-poly(ϵ -caprolactone) conjugated with doxorubicin through hydrazone linker

PEO-*b*-P(DMA-*stat*-NAS)-*b*-NIPAM; PEO-*b*-((N,N-dimethylacrylamide)-*stat*-(N-acryloxysuccinimide))-*b*-(N-isopropylacrylamide)

PEO-*b*-P(His); PEO-*b*-poly(L-histidine)

PEO-*b*-P(His); Poly(ethylene oxide)-*b*-poly(L-histidine)

PEO-*b*-P(Lys); PEO-*b*-poly(lysine)

PEO-*b*-P(α,β -Asp); PEO-*b*-poly(α,β -aspartic acid)

PEO-*b*-PBCL; PEO-*b*-poly(α -benzyl carboxylate- ϵ -caprolactone)

PEO-*b*-PCCL; PEO-*b*-poly(α -carboxyl- ϵ -caprolactone)

PEO-*b*-PCL; Poly(ethylene oxide)-*block*-poly(ϵ -caprolactone)

PEO-*b*-PCL-*b*-PEO; Poly(ethylene oxide)-*block*-poly(ϵ -caprolactone)-*block*-poly(ethylene oxide)

PEO-*b*-PDMA-*b*-PDEA; PEO-*b*-poly(2-(dimethylamino)ethyl methacrylate)-*b*-poly(2-(diethylamino) ethyl methacrylate)

PEO-*b*-PEI; PEO-*b*-poly(ethylene imine)

PEO-*b*-PHSA; PEO-*b*-poly(*N*-hexyl stearate L-aspartamide)

PEO-*b*-PLA; Poly(ethylene oxide)-*b*-polylactide

PEO-*b*-PLAA; PEO-*b*-P(L-amino acid)

PEO-*b*-PLDTP; PEO-*b*-poly(L-lysine-dithiopyridine)

PEO-*b*-PLLA; PEO-*b*-P(L-lactide)

PEO-*b*-PUNB-*b*-PEO; Poly(ethylene oxide)-*block*-poly(urethane containing *o*-nitrobenzyl methyl ester)-*block*-poly(ethylene oxide

PEO-DSPE; 1,2-distearoyl-sn-glycero-3-phosphoethanolamine-*N*-[amino(polyethylene glycol)-5000]

PET; positron emission tomography

PEVP; poly(*N*-ethyl-4-vinylpyridinium)

P-gp; P-glycoprotein

PHEMA-*co*-His-*g*-PLA; poly(2-hydroxyethyl methacrylate-*co*-histidine)-*g*-PLA

PIC; Polyion complex

PLA; poly(lactide)

PLGA; Poly-(D,L-lactide-*co*-glycolide)

PMAa; PEO-*b*-poly(methacrylic acid)

PPEGMA-*b*-PESPMA; poly(PEG-methacrylate)-*b*-poly(triethoxysilyl propylmethacrylate)

PS; phosphatidylserine

PS; poly(styrene)

PSMA-*b*-PSTY; poly(styrene-*alt*-maleic anhydride)-*b*-polystyrene

p-STAT3; tyrosine-phosphorylated STAT3

PStS; poly(styrene sulphonate)

PTX; Paclitaxel

pTyr; phopho-tyrosine

RGD; Arg-Gly-Asp

RGD4C; Cys-Asp-Cys-Arg-Gly-Asp-Cys-Phe-Cys

RISC; RNA-induced silencing complex

RNA; ribonucleic acid

RNAi; RNA interference

ROP; ring-opening polymerization

RT PCR; Real-time PCR

S.C.; subcutaneous

sCLU; secretory clusterin

SEC; size exclusion chromatography

SH2; Src-homology 2

siRNA; small interfering RNA

Sn(Oct)₂; Stannous octate

SP; spermine

SPECT; single photon emission computed tomography

STAT; Signal transducers and activators of transcription

TAA; tumor associated antigen

TDSF; tumor-derived soluble factors

TEM; transmission electron microscopy

TEM; Transmission electron microscopy

TGF; tumor growth factor

THF; Tetrahydrofuran

TLC; Thin-layer chromatography

TLR; toll like receptor

TNBC; Triple negative human breast cancer

TNF- α ; tumor necrosis factor α

TP; tetraethylenepentamine

T_{reg}; regulatory T-cell

US; ultrasound

UV; ultraviolet

VEGF; Vascular endothelial growth factor

WT; Wild type

ϵ -CL; ϵ -Caprolactone

Chapter One

Introduction

Section 1.2 of this chapter has been published in
**Engineering of amphiphilic block copolymers for polymeric micellar drug and gene
delivery**
in
Journal of Controlled Release 2011, 155, 247 - 261

Xiao-Bing Xiong¹, Arash Falamarzian¹, Shyam M Garg¹, Afsaneh Lavasanifar^{1,2}

¹Faculty of Pharmacy and Pharmaceutical Sciences, University of Alberta, Edmonton, AB

²Department of Chemical and Materials Engineering, Faculty of Engineering, University of
Alberta, Edmonton, AB

Reprinted from Reference,¹ Copyright (2011), with permission from Elsevier

1.1 Nanotechnology in Cancer therapy

Nanotechnology encompasses the engineering of materials at the atomic, molecular and supramolecular scale in order to modify their properties for an intended application. During the past few decades, advancement in the development and application of nanotechnology in drug and gene delivery has offered exciting new possibilities in the field of nano-medicine. The application of nanotechnology can ultimately improve the delivery and bioavailability of poorly water soluble drugs at the site of drug action. The utility of nanotechnology in medicine has led to the creation of materials that can interact with the biological system at sub-cellular levels with high degree of specificity. All these can potentially translate into maximum therapeutic benefits with limited adverse effects for existing or emerging therapeutics.²⁻⁵ Nanoscale drug delivery was largely introduced in the mid-1960s when liposomes were utilized as carriers of proteins and drugs to treat different diseases. Therefore, liposomes can be regarded as one of the first nanomedicines.^{6, 7} Since then numerous nanoscale drug delivery systems have been investigated.^{2, 8-10} In the field of cancer, nanomedicine can play an important part in improving therapy and diagnosis.¹¹

Today, around 50% of all humans diagnosed with malignant tumors die from this disease.¹² In Canada, cancer is the leading cause of death and is responsible for nearly 30% of all deaths.¹³ Nanomedicine is expected to make a strong impact in the field of cancer diagnosis and therapy. Nanotechnology can be used for:

- a) Targeted therapy of anti-cancer drugs at the tumor site while reducing toxicity to other healthy organs and tissues.
- b) Better resolution in diagnostic imaging.
- c) Improving the pharmacokinetics and bioavailability of anti-cancer drugs.

d) Delivery of two or more drugs or therapeutic modalities.

e) Development of theranostics in cancer therapy.^{2, 14, 15}

Additionally, various nanotechnology modalities such as drug conjugates, lipid- and polymer-based nanocarriers, inorganic nanoparticles and viral nanoparticles have also been investigated for use in cancer detection and treatment (Figure 1.1).^{11, 14} Among these, polymer-based carriers like polymeric micelles have been receiving great attention due to the flexibility of their chemical structure and easy adaptation to engineering strategies. In this thesis, we have taken advantage of the chemical flexibility of polymeric micelles by engineering their core/shell structure to develop chemotherapeutic, immunotherapeutic, and gene silencing strategies to fight cancer.

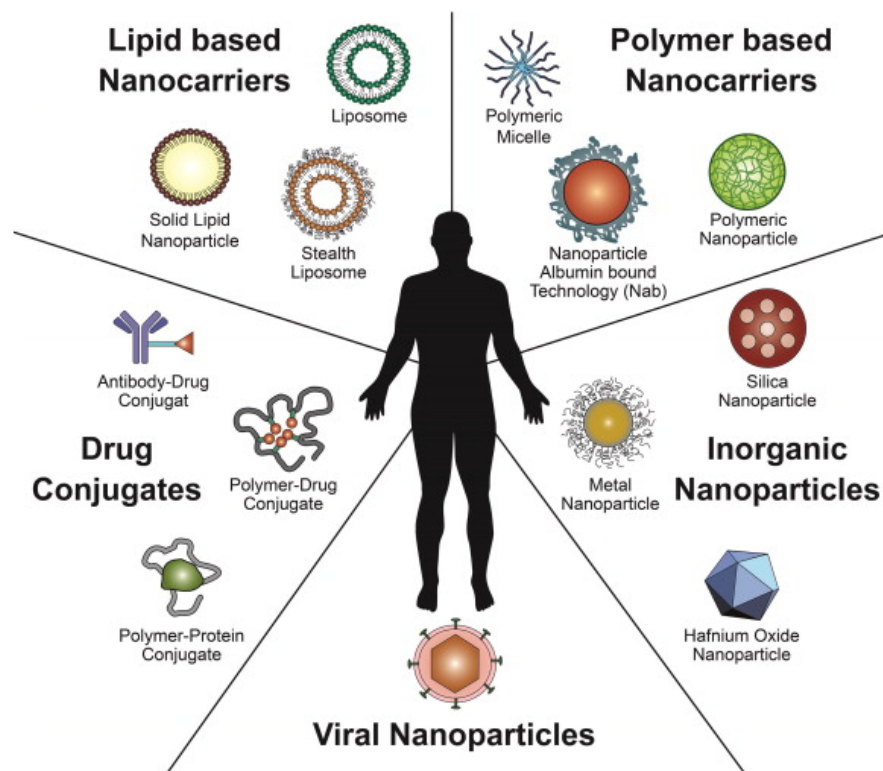


Figure 1.1 Schematic illustration of established nanotherapeutic platforms. Different nanomedicine products such as drug conjugates, lipid-based nanocarriers, polymer-based nanocarriers, inorganic nanoparticles, and viral nanoparticles are used in clinical cancer care. (Reprinted from Reference¹¹, Copyright (2014), with permission from Elsevier).

1.2 Polymeric micelles: Advantages and Challenges

Over the last few decades, block copolymers have emerged as an interesting class of biomaterials due to their versatile applications in pharmaceutical science and drug delivery. Of particular interest are amphiphilic block copolymers which self-assemble into polymeric micelles (average diameters of 20 to 100 nm) above the critical micelle concentration (CMC).¹⁶⁻¹⁸ In an aqueous environment, polymeric micelles are characterized with a core-shell architecture, where the hydrophobic core is segregated from the aqueous exterior by a hydrophilic shell. The widespread application of polymeric micelles in drug delivery is linked to their unique core-shell architecture, in which the hydrophobic core of micelles creates a space for the encapsulation of hydrophobic drugs, proteins or DNA through physical or chemical means. The hydrophilic shell of polymeric micelles, on the other hand, is a brush-like corona masking the hydrophobic core from the biological milieu. Since the hydrophilic shell minimizes protein adsorption on micelles and their cellular adhesion, polymeric micelles have the ability to evade non-specific capture by the mononuclear phagocyte system (MPS). The size of polymeric micelles is also above the threshold for filtration by kidneys. Thus, polymeric micelles can potentially sequester several drugs; they have demonstrated prolonged circulation,¹⁹⁻²¹ and can act as depot release nano-carriers in blood and/or passively accumulate in sites with leaky vasculature (e.g., solid tumors and sites of inflammation) because of the enhanced permeability and retention (EPR) effect.^{19, 21} Polymeric micelles consisting of PEO-*b*-polypropylene oxide (PPO), PEO-*b*-poly(ester)s and PEO-*b*-poly(amino acid)s have been extensively investigated for drug solubilization, controlled drug release and drug targeting.^{19, 21, 22} Several excellent reviews have been

published on polymeric micelles based drug/gene delivery systems, and a few micellar drug delivery systems have moved from bench to clinical trials (Table 1.1).

In spite of their advantages as drug delivery system, challenges still exist which greatly limit the micelle delivery system for clinical use. The major hurdles include low drug loading efficiency, poor blood stability after injection, and difficulty in transporting through cell membranes.²³ Clinical use of polymeric micelle formulations greatly depends on addressing these issues. The chemical flexibility of block copolymers makes it possible to engineer both the core and shell to achieve maximum therapeutic effect. Efforts for core engineering have been directed towards increasing drug loading capacity, enhancing micelle stability, achieving controlled drug release and encapsulating genetic cargos such as gene and siRNA. The micellar shell, on the other hand, has been engineered towards achieving active targeting, enhanced cellular uptake, or stimuli responsive drug release. Finally, simultaneously engineering the core and shell would lead to next generation of multifunctional polymeric micelles which integrate many functions into one nanocarrier providing a wide range of solutions to the unmet problems in drug delivery.

Table 1.1 Polymeric micellar delivery systems in clinical trials.²⁴⁻³³

Trade Name	Block Copolymer	Drug	Clinical Phase	Indication
NK911	PEG- <i>b</i> -poly(α,β -aspartic acid)	Doxorubicin	Phase II	Various solid tumors
NK105	PEG- <i>b</i> -poly(α,β -aspartic acid)	Paclitaxel	Phase III	Metastatic or recurrent Breast cancer
NK012	PEG- <i>b</i> -poly(L-glutamic acid)	SN-38	Phase II	Triple negative breast cancer/small cell lung cancer
NC-6004	PEG- <i>b</i> -poly(L-glutamic acid)	Cisplatin	Phase III	Pancreatic cancer
NC-6004	PEG- <i>b</i> -poly(L-glutamic acid)	Cisplatin	Phase I/II	Non-small cell lung cancer/solid tumors
SP1049C	Pluronic L61, F127	Doxorubicin	Phase III	Gastric cancer
Genexol-PM	PEG- <i>b</i> -poly(D,L-lactide)	Paclitaxel	Phase II,III	Various solid tumors
NC-4016	PEG- <i>b</i> -poly(L-glutamic acid)	Oxaliplatin	Phase I	Various solid tumors/lymphoma
NC-6300	PEG- <i>b</i> -poly(aspartate-hydrazone)	Epirubicin	Phase I	Various solid tumors

1.2.1 Engineering of Micellar Core for Improved Properties in Drug Delivery

1.2.1.1 Enhancing Micelle Stability

Micelle instability upon administration is one of the main obstacles precluding the use of effective micellar drug carriers. The existence of a hydrophilic PEO brush on polymeric micelles can introduce steric effects and thus decrease their interaction with opsonins that lead to early micellar elimination by the MPS. Also, the size of polymeric micelles is large enough to avoid removal by kidneys. If the micellar structure can stay intact and retain the drug, the normal biodistribution of the encapsulated drug becomes similar to that of the carrier.

Under highly diluted conditions in the biological system, the stability of a particular polymeric micellar structure will be determined by its thermodynamic, as well as its kinetic stability. The critical micelle concentration (CMC), which is largely dependent on the hydrophobicity of block copolymers, reflects the micellar thermodynamic stability. Micelles with low CMC will have a better chance of staying in a micellar form under diluting conditions of blood circulation. The kinetic stability refers to the rate at which the micelle disassembles into single chains once the copolymer concentration falls below the CMC. The kinetic stability is largely influenced by the physical state of the core (i.e. amorphous or semi-crystalline nature). Both thermodynamic and kinetic stabilities are very important in determining the *in vivo* fate of micelles. Upon intravenous injection, micelles are also subjected to interactions with numerous blood components such as proteins and cells, which may lead to their early elimination.^{34, 35} Degradation of the polymer backbone can also significantly influence the thermodynamic stability of the micelles and provides an additional degree of freedom to control the longevity of block copolymer micelles in the body.³⁶

Several strategies have been investigated to increase micellar stability, including the modification of the core-forming block to reduce CMC and/or decrease rate of degradation, enhancement of intramicellar physical interactions through core crystallization, and covalent crosslinking of the micellar core.³⁷⁻⁴⁷

1.2.1.1.1 Reducing CMC

The most common strategy for reducing the CMC of amphiphilic block copolymers is to increase the hydrophobicity of the block copolymer through attachment of more hydrophobic moieties. For example, the attachment of various fatty acids to the core of PEO-*b*-poly(L-aspartamide) micelles was shown to decrease their CMCs.⁴² Chemical conjugation of doxorubicin (DOX) into the micelle core also increased the thermodynamic stability of the PEO-*b*-poly(aspartic acid) micelles as reflected by a reduced CMC.⁴⁴ Studies on PEO-*b*-peptide based micelles demonstrated the effect of more aliphatic and aromatic peptides in reducing the CMC.⁴⁸ Pluronic® micelles have been extensively studied as drug and gene delivery systems.^{49, 50} Problems associated with their use include low thermodynamic stability (high CMC) and relatively rapid *in vivo* drug release.⁵⁰ In order to overcome this disadvantage, chemically modified Pluronics® have been developed. Lee et al. have synthesized PCL-Pluronic®-PCL by ring-opening polymerization of ϵ -caprolactone (ϵ -CL) using the Pluronic® copolymers as the initiator and stannous octoate (Sn(Oct)₂) as the catalyst.^{51, 52} The PCL-Pluronic®-PCL copolymers self-assembled into micelles in water at a lower CMC than Pluronic® alone.

Another strategy is to increase the length of the hydrophobic chain of the block copolymer. Adams et. al synthesized PEO-*b*-poly(*N*-hexyl-aspartamide)-acyl conjugates with

various acyl chain lengths and found that increasing the acyl chain length results in a decreased CMC.^{37, 38} Another study demonstrated that an increase in the length of the PCL block in PEO-*b*-PCL-*b*-PEO triblock copolymer micelles led to a decrease in the CMC of the prepared micelles.⁵³ However, increasing the hydrophobic chain length beyond a certain point can result in non-spherical aggregates.⁵⁴

1.2.1.1.2 Reducing rate of degradation

Rapid degradation of block copolymers in the aqueous environment may prove to be a major obstacle in the development of effective micellar drug carriers. The thermodynamic stability of micelles, which is characterized by the CMC of block copolymers, depends on the hydrophobicity and/or length of the hydrophobic block.^{1, 54} In this regard, rapid degradation of the polymer backbone may lead to a reduction in hydrophobicity and an increase in CMC for block copolymers over time.³⁶ The degradation rate of micelle forming block copolymers can, not only affect the physical and biological stability, but it may also influence drug encapsulation and release characteristics of polymeric micelles.^{55, 56} For PEO-*b*-poly(ester) micelles, hydrolytic degradation via hydrolysis of the ester bonds has been reported to be the major route of degradation.^{36, 45, 47, 55, 57-59} Previous reports have proposed two-stage degradation mechanisms for PEO-*b*-poly(ester) micelles with slow interfacial erosion first occurring at the core-shell interface leading to swelling of the micelles. This is proposed to be followed by formation of caves and channels which leads to rapid degradation in the core.^{45, 55, 56} Carsten et al.,⁵⁷ on the other hand, proposed random scission as the mechanism for the degradation of micelles rather than preferential cleavage as described by the previous studies.

Li et al.⁶⁰ found that the enzymatic degradation of PEO-*b*-PCL films was not affected by the addition of PEO when compared to PCL homopolymer. However, Hu et al.⁵⁵ found that the degradation of PCL-*b*-PEO-*b*-PCL micelles in aqueous solution was faster compared to bulk materials such as films with changes in size and morphology during the degradation period.⁶¹ Yang et al.⁴⁷ studied the hydrolytic degradation of PEO-*b*-polylactide (PEO-*b*-PLA) micelles in aqueous solution and found that micelles having longer hydrophobic PLA blocks were more stable in size during degradation. Shen et al.⁴⁵ studied the hydrolytic degradation behavior of monomethoxy PEG-PCL nanoparticles in aqueous solution and found that the degree of polymerization of the PCL block significantly affects the rate of degradation of micelles with shorter PCL blocks degrading faster.

Apart from increasing the length of the hydrophobic block, introducing interactions between the hydrophobic chains can also reduce the rate of degradation. Yang et al.⁴⁷ found that stereocomplexation between poly(L-lactide) and poly(D-lactide) blocks is the reason why micelles prepared by mixtures of PEO-*b*-poly(L-lactide) and PEO-*b*-poly(D-lactide) were able to keep their micellar integrity for up to six weeks as compared to micelles prepared from PEO-*b*-poly(L-lactide) or PEO-*b*-poly(D-lactide) alone which lost their structural integrity within two weeks. Controlling the rate of degradation by using stimuli-responsive core is another way of modifying the stability of the micelles. Han et al.⁶² synthesized triblock copolymers of PEO-*b*-PUNB-*b*-PEO in which the PUNB block is composed of hydrophobic polyurethane containing *o*-nitrobenzyl methyl ester groups. The *o*-nitrobenzyl methyl esters can be rapidly photocleaved thus accelerating the rate of degradation of the micelles on exposure to UV light. In further studies, they modified the core of these triblock copolymers using click chemistry to contain both disulfide and *o*-

nitrobenzyl methyl ester groups. This allowed them to control the rate of degradation of the micelles by using either UV to rapidly photocleave the *o*-nitrobenzyl methyl esters or a reducing agent to slowly cleave the disulfide bonds in the core.⁶³

1.2.1.1.3 Increasing Intramicellar Interactions

To increase the kinetic stability of polymeric micelles, modification of micellar core with structures capable of intramicellar interactions has been attempted. For instance, introduction of benzyl groups to PEO-*b*-PCL increased the rigidity of the micellar core, possibly through intramicellar π - π interactions.⁴³ Recently, the stability of PEO-*b*-poly(*N*-hexyl stearate L-aspartamide) (PEO-*b*-PHSA) micelles having nine stearic acid side chains was studied and compared to that of 1,2-distearoyl-sn-glycero-3-phosphoethanolamine-*N*-[amino(polyethylene glycol)-5000] (PEO-DSPE) micelles in the presence of serum proteins by fluorescence resonance energy transfer (FRET).⁶⁴ The PEO-*b*-PHSA micelles were remarkably stable in the presence of serum while PEO-DSPE micelles were disrupted within 2 h. Both PEO-*b*-PHSA and PEO-DSPE micelles could efficiently solubilize Amphotericin B (AmB) in their aliphatic cores, but only PEO-*b*-PHSA micelles liberated AmB gradually in the presence of alpha and beta globulins, while PEO-DSPE micelles demonstrated rapid release of AmB. Another class of micelles capable of intramicellar interactions are the diacyllipid-PEO based micelles. The presence of two acyl chains introduces hydrophobic interactions inside the core thereby decreasing the CMC to the nanomolar or micromolar range. Various acyl chains such as stearyl or palmityl can be used to modify the stability of the core which can consist of diacyllipids such as phosphatidyl ethanolamine (PE).^{65, 66} Gao et. al.⁶⁵ used these PEO-PE based micelles for successfully encapsulating m-porphyrin,

tamoxifen, and PTX. In the case of PTX, which is a poorly water soluble drug, the encapsulation efficiency increased as the HLB of the PEG-PE micellar system was lowered. Another study indicated that PEG-PE micelles maintained their kinetic stability for a prolonged period of time in the high dilution conditions of the blood after intravenous administration.⁶⁷

To introduce hydrogen-bond interaction in the core-forming block, PEO-*b*-poly(ethyl-*random*-urea carbonate) block copolymers were synthesized by ring-opening polymerization of functionalized cyclic carbonates derived from 2,2-bis(methylol)propionic acid (bis-MPA).⁴¹ The incorporation of urea functional groups into the block copolymers led to improved kinetic stability of micelles in the presence of a destabilizing agent.

Micelle formation driven by the electrostatic ionic interaction of oppositely charged block copolymers can form stable polyion complex (PIC) micelles. Examples includes the pairs of PEO-*b*-poly(lysine) (PEO-*b*-P(Lys)) and PEO-*b*-poly(α,β -aspartic acid) (PEO-*b*-P(α,β -Asp)), PEO-*b*-poly(methacrylic acid) (PMAa) and poly(N-ethyl-4-vinylpyridinium) (PEVP), or PEO-*b*-poly(2-vinylpyridinium) (P2VP) and poly(styrene sulphonate) (PStS).⁶⁸⁻⁷⁰

1.2.1.1.4 Core Crosslinking

Covalent crosslinking of the micellar core can effectively enhance the stability of the micelles and avoid their dissociation in the extreme dilution conditions of the blood below CMC.⁷¹ Crosslinking of the hydrophobic core may be attained by various strategies including thermal- or photo-induced polymerization, using disulphide linkages in the hydrophobic block, or more recently, using click chemistry in the presence of an external reagent.^{39, 40, 46,}

⁷²⁻⁷⁵ One of the first examples of core crosslinking was reported by Tuzar et al. who

stabilized poly(styrene)-poly(butadiene)-poly(styrene) micelles with core of poly(butadiene) by UV radiation in the presence of a photo-initiator.^{76, 77} Kataoka et al. reported the synthesis of amphiphilic PEO-*b*-poly(lactide) (PEO-*b*-PLA) block copolymers having a polymerizable methacryloyl group at end of PLA block.^{39, 72} After micellization, the methacryloyl group located in the core of micelles was thermally or photo-chemically polymerized to produce core crosslinked micelles. The micelles were found to be stable up to 60 °C and in organic solvent. Liu et al. synthesized block copolymers having polymerizable groups laterally distributed on the hydrophobic block of poly(2-cinnamoyl ethyl methacrylate) (PCMA), where more than one polymerizable group can participate in the photo-crosslinking.^{75, 78-80}

Recently, click chemistry has emerged as a specific and useful method for core crosslinking under mild conditions. Click chemistry is a highly efficient technique, providing attractive possibilities for the synthesis of polymers with different architectures. It offers advantages including ambient reaction conditions, quantitative yields, easily obtained starting materials, and in particular high specificity which makes the reaction viable for molecules bearing extra functional groups avoiding the need for protection/deprotection reactions.⁸¹⁻⁸⁴ The philosophy was first recognized by Linus Pauling in 1933,⁸⁵ but in 2001, Sharpless and coworkers⁸² completely described the concept of click chemistry reactions of which the Cu(I)-catalyzed Huisgen 1,3-dipolar cycloaddition reaction between terminal alkynes and azides is one of the most popular and commonly used.^{86, 87}

Block copolymers of poly(N,N-dimethylacrylamide)-*b*-poly(N-isopropylacrylamide-*co*-3-azidopropylacrylamide) (PDMA-*b*-P(NIPAM-*co*-AzPAM)) containing azide moieties in the thermosensitive P(NIPAM-*co*-AzPAM) block were core crosslinked via click chemistry in either aqueous or organic solvent.⁸⁸ O'Reilly et al. also reported the successful

crosslinking of amphiphilic diblock copolymers of poly(acrylic acid)-*b*-poly(styrene) (PAA-*b*-PS) that contained alkynyl functionality on PS block, by click chemistry.⁸⁹ Dendrimers of the zero to third generations, having increasing numbers of azide terminating groups ((N₃)₂-[G-0], (N₃)₄-[G-1], (N₃)₈-[G-2], (N₃)₁₆-[G-3]), were used as cross linker.

Although these strategies can effectively increase micelle stability by forming stable covalent bonds in the core, they may cause safety problems, such as difficult clearance of nano-carrier from the body. To avoid this problem, Zhao et al. reported photo-reversible crosslinked nano-gels, prepared by synthesizing novel coumarin-containing ABCs at $\lambda > 310$ nm. They further demonstrated de-crosslinking by photo induced cleavage at $\lambda < 260$ nm, leading to disintegration of the micellar aggregates.^{40, 90} Jin et al. reported successful preparation of temperature and pH responsive micelles with similar reversible photo-crosslinking. The diblock copolymers formed shell or core crosslinked micelles and nano-gels by adjusting the temperature and pH.⁹¹ Kakizawa et al. reported the synthesis of polyion complex micelles core crosslinked by disulfide bonds.⁹² P(Lys) and P(α , β -Asp) composed the core of the micelles and crosslinking was carried out by oxidation of thiols introduced in the side chains of the lysine units of PEO-*b*-P(Lys). The crosslinked micelles were expected to be stable in circulation, but dissociate in response to the stronger reducing environment inside the cell. A similar method was carried out by Heffernan and Murthy, who cross-linked micelles of block copolymer PEO-*b*-poly(L-lysine-dithiopyridine) (PEO-*b*-PLDTP) with a dithiol, generating disulfide crosslinked polyion micelles (DCPM).⁹³

1.2.1.2 Development of Traceable Micelles for Imaging in Live Animals

Non-invasive imaging can give important information regarding the *in vivo* fate and biodistribution of nanocarriers. Some of the commonly used imaging methods are computed tomography (CT),^{94, 95} magnetic resonance (MR),^{96, 97} single photon emission CT (SPECT),^{98, 99} positron emission tomography (PET),¹⁰⁰ ultrasound (US),¹⁰¹ and optical imaging.^{99, 102} Optical imaging using fluorescence has been associated with numerous advantages such as high sensitivity, low cost, and lack of exposure to radiation. However, disadvantages such as low tissue penetration and high absorption and scattering from tissues have limited their use.¹⁰¹ Near infra-red probes (NIR), which have their absorption and emission spectra at wavelengths of 700-1000 nm, are better suited for optical imaging since at this wavelength most biological tissues exhibit low scattering and minimal absorption thus enabling deeper tissue penetration and imaging.^{101, 102} In the case of block copolymer micelles, NIR probes have been widely used to track the *in vivo* biodistribution of the nanocarriers.^{53, 99, 102-105}

NIR probes can either be encapsulated¹⁰⁴ or conjugated^{53, 102} to the hydrophobic core of micelles.^{103, 106} Rodriguez et al.¹⁰⁴ encapsulated the FDA-approved NIR probe indocyanine green (ICG) into poly(styrene-*alt*-maleic anhydride)-*b*-polystyrene (PSMA-*b*-PSTY) block copolymer micelles. They found that encapsulating the probe can protect it from aqueous and thermal degradation for up to three weeks indicating the potential of these systems in diagnosis. In another study, NIR probe DiR (1,1'-dioctadecyltetramethyl indotricarbocyanine iodide) was physically encapsulated into the core of apoptosis-targeting GFNFRLKAGAKIRFGS-PEO-*b*-PCL micelles and injected into nude mice bearing ES-2-luc xenograft.¹⁰⁷ The peptide binds to phosphatidylserine (PS), the appearance of which, in the

outer leaflet of the plasma membrane indicates early or intermediate apoptosis.¹⁰⁸ The peptide modified PEO-*b*-PCL micelles homed to the site of apoptosis in peritoneally metastatic ES-2-luc xenograft of ovarian cancer facilitating the removal of the apoptotic tumor cells from the peritoneum.¹⁰⁷ However, physical encapsulation of NIR probe into the hydrophobic core can lead to release of the probe from the micellar system.

Kim et al.¹⁰⁹ reported the conjugation of NIR probe cy5.5 to pH sensitive PEO-*b*-poly(L-histidine) (PEO-*b*-P(His)) based block copolymer micelles. Cy5.5 bis-NHS ester was successfully conjugated to the primary amine group of the poly(benzyl-His) block. The cy5.5 loaded block copolymer was mixed with folate-conjugated or plain PEO-*b*-PLLA and DOX was encapsulated within the core of these mixed micelles. pH sensitive micelles showed a 1.5-fold increase in fluorescent intensity in KB epidermoid xenograft mouse model, when compared to pH insensitive micelles. This was postulated to be due to the destabilization of pH sensitive micelles in the acidic pH of the tumor microenvironment or endosomes resulting in the release of cy5.5, thus removing the quenching effect on the dye when encapsulated into the micelles, and showing an increased fluorescence. In our lab, cy5.5 was conjugated to the primary amine of the polyamine spermine in PEO-*b*-PCL based micelles bearing spermine (PEO-*b*-P(CL-*g*-SP)). The cy5.5 conjugated (PEO-*b*-P(CL-*g*-SP)) micelles were mixed with RGD4C modified PEO-*b*-PCL micelles conjugated with DOX through a hydrazone linker (RGD4C-PEO-*b*-P(CL-Hyd-DOX)) (Figure 1.2). The biodistribution of the NIR probe was investigated in nude mice bearing MDA-MB-435/LCC6 MDR-1 resistant tumors. It was found that RGD4C modified micelles preferentially accumulated in the tumor whereas non-targeted micelles showed distribution the liver and kidneys.¹⁰²

1.2.1.3 Development of Micellar Carriers for Controlled Drug Release

Drug release from polymeric micellar nano-containers, drug conjugates and PIC micelles is governed by several different mechanisms.¹⁹ To achieve controlled drug release from micellar nano-containers, engineering efforts have focused on developing polymeric cores that can interact strongly with a specific drug. For example, micelles of PEO-*b*-PHSA having aliphatic structures in their core were prepared and used for the solubilization of AmB. In this study, an increase in the level of aliphatic chain substitution was found to enhance the encapsulation efficiency while reducing the release of AmB.¹¹⁰ Recently, the core of PEO-*b*-PCL micelles was modified by introducing benzyl groups and paclitaxel (PTX), to physically load PTX. Core structures containing benzyl groups demonstrated slower drug release.¹¹¹ Higher release of PTX from the P(CL-PTX) core coincided with a lower rigidity of this structure (Figure 1.3).

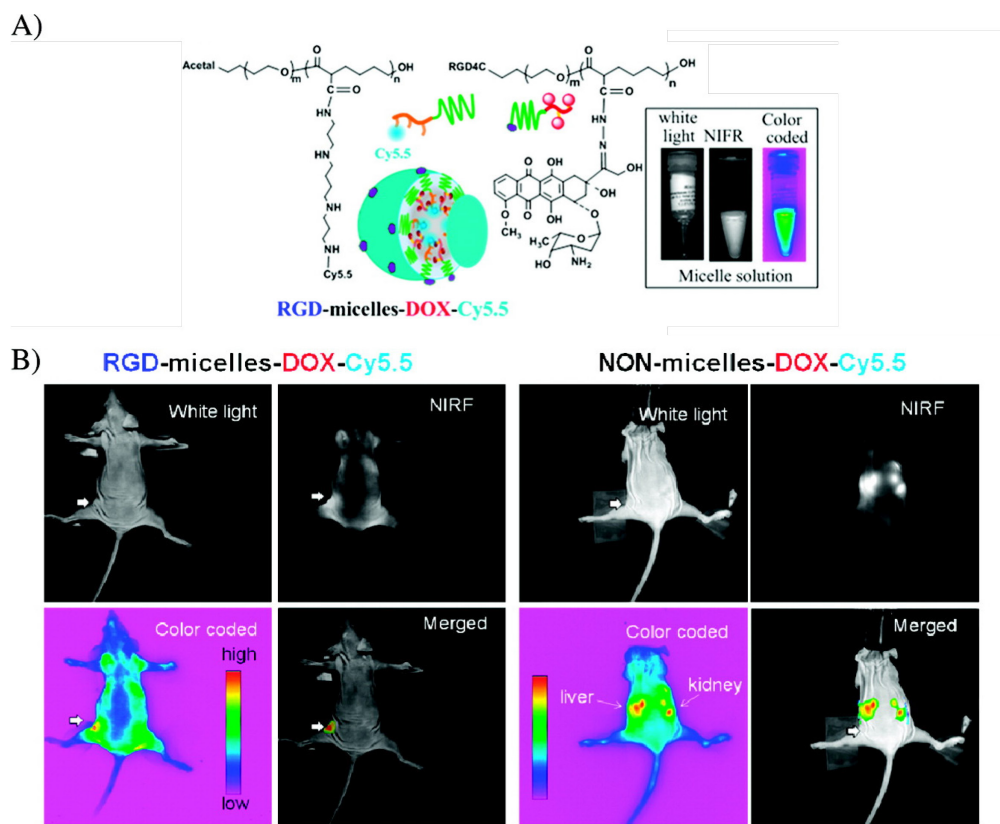


Figure 1.2 (A) Schematic illustration of polymer structures and assembled RGD-functionalized micelles containing NIRF imaging probes. The insets show images of one of those NIRF formulations. (B) Athymic nude mice bearing MDA-MB-435/LCC6MDR1-resistant tumors injected with RGD- and NON-micelles-DOX-Cy5.5. The intensity of fluorescence is expressed by different colors, with violet reflecting the lowest intensity (background) and red reflecting the highest intensity. The tumor is indicated by the thick arrow. (Adapted with permission from¹⁰². Copyright (2011) American Chemical Society).

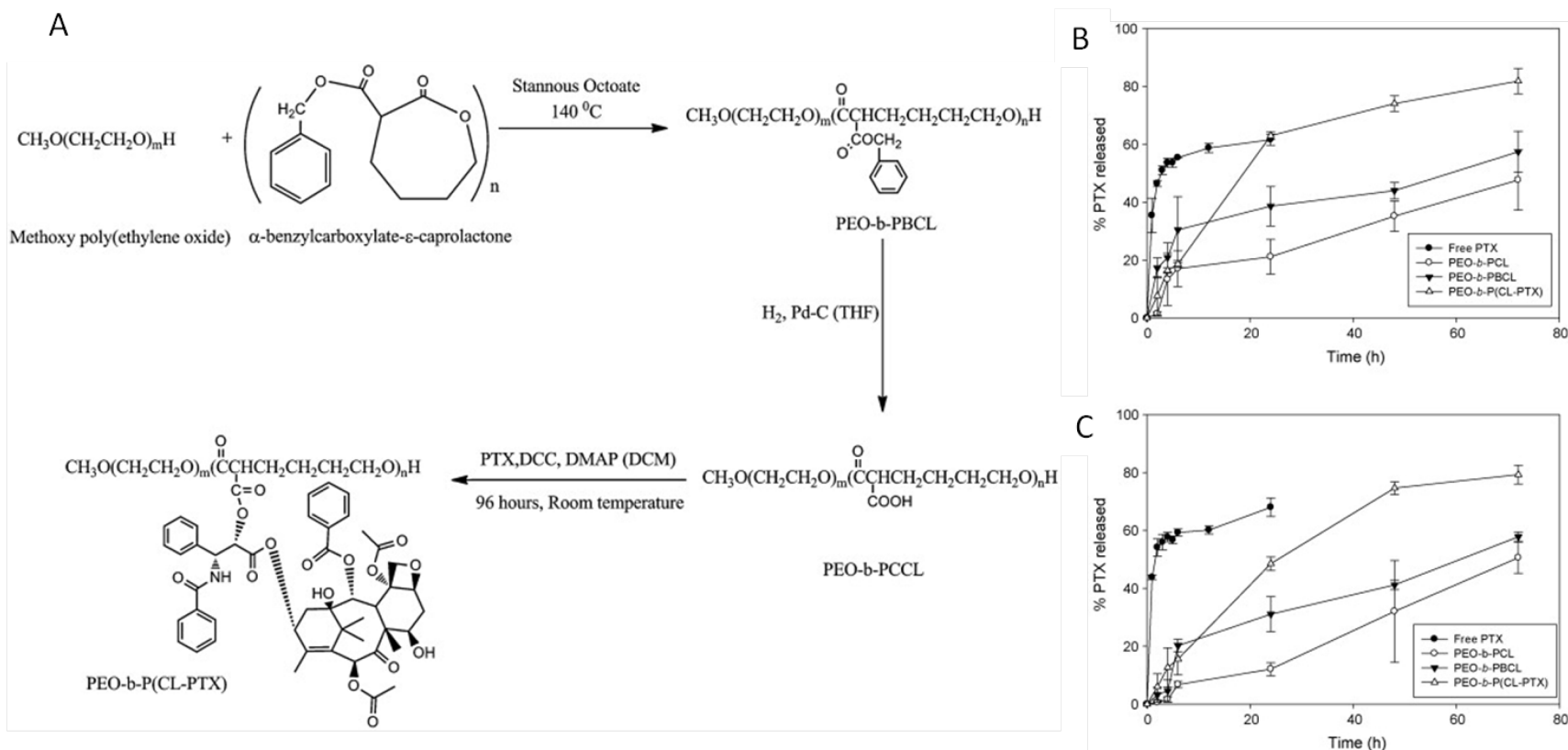


Figure 1.3 A) Synthesis of PEO-b-P(CL-PTX) block copolymer; *in vitro* release profile of physically loaded PTX from different micellar formulations at (B) pH 7.4 and (C) pH 5.0 at 37 °C. (Adapted from reference ¹¹¹, Copyright (2010), with permission from Elsevier).

Engineering of amphiphilic block copolymers (ABCs) has also been directed towards the development of micellar nano-containers that provide enhanced drug release in response to internal stimuli such as pH. This strategy can be used to achieve the preferential release of incorporated drugs in the acidic microenvironment of the tumor, or endosomes inside tumor cells. For example, micellization of the triblock copolymer, composed of PEO as the shell forming block and poly(2-(dimethylamino)ethyl methacrylate)-*b*-poly(2-(diethylamino)ethyl methacrylate) as the core forming block (PEO-*b*-PDMA-*b*-PDEA) can be induced by adjusting the pH above 7.0. The micellar structure completely dissolves in acidic media due to the protonation of the tertiary amine on the DMA and DEA chains.¹¹² The feasibility of PEO-*b*-poly(L-histidine) (PEO-*b*-P(His)) block copolymers to construct an effective pH sensitive micellar carrier was investigated by Bae et al.¹¹³ The presence of an electron ion pair on the unsaturated nitrogen of the imidazole ring endows P(His) with an amphoteric nature. Protonation of the imidazole group at lower pHs causes a reduction in the hydrophobicity of P(His), leading to an increase in CMC at pHs below 7.2. Gillies et al. reported a new approach to develop pH sensitive nano-carriers where the hydrophobic groups were attached to one block of the copolymer via an acid sensitive linkage. Upon hydrolysis of the linkage, the hydrophobic block became more hydrophilic, thus destabilizing the micelle and enabling escape of the encapsulated drug.¹¹⁴ Bromberg has synthesized Pluronic® grafted with poly(acrylic acid) (PAA) by dispersion/emulsion polymerization.¹¹⁵ Pluronic®-g-PAA graft polymers have shown a dual responsive property to pH and temperature. In addition, grafting PAA onto the Pluronic® copolymers has improved the bioadhesive properties of Pluronics®.^{115, 116}

Polymeric micellar drug conjugate design has been extensively explored to achieve sustained and/or triggered drug release. Early efforts were directed to reduce premature drug release by preparing drug-polymer conjugates through relatively stable linkers (e.g. amide and ester bond). The first example of a polymeric micellar system of this type was developed by Ringsdorf et al., who reported on the preparation of micelle-forming conjugates of cyclophosphamide (CP) sulfide and PEO-*b*-P(Lys).¹¹⁷ Later, covalent conjugation of drugs (e.g. DOX, PTX and methotrexate) to the core of PEO-*b*-P(L-amino acid) (PEO-*b*-PLAA) and PEO-*b*-poly(ester) block copolymers was attempted by several groups.^{111, 118-122} In this case, the excessive stability of the polymeric pro-drug may lead to inactivity of the final product. Incorporation of hydrophilic moieties, formation of pH sensitive bonds between polymer and drug, and changes in the molecular weight of the core-forming block have been used to modify micellar stability and drug release properties from micelle-forming drug conjugates.

Design of pH-responsive polymeric drug conjugate micelles has provided an exciting opportunity to achieve the site-specific release of incorporated drug from its carrier. This method involves formation of an acid-labile linkage between the therapeutic agent and the micelle forming copolymer. The linkage is stable at physiological pH, but will be cleaved at the acidic pH of a tumor extracellular space or its endosomes, leading to the site specific release of the parent chemotherapeutic agents from their micellar nano-conjugates.¹²³ Park et al. have developed one of the first pH-sensitive micelle forming drug conjugates through linking DOX to the terminal end of PEO-*b*-PLLA via two acid-cleavable bonds, i.e. hydrazone and cis-aconityl bond.¹²⁴ The pH sensitivity was more noticeable in the case of cis-aconityl linkages, which showed about 10 times higher DOX release at pH 3.0 than at pH

7.0. However, this linkage generated chemically modified DOX after release, whereas a hydrazone linkage resulted in the generation of intact DOX. DOX was also conjugated to the P(Asp) through a hydrazone linker and drug release in media with different pHs has been investigated.¹²⁵

This new paradigm in cancer therapy needs precise control over the exposure of tumor associated cells to anti-cancer drugs. Maximum therapeutic efficacy may be obtained by regimens that can control drug concentration levels, dosing intervals, and drug retention in tumors. It was suggested that cancer cells exposed to small amounts of drug over longer periods appear to be more sensitive to chemotherapy than cells incubated with a higher drug dose for shorter exposure times. In this context, polymeric drug conjugates with pH-dependent tunable drug release have been proposed to allow spatial and temporal control of drug delivery for maximum therapeutic effect in cancer treatment.¹²⁶ To meet this demand, DOX was conjugated to the P(Asp) section of PEO-*b*-P(Asp) by different spacers (e.g., glycine (Gly) or 4-aminobenzoate (Abz)) through a hydrazone linkage. It was found that drug release patterns of both Gly and Abz micelles were pH-dependent and tunable. The spacers appeared to play a crucial role in controlling drug release and stability of polymer micelles in combination with block copolymer chain lengths. Polymeric micelles with tunable drug release may provide means for both early-prompt and/or late-prolonged chemotherapeutic treatment.

Using the same concept, PTX was incorporated into a polymeric drug conjugate to permit its pH-dependent controlled and/or continuous low dose release, with the aim to prepare PTX-loaded micelles with anticancer activity or anti-angiogenic activity.¹²⁷ Toward this goal, PEO-*b*-P(Asp) was modified by either levulinic acid (LEV) or 4-acetyl benzoic

acid (4AB) attached to P(Asp) via hydrazone bonds. PTX was then conjugated to the linkers to form PEO-*b*-P(Asp-Hyd-LEV-PTX) and PEO-*b*-P(Asp-Hyd-4AB-PTX). It was found that PEO-*b*-P(Asp-Hyd-LEV-PTX) micelles release LEV-PTX in a pH-dependent manner, while no obvious release of 4AB-PTX for PEO-*b*-P(Asp-Hyd-4AB-PTX) was observed. Due to the hydrophobicity of PEO-*b*-P(Asp-Hyd-4AB-PTX), the mixed micelles of PEO-*b*-P(Asp-Hyd-LEV-PTX) and PEO-*b*-P(Asp-Hyd-4AB-PTX) can more effectively moderate the release of LEV-PTX compared to PEO-*b*-P(Asp-Hyd-LEV-PTX) micelles.

1.2.1.4 Attaining Polycationic Core for Efficient Gene Delivery

Block copolymers composed of polycationic segments have attracted increasing attention as non-viral gene vectors. In this case, neutralization of the positive charge on the polycation by the negatively charged DNA will lead to micelle formation. PEO-*b*-P(Lys) has been extensively used for this purpose.¹²⁸⁻¹³⁰ To increase the stability of PEO-*b*-P(Lys) micelles against dissociation and at the same to maintain their ability to bind DNA, certain fractions of the lysine residues in the core were replaced by thiol groups that can readily form disulfide cross-links with other sulfide substituted PEO-*b*-P(Lys) and develop a network in the micelle core after DNA complexation. The cross-linked core of the micelles is cleavable inside cells which show increased levels of glutathione (~1-5 mM), but not in blood (~1 mM).¹³¹⁻¹³³ To achieve a ‘proton sponge effect’ which can result in endosomal disruption and gene release,^{134, 135} PEO-*b*-P(Asp) block copolymer containing two amino groups in their side chain was synthesized. The primary amine group located at the distal end of the side chain was used for complexation with phosphate groups of siRNA or DNA, while the

secondary amine, which was located closer to the polymeric backbone and had a lower pKa, provided buffering capacity for proton sponge effect.¹³⁶⁻¹³⁸

Copolymers of PEO-*b*-PCL with grafted polyamine (e.g., spermine, SP, and tetraethylenepentamine, TP) in the PCL block were synthesized in our lab for siRNA delivery (Figure 1.4).¹³⁹ These amphiphilic polycationic copolymers can effectively bind siRNA, self-assemble into micelles and protect siRNA from degradation by nuclease in serum. Our lab also showed that PEO-*b*-P(CL-*g*-SP) and PEO-*b*-P(CL-*g*-TP) micelles can efficiently deliver siRNA into cytoplasm by endocytosis and show endosomal escape after cellular uptake. MDR1-targeted siRNA formulated in PEO-*b*-P(CL-*g*-SP) and PEO-*b*-P(CL-*g*-TP) exhibited efficient silencing of MDR-1 gene expression leading to down-regulation of P-gp.

Pluronic® copolymer has been grafted to PEI for gene and ODNs delivery. Pluronic®-*g*-PEI block copolymer complexes are promising non-viral vectors for gene delivery because of their high stability and high transfection activity.^{140, 141}

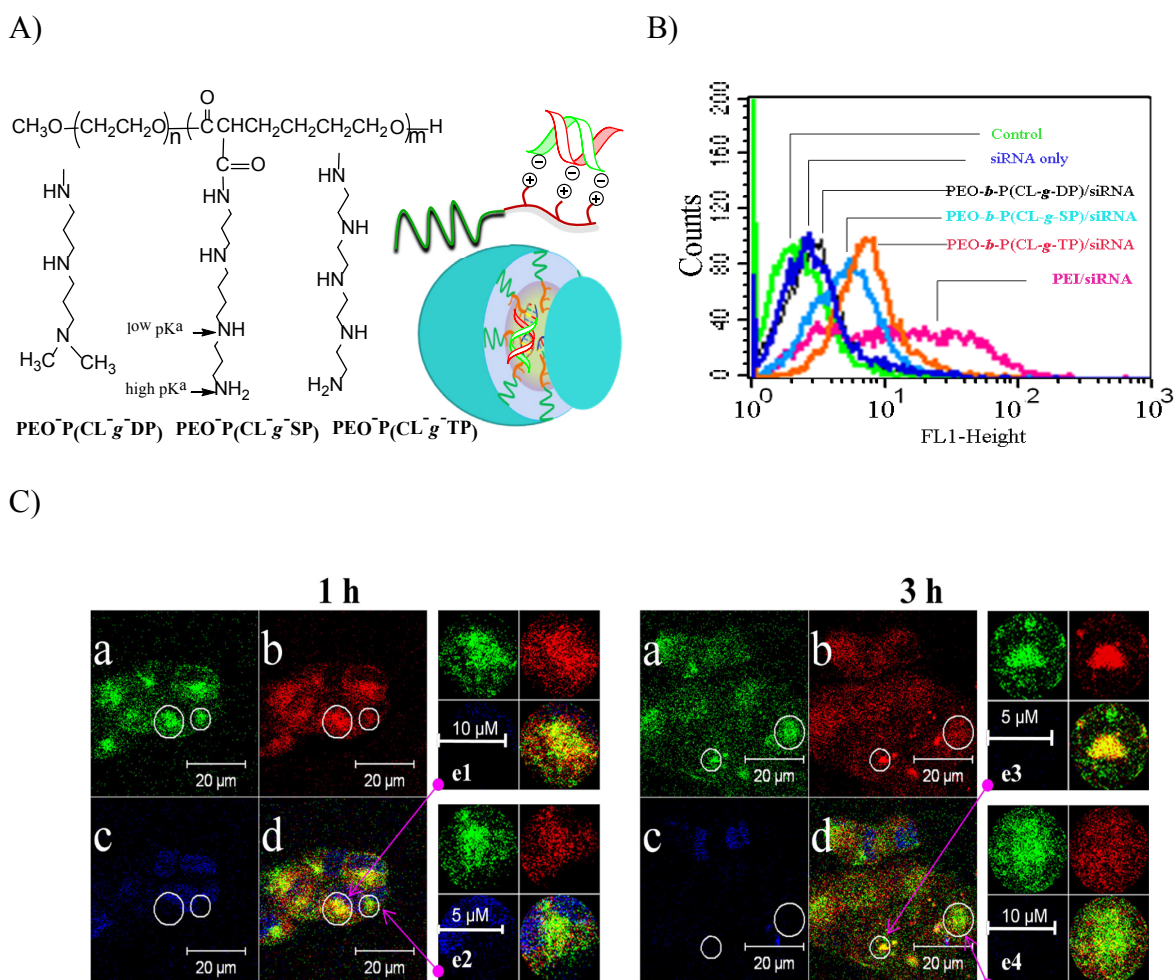


Figure 1.4 PEO-*b*-P(CL-polyamine) micelles for siRNA delivery. A) Schematic structures of PEO-*b*-P(CL-polyamines) and siRNA complexed micelles. B) Cellular uptake of FAM-siRNA from different PIC micelles or from PEI/siRNA PICs by MDA-MB-435/LCC6 cells. C) Endosome escape of siRNA formulated PEO-*b*-P(CL-g-TP) micelles after endocytosis upon 1 and 3 h incubation by confocal microscopy. SP: spermine; TP: tetraethylenepentamine; DP: N,N-dimethyldipropylenetriamine (Reprinted from Reference¹, Copyright (2011), with permission from Elsevier; Adapted from Reference¹³⁹, Copyright (2009), with permission from Elsevier).

1.2.2 Engineering of the Micellar Shell for Improved Properties in Drug Delivery

1.2.2.1 Micelle Biological Stability

The MPS is designed to protect the body against invading pathogens and other foreign materials and represents a group of cells including macrophages and macrophage precursors, specialized endothelial cells lining the sinusoids of the spleen, liver and bone marrow. They are either freely circulating in the blood or fixed to connective tissue and are capable of phagocytosis. Any foreign material is then removed by the MPS if the surface of the material promotes a mechanism called opsonization that tags a particle for removal by macrophages or by acting as ligand for receptors expressed on macrophage surfaces.^{142, 143}

Phagocytosis by macrophages is greatly enhanced when the particle surface is coated with certain serum protein ligands called ‘opsonins’ and their adsorption on the particle surface is called ‘opsonization’. They act as ligands on the particle surface and are responsible for the recognition and initial attachment by phagocyte receptors, thus facilitating phagocytosis of the foreign particles. Non-opsonic serum proteins can also play a role in clearance. They adsorb on the particle surface leading to conformational changes which act as ligands for phagocyte receptors or other blood opsonins.¹⁴²

Because nanocarriers are foreign particles, the circulation time as well as the efficacy of nanocarriers to target specific organs is greatly dependent on the interaction between serum proteins and the nanocarrier surface. This, in turn, is influenced by factors such as size, size distribution, surface hydrophobicity, and the surface charge on the nanocarrier.^{144,}
¹⁴⁵ One of the main limiting factors for successful delivery of nanocarriers is their uptake by the MPS.^{144, 146} Serum protein adsorption is regarded as the key factor in the uptake of

nanocarriers by the MPS.¹⁴⁷ A major challenge for formulation scientists is to avoid MPS uptake and maintain prolonged circulation of the nanocarriers.

Following the intravenous administration of a drug-loaded micellar system, there are two possibilities by which protein adsorption might affect the fate of the delivery system. Firstly, the proteins might adsorb on the surface of the nanocarrier which can cause its removal by the MPS. Secondly, if the drug has a higher affinity for the proteins rather than the core of the micelles, the protein might alter the release of the drug from the micellar system.¹⁴⁸

Coating or linking polymers with polyethylene glycol (PEG), or PEGylation has proven to be the most effective way to prevent phagocytosis as compared to other strategies reported, such as, polyvinyl alcohol,^{149, 150} poloxamer,^{150, 151} dendrimers,¹⁴⁶ and polysaccharides.^{150, 152} For PEGylation, the interfacial chain density, chain length, and chain conformations are important factors determining protein resistance. A density of higher than 0.1 chains/nm²¹⁵³ upto 0.5 chains/nm²¹⁵⁴ depending on the molecular weight of PEG shows minimal protein adsorption on the PEG surface. Increase in MW and length of PEG chain also was found to show higher hydrophilicity of the surface with maximal reduction in protein adsorption for a PEG MW of 5000 g/mole.^{155, 156} Influence of PEGylation on protein adsorption for nanoparticles^{156, 157} and liposomes^{158, 159} have been studied extensively, however very few studies have been done to see the effect of protein adsorption on micellar systems.

Lo et al¹⁶⁰ and found that micelles having PEG as the hydrophilic shell were stable in size even after 25 h incubation in solutions containing albumin. Li et al¹⁶¹ prepared thermo-sensitive micelles which were stable in size at 37 °C for 40 h in solution containing BSA but

were unstable within 6 m at 43 °C when the shell became hydrophobic due to change in temperature. Yang et al¹⁶² showed that micelles containing PEG as shell were stable in size even after 24 h of incubation in 10% fetal bovine serum. Stability in size and absence of aggregates indicates that there is absence of/minimal protein adsorption on the surface of the micelles. Kabanov et al¹⁶³ showed that protein had no impact on the size and sedimentation coefficient of Pluronic triblock copolymer micelles. They also found that BSA did not alter the CMC of these micelles. However, size measurement alone does not give enough information regarding protein adsorption and further studies are required to show the true nature and quantity of protein adsorption.

Size exclusion chromatography or GPC can also be used to study the amount of protein adsorption on micellar surface. In this case, only proteins that are associated with the micelles for the entire duration of passage through the column are recovered in the same fraction as the nanoparticles, and can then be quantified for protein content.^{145, 148, 164, 165} Kataoka et al⁴⁴ used GPC to study the stability of adriamycin-conjugated PEO-*b*-poly(Asp) micelles in the presence of rabbit serum. It was revealed that longer PEG chains and shorter adriamycin-conjugated poly(Asp) chains gave more stable micelles.

1.2.2.2 Shell Crosslinking

Crosslinking of the micellar shell can affect the permeability of the corona and can be used to fine-tune the rate of drug release.⁷¹ Since the hydrophilic shell of polymeric micelles is responsible for preventing attachment of serum proteins, the effect of cross linking on protein adsorption, which could lead to their early removal by MPS, should also be considered.

One of the earliest examples of shell crosslinking was reported by Thurmond et al.¹⁶⁶ Since then, numerous strategies have been developed for crosslinking the micellar shell. For instance, the PAA shell of micelles having polystyrene,¹⁶⁶⁻¹⁶⁹ PCL,^{170, 171} or polyisoprene^{172, 173} cores was crosslinked with diamino compounds by formation of amide bonds in the presence of carbodiimide as a condensation agent. Wei et al. used inorganic 1,1'-ferrocenedicarboxylic acid as the crosslinker to prepare crosslinked micelles via carbodiimide chemistry.¹⁷⁴ Use of the inorganic crosslinker resulted in micelles which exhibited antitumor activity and had improved stability. A similar crosslinking strategy has been reported for peptide-containing micellar shells.¹⁷⁵ Poly(2-(dimethylamino)ethyl methacrylate) shells were crosslinked via quaternization with 1,2-bis(2-iodoethoxy)ethane (BIEE).¹⁷⁶ Glutaraldehyde was used to crosslink the primary amines of lysine units in the P(Lys) block of micelles of poly(isoprene-*b*-L-lysine).¹⁷⁵ Recently, a novel strategy was used by Joralemon et al. in which alkyne functionalized PAA shell of micelles was crosslinked via click chemistry with azide terminating groups of dendrimers, giving a crosslinked shell.⁸¹ A similar strategy was further explored by Jiang et al.¹⁷⁷

Photo or UV-crosslinking of polymerizable groups in the micellar shell takes place by UV irradiation and does not need the addition of cross-linker. Liu et al. first reported the photo-crosslinking of the shells of poly(isoprene)- or poly(styrene)-*b*-poly(2-cinnamoyl ethyl methacrylate) copolymer micelles in a tetrahydrofuran (THF)-acetonitrile mixture by UV irradiation.^{178, 179} Similar strategy was reported by Sugihara et al. who prepared shell crosslinked micelles by UV irradiation in aqueous solution.¹⁸⁰

Shell crosslinking of diblock copolymer micelles can result in intermicellar crosslinking leading to micellar fusion and, therefore, it has to be carried out at high dilution.

This poses a difficulty at the industrial scale, and was overcome by Butun et al., who used triblock copolymers which are generally prepared by ATRP using a PEO-based macro-initiator.¹⁸¹ The same strategies involving covalent crosslinking of diblock copolymer micelles can be used for the crosslinking of triblock copolymer micelles. Examples of strategies used for shell crosslinking of triblock copolymer micelles include carbodiimide chemistry,¹⁸² click chemistry,¹⁷⁷ and UV irradiation.¹⁸³

There is a concern that the body may be unable to eliminate crosslinked micelles. Reversible crosslinking would provide a solution to this concern. Reversible disulfide crosslinking in which the disulfide bonds are expected to cleave in the stronger reducing environment inside the cell provides a means for the degradation of crosslinked micelles. Li et al. prepared micelles of thermoresponsive triblock copolymer PEO-*b*-((N,N-dimethylacrylamide)-*stat*-(N-acryloxysuccinimide))-*b*-(N-isopropylacrylamide) (PEO-*b*-P(DMA-*stat*-NAS)-*b*-NIPAM) which was crosslinked using cystamine via thiol-disulfide exchange.¹⁸⁴ Similar crosslinking via disulfide-thiol exchange has been reported by many other groups.^{185, 186} Photo-reversible crosslinking of micelles has also been reported as a novel approach in which coumarin-containing block copolymers have been shell-crosslinked by photo-induced dimerization of the coumarin groups at $\lambda > 310$ nm and further de-crosslinked by photo-induced cleavage at $\lambda < 260$ nm leading to disintegration of the micellar aggregates.^{91, 187}

1.2.2.3 Ligand attachment to Micellar Shell for Active Targeting

The introduction of targeting ligands to the surface of polymeric micelle can provide a mechanism to cross the cell membrane barrier for drug delivery. The micellar shell can be

extensively engineered with various ligands such as peptides and proteins to promote binding to cancer cells.

Peptides containing the RGD sequence can recognize integrins that are over-expressed on the tumor cells or the angiogenic endothelial cells of the tumor vasculature. Nasongkla et al. developed polymeric micelles to selectively deliver hydrophobic drugs to angiogenic tumor endothelial cells which overexpress $\alpha\beta_3$ integrins.¹⁸⁸ To couple the cyclic pentapeptide cyc(Arg-Gly-Asp-d-Phe-Lys) (cRGDfK) which contains a thiol group, they synthesized maleimide-terminated PEO-*b*-PCL (MAL-PEO-*b*-PCL). After micellization, cRGDfK was coupled onto the micelle surface by electrophilic addition to form a thioether bond between the thiol group on the peptide and the ethylenic bond on the maleimide. The cRGDfK-PEO-*b*-PCL micelle, with 76% (molar ratio) peptide density, was used for DOX delivery to angiogenic tumor endothelial cells. Confocal laser scanning microscopy showed 30 times greater accumulation of DOX-loaded cRGDfK-modified micelles compared to unmodified micelles into human Kaposi sarcoma tumor endothelial SLK cells. This system has recently been used for the co-delivery of DOX and supramagnetic iron oxide as a contrast agent for magnetic resonance (MRI) imaging.¹⁸⁹ Our group has synthesized acetal-terminated PEO-*b*-PCL through anionic ROP of ϵ -CL by acetal-PEO.¹⁹⁰ After formation of micelles, the acetal group was converted to an aldehyde at acidic pH and used for the conjugation of peptide GRGDS to the micellar surface by Schiff base reaction. Fluorescent spectroscopy and microscopy analysis have shown 4.5 times higher uptake of GRGDS micelles compared to unmodified micelles after 3 h incubation in mouse melanoma B16-F10 cells. To extend the research, an acetal-PEO-*b*-poly(α -benzyl carboxylate- ϵ -caprolactone) (acetal-PEO-*b*-PBCL) block copolymer was synthesized and then reduced to produce acetal-

PEO-*b*-poly(α -carboxyl- ϵ -caprolactone) (acetal-PEO-*b*-PCCL). The anticancer drug DOX was then covalently conjugated to the free side carboxyl groups on the PCCL block by an amide bond to form acetal-PEO-*b*-P(CL-Ami-DOX). After conversion of the acetal group into aldehyde, RGD containing peptides such as GRGDS were attached to the surface of aldehyde-PEO-*b*-P(CL-Ami-DOX) micelles. The RGD-modified micelles bearing conjugated DOX demonstrated higher cytotoxicity against B16–F10 cells than the conjugates without peptide.¹⁹¹

Another peptide, P18-4 (WxEAAYQrFL; Figure 1.5), has been identified as a stable derivative of peptide P160 and has increased affinity for breast cancer cells. The receptors for this peptide are still unknown however, they show excellent affinity for MDA-MB-435, MDA-MB-231, and MCF-7 cells while showing a low affinity for non-cancerous cell lines MCF-10A and HUVEC cells.¹⁹² DOX-loaded liposomes decorated with the P18-4 peptide on the surface increased the efficacy of DOX at the tumor site leading to a 4.8-fold reduction in tumor volume in MDA-MB-435 tumor models when compared with plain DOX-loaded liposomes indicating the increased affinity of P18-4 peptide for the MDA-MB-435 cancer cells.¹⁹³

Human transferrin is a relatively large serum glycoprotein (80 kDa). Transferrin receptors are elevated 2–10 times on various types of cancer cells. The level of elevation in transferrin receptor correlates with the proliferative ability of the tumor cells. Vinogradov et al. proposed transferrin receptor-mediated delivery of phosphorothioate ODNs by using polyion complex micelles formed with transferrin-conjugated PEO-*b*-PEI.¹⁴¹ Transferrin was attached to the PEO corona using an avidin/biotin construct. Compared to unmodified micelles, fluorescent-labeled transferrin-micelles showed a significantly higher accumulation

in resistant human oral epidermoid carcinoma (KBv) cells. Delivery of antisense ODNs against the expression of P-glycoprotein (P-gp) human *mdr1*-mRNA by transferrin modified PEO-*b*-PEI nanocarriers resulted in a significantly higher inhibition of P-gp efflux in MCF-7/ADR cells that over-express P-gp compared to cells treated with unmodified micelles. Transferrin was conjugated to the PEO end of PEO-*b*-PEI by various procedures.¹⁹⁴ Complexes were generated by mixing of plasmid DNA, linear PEI (PEI₂₂, 22 kDa) as the main DNA condensing agent, PEO-*b*-PEI for surface shielding, and transferrin-PEO-*b*-PEI to provide a ligand for receptor-mediated cell uptake. The systemic application of freeze-thawed complexes exhibited *in vivo* tumor-targeted expression; for complexes containing the luciferase reporter gene the highest expression was found in tumor tissue of mice. The optimum formulation for *in vivo* application, i.e., PEI₂₂/transferrin-PEO-*b*-PEI/PEI₂₂-PEO₅, containing plasmid DNA encoding for the tumor necrosis factor (TNF- α), inhibited tumor growth in three different murine tumor models.

1.2.2.4 Labeling of Micellar Shell for *in vivo* Imaging

Apart from the hydrophobic core,^{103, 106} NIR probes can also be conjugated to the hydrophilic shell of the micellar system.¹⁰⁵ Tsai et al.¹⁰⁵ prepared mixed micelles composed of poly(2-hydroxyethyl methacrylate-*co*-histidine)-*g*-PLA (PHEMA-*co*-His-*g*-PLA) and diblock copolymer PEO-*b*-PLA. NIR dye Cy5.5 and folate was conjugated to the PEO end of PEO-*b*-PLA. Mixed micelles of PHEMA-*co*-His-*g*-PLA, cy5.5-PEO-*b*-PLA, and folate-modified or plain PEO-*b*-PLA were synthesized and encapsulated with DOX. *In vivo* NIR imaging showed that folate modified micelles exhibited higher fluorescence at tumor sites compared to unmodified micelles. Another study by the same group used fluorescein

isothiocyanate (FITC) and galactosamine (Gal) to decorate the surface of PEO-*b*-PLA micelles and mixed these with poly(*N*-isopropyl acrylamide-*co*-methacryl acid)-*g*-PLA (P(NIPAAm-*co*-MAAc)-*g*-PLA) and encapsulated DOX into the hydrophobic core. The micelles were investigated against HepG2 cells.¹⁹⁵

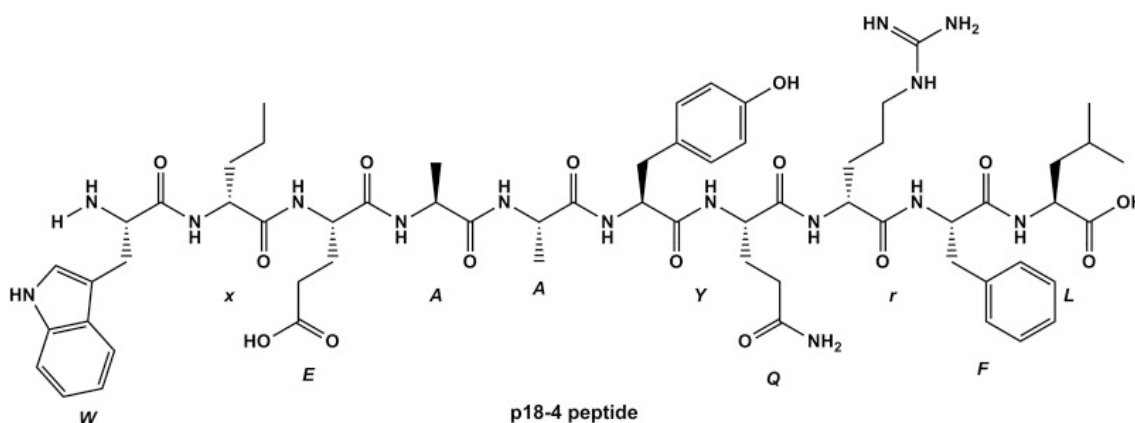


Figure 1.5 Chemical structure of P18-4 peptide. (Reprinted from Reference,¹⁹³ Copyright (2013), with permission from Elsevier).

1.2.3 Simultaneous Engineering of Core and Shell

The unique structure of polymeric micelles allows for the integration of multiple functional components in a single structure. Polymeric micelles can combine tumor targeting and stimulus-triggered drug release. A typical example of multifunctional polymeric micelles developed through simultaneous engineering of the micellar core and shell include polymeric micelles consisting of a ligand-installed shell for active targeting and a pH-sensitive core for triggered drug release. Bae et al. developed PEO-*b*-P(Asp) based micelles which are composed of a targeting ligand (i.e. folate) modified shell and a pH-sensitive core for DOX delivery.¹⁹⁶ Chemical modification of the core-forming P(Asp) block with a hydrazone

linkage allows the polymeric micelles to release drugs selectively at acidic pH (4–6), while installation of folic acids on the micelle surface improves cancer cell-specific drug delivery. An *in vitro* study using human pharyngeal cancer KB cells which express folate-binding protein (FBP) receptors, showed that these intelligent micelles, i.e. folate-PEO-*b*-P(Asp-Hyd-DOX), were capable of increased cell internalization at short exposure times (3 h) compared to non-targeted micelles. The cytotoxicity of folate polymeric micellar drug conjugates against FBP-expressing KB cells after 24 h incubation was equal to free DOX and 8-fold higher than polymeric micellar DOX conjugates without folate. An *in vivo* study revealed long circulation, improved activity and reduced toxicity of folate-PEO-*b*-P(Asp-Hyd-DOX) micelles in mice bearing KB tumors compared to non-targeted micelles. An excellent example of multifunctional polymeric micelles was given by Zhu et. al.¹⁹⁷ who synthesized stimuli-responsive micelles consisting of a cell-penetrating peptide i.e. TAT and a PTX-based prodrug. The group synthesized PEO₂₀₀₀-PTX conjugate with a matrix metalloproteinase 2 (MMP2) cleavable peptide between PEO and PTX. The PTX containing polymer was then mixed with TAT-PEO₁₀₀₀-PE and PEO₁₀₀₀-PE to form mixed micelles. The PTX was hidden in the core of the micelles whereas the TAT peptide was hidden in the core-shell interphase due to the shorter PEO length. In the blood, where MMP2 levels are low, the micellar system avoided the premature release of the conjugated drug. However, in the extracellular tumor microenvironment, where MMP2 is upregulated, the PEO₂₀₀₀-PTX conjugate cleaved, thus releasing the active drug and exposing the TAT peptide, which facilitated their entry into the tumor cells. *In vivo* studies in a non-small cell lung carcinoma (NSCLC) tumor model showed an improved anti-tumor efficacy of these micelles when

compared with those with MMP2 non-sensitive PTX linker and/or without TAT peptide modification in the shell.¹⁹⁷

Multifunctional polymeric micelles based on PEO-*b*-PCL for DOX delivery were developed in our lab.¹⁹⁸ DOX was chemically conjugated to the micellar core by amide or hydrazone linkages, while RGD4C's specific homing to integrin $\alpha\beta3$ receptors expressed on cancer cells (e.g. MDA435/LCC6 sensitive and resistant cells) was used to functionalize the micellar shell. These targeted micelles showed markedly increased uptake of DOX in cancer cells. The RGD4C-PEO-*b*-P(CL-Hyd-DOX) conjugated micelles showed pH-triggered drug release of intact DOX, leading to preferential accumulation of DOX in the nucleus of sensitive cells and showed a better activity against these cells when compared to free DOX. Micelles containing amide-linked DOX, on the other hand, showed insignificant release of free DOX, but very slow release of DOX-6-hexanoic acid at acidic pH, and led to preferential accumulation of DOX in the mitochondria of sensitive and resistant cancer cells. These micelles showed equal activity to that of free DOX in sensitive cells but a significantly higher cytotoxicity to that of free DOX in resistant cells. The IC₅₀ of DOX as part of the latter formulation was 10 times lower than that of free DOX in sensitive cells, pointing to the hyper-sensitization of resistant cells to DOX, perhaps through a mitochondrial related mechanism of cytotoxicity. In animal studies, treatment with RGD4C-PEO-*b*-PCL-DOX conjugates with hydrazone and amide links showed not only better activity than free DOX, but also led to longer survival of SCID mice bearing sensitive and resistant MDA-MB-435 tumors, respectively. The main target for the activity of DOX is located in the nucleus. Highly lipophilic and unaminated anthracyclines have shown selective accumulation in cytoplasm, and demonstrated the ability to circumvent multi-drug resistance (MDR).^{199, 200}

This indicates an alternative intracellular target for lipophilic derivatives of DOX, which can be used to overcome P-gp mediated resistance to DOX. The RGD4C–PEO-*b*-P(CL-Ami-DOX) micelles may behave in a similar manner.

The core and shell of micelles can also be engineered for dual imaging. Yang et al.⁹⁹ used poly(PEG-methacrylate)-*b*-poly(triethoxysilyl propylmethacrylate) (PPEGMA-*b*-PESPMA) block copolymer micelles for entrapment of a modified NIR probe cy7 to the core and chelation of ¹¹¹In to the surface of the micelles. The dual imaging provided more detailed information as the NIR probe provided good detection of the superficial tumors via optical imaging whereas the ¹¹¹In on the surface of the micelles provided information regarding the distribution of micelles in internal organs via gamma scintigraphy.

The core and shell of PEO-*b*-PCL based micelles were also engineered for effective siRNA delivery.²⁰¹ The micellar shell was decorated with virus-related peptides such as RGD4C and/or cell penetrating peptide (TAT), while the micellar core was modified with a polycation (spermine) for siRNA binding, protection and endosome disruption. The peptide-functionalized micelles especially those with dual functionality (RGD/TAT-micelles), demonstrated increased cellular uptake and effective endosomal escape of siRNA compared to unmodified micelles (NON-micelles) when tested in MDA435/LCC6 resistant cells. Transfection of these cells with MDR-1 siRNA formulated in peptide-modified micelles led to P-gp down regulation both at the mRNA and protein level, and increased DOX accumulation in the cytoplasm and nucleus of the cells. Compared to RGD- or TAT-micelles, RGD/TAT-micellar siRNA complexes produced improved cellular uptake, P-gp silencing, DOX cellular accumulation, DOX nuclear localization and DOX-induced

cytotoxicity in MDA435/LCC6 cells, pointing to the potential of RGD/TAT-functionalized virus-like micelles for efficient siRNA delivery.

1.3 Immune System and Cancer

Although once controversial, increasing evidence supports the idea that our immune system is capable of recognizing tumor cells and can play an important role in tumor control and progression. The recognition of malignant cells by the immune system leading to an immune response capable of destruction of the malignant cells has been termed “immunosurveillance”.²⁰²⁻²⁰⁴ However, this concept was not able to explain how pre-clinical cancers develop into detectable tumors in the presence of a functioning immune system. This prompted the development of the concept “cancer immunoediting” which is a dynamic process composed of three phases: elimination, equilibrium, and escape. Elimination represents “cancer immunosurveillance” where the immune cells detect and destroy the cancer, thus protecting the host. However, some tumor cells can withstand the responses created by the immune system and enter a period of latency where a dynamic equilibrium exists between cancer cells and immune system leading to the growth of more resistant mutations of cancer cells which are finally able to outstrip the immunological restraints of the equilibrium phase and escape into a clinically detectable tumor leading to the escape phase.²⁰² The immune resistant cells in escape phase have several mechanisms to evade anticancer immune responses and develop to clinically apparent tumors.²⁰⁴

Dendritic cells (DCs) are best known for their roles in regulating immune responses and provide a direct link between innate and adaptive immunity. Innate immunity is the first line ‘generic’ response to anything the body recognizes as foreign. These responses involve

phagocytosis of invading cells, production of cytokines and chemokines, and recruitment of immune cells to the site of infection. The mechanisms of such responses are broad, non-specific and do not confer long-lasting immunity against the foreign substance. However, the cells of the innate immune system, such as the DCs and macrophages, play a crucial part in the initiation and subsequent direction of adaptive immune responses, which involve the T and B lymphocytes, and are responsible for quick, strong, and specific responses against the invading pathogen.²⁰⁵⁻²⁰⁸ DCs are the most professional antigen presenting cells (APCs) and are the ‘sentries’ of the body. They are bone-marrow derived cells and travel through blood and localize in peripheral tissues especially body surfaces exposed to the external environment. The functional maturation of DCs is a critical step in the induction of adaptive immunity. Before antigen encounter, DCs are in the immature state. As they encounter microbes such as bacteria, fungi, and viruses they engulf them through phagocytosis.²⁰⁹ This results in activation of a large number of genes including CD80, CD86, CD40, major histocompatibility complex class II (MHC-II) and IL-12 leading to their maturation. At this stage, DCs have switched from ‘antigen capture’ mode to ‘antigen presentation’ mode. Mature DCs migrate to draining lymph nodes where, in association with MHC class I and class II molecules, they present the processed antigen to naïve T cells resulting in T cell activation. The microenvironment of antigen capture and antigen presentation by DCs controls the direction and magnitude of immune responses.^{204, 205, 210}

1.4 Cancer Immunotherapy

Recently, cancer immunotherapy has significantly developed as an alternate modality of treatment, which utilizes the tremendous specificity and cytotoxicity of the immune

system, in creating an immune response against cancer. Strategies are based on complementation or stimulation of the immune system via a plethora of compounds including lymphokines, monoclonal antibodies, cancer vaccines, and *in vitro*-stimulated effector cells.²¹¹⁻²¹³ Immunotherapy utilizes the body's own defence mechanism in eradicating the tumor and can thus reach areas, where chemotherapy, radiation therapy or surgery cannot. Cancer immunotherapy can be divided into two main strategies: passive and active immunization against cancer. Passive immunotherapy strategies establish the link between Tumor Associated Antigens (TAAs) and the individual (native) immune system. In this type of immunotherapy, tumor-antigen specific antibodies, cytokines, or other immune system components are made outside of the body and administered to the patient to interact with the immune system of the host and provide immunity against cancer. Monoclonal antibody (mAb) therapy is the most widely used form of passive therapy. Passive cancer immunotherapy, however, requires high amounts of tumor-antigen specific antibodies, and is of limited duration.^{204, 211, 214}

In active immunotherapy, TAAs are delivered to the APCs which process them and present them to the T cells to create an immune response rather than a direct activation of T cells as in passive immunotherapy.²¹¹ Generation of active immunotherapy is more desirable since it induces an endogenous anti-tumor response, which can initiate long-term immunological memory. The ultimate goal of vaccine-based cancer immunotherapy is to elicit a potent anticancer immune response that will not only eradicate the tumor, but also generate a long-term memory response against the tumor, thus keeping the cancer in check.²⁰⁴

Although the immunological basis for cancer immunotherapy is sound, clinical studies with cancer vaccines have only achieved limited success.²¹⁵⁻²¹⁷ A major limitation of current cancer vaccines is that the immune responses elicited by cancer vaccines are weak. This is mainly due to the ability of cancer to develop several strategies to thwart anti-tumor immune responses by establishing an immunosuppressive microenvironment leading to the activation of immunosuppressive immune cells, impairment of immune effectors cells, and the activation of co-inhibitory signals.²⁰⁴

1.5 Cancer Immunosuppression

One of the major obstacles of effective cancer immunotherapy is the ability of the tumor to promote an immunosuppressive microenvironment that limits the activation of the immune system against the disease.²⁰⁴ Cancer immunosuppression evolves by constitution of an immunosuppressive network extending from a primary tumour site to secondary lymphoid organs and peripheral vessels. It is mediated by the production of several tumour-derived soluble factors (TDSFs) such as interleukin-10 (IL-10), transforming growth factor- β (TGF- β) and vascular endothelial growth factor (VEGF), and the lack of pro-inflammatory cytokines in tumor microenvironment.²¹⁸ TDSFs induce the activation of immunosuppressive cells including tolerogenic DCs and regulatory T (T_{reg}), and Th17 cells in accordance with tumour progression, which are the major cellular effectors of tumor immunosuppression. Tolerogenic DCs are incapable of producing a strong anti-tumor response, whereas T_{reg} cells are important in suppressing the activation and function of effector T cells.^{204, 218} This leads to effector cell tolerance or “exhaustion” of function due to inappropriate stimulation, or metabolic changes caused by limited access to proper cell function or proliferation in the

tumor microenvironment.²⁰³ The molecular mechanisms leading to cancer immunosuppression are not completely understood. However, recent studies have identified important molecules involved in tumor-induced immunosuppression. One of these molecules is an important oncogenic protein called STAT3.^{204, 219}

1.6 STAT3 in Cancer

1.6.1 Introduction to STAT3

Signal Transducer and Activator of Transcription (STAT) proteins make up one of the recently recognized signaling pathways. This family is comprised of seven members including STAT1 to STAT4, STAT5a, STAT5b, and STAT6 proteins. These proteins play an important role as cytoplasmic transcription factors regulating various genes involved in cell growth and survival.²²⁰ STAT proteins comprise of various domains having distinct functions such as the N-terminal which is important in STAT mediated cellular responses; the DNA binding domain which interacts with the DNA to mediate STAT transcriptional activity; the Src-homology 2 (SH2) domain which engages in dimerization between two activated monomeric STATs through reciprocal phospho-tyrosine (pTyr)-SH2 domain interactions; and the C-terminal which is involved in transcriptional activation.²²¹ Extracellular binding of ligands such as cytokines and growth factors, to their respective cell surface receptors, leads to the activation of either the non-receptor tyrosine kinases such as Janus Kinase (JAK), and Src; or intrinsic receptor tyrosine kinases. The activated tyrosine kinases recruit the STAT monomers to dock to the cytoplasmic domain of the receptor, where they are phosphorylated at a specific tyrosine residue (Tyr₇₀₅ in case of STAT3), leading to their dimerization via reciprocal (pTyr)-SH2 domains. The activated dimer transports into the nucleus where it

binds with DNA to regulate the transcription of many genes (Figure 1.6).^{204, 220-222} Under normal conditions, STAT3 activation is rapid and transient. However, constitutive activation of STAT3 protein is associated with many human cancers.²²¹

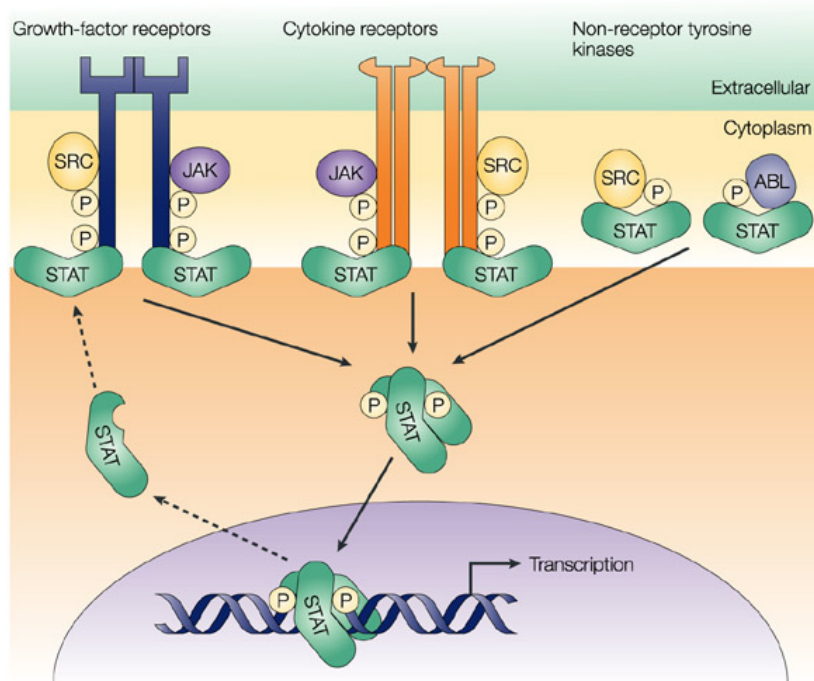


Figure 1.6 STATs are an important point of convergence for many signalling pathways that are commonly activated in cancer cells. Binding of growth factors or cytokines to their receptors results in the activation of intrinsic receptor-tyrosine-kinase activity or of receptor-associated kinases, such as JAK or SRC tyrosine kinases. These tyrosine kinases subsequently phosphorylate the cytoplasmic tails of the receptor to provide docking sites for the recruitment of monomeric STATs. Once they have been recruited, STATs become substrates for tyrosine phosphorylation. Non-receptor tyrosine kinases, such as the oncoproteins SRC and BCR–ABL (a fusion of the breakpoint-cluster region (BCR) and Abelson leukaemia (ABL) proteins), can phosphorylate STATs independently of receptor engagement. Phosphorylated STATs dimerize and translocate to the nucleus, where the dimers directly regulate gene expression. Dashed arrows indicate the 'recycling' of STAT proteins from the nucleus to the cytoplasm. (Reprinted by permission from Macmillan Publishers Ltd: Nature Reviews Cancer,²²⁰ copyright (2004))

1.6.2 Role of STAT3 in tumor growth

A large number of studies have provided evidence for the incidence of constitutive STAT3 activity in human tumors. Solid tumors, including breast, brain, colon, prostate, lung, pancreatic, pituitary, gastrointestinal, ovarian, and cervical tumors, HNSCC, and melanoma, as well as hematological malignancies such as lymphomas and leukemias, all harbor persistently activated STAT3.²²¹ Constitutively activated STAT3 contributes to cancer progression by regulating the expression of genes that are involved in cell proliferation, survival, angiogenesis, metastasis, and cancer immune evasion.²⁰⁴ STAT3 hyper-activation favors proliferation of malignant cells by exerting an anti-apoptotic effect by inducing factors that drive angiogenesis and metastasis including VEGF and metalloproteases. STAT3 has been shown to upregulate the expression of the genes involved in uncontrolled cell proliferation and survival. Over-expression of STAT3 in tumors also has a major effect on recruiting tumor-infiltrating immune cells by controlling production of various inflammatory chemotactic factors and chemokines. Many factors released by the tumor, such as VEGF, IL-6, and IL-10, not only play an important role in STAT3 over-expression, but are themselves transcriptionally regulated by STAT3, thus creating a positive feedback loop.²²³ Since constitutively activated STAT3 plays an important role in the progression of many human cancers, blocking its hyper-activation has been suggested as a novel approach for inducing cancer cell apoptosis.²⁰⁴

1.6.3 Role of STAT3 in tumor-induced immunosuppression

In addition to the effects of STAT3 in cancer progression, hyperactivation of STAT3 in tumors has been found to lead to immune evasion by blocking both, the production and

sensing of inflammatory signals by multiple components of the immune system, in particular DCs.²²⁴⁻²²⁷ Previous studies have reported that the inhibition of STAT3 activation in tumor cells can reverse tumor-induced immunosuppression in DCs giving them the ability to present antigen and induce T-cell activation against the tumor cells. Constitutive activation of STAT3 in tumor cells leads to the release of tumor-derived factors like IL-10 and VEGF in the tumor microenvironment. These soluble factors are taken up by DCs rendering them either immunosuppressive or dysfunctional.^{219, 228, 229} Recent evidence has shown that both IL-10 and VEGF lead to constitutive activation of STAT3 in DCs.²²⁵ Hyperactivation of STAT3 in DCs has been found to suppress myeloid differentiation into DCs, inhibit DC functional maturation and induce the activation of tolerogenic DCs.^{227, 228, 230-233} Inhibition of DC maturation inhibits their ability to induce T-cell activation whereas activation of tolerogenic DCs can induce the activation of T_{reg} cells which further inhibit the function of DCs and effector T-cells.²³⁴ Since constitutively activated STAT3 in DCs suppresses their ability to induce an immune response, inhibition of STAT3 in DCs is an attractive target for cancer immunotherapy.

1.6.4 Targeting STAT3 for cancer immunotherapy

Since 2001,²³⁵ STAT3 inhibitor development has gained high interest as a potential target for cancer therapy. As already mentioned in Section 1.6.1, STAT proteins such as STAT3 have various domains with distinct functions, hence targeting these domains can directly inhibit STAT3 (Table 1.2).

Platinum based compounds have been found to inhibit the STAT3 DNA binding activity. Platinum complexes like cisplatin have been used as anticancer agents targeting

STAT3 in various human cancers.²³⁶ IS3 295 has been shown to interact with the DNA binding domain of STAT3 however, the exact mechanism is still unclear.²³⁷ Additional platinum compounds like CPA-1 and CPA-7 have been identified as STAT3 inhibitors which can diminish STAT3-mediated gene regulation.²³⁸ Recently, various peptide analogs have been identified which can interact with the DNA binding domain and inhibit STAT3-mediated transcription.^{236, 239} SH2 targeting compounds can either prevent phosphorylation of STAT3 by binding to Tyr₇₀₅ or by preventing the dimerization of STAT3. STA-21,²⁴⁰ LLL-3,²⁴¹ S3I-201,²⁴² and Stattic²⁴³ are all small molecule inhibitors which can bind to the SH2 domain of STAT3 preventing their dimerization, inhibiting their translocation into the nucleus. Another inhibitor, named LLL-12 exerts its effects by binding directly to the Tyr₇₀₅ site on STAT3, inhibiting its ability to phosphorylate.²⁴⁴ The N-terminal domain of STAT3 is comprised of nearly 130 amino acids containing 8 helices. Recently, a category of short peptides, derived from the helices of the N-terminal domain have been investigated for their STAT3 inhibitory effects.^{236, 239} The LDTRYLEQLHKLY motif of these short peptides can bind to full-length STAT3 with good selectivity leading to STAT3 inhibitory activity without affecting its phosphorylation.²³⁶

Another approach to directly inhibit STAT3 is by inhibiting STAT3 gene expression using siRNA. Previous studies in our lab used STAT3 siRNA for knockdown of STAT3 in B16 tumor cells both *in vitro* and *in vivo*. Their results showed a regression in tumor growth *in vivo* after treatment.²⁴⁵ Another study from our lab investigated the efficacy of various lipid-modified PEI/STAT3 siRNA complexes and found that linoleic acid substituted PEI (PEI-LA) was most efficient in down-regulation of STAT3 at both mRNA and protein levels, leading to loss of viability in MDA-MB-435 cancer cells. Furthermore, they found that pre-

treatment with STAT3 siRNA renders MDA-MB-435 drug resistant cells, susceptible to the cytotoxic effects of both doxorubicin and paclitaxel.²⁴⁶

Table 1.2 Agents used for STAT3 targeting.^{236, 239, 247}

Agent	Target Site	Mode of STAT3 inhibition	Cell line
S3I-201	STAT3 SH2	Dimerization	NIH3T3/vSrc, MDA-MB-231, MDA-MB-435
Stattic	STAT3 SH2	Dimerization	MDA-MB-231, MDA-MB-435, HepG2
STA-21	STAT3 SH2	Dimerization	MDA-MB-231, MDA-MB-435, MDA-MB-468
LLL-3	STAT3 SH2	Dimerization	U87, U373, U251
LLL-12	STAT3 SH2	Phosphorylation	MDA-MB-231, SKBR3, HPAC, U87
IS3 295	STAT3 DBD	DNA binding	NIH3T3/vSrc, MDA-MB-468, MDA-MB-435
CPA-1, CPA-7	STAT3 DBD	DNA binding	NIH3T3/vSrc, MDA-MB-231, MDA-MB-435, CT26
JSI-124	JAK	Phosphotyrosine STAT3 level	NIH3T3/vSrc, MDA-MB-468, A549, B16-F10, MDA-MB-435
siRNA	STAT3 mRNA	STAT3 expression	B16-F10, MDA-MB-435

Targeting the ligand-receptor interaction at the extracellular surface by inhibiting the Tyr kinases can provide an indirect, but effective method in inhibiting STAT3 activation in various cancer cells. Various inhibitors been identified to indirectly modulate STAT3 signaling including the receptor Tyr kinase inhibitors, like tyrphostins,²⁴⁸ the JAK kinase inhibitors, like AG490, WP1066, and JSI-124;²⁴⁹⁻²⁵¹ and the Src kinase inhibitors, like TG101209, resveratrol, and indirubin.²⁵²⁻²⁵⁴

1.6.4.1 STAT3 inhibitor JSI-124

JSI-124 has been identified as a potent inhibitor of the JAK/STAT3 pathway and has been studied extensively for its direct anti-tumor effect and role in enhancing cancer immunotherapy in several human and murine models.^{226, 231, 249, 255-258} JSI-124 belongs to a group of natural products called cucurbitacins, which have been isolated from various plant families such as *Cucurbitaceae*.²⁵⁹ JSI-124 has previously demonstrated its STAT3 inhibitory activity by selectively inhibiting the activation of JAK2 and STAT3 but not Src, Akt, Erk, and Jnk.²⁴⁹ Other studies suggested the role of JSI-124 in activation of phosphatases or in activation of certain physiological inhibitors that can directly or indirectly regulate STAT3 activation.^{249, 260}

Previous studies showed that JSI-124 was successful in directly inhibiting tumor growth in mice bearing tumors having constitutively activated STAT3 like A549, MDA-MB-468, and B16 melanoma, however, it did not affect the growth of tumors which were independent of STAT3 or which had low levels of activated STAT3.^{249, 261} Furthermore, other studies have shown that JSI-124 can activate the anti-tumor immune response by inhibiting the tumor-induced activated STAT3 in DCs *in vitro*.^{226, 228, 231, 257} Nefedova et al.²³¹

demonstrated that treatment of JSI-124 can reverse the tumor-induced immune suppression of DCs by promoting their differentiation into mature DCs. The activation manifested in up-regulation of MHC class II, co-stimulatory molecules and the increase in the ability to stimulate T-cells.

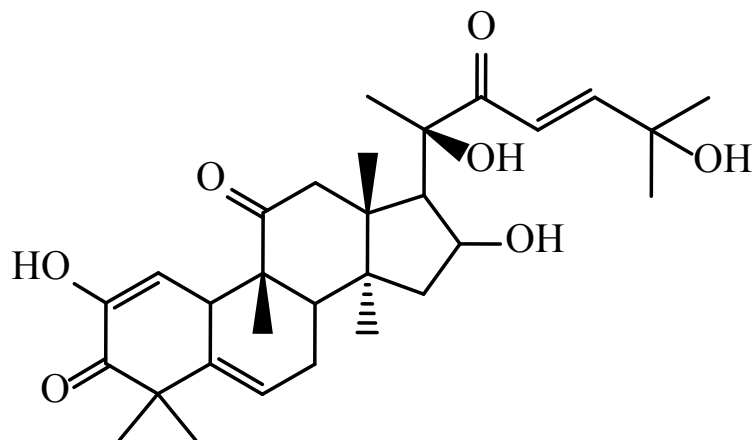


Figure 1.7 Chemical structure of JSI-124

In another study, systemic administration of JSI-124 in glioma-bearing immunocompetent mice resulted in their prolonged survival, and also promoted the maturation of tumor-infiltrating DC and activation of tumor-conditioned cytotoxic T cells.²⁶² Previous studies in our lab showed that JSI-124 conjugated to PLGA nanoparticles was able to successfully suppress the constitutively activated STAT3 in B16 melanoma cells and also in tumor-exposed DCs. In combination with CPG, the PLGA JSI-124 conjugate was able to reverse immunosuppression in tumor-exposed DCs resulting in higher T-cell proliferation by DCs *in vitro*.²⁵⁷ *In vivo* studies by our group showed the synergistic antitumor effects of combining CPG and JSI-124 in a B16-F10 melanoma tumor model. Moreover, the combination therapy resulted in significantly higher intratumoral levels of several pro-

inflammatory, T_H1-related cytokines, increase in intra-tumoral CD8⁺ and CD4⁺ T cells expressing activation/memory markers and NK cells, and increase in activated DCs in the tumors and regional lymph nodes.²⁵⁵

1.7 Role of Myeloid Cell Leukemia-1 (MCL-1) in Cancer

Apoptosis is the process of programmed cell death which is generally characterized by energy-dependent biochemical mechanisms and distinct morphological changes including cell shrinkage, pyknosis, membrane blebbing, and karyorrhexis, finally leading to uptake by phagocytic cells.^{263, 264} The culmination of apoptosis involves the activation of a family of cysteine proteases (caspases), which when activated cause cellular destruction by dismantling the cell's components.^{265, 266} One of the key regulators of apoptosis, apart from caspases, is the Bcl-2 family of proteins which is comprised of structurally related proteins that are either pro-apoptotic or anti-apoptotic.²⁶⁷ Dysregulation in the expression of the Bcl-2 family members has been found to play a key role in the resistance to apoptosis in cancer leading to cancer survival and progression.²⁶⁸

MCL-1 is a anti-apoptotic member of the Bcl-2 family of proteins that was initially identified as a gene that is expressed early in the induction of differentiation of the myeloid cell line, ML-1.²⁶⁹ MCL-1 maintains survival of cells by inhibiting cytochrome c release via binding and sequestering pro-apoptotic Bcl-2 proteins Bak (Bcl-2 homologous antagonist killer) and Bax (Bcl-2 associated X).^{266, 270, 271} Up-regulation of MCL-1 has been found to play a role in cancer survival and is found to be over-expressed in a variety of human hematological cancers^{266, 272} and solid tumors²⁶⁸ including breast cancer,²⁷³ whereas, down-

regulation of MCL-1 has been found to induce apoptosis²⁶⁴ and can be a potential target in the treatment of a number of cancer cell types.

1.7.1 Targeting MCL-1

The strategies involving the down-regulation of MCL-1 can be divided into two categories, namely, non-specific and specific treatments.²⁶⁴ Under non-specific treatments, many synthetic chemicals and natural products have been investigated which include treatment with cyclin-dependent kinase inhibitors like flavopiridol,²⁷⁴ tyrosine kinase inhibitors like sorafenib,²⁷³ or STAT3 inhibitors like resveratrol.²⁷⁵ Flavopiridol inhibits MCL-1 mRNA via inhibition of RNA polymerase-II dependent transcription, whereas sorafenib inhibits translation and rapidly reduces the levels of MCL-1 protein. Since MCL-1 transcription is regulated by STATs, inhibition of STAT3 indirectly inhibits the transcription of MCL-1. All of these compounds, however, lack specificity and may affect multiple targets by different signaling pathways.²⁶⁴

Specific treatments include BH3 mimetics or gene-specific treatments. BH3 mimetics exert their effects by antagonizing the interaction between anti-apoptotic proteins and pro-apoptotic proteins in the mitochondria. BH3 mimetics like Obatoclax and Bim_s2A can efficiently antagonize the interaction of MCL-1 and overcome the resistance to apoptosis.^{264, 268, 276, 277} However, many of these compounds have shown to cause cell death by non-mechanism based toxicity like damaging mitochondria.²⁶⁸ An alternative approach in down-regulating MCL-1 is by using siRNA which can specifically inhibit MCL-1 expression.

1.7.1.1 siRNA Delivery and Challenges

RNA interference (RNAi) is a sequence-specific evolutionary mechanism where sequence-specific double stranded small interfering RNA molecules (siRNA) are used for regulation of gene expression.^{247, 278, 279} In the presence of endogenous RNA Induced Silencing Complex (RISC), the double stranded siRNA unwinds and the antisense strand binds to specific sequences of messenger RNA (mRNA). This binding leads to cleavage of the target mRNA thus eliciting highly sequence-specific gene silencing.²⁸⁰ Therapeutically, RNAi can be employed to silence any specific gene, making it highly specific and advantageous over other drugs which can have numerous targets resulting in toxicity. However, despite their great promise, translation of this approach to clinical practice particularly following systemic administration has been challenging. This is mostly due to the instability of siRNA and other gene silencing entities in plasma, poor distribution in target tissue and inadequate access to their molecular target within the target cells. The lack of an efficient delivery system to encapsulate the siRNA and deliver it to the target site is one of the major limitations of siRNA delivery. This is mainly due to nonspecific toxicity imposed by the siRNA carrier, their uptake by the MPS, insufficient stability in blood, or lack of specific interaction and distribution in the target tissue.^{278, 279, 281}

Optimal systemic delivery systems for siRNA should be biocompatible, biodegradable, and non-immunogenic. At the same time, the system should be able to efficiently encapsulate the siRNA, deliver it to the target site, be taken up by cells and ensure release of the siRNA into the cytoplasm to allow its interaction with RISC. Various types of non-viral delivery systems have been studied. These include cationic emulsions,²⁸² liposomes,^{283, 284} lipid nanoparticles,^{285, 286} polymeric micelles,^{139, 201} and nanoparticles.^{287, 288}

1.7.1.2 Polymeric micelles for siRNA delivery

Polymeric micelles for delivery of siRNA can be classified into two major types. The first is formed by direct conjugation of PEO to siRNA followed by condensation of the siRNA using polycations. The second is formed by complexation of the block copolymer containing a polycation with the siRNA.²⁴⁷

PEO-siRNA conjugates have been studied extensively. Kim et al.²⁸⁹ synthesized PEO-siRNA conjugate via disulfide linkage using VEGF siRNA and then condensed the siRNA using PEI25K. The micelles formed were found to protect the VEGF siRNA from degradation in serum for up to 48 h whereas the PEO shell protected the micelles against serum protein adsorption. *In vivo* studies after intratumoral or systemic administration resulted in significant downregulation of VEGF protein when compared to the untreated group.²⁹⁰ Other studies showing the success of targeting of PEO-siRNA conjugates using luteinizing hormone releasing hormone (LHRH) as the targeting moiety have also been carried out.²⁹¹

Block copolymer complexes with siRNA have also been used extensively for the development of effective siRNA delivery systems. Sutton et al.²⁹² synthesized graft polymers of PEO-g-PEI with different PEO densities. They found that PEG densities of 9.7 per PEI chain were most efficient in delivering secretory clusterin (sCLU) siRNA in MCF-7 breast cancer cells. In another study, a series of cationic comb type copolymers (CCCs) having a poly(L-lysine) (PLL) backbone and different densities of PEO side chain were synthesized. It was found that higher PEO densities were able to protect siRNA for longer periods of time both *in vitro* and *in vivo*.²⁹³ Musacchio et. al. reversibly conjugated GFP siRNA to

phosphothioethanol (PE) via disulfide linkage (siRNA-S-S-PE) and prepared mixed micelles of PEO-PE and siRNA-S-S-PE. The micelles exhibited a small size of 10 nm and successfully down-regulated GFP production in GFP-C166 endothelial cells, 50 times more efficiently than free siRNA.²⁹⁴ In further studies, the group used a similar approach to target the anti-apoptotic factor survivin by conjugating survivin siRNA to PE and testing their ability in chemosensitizing sensitive and resistant cancer cells to PTX therapy. The siRNA-S-S-PE/PEO-PE micellar complex was able to effectively downregulate survivin protein levels and chemosensitize both sensitive (MDA-MB-231 and SKOV3) and resistant (SKOV3-tr) cells to paclitaxel therapy.²⁹⁵ Next, they also showed the success of survivin siRNA-S-S-PE/PEO-PE micellar complex and PTX in mice bearing PTX-resistant SKOV3-tr ovarian cancer xenografts.²⁹⁶

PEI-lipid based siRNA complexes have also been used successfully for siRNA delivery and reduce the toxicity exhibited by PEI. Navarro et. al. modified PEI (1.8 kDa) with dioleoylphosphatidylethanolamine (DOPE) to form DOPE-PEI complexes. The complexes showed a 10-fold reduction in the toxicity of the PEI polymer when compared to PEI25K (25kDa) but exhibited comparable transfection efficiency of siRNA in downregulating green fluorescent protein (GFP) expression.²⁹⁷ Similar results were seen in another study where the authors modified PEI2K with various fatty acids such as caprylic acid, stearic acid, palmitic acid, linoleic acid, and oleic acid. The lipid modified PEI reduced the toxicity of PEI25K whereas modification with caprylic or linoleic acid showed higher efficacy of siRNA complexes in downregulation of p-gp when compared to PEI25K.²⁹⁸

Our research group has reported on the development of a biodegradable and biocompatible siRNA delivery system based on self-associating PEO-*b*-PCL block

copolymers bearing spermine (SP) on the α -carbons of ϵ -caprolactone in the PCL block. The PEO-*b*-P(CL-*g*-SP) micelles were able to protect siRNA from degradation by serum nucleases, be taken up by cancer cells and effectively down-regulate MDR-1 through delivery of its siRNA leading to a significant decrease in the expression of P-glycoprotein in MDA-MB-435 cells.¹³⁹ Further modification of PEO-*b*-P(CL-*g*-SP) micellar shell with cancer targeting and cell penetrating peptides, i.e., RGD4C and TAT, respectively, increased the transfection efficiency of the MDR-1 siRNA *in vitro*.²⁰¹ Systemic administration of RGD4C modified PEO-*b*-P(CL-*g*-SP) enhanced the localization of siRNA in tumor in an MDA-MB-435 xenograft model pointing to the potential of this nanocarrier for siRNA delivery following systemic administration.¹⁰²

1.7.1.3 MCL-1 siRNA delivery

Advanced delivery systems have been developed for delivery of MCL-1 siRNA. Yu et. al. showed improved anticancer activity against human epithelial carcinoma KB cells when treated with solid cationic lipid nanoparticles loaded with paclitaxel and MCL-1 siRNA.²⁹⁹ Similar results were seen by Chang et. al. when combining MCL-1 siRNA with mitoxantrone in lipid nanoparticles.³⁰⁰ Aliabadi et. al. used a lipid-modified cationic polymeric delivery system based on PEI for successfully silencing both MCL-1 and P-gp in drug-resistant MDA-MB-435 cancer cells sensitizing them to chemotherapy.²⁷¹

1.8 Research Proposal

1.8.1 Central Hypothesis

The central hypothesis of this project is that functionalizing the PCL core of PEO-*b*-PCL block copolymer micelles by attaching various pendent groups, or the PEO shell by covalently conjugating various peptide ligands can enhance the activity of these nanocarriers in delivering their drug and/or siRNA cargo to the tumor *in vitro* and *in vivo*. Two main objectives were set to test this hypothesis:

1) To assess the effect of the pendant group on the PCL block of PEO-*b*-PCL micelles in increasing the physicochemical stability and biocompatibility; reducing the immunogenicity and rate of degradation; increasing the accumulation in the tumor; and increasing the efficacy of drug and siRNA delivery when compared with unmodified PEO-*b*-PCL based micelles.

2) To assess the effect of covalent attachment of a tumor targeting peptide ligand to the PEO shell of PEO-*b*-PCL micelles in increasing the homing and/or cargo delivery of the nanocarrier at the tumor site when compared to plain unmodified micelles.

1.8.2 Rationale

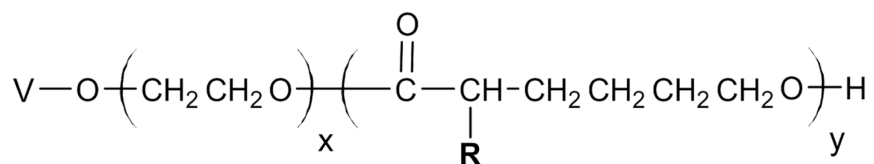
In spite of great advantages, development of successful polymeric micellar delivery systems for different therapeutic entities (e.g., drugs of different physiochemical structure and nucleic acid based therapeutics) is still challenging. Evidence from the literature suggests that chemical modification of the micellar core and/or shell in polymeric micelles is an effective strategy that can be utilized to optimize their function in the delivery of given therapeutic/diagnostic agents.

Our research group has developed a micelle-forming polymer platform technology based on poly(ethylene oxide)-*block*-poly(ϵ -caprolactone) (PEO-*b*-PCL) with functional pendant groups on the α -carbon of PCL.^{43, 102, 111, 121, 139, 191, 301-306} The members of this library differ from each other by the chemical structure of the pendent group (Scheme 1.1) which can influence the physicochemical properties of the micelles or change the encapsulation and release of certain therapeutic molecules. For instance, benzyl carboxylate has been added as the functional group to enhance the thermodynamic and kinetic stability of micelles, and/or make them more suitable for the encapsulation and release of hydrophobic drugs.^{43, 301, 304} Pendent carboxyl groups have been introduced to further functionalize the nanocarriers for conjugating drugs^{111, 121, 191, 305}, NIR probes,¹⁰² substituents to improve drug delivery,^{302, 303, 306} or polyamines¹³⁹ to improve siRNA delivery. However, further investigations on the effect of pendent groups like benzyl carboxylate and carboxyl groups on the biodistribution, rate of degradation, biocompatibility, and immunogenicity of PEO-*b*-PCL based micelles are scarce. Thus, we evaluated these effects and compared them against unmodified PEO-*b*-PCL micelles.

As mentioned in Section 1.2.1.1.4, click chemistry is a useful tool for crosslinking the core of micelles, which can prevent their dissociation in the high dilution conditions of the blood thereby increasing their stability. Click chemistry is a mild technique which can be carried out at room temperatures, thereby, not exposing the encapsulated material to the harsh conditions of some other cross-linking techniques.^{71, 81-84} However, previous work with PEO-*b*-poly(esters) is scarce due to lack of functionalization in the poly(ester) block. We proposed to introduce click crosslinkable groups by functionalizing the core of PEO-*b*-PCL micelles and assessing their stability against unmodified PEO-*b*-PCL micelles.

STAT3 inhibitor JSI-124 has previously been shown to have potent anti-cancer and immune modulatory effects in several human and murine models.^{226, 231, 249, 255-258} However, its poor water solubility and non-specific toxicity has limited its clinical application.²⁰⁴ Previously, PEO-*b*-PCL based micelles have successfully solubilised JSI-124, but were unable to control its release.^{261, 301} We proposed to covalently conjugate JSI-124 to the core of PEO-*b*-PCL based micelles to sustain the release of JSI-124 thus providing an opportunity to successfully deliver it to the tumor site.

As mentioned previously, our lab has modified PEO-*b*-PCL based block copolymers with polyamines like spermine to aid in siRNA delivery and further investigated the role of cholesteryl substitution in improving siRNA delivery *in vitro*.^{139, 247} We further proposed to investigate the role of cholesteryl modification in improving siRNA delivery *in vivo* after local or systemic administration.



R: H
 COOH
 CO-Obz
 CO-Ochol
 CO-O-(CH₂)_n-CH₃
 CO-drug
 CO-poly(amine)

V: CH₃
 acetal
 Peptides (RGDfK, RGD4C, NGR, GE11, P160)
 mAbs
 COO-CH(R)-(CH₂)₄-OH

x: 45 – 295

y: 15 - 210

Scheme 1.1 The developed library of functionalized PEO-PCL polymers.

1.8.3 Working Hypotheses

1) a) Increasing the hydrophobicity of the PCL core of PEO-*b*-PCL block copolymers with pendant benzyl carboxylate group will increase the thermodynamic and kinetic stability, decrease the rate of degradation, and maintain the high biocompatibility, and low immunogenicity of the generated polymeric micelles when compared with unmodified PEO-*b*-PCL.

b) Decreasing the hydrophobicity of the PCL core of PEO-*b*-PCL block copolymers with pendant carboxyl group will decrease the thermodynamic and kinetic stability, increase the rate of degradation, and maintain the high biocompatibility, and low immunogenicity of the generated polymeric micelles when compared with unmodified PEO-*b*-PCL.

2) a) Owing to better thermodynamic and kinetic stability, micelles formed from PEO-*b*-PCL block copolymers with pendant benzyl carboxylate groups on PCL, will provide better passive intake in orthotopic MDA-MB-231 breast tumors when compared with micelles formed from unmodified PEO-*b*-PCL block copolymers.

b) Modifying the PEO shell of the micelle with the breast cancer targeting peptide, P18-4, will provide higher intake in orthotopic MDA-MB-231 breast tumors when compared with micelles having no modification on the PEO shell.

3) Covalently crosslinking the core of PEO-*b*-PCL based block copolymer micelles will prevent them from dissociating in high dilution conditions below CMC, thus increasing their thermodynamic stability and preventing premature release of model drugs PTX and JSI-124 when compared to PEO-*b*-PCL based micelles bearing no crosslinks in the core.

4) Covalently conjugating a STAT3 inhibitor JSI-124 to the core of PEO-*b*-PCL based block copolymer micelles via a hydrolysable ester bond will sustain the release of the drug while still maintaining its STAT3 inhibitory effects in B16 melanoma cells and immune-suppressed DCs when compared with free JSI-124.

5) a) Chemical modification of PEO-*b*-P(CL-*g*-SP) core by covalently conjugating hydrophobic groups such as cholesteryl to SP will increase the thermodynamic stability of the micelles thus increasing the efficacy of these carriers in MCL-1 siRNA delivery to MDA-MB-435 tumors after local or systemic administration when compared with PEO-*b*-P(CL-*g*-SP) not modified with cholesteryl groups.

b) Modifying the PEO shell of the micelle with the integrin targeting peptide, RGD4C, will increase the efficacy of these carriers in MCL-1 siRNA delivery to MDA-MB-435 tumors (over-expressed with integrins) after systemic administration when compared with micelles having no modification on the PEO shell.

1.8.4 Specific Objectives

1) To synthesize a library of 10 block copolymers based on PEO-*b*-PCL, having either no modification, or bearing different pendant groups on the PCL block i.e. benzyl carboxylate and carboxyl, varied PCL backbone lengths, and assess the effect of these structural changes on the thermodynamic and kinetic stability, rate of degradation, biocompatibility, and immunogenicity of the prepared micelles.

2) To synthesize traceable polymeric micelles based on PEO-*b*-PCL, having either no modification, or bearing pendant benzyl carboxylate group on the PCL block, and assess the effect of changes in micellar core on its *in vivo* biodistribution and tumor accumulation in orthotopic MDA-MB-231 breast tumors. Further, to modify the PEO shell of the prepared micelles with P18-4 peptide and assess the effect of changes in micellar shell on its *in vivo* biodistribution and tumor accumulation in orthotopic MDA-MB-231 breast tumors.

- 3) To synthesize PEO-*b*-PCL based block copolymer micelles with degradable crosslinks in the core and assess the effect of this structural change on the thermodynamic stability of the micelles as well as encapsulation and release profile of model drugs PTX and JSI-124.

- 4) To covalently conjugate JSI-124 to the core of PEO-*b*-PCL based block copolymer micelles and assess the encapsulation and release profile of the micellar conjugate, and its ability to maintain the STAT3 inhibitory activity of the free drug in B16 melanoma cells and DCs, and the immune modulatory effect of the free drug in DCs.

- 5) To synthesize cholesteryl substituted PEO-*b*-P(CL-*g*-SP)/MCL-1 siRNA complexes with or without RGD4C modification in the shell and assess the effects of cholesteryl and RGD4C modification on MCL-1 siRNA delivery after local and systemic delivery in *in vivo* MDA-MB-435 tumor models.

Chapter Two
Polymeric Micelles based on Poly(ethylene oxide) and α -carbon
Substituted Poly(ϵ -caprolactone): An *In Vitro* Study on the Effect of Core
Forming Block on Polymeric Micellar Stability, Biocompatibility, and
Immunogenicity

A version of this chapter has been published in

Colloids and Surfaces B: Biointerfaces 2015, 132, 161-170

Shyam M Garg¹, Mohammad Reza Vakili¹, Afsaneh Lavasanifar^{1,2}

¹Faculty of Pharmacy and Pharmaceutical Sciences, University of Alberta, Edmonton, AB

²Department of Chemical and Materials Engineering, Faculty of Engineering, University of
Alberta, Edmonton, AB

Reprinted from Reference,³⁰⁷ Copyright (2015), with permission from Elsevier

2.1 Introduction

Amphiphilic block copolymers based on poly(ethylene oxide)-*b*-poly(esters) such as poly(ethylene oxide)-*b*-poly(ϵ -caprolactone) (PEO-*b*-PCL),³⁰⁸⁻³¹¹ poly(ethylene oxide)-*b*-poly(lactide) (PEO-*b*-PLA),^{312, 313} and poly(ethylene oxide)-*b*-poly(lactide-co-glycolide) (PEO-*b*-PLGA)^{122, 314} have emerged as self-associating synthetic biomaterials with tremendous potential for pharmaceutical applications.^{16, 17} The interest towards the use of PEO-*b*-poly(ester)s for application in biological systems is owed to the biocompatibility of PEO and biodegradability of poly(ester) structure through enzymatic and/or hydrolytic degradation into biocompatible catabolites.^{47, 315} In spite of these advantageous features, the lack of functional groups on the poly(ester) block has restricted opportunities for the chemical engineering of PEO-poly(ester)s towards development of biomaterials for broad range of applications. To address this shortcoming, our research group has developed a library of PEO-*b*-PCL block copolymers with functional pendent groups on the α -carbons of the PCL block.^{43, 111, 139, 302, 316} The members of this library differ from each other by the chemical structure of the pendent group. The aim of this study was to investigate the effect of the chemistry of the pendent group on the PCL block on the physicochemical and biological stability of associated polymeric micelles, under *in vitro* conditions mimicking that of biological system. The results of this study can be used as a primary step in defining the effect of the core-forming structure in this class of polymeric micelles on their *in vivo* fate.

The *in vivo* fate of polymeric micellar delivery system is primarily governed by: i) the stability of the micellar structure against dissociation in blood stream; ii) its degradation behavior; iii) its interaction with different blood components (e.g., proteins, lipoproteins and cells); and iv) its ability to create an immune response.^{45, 60} The stability of micellar structure

against dissociation in blood is determined by the thermodynamic as well as kinetic stability of micelles. The thermodynamic stability of micellar structure, characterized by the critical micelle concentration (CMC) of block copolymers, is known to be dependent on the hydrophilic lipophilic balance (HLB) of block copolymers constructing the micelles. Block copolymers of lower HLB usually show higher tendency towards micelle formation (characterized by lower CMCs). In other words, micelles from low HLB block copolymers are thermodynamically more stable.^{1, 54} Kinetic stability of micellar structures, on the other hand, refers to the rate of micellar dissociation at concentrations below CMC. Polymeric micelles with rigid and semi-crystalline core structures are known to show higher kinetic stability and resistance towards dissociation below CMC.

The degradation behavior of micelles also play an important role in their fate in the body. The degradation of the core-forming block can influence both thermodynamic as well as kinetic stability of polymeric micelles through changing the HLB and rigidity of block copolymers over time, respectively.³⁶ Few studies have been carried out on the degradation of PEO-b-PCL block copolymer micelles,^{45, 55, 57} however, none have investigated the influence of the PCL core chemistry on the degradation.

The *in vivo* stability and blood circulation time of polymeric micellar structures, is also affected by the adsorption of opsonins (mostly proteins) present in plasma on the micellar surface. Adsorption of opsonins on nano-carrier surfaces can enhance the uptake of these carriers by the MPS and lead to their early removal from blood circulation.^{144, 146} Numerous methods have been used to study the protein adsorption on micelles.^{64, 145, 148} Influence of PEGylation on protein adsorption has been well documented in the literature,^{145, 156, 159, 160} however, there is little work done on the influence of core chemistry on protein

adsorption.³¹⁷ Biocompatibility of micellar structures is further characterized by their ability in the induction of immune response by key cells of the immune system. Dendritic cells (DC)s are key players in this regard known to play a pivotal role in initiating an immune response against any foreign substance presented to blood or peripheral tissue.^{147, 318} Previous literature on the immunogenicity of nanocarriers to DCs is scarce.^{318, 319}

In this study we prepared PEO-*b*-PCL block copolymers containing either free carboxyl or benzyl carboxylate pendent groups on their PCL segment and investigated the influence of pendent group chemistry and the degree of polymerization of the hydrophobic segment on the physicochemical, thermodynamic as well as kinetic stability of formed polymeric micelles. Comparisons were made with PEO-*b*-PCL micelles without pendent groups. The effect of PCL chemistry on the degradation of micellar structure was also investigated. In further studies, the effect of PCL chemistry on the biological interactions of resulted polymeric micelles with plasma proteins as well as induction of immune responses by bone marrow derived DCs (BMDC)s, was investigated *in vitro*, as an indication of micellar *in vivo* stability and immunogenicity, respectively. To the best of our knowledge, this is the first study investigating the effect of pendant groups on the PCL core on the thermodynamic and kinetic stability, degradation, and biocompatibility of micelles. It is also the first study investigating the immunogenicity of micellar systems to DCs.

2.2 Experimental Section

2.2.1 Materials

Methoxy-polyethylene oxide (PEO) (average molecular weight of 5000 g/mol), sodium (in kerosene), palladium on charcoal, and bovine serum albumin (BSA) powder were purchased from Sigma (St. Louis, MO). ϵ -Caprolactone was purchased from Lancaster Synthesis (UK). α -Benzyl carboxylate- ϵ -caprolactone monomer was synthesized by Alberta Research Chemicals Inc (Edmonton, AB) according to a previously published procedure.⁴³ Stannous octoate was purchased from MP Biomedicals Inc. (Germany). Quick-Start™ Bradford Protein Assay kit and bovine serum albumin standards were purchased from Bio-Rad Laboratories (Hercules, CA). Cell culture media RPMI 1640, fetal bovine serum (FBS), and penicillin-streptomycin-L-glutamine were purchased from GIBCO, Life Technologies Inc. (Burlington, ON, Canada). Murine Interleukin-12 (IL-12) p70 ELISA (enzyme-linked immunosorbent assay) Ready-SET-Go® kit, Fluorescein isothiocyanate (FITC) conjugated anti-mouse CD-86 (B7-2) (GL7) mAb, and Phycoerythrin-Cy5 (PE-Cy5) conjugated anti-mouse CD40 mAb, and purified anti-mouse CD16/CD32 (Fc γ -III/II receptor) were purchased from e-Biosciences (San Diego, CA). Spectra/por dialysis tubing (MWCO - 3.5 kDa) was purchased from Spectrum Laboratories (Rancho Dominguez, CA). All other chemicals were reagent grade.

2.2.2 Mice

C57Bl/6 mice were purchased from the Jackson Laboratory (Bar Harbor, ME). All experiments were performed using 6 to 12 week-old female mice. All experiments were

performed in accordance with the University of Alberta guidelines for the care and use of laboratory animals.

2.2.3 Synthesis of Block Copolymers

Block copolymers of PEO-*b*-PCL and PEO-*b*-PBCL with different degrees of polymerization for the PCL and PBCL segment were synthesized by ring-opening polymerization of ϵ -caprolactone or α -benzyl carboxylate- ϵ -caprolactone, respectively, using methoxy-PEO (M_w : 5000 g/mol) as initiator and stannous octoate as catalyst according to a method described previously.^{43, 308, 320} Briefly, methoxy PEO (M_w : 5000 g/mol) (0.5 g), ϵ -caprolactone (0.25, 0.5, 0.75, 1.0 g) or α -benzyl carboxylate- ϵ -caprolactone (0.5, 0.8, 1.6 g), and stannous octoate (0.1% weight/weight of the polymer) were added to a 10 mL previously flamed ampoule and sealed under vacuum. The polymerization reaction was allowed to proceed for 4 h at 140 °C in an oven. The reaction was terminated by cooling the mixture to room temperature. The product was then dissolved in dichloromethane and precipitated in hexane. The mixture was centrifuged at 3000 rpm and the supernatant was discarded and the product was further washed in diethyl ether. The final product was dried under vacuum for further use.

Block copolymers of PEO-*b*-PCCL were synthesized by catalytic debenzylation of PEO-*b*-PBCL in the presence of H_2 to obtain PEO-*b*-PCCL according to a method described previously with slight modifications.⁴³ Briefly, a solution of PEO-*b*-PBCL (1 g in 50 mL dry THF) was placed into a cylindrical flask. Palladium on charcoal (300 mg) was dispersed in the solution. The mixture was stirred vigorously with a magnetic stirrer under the continuous

flow of hydrogen gas at 0.2 L/min for 6 - 16 hrs (depending on degree of polymerization of PBCL block) at room temperature. The reaction mixture was centrifuged at 3000 rpm to remove the catalyst. The supernatant was collected, condensed under reduced pressure and precipitated in diethyl ether. The final product was dried under vacuum for further use.

2.2.4 Characterization of Synthesized Block Copolymers and Preparation of Micelles

The number-average molecular weight of PEO-*b*-PCL, PEO-*b*-PBCL, and PEO-*b*-PCCL block copolymers was determined from the ¹H NMR spectrum of the block copolymers in CDCl₃ at 600 MHz (Bruker Avance III spectrometer, Bruker BioSpin Corporation, Billerica, MA) by comparing the peak intensity of PEO (-CH₂CH₂O-, δ = 3.65 ppm) to that of PCL, PBCL, or PCCL backbone (-OCH₂-, δ = 4.05 ppm), considering a 5000 g/mol molecular weight for PEO.

The polydispersity of the synthesized polymers was assessed by gel permeation chromatography (GPC). Briefly, 20 μ L of polymer solution (10 mg/mL in THF) was manually injected into a 7.8 \times 300 mm Styragel HT3 column (Waters Inc., Milford, MA) heated to 35 $^{\circ}$ C which was attached to a Shimadzu LC-10AD HPLC pump (Shimadzu Corp., Kyoto, Japan). The column was eluted with THF (1 mL/min). The elution pattern was detected by refractive index and viscometry detectors (Viscotek TDA 305, Malvern Instruments Ltd., Malvern, Worcestershire, UK) using the OmniSEC 4.7 software (Malvern Instruments Ltd., Malvern, Worcestershire, UK). The polydispersity of the polymers was determined using universal calibration which was accomplished with PEO standards with molar masses ranging from 1400 to 24500 g/mol.

Micellization of PEO-*b*-PCL, PEO-*b*-PBCL, and PEO-*b*-PCCL block copolymers was achieved by a co-solvent evaporation method as described previously.^{43, 308} Briefly, the synthesized block copolymers of PEO-*b*-PCL, PEO-*b*-PBCL, or PEO-*b*-PCCL (50 mg) were dissolved in acetone (1 mL). This solution was added to 5 mL of deionized water in a drop-wise manner under moderate stirring at room temperature, followed by the evaporation of acetone under vacuum. The prepared micellar solution was then centrifuged to remove any aggregates.

The size and size distribution of micelles was measured by dynamic light scattering (DLS) using a commercial Zetasizer Nano-ZS (Malvern Instruments, Worcestershire, UK). All DLS measurements were made at 25.0 ± 0.1 °C with a 173° scattering angle. The samples were dissolved with deionized water and centrifuged prior to analysis. The morphology of the micelles was investigated by transmission electron microscopy (TEM) using a Morgagni TEM (Field Emission Inc., Hillsboro, OR) with Gatan digital camera (Gatan, Pleasanton, CA) according to a method described previously.³¹⁶ Briefly, an aqueous droplet of micellar solution (10 μL) with a polymer concentration of 1 mg/mL was placed on a copper-coated grid. The grid was held horizontally for 1 minute to allow the colloidal aggregates to settle, after which, the excess fluid was removed by filter paper. A drop of 2% solution of phototungstic acid (PTA) in PBS (pH 7) was then added to provide the negative stain. After 20 sec, the excess fluid was removed by filter paper. The samples were then air-dried and loaded into a Morgagni TEM (Field Emission Inc., Hillsboro, OR) with Gatan digital camera (Gatan, Pleasanton, CA). Images were obtained at a magnification of 110,000X at 75 kV. Size measurements were taken using the DigitalMicrograph™ software (Gatan, Pleasanton, CA).

2.2.5 Assessing the Physicochemical Stability of Polymeric Micelles

2.2.5.1 Measuring the critical micellar concentration (CMC) of block copolymers

The CMC of polymeric micelles was determined using the DLS technique according to a previously published procedure.³²¹ Briefly, micellar solutions of PEO-*b*-PCL, PEO-*b*-PBCL, and PEO-*b*-PCCL having concentrations ranging from 1000 - 0.24 $\mu\text{g/mL}$ were prepared in vials. The intensity of scattered light at 173° was measured by DLS in a polystyrene cell at 25°C .

2.2.5.2 Stability of micellar solutions against aggregation over time

Micellar solutions (15 mL) of PEO-*b*-PCL, PEO-*b*-PBCL, and PEO-*b*-PCCL having concentrations of 10 mg/mL were prepared in vials using phosphate buffer saline (PBS; pH 7.4) containing 0.01% (w/v) sodium azide which was added to prevent the growth of fungus and bacteria. The vials were kept at 37°C . Aliquots (2 mL) were withdrawn at predetermined intervals and analyzed for micellar size and size distribution by DLS as described in the previous section.

2.2.5.3 Stability of micelles against dissociation

Micelles were incubated with a destabilizing agent, sodium dodecyl sulfate (SDS) according to previously published methods.^{185, 322} Briefly, micellar solutions of PEO-*b*-PCL, PEO-*b*-PBCL, and PEO-*b*-PCCL having concentrations of 3 mg/mL were mixed with aqueous solution of SDS (20 mg/mL) at a ratio of 2:1 v/v. Samples were analyzed at

predetermined time intervals by DLS for intensity and volume distribution as well as polydispersity index (PDI).

2.2.5.4 Degradation of Polymeric Micelles

Degradation of PEO-*b*-PCL, PEO-*b*-PBCL, and PEO-*b*-PCCL micelles over time was measured using ^1H NMR. Briefly, micellar solutions (15 mL) of PEO-*b*-PCL, PEO-*b*-PBCL, and PEO-*b*-PCCL having concentrations of 10 mg/mL of polymer were prepared using PBS (pH 7.4) containing 0.01% (w/v) sodium azide (added to prevent the growth of bacteria). The vials were kept at 37 °C and aliquots (2 mL) were withdrawn at predetermined intervals and dialyzed (MWCO – 3.5 kDa) for 24 hrs against water, lyophilized, and then analyzed by ^1H NMR in CDCl_3 to determine the MWt of remaining polymer. The MWt of the remaining polymer was determined by comparing the peak intensity of PEO ($-\text{CH}_2\text{CH}_2\text{O}-$, $\delta = 3.65$ ppm) to that of PCL, PBCL, or PCCL backbone ($-\text{OCH}_2-$, $\delta = 4.05$ ppm), considering a 5000 g/mol molecular weight for PEO.

2.2.6 Evaluation of Protein Adsorption from Serum on Polymeric Micelles

For measurement of the level of protein adsorbed to the surface of micelles, a procedure involving GPC was used.¹⁴⁸ Briefly, micellar solutions (16 mg/mL) were mixed with equal volume of FBS solution and incubated for 4 h at 37 °C. Micellar solutions mixed with equal volume of PBS were used as control. After incubation, solution samples of 20 μL were injected into a GPC system with an Ultrahydrogel 2000 (7.8mm \times 300mm) column (Waters Inc., Milford, MA) at 25 °C. The elution pattern was detected at 35 °C by

differential refractometer detector (model 410, Waters Inc.). 0.01 M PBS (pH 7.4) (0.8 mL/min) was used as eluent. Eluate containing the micellar fraction was collected and the concentration of protein in the eluate was measured using the Bradford Protein assay kit at 595 nm (Bio-Rad, Hercules, CA).

2.2.7 Assessing the *in vitro* immunogenicity of polymeric micelles against BMDCs

BMDCs were generated from murine bone marrow precursors from femurs of C57Bl/6 mice in complete media in the presence of GM-CSF as described previously with minor modifications.³²³ Briefly, femurs of C57Bl/6 mice were removed and purified from surrounding tissue. Both ends of the intact bone were cut with scissors and the bone marrow was flushed with sterile PBS using an insulin syringe. Cells were triturated and filtered through a nylon screen (40 μ m cell strainer) to obtain a single cell suspension. Cells were washed and 2×10^6 cells were seeded in 100 mm non-treated cell culture dishes with 10 mL DC complete medium (RPMI-1640 with penicillin-streptomycin-L-glutamine, 10 % heat-inactivated FBS) supplemented with 20 ng/mL of GM-CSF. At day 3, another 10 mL complete medium containing 20 ng/mL GM-CSF was added to the plates. At day 6, 10 mL of culture media was replaced with 10 mL fresh complete medium containing 20 ng/mL of GM-CSF. At day 7, cells can be used for experiment.

On day 7, BMDCs were treated with different micellar formulations (polymer concentration 50 μ g/mL). Untreated DCs were used as the negative control. For positive control, 100 ng/mL lipopolysaccharide (LPS) was added to the BMDCs. After 24 h treatment, cells were harvested and the supernatant was collected and stored in -20 °C until

further use. The cells were then washed twice with sterile PBS. Cell suspensions consisting of 5×10^5 cells/100 μ L were prepared in FACS buffer (PBS containing 2% FBS) and incubated with anti-CD86 with FITC-conjugated secondary antibody, or anti-CD40 with PE-Cy5-conjugated secondary antibody. The samples were acquired on a BD FACSCalibur™ flow cytometer (BD Biosciences, Franklin Lakes, NJ) and the data was analyzed with FCS Express™ software (De Novo Software, Los Angeles, CA). The previously collected supernatants were analyzed for the level of IL-12 by ELISA using the commercially available ELISA kits in a 96-well microplate using a microplate reader Powerwave with KC Junior Software (BioTek, Winooski, VT) at OD of 450 nm according to the manufacturer's directions. The minimum detection level of the cytokine was 15 pg/mL.

2.2.8 Statistical Analysis

Values are presented as mean \pm standard deviation (SD) of triple measurements. Statistical significance of difference was tested using unpaired Students' t-test or one-way ANOVA as indicated in the text. The level of significance was set at $\alpha = 0.05$.

2.3 Results

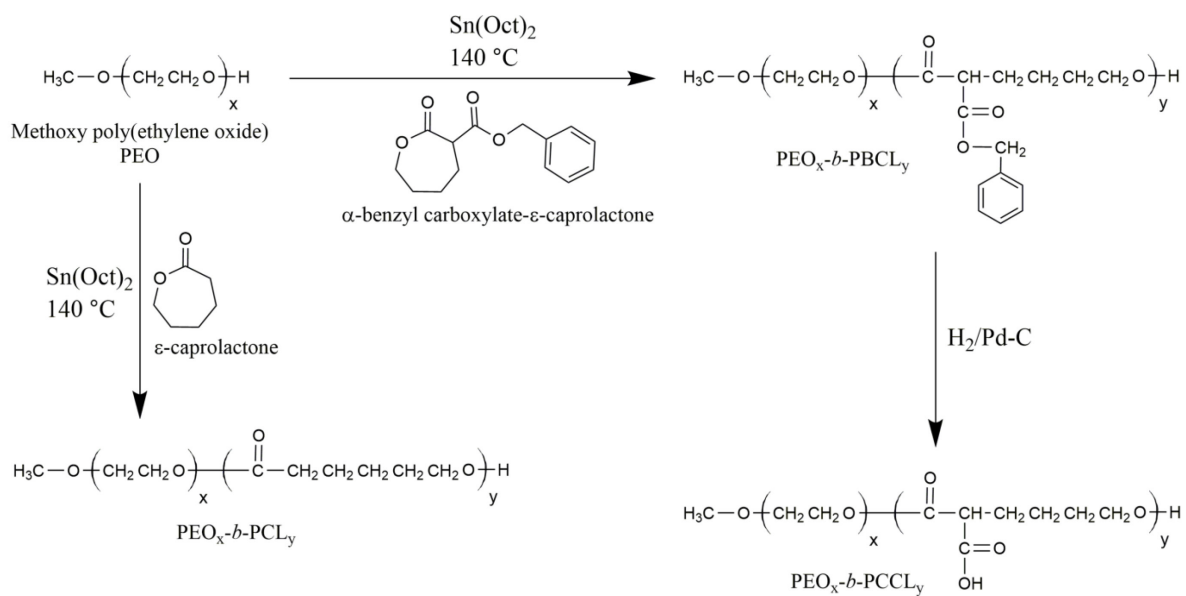
2.3.1 Synthesis and Characterization of Block Copolymers

The conversion of ϵ -caprolactone and α -benzyl carboxylate- ϵ -caprolactone monomers to their respective copolymers, i.e., PEO-*b*-PCL, and PEO-*b*-PBCL (Scheme 2.1, Figures 2.5 and 2.6), and catalytic hydrogenolysis of PEO-*b*-PBCL to PEO-*b*-PCCL (Scheme 2.1, Figures 2.7) was analyzed and confirmed by ^1H NMR according to previously published

methods.^{43, 308} The polydispersity for PCL, PBCL, and PCCL containing block copolymers as calculated by GPC decreased with an increase in the degree of polymerization of the hydrophobic section of the block copolymer. The characteristics of synthesized polymers under study are summarized in Table 2.1.

2.3.2 Micellization of Block Copolymers

Synthesized block copolymers were assembled to polymeric micelles by a co-solvent evaporation method as described previously.^{43, 308} The characteristics of prepared polymeric micelles in terms of average size and size distribution are listed in Table 2.1. The average size of micelles formed from PCL, PBCL, and PCCL containing block copolymers increased with an increase in the degree of polymerization of the core-forming block in most cases, similar to previously documented results.³²⁴ The average polydispersity index (PDI) of micelles as measured by DLS for PCL, PBCL, and PCCL containing block copolymers decreased with an increase in the degree of polymerization of the hydrophobic section of the micelles in most cases.⁵⁵ All micelles showed spherical morphology with clear boundary as shown by TEM (Figure 2.1). In line with the DLS observations, TEM showed a similar trend in the size of polymeric micelles as a function of the degree of polymerization of hydrophobic blocks (Table 2.1). The difference in size measured by TEM and DLS was due to the acquirement of TEM images in a dry state as compared to DLS that measures the particles in a hydrated state in aqueous solutions.³¹⁶



Scheme 2.1 General synthesis scheme for the preparation of PEO-*b*-PCL, PEO-*b*-PBCL, and PEO-*b*-PCCL block copolymers.

Table 2.1 Characteristics of prepared block copolymers and block copolymer micelles

Block Copolymer ^a	Theoretical mol wt (g/mol)	M_n (g/mol) ^b	Polydispersity (M_w/M_n) ^c	Average micellar size \pm SD (nm) ^d	PDI \pm SD ^e	Average micellar Size \pm SD (nm) ^f	CMC \pm SD (μ M) ^g
PEO ₁₁₄ - <i>b</i> -PCL ₂₀	7500	7310	1.606	55.5 \pm 0.2	0.174 \pm 0.010	21.7 \pm 4.6	1.002 \pm 0.065
PEO ₁₁₄ - <i>b</i> -PCL ₄₂	10000	9790	1.573	78.9 \pm 0.5	0.129 \pm 0.010	28.3 \pm 4.0	0.427 \pm 0.027
PEO ₁₁₄ - <i>b</i> -PCL ₆₂	12500	12050	1.400	109.1 \pm 0.4	0.119 \pm 0.004	38.3 \pm 5.1	0.189 \pm 0.006
PEO ₁₁₄ - <i>b</i> -PCL ₇₉	15000	14060	1.230	120.4 \pm 1.6	0.120 \pm 0.008	52.5 \pm 3.7	0.096 \pm 0.017
PEO ₁₁₄ - <i>b</i> -PBCL ₁₉	10000	9700	2.171	52.8 \pm 0.3	0.169 \pm 0.002	23.3 \pm 6.0	0.258 \pm 0.002
PEO ₁₁₄ - <i>b</i> -PBCL ₃₁	13000	12590	1.966	53.9 \pm 0.6	0.172 \pm 0.003	31.7 \pm 7.0	0.077 \pm 0.000
PEO ₁₁₄ - <i>b</i> -PBCL ₅₈	21000	19300	1.732	86.1 \pm 0.8	0.111 \pm 0.005	48.3 \pm 9.1	0.043 \pm 0.004
PEO ₁₁₄ - <i>b</i> -PCCL ₁₉	8200	7990	1.938	54.4 \pm 1.1 (17.37 \pm 0.3; 14.3%) ^h	0.457 \pm 0.024	24.2 \pm 1.9	9.089 \pm 0.214
PEO ₁₁₄ - <i>b</i> -PCCL ₃₀	10100	9730	1.808	68.3 \pm 1.3	0.196 \pm 0.005	28.3 \pm 4.6	8.040 \pm 0.106
PEO ₁₁₄ - <i>b</i> -PCCL ₄₆	15200	12260	1.608	89.0 \pm 1.1	0.088 \pm 0.020	28.3 \pm 5.2	3.301 \pm 0.033

^a The number shown in the subscript indicates the polymerization degree of each block determined by ¹H NMR spectroscopy

^b Number-average molecular weight measured by ¹H NMR

^c Polydispersity index measured by GPC

^d Average micellar size estimated by the DLS technique ($n = 3$).

^e Average polydispersity index (PDI) of micellar size distribution ($n = 3$)

^f Average size estimated by TEM ($n = 6$)

^g Measured from the onset of rise in the intensity values of scattered light as a function of concentration of block copolymer ($n = 3$)

^h Numbers in parentheses indicate the size and frequency (%) of secondary peaks in micellar population.

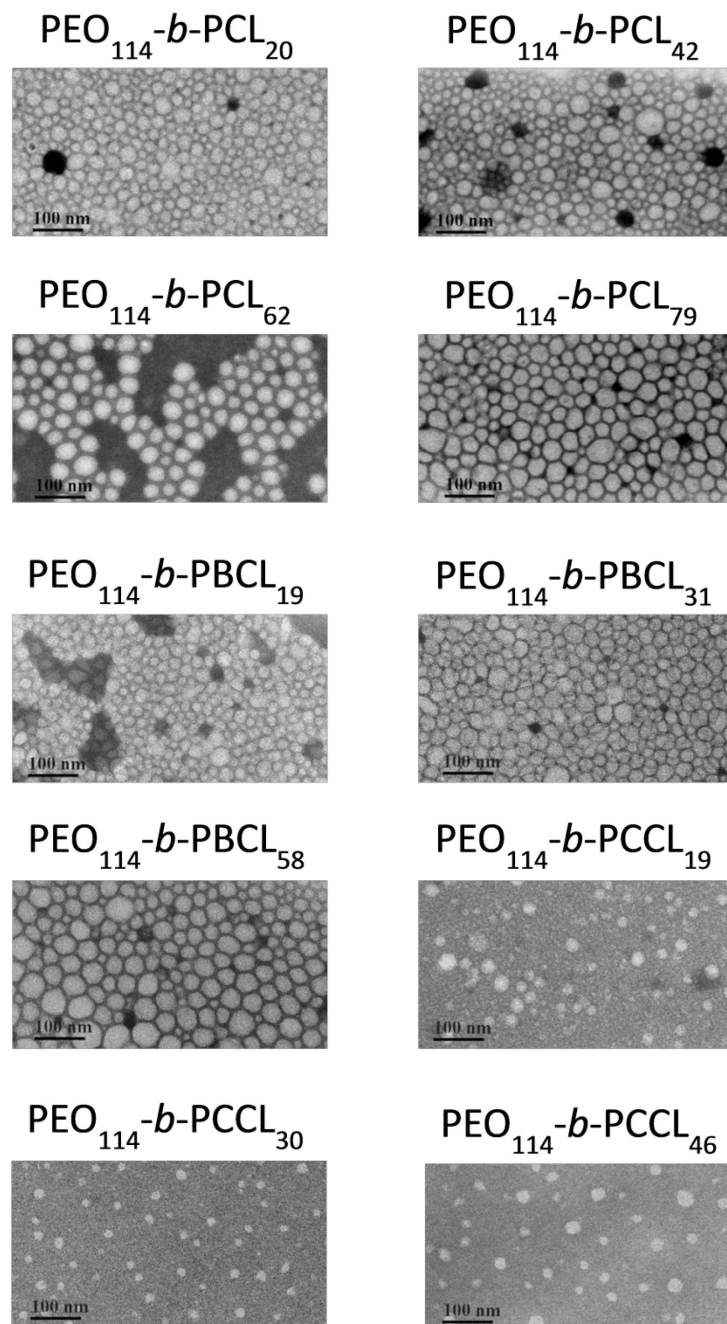


Figure 2.1 TEM picture of PEO-*b*-PCL, PEO-*b*-PBCL, and PEO-*b*-PCCL block copolymer micelles (110,000X). The bar in the bottom left corner of each image indicates a scale of 100 nm.

The CMC of all diblock copolymers was determined by DLS technique using the intensity values of scattered light as a function of block copolymer concentration.³²¹ In line with previous findings for other block copolymers, the average CMC of PCL, PBCL, and PCCL containing block copolymers decreased with an increase in the degree of polymerization of the core-forming block.^{43, 54} At similar degree of polymerization, PBCL containing block copolymers have shown lower CMC compared to PCL and PCCL containing block copolymers. For instance for a degree of polymerization of around 20 for the core forming block, the CMC was measured at 1.002, 0.258, and 9.089 μM for PEO-*b*-PCL, PEO-*b*-PBCL, and PEO-*b*-PCCL, respectively.

2.3.3 The Effect of Pendent Group on PCL on the Physical Stability of Polymeric Micelles

The average hydrodynamic diameter and polydispersity index of different micelles upon incubation in PBS solution (pH 7.4) at 37 °C was determined by DLS at specific time intervals over a period of 100 days (Figure 2.2). PEO₁₁₄-*b*-PCL₆₂, and PEO₁₁₄-*b*-PCL₇₉ showed no significant change in their average diameter during the first 60 days of incubation ($P > 0.05$; one-way ANOVA) followed by a slight but significant decrease in size on day 100 ($P < 0.05$) (Figure 2.2A). For PEO₁₁₄-*b*-PCL₂₀ micelles, there was a significant increase in the average size during the first 15 days of incubation ($P < 0.05$). This increase in average diameter coincided with the broadening of the micellar peak during the same time period (Figure 2.2A and 2.3A). Further increase in the average size and polydispersity of micelles (Figure 2.2A) at longer incubation times for this structure was due to the formation of

aggregates (Figure 2.3A). In contrast to PEO₁₁₄-*b*-PCL₂₀ micelles, PEO₁₁₄-*b*-PCL₆₂, and PEO₁₁₄-*b*-PCL₇₉ showed no change in polydispersity during the entire period of incubation ($P > 0.05$; one-way ANOVA) (Figure 2.2A). PEO₁₁₄-*b*-PCL₄₂ showed a significant increase in polydispersity ($P < 0.05$) (Figure 2.2A) and broadening of the micellar peak (Figure 2.3A) only on the 100 day incubation period, but were found to be stable before that.

In the case of PEO-*b*-PBCL micelles, no significant change in the average diameter of micelles was observed during the 100 days of incubation ($P > 0.05$) (Figure 2.2B). Only PEO-*b*-PBCL micelles of relatively short PBCL chain length, i.e. PEO₁₁₄-*b*-PBCL₁₉ micelles, showed a significant increase in their polydispersity ($P < 0.05$) on day 60 onwards (Figure 2.2B). This was attributed to the formation of few aggregates as seen in Figure 2.3B. PEO₁₁₄-*b*-PBCL₃₁ and PEO₁₁₄-*b*-PBCL₅₈, both showed stability in PDI and size distribution throughout the 100 days of incubation (Figure 2.2B and 2.3B, respectively).

In contrast, PEO₁₁₄-*b*-PCCL₁₉, and PEO₁₁₄-*b*-PCCL₃₀ failed to show readings on Day 15 and Day 30 of incubation (Figure 2.2C, 2.3C). PEO₁₁₄-*b*-PCCL₄₆ micelles, on the other hand, showed a single peak during the 30 days of incubation (Figure 2.3C) with no significant change in the average diameter ($P > 0.05$). (Figure 2.2C). Only an increase in the polydispersity of PEO₁₁₄-*b*-PCCL₄₆ micelles was seen within 30 day incubation. All PEO-*b*-PCCL micelles however, failed to show readings on day 60.

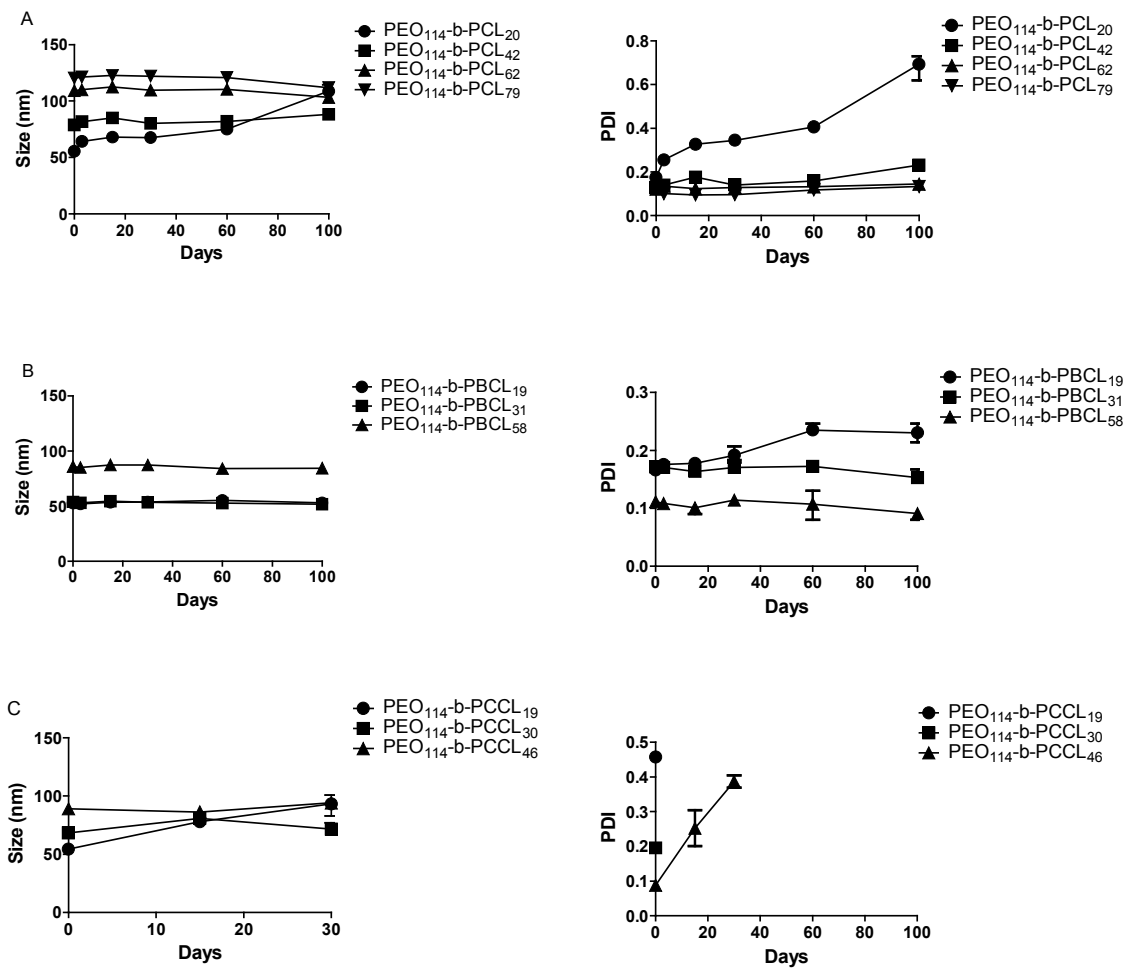


Figure 2.2 Average size (Z-average) and polydispersity index (PDI) changes of A) PEO-*b*-PCL, B) PEO-*b*-PBCL, and C) PEO-*b*-PCCL micelles as a function of time in PBS solution (pH 7.4) containing 0.01% (w/v) sodium azide. Each point represents mean \pm SD ($n = 3$).

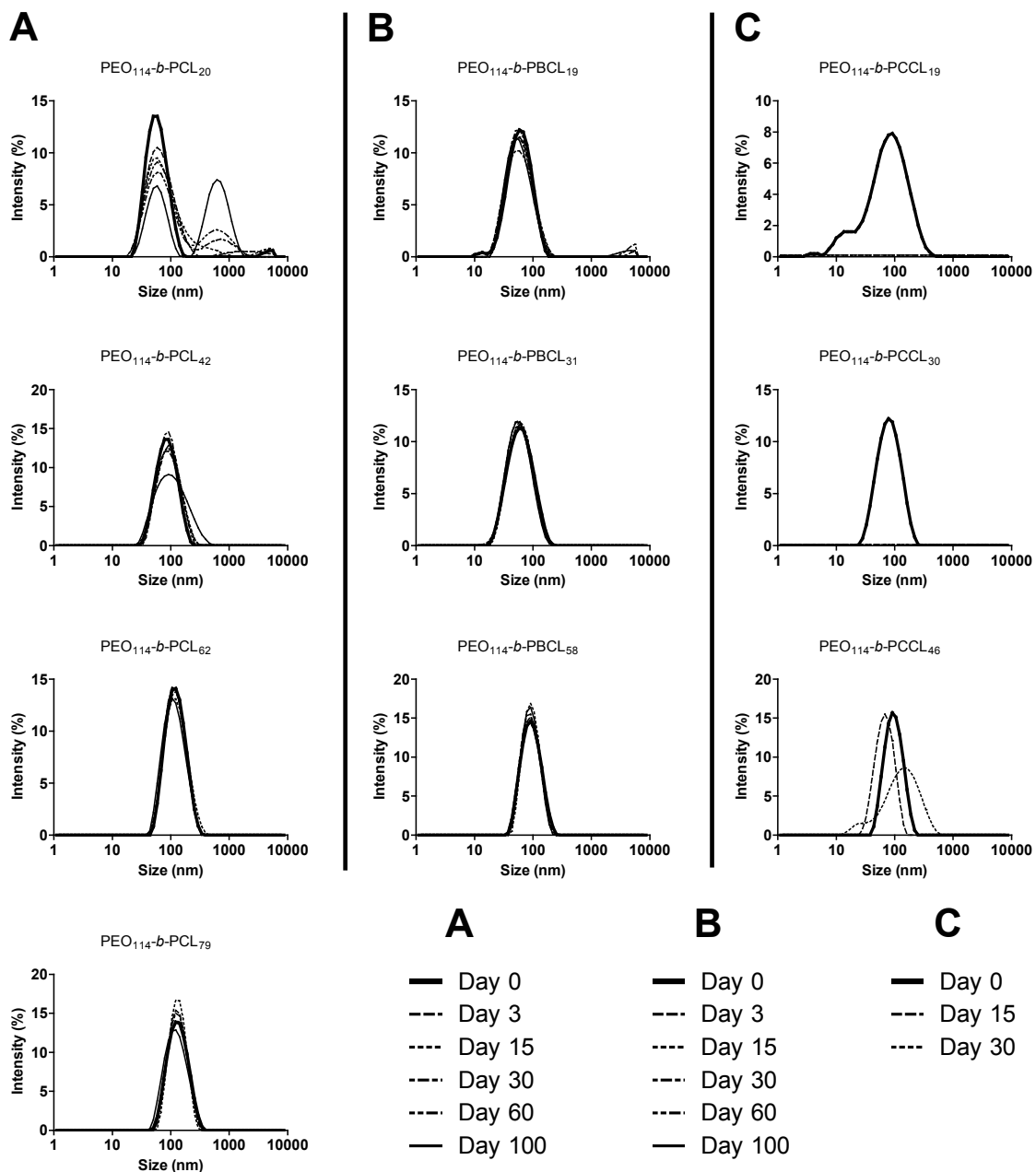


Figure 2.3 Intensity size distributions of A) PEO-*b*-PCL, B) PEO-*b*-PBCL, and C) PEO-*b*-PCCL micelles as a function of incubation time in PBS solution (pH 7.4) containing 0.01% (w/v) sodium azide.

The kinetic stability of micelles was studied using DLS after the addition of a destabilizing agent, SDS. Figure 2.4A shows the % intensity of the micellar peak for PEO-*b*-PCL micelles over time in the presence of SDS. PEO₁₁₄-*b*-PCL₂₀ showed a drastic decrease ($P < 0.05$) in the signal intensity of the micellar peak within 2 hrs of incubation after which the signal remained between 25-30 %. In the case of PEO₁₁₄-*b*-PCL₄₂ micelles, a significant decrease ($P < 0.05$) in signal intensity was seen within 6 hrs after which the signal remained around 65 %. PEO₁₁₄-*b*-PCL₆₂, and PEO₁₁₄-*b*-PCL₇₉, on the other hand, maintained a signal around 100 %. Hence, an increase in the degree of polymerization of the core forming block resulted in improved stability against SDS. These results are in line with the data shown for increase in PDI over time upon incubation with SDS (Figure 2.4A).

All PEO-*b*-PBCL micelles maintained a signal of 100 % throughout the incubation period (Figure 2.4B). As seen in Figure 2.4B, all PEO-*b*-PBCL micelles showed no significant change in PDI ($P > 0.05$) after addition of SDS for the entire period of incubation. However, in the case of PEO-*b*-PCCL micelles, the polymer micelles were completely destabilized after addition of SDS (Figure 2.4C; no PDI recorded).

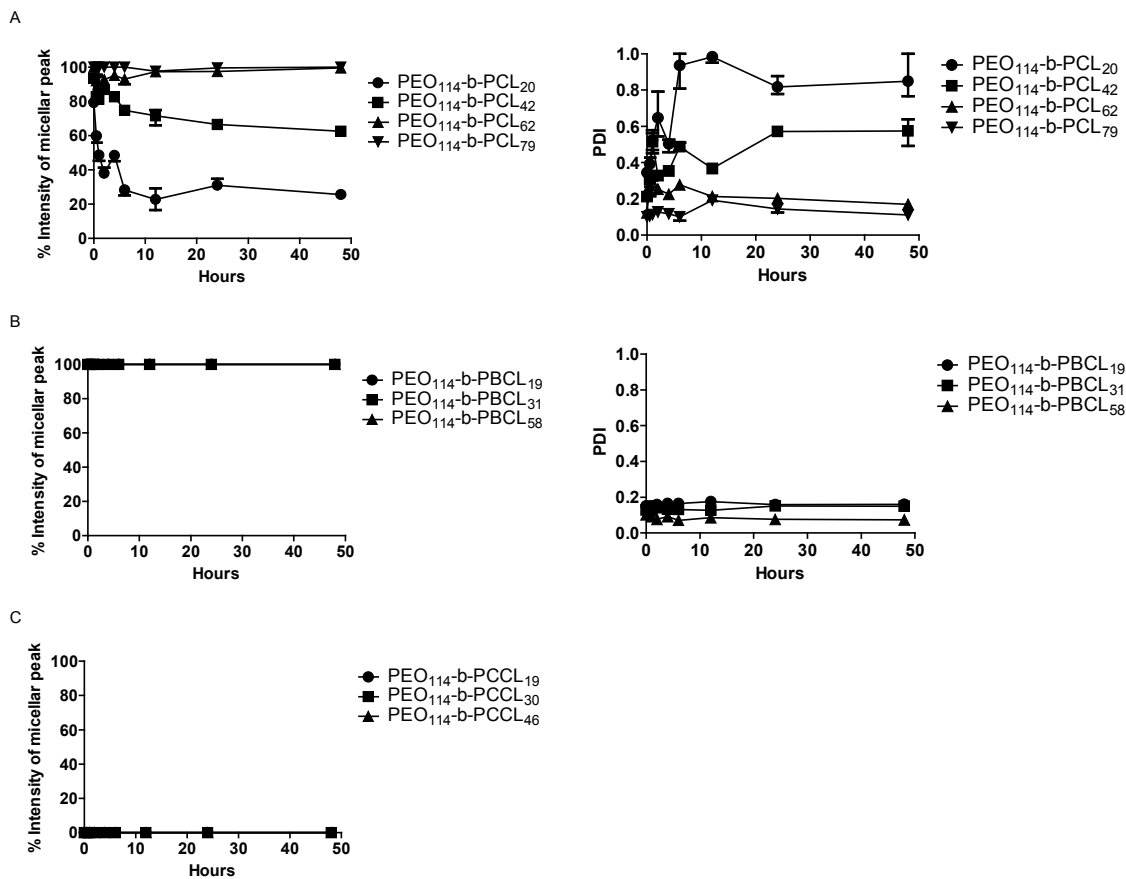


Figure 2.4 Percentage intensity and polydispersity index (PDI) of A) PEO-*b*-PCL, B) PEO-*b*-PBCL, and C) PEO-*b*-PCCL (no PDI data) micellar peak (2 mg/mL) as a function of time in the presence of SDS (6.7 mg/mL). Each point represents mean \pm SD ($n = 3$).

2.3.4 The Effect of Pendent Group Chemistry on the Hydrolytic Degradation of Polymeric Micelles

^1H NMR spectroscopy was used to characterize the chemical stability of polymeric micelles upon incubation in PBS. To remove the degradation products, the polymeric micelles incubated at different time periods with PBS were dialyzed against water first, freeze-dried, dissolved in CDCl_3 and assessed for their molecular weight by ^1H NMR spectroscopy. Core degradation was then estimated by calculating the molecular weight of the core forming block at different time intervals comparing characteristic peaks for PCL, PBCL, or PCCL to that of PEO and assuming a degree of polymerization of 114 for PEO during the study (MW = 5000 Da). A typical ^1H NMR spectra of $\text{PEO}_{114}\text{-}b\text{-PCL}_{42}$, $\text{PEO}_{114}\text{-}b\text{-PBCL}_{19}$, and $\text{PEO}_{114}\text{-}b\text{-PCCL}_{19}$ block copolymers in CDCl_3 , at the initial time-point and after 30 days of incubation of micelles in PBS following dialysis is shown in Figure 2.5, 2.6, and 2.7, respectively. The changes in the molecular weight of hydrophobic block for PEO-*b*-PCL, PEO-*b*-PBCL, and PEO-*b*-PCCL micelles at different incubation time periods is plotted in Figure 2.8. An increase in the ratio of the integration of the ethylene glycol related peak to the integration of peak related to the poly(ester) block indicates degradation of the poly(ester) block.⁴⁷ For all block copolymers under study, the molar ratio of PEO/hydrophobic block increased as incubation time progressed confirming the degradation of the poly(ester) block upon incubation of micelles in PBS. The kinetic of degradation was dependent on the structure of poly(ester) block. PEO-*b*-PCL micelles showed an initial decrease in molecular weight of core forming block from 100 % to 95 % in the first 3 days of incubation followed by slow degradation (2 %) in the later days. After 60 days of incubation,

micelles of PEO-*b*-PCL still maintained more than 90 % of their molecular weight. In the case of PEO-*b*-PBCL, two points of degradation are present (two ester bonds); one along the polymer backbone and the other along the ester bond on the α -benzyl carboxylate side chain. Using both points of degradation i.e. PEO-*b*-PBCL (backbone) and PEO-*b*-PBCL (side-group), an initial sharp loss of molecular weight in the first 3 days of incubation followed by slow degradation in later days was observed. Similar to PEO-*b*-PCL polymers, PEO-*b*-PBCL polymers maintained more than 90% of their molecular weight after 60 days. For both PEO-*b*-PCL and PEO-*b*-PBCL, an increase in the degree of polymerization of the hydrophobic block resulted in a decrease in their degradation rate.

PEO-*b*-PCCL micelles showed faster degradation of the core as compared to PEO-*b*-PCL and PEO-*b*-PBCL micelles. PEO₁₁₄-*b*-PCCL₁₉, PEO₁₁₄-*b*-PCCL₃₀, and PEO₁₁₄-*b*-PCCL₄₆ showed 57.1, 73.2, and 86.6 % degradation of the core, respectively, within 30 days of incubation in PBS (pH 7.4) at 37 °C. In contrast to PEO-*b*-PCL and PEO-*b*-PBCL micelles, for PEO-*b*-PCCL micelles, the rate of degradation increased with an increase in the degree of polymerization of the core, due to the increase in the number of free COOH groups on PCCL.

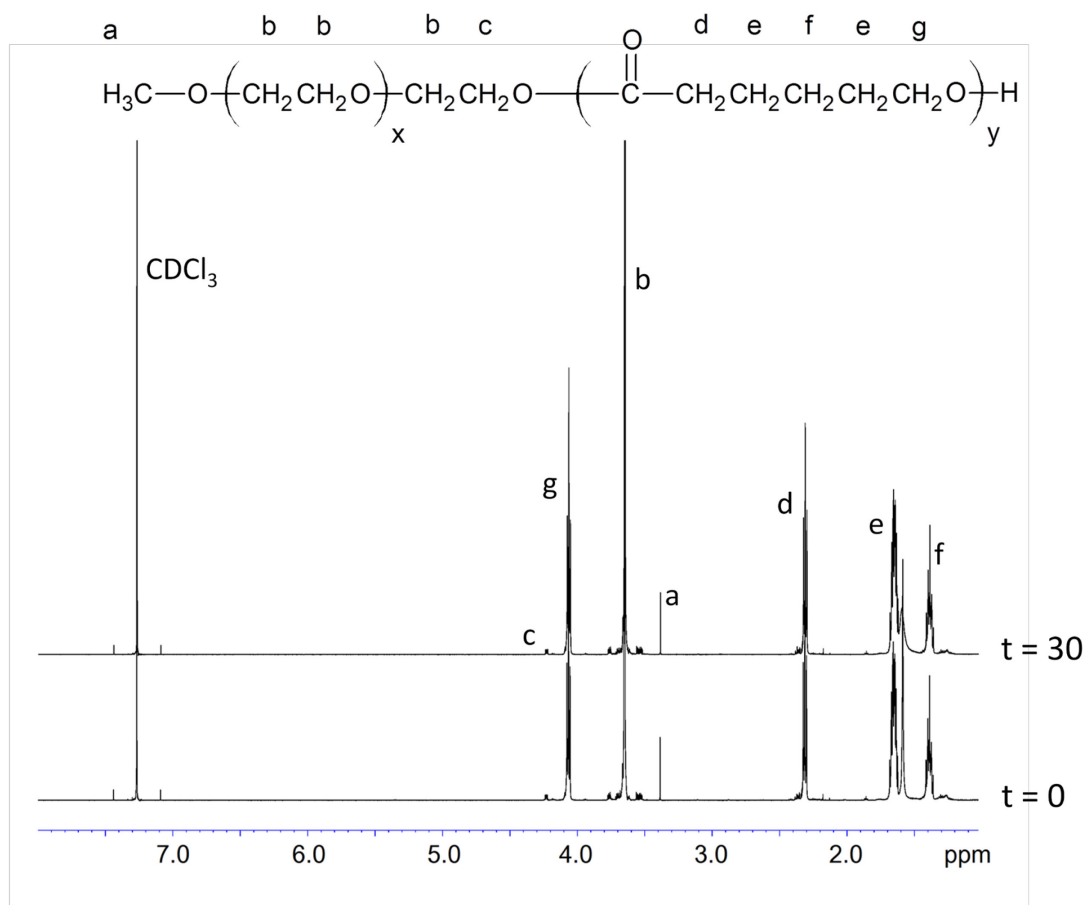


Figure 2.5 ^1H NMR spectrum of $\text{PEO}_{114}\text{-}b\text{-PCL}_{42}$ block copolymer in CDCl_3 and peak assignments. Core degradation is calculated by finding the molecular weight at different time intervals by measuring the integration of peak (b) for PEO and peak (g) for PCL assuming a degree of polymerization of 114 for PEO.

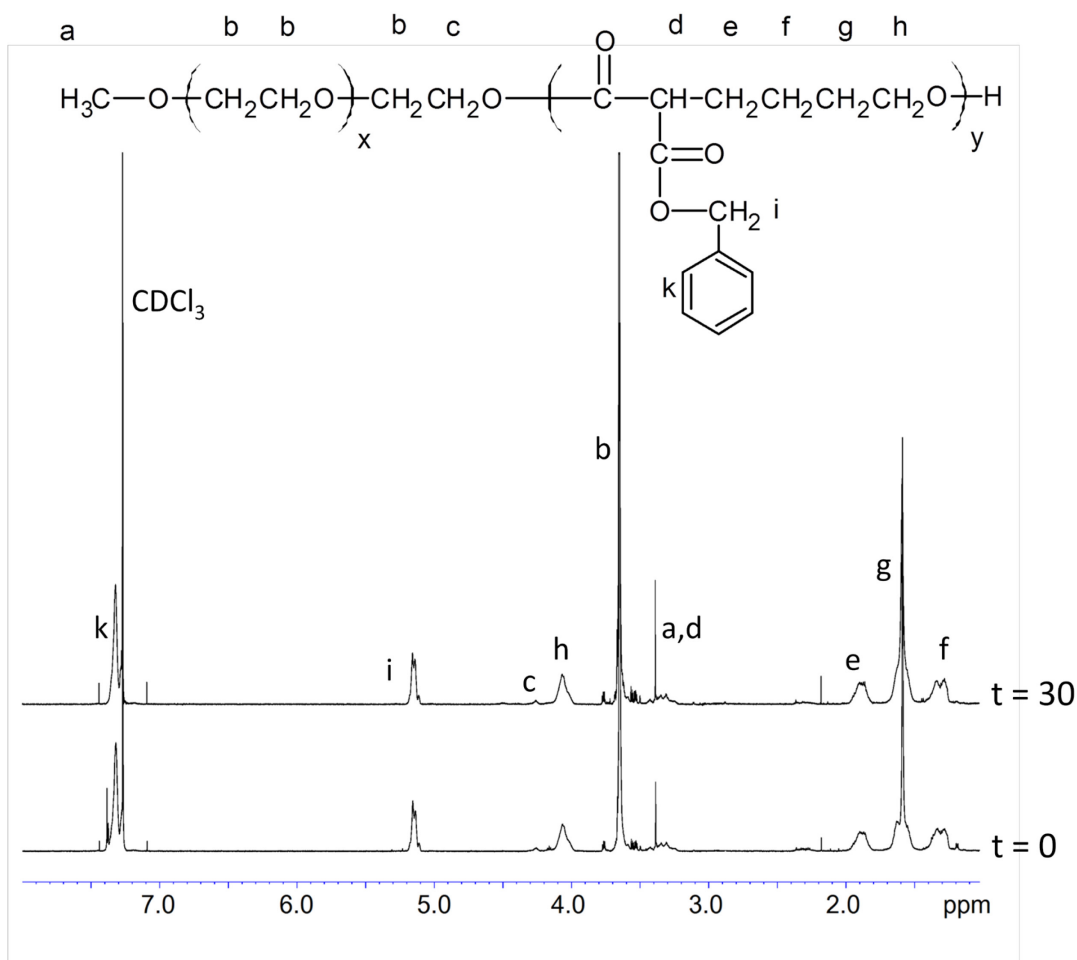


Figure 2.6 ^1H NMR spectrum of $\text{PEO}_{114}\text{-}b\text{-PBCL}_{19}$ block copolymer in CDCl_3 and peak assignments. Core degradation is calculated by finding the molecular weight at different time intervals by measuring the integration of peak (b) for PEO and peak (h) for PBCL back-bone or peak (i) for PBCL side-group assuming a degree of polymerization of 114 for PEO.

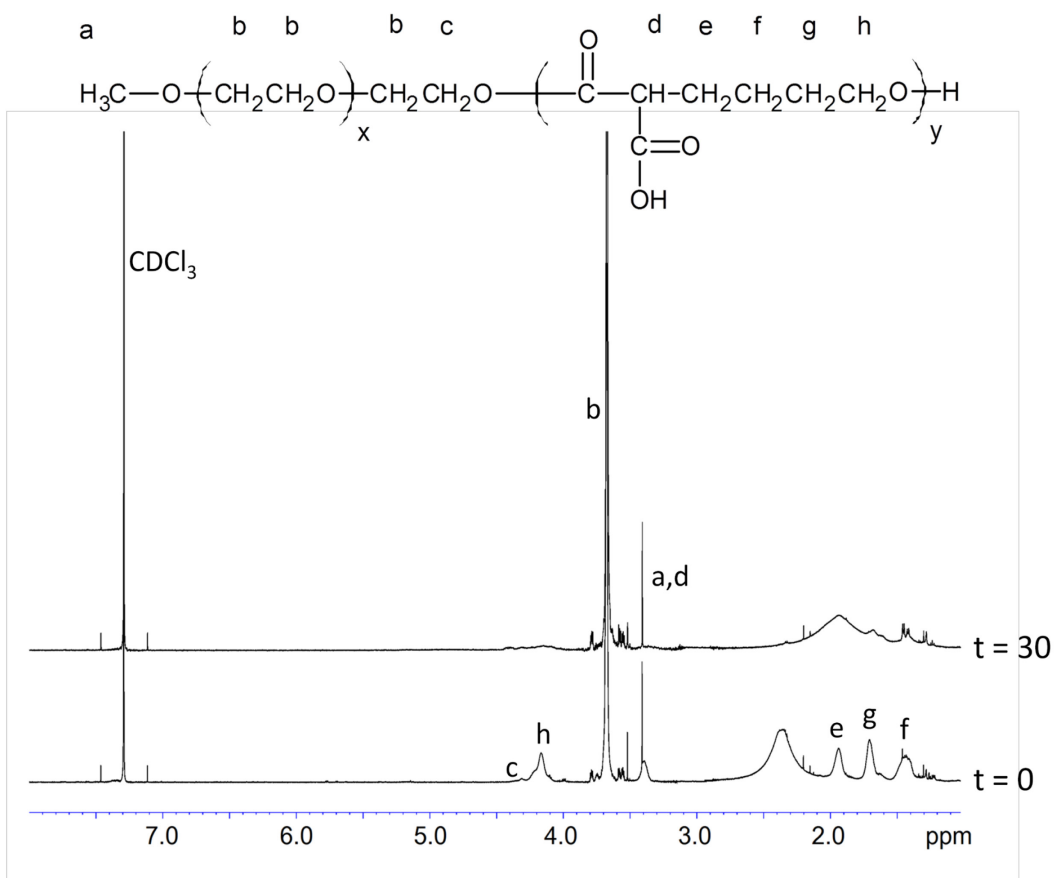


Figure 2.7 ^1H NMR spectrum of $\text{PEO}_{114}\text{-}b\text{-PCCL}_{19}$ block copolymer in CDCl_3 and peak assignments. Core degradation is calculated by finding the molecular weight at different time intervals by measuring the integration of peak (b) for PEO and peak (h) for PCCL assuming a degree of polymerization of 114 for PEO.

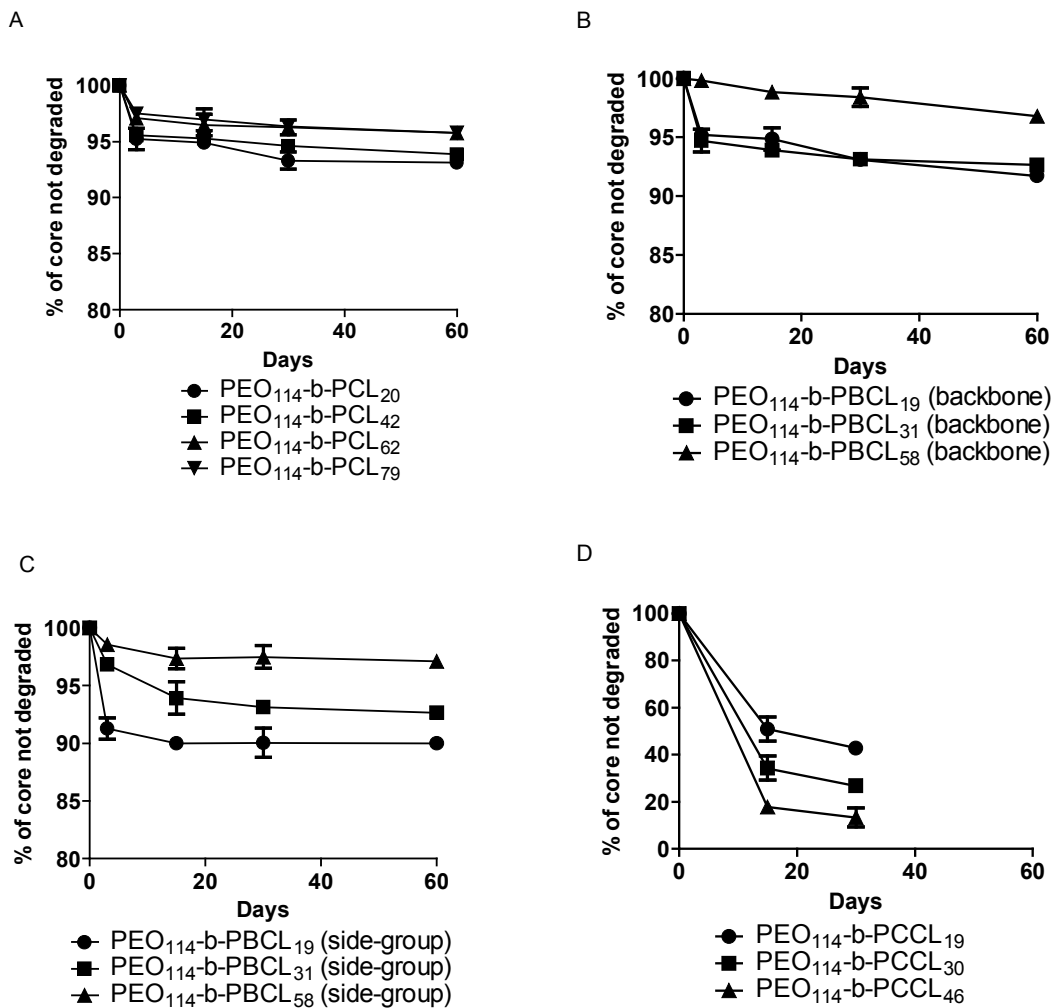


Figure 2.8 Degradation of the core of A) PEO-*b*-PCL, B) PEO-*b*-PBCL (backbone), C) PEO-*b*-PBCL (side-group), and D) PEO-*b*-PCCL micelles incubated in PBS solution (pH 7.4) at 37 °C as a function of time by ¹H NMR. Each point represents mean ± SD (*n* = 3). (y-axis scale for A, B, and C is from 80 - 100 % whereas for D it is 0 - 100 %).

2.3.5 The Effect of Micellar Core Structure on Serum Protein Adsorption

The extent of protein adsorbed on the surface of the micelles after incubation with FBS was measured by Bradford protein assay after separation of protein adsorbed micelles from free protein by GPC.^{145, 148} Micelles were found to elute from the column at 6-10 min. The elution time of FBS was found to be between 12-18 min. No free protein was detectable between 6-10 min. Hence, any protein detected in the micellar eluate would be due to the protein closely associated with or adsorbed on the surface of the micelles. After incubation for 4 h with FBS, there was no change in the size of the micelles when measured with DLS (data not shown). Also, the elution peak for the micelles remained the same. Overall, all micelles showed insignificant adsorption of protein suggesting that the hydrophilic PEO shell provides sufficient coverage of the hydrophobic core of the micelles (Figure 2.9). Within this low protein binding range, some micelles showed significantly higher protein adsorption compared to others. For instance, protein binding on micelles significantly increased ($P < 0.05$; one-way ANOVA) with an increase in the degree of polymerization of the hydrophobic core forming block. On the other hand, micelles formed from PEO-*b*-PBCL showed higher protein adsorption than those from PEO-*b*-PCL, whereas, micelles formed from PEO-*b*-PCCL showed extremely less protein adsorption as compared to both PEO-*b*-PCL and PEO-*b*-PBCL. This could be due to lower coverage of the micellar core or interface by the specific molecular weight of PEG applied here.

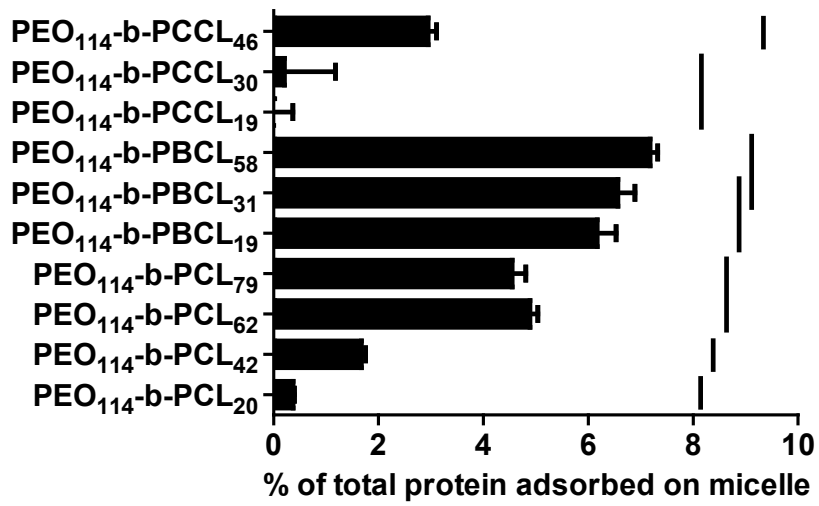


Figure 2.9 Percentage of total protein adsorbed on PEO-*b*-PCL, PEO-*b*-PBCL, and PEO-*b*-PCCL micelles after incubation in FBS for 4 hrs. Each bar is mean \pm SD ($n = 3$). Each single row of lines above the bar indicates bars with no significant difference. Lines in different rows show significant difference between the bars ($P < 0.05$; one-way ANOVA (Tukey's multiple comparison test)).

2.3.6 Assessing the *In Vitro* BMDC Mediated Immunogenicity of Polymeric Micelles

Micelles were incubated with BMDCs and flow cytometry was employed to detect the surface maturation markers CD40 and CD86 on BMDCs as a measure of immunogenicity.^{318, 319} LPS was used as positive control to induce DC maturation whereas untreated DCs were used as the negative control. Up-regulation of surface maturation markers was considered notable only when the treatment group induced a statistically significant ($P < 0.05$) and biologically substantial ($> 30\%$) increase in the CD40/CD86 % positive DCs above the untreated group.³²⁵ Figure 2.10 represents the regulation of the two phenotypes with their % positive cell values among different groups. It can be seen that the LPS treated DCs showed significantly higher ($P < 0.05$; one-way ANOVA) and biologically substantial ($> 30\%$) expression of CD40/CD86 % positive cells than the negative control and micelle groups. From different micellar groups, none have shown significantly higher ($P < 0.05$; one-way ANOVA) or biologically substantial ($> 30\%$) percentage of CD40/CD86 positive DCs after treatment compared to the untreated group (Figure 2.10A and 2.10B). Secretion of IL-12 was also tested in the DCs supernatant using ELISA kit (Figure 2.10C). Similar to previous results, secretion of IL-12 by LPS treated DCs was significantly higher ($P < 0.05$) and biologically substantial ($> 30\%$) compared to the untreated DCs.³²⁵ This was not the case with all PEO-*b*-PCL, PEO-*b*-PBCL, and PEO-*b*-PCCL micelles which showed IL-12 secretion levels below the detection level of the kit.

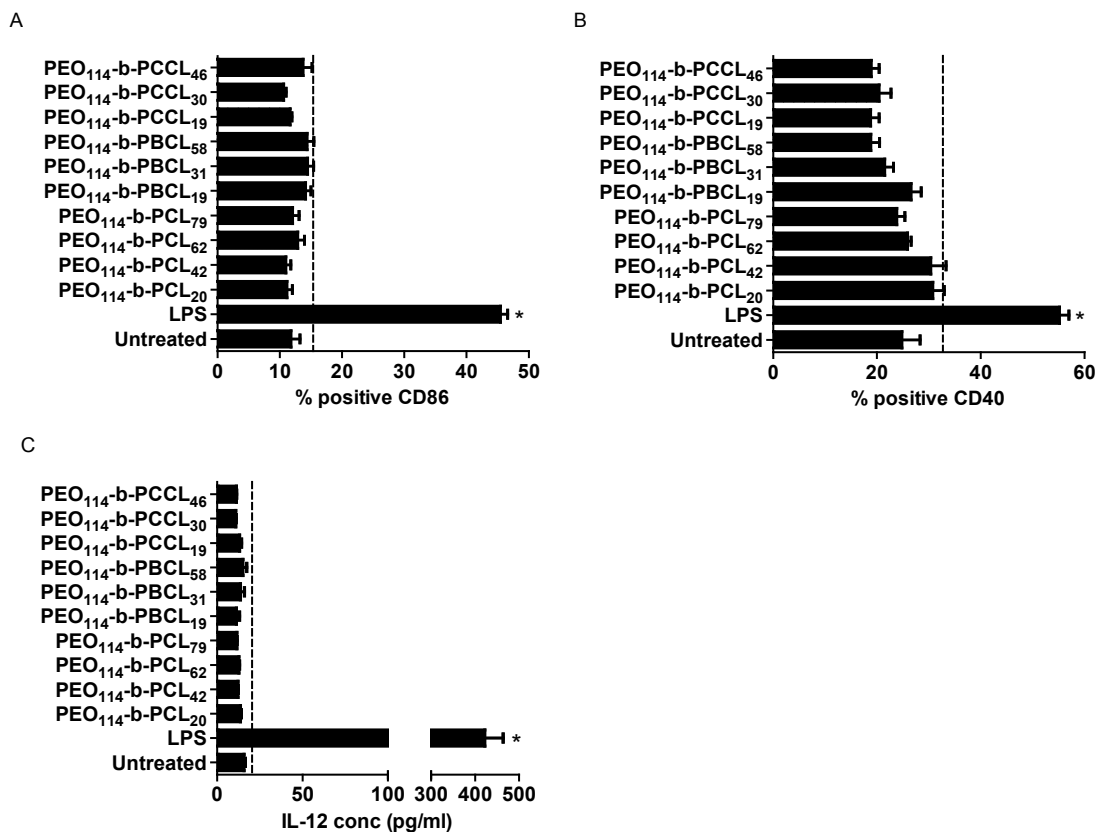


Figure 2.10 Immunogenicity of micelles measured in terms of promoting the phenotype maturation and cytokine secretion by DCs. A) DCs examined for % CD86 and B) % CD40 surface marker expression after treating them with different micellar groups. C) DC supernatants examined for IL-12 secretion (pg/mL) after treating them with different micellar groups. Each bar is mean \pm SD ($n = 3$). Broken line indicates the reading at 30 % above the untreated group. '*' indicates bar(s) which are statistically significant ($P < 0.05$; one-way ANOVA; Tukey's multiple comparison test) from the untreated group.

2.4 Discussion

The PEO-*b*-PCLs are one of the most highly researched block copolymers as self-associating vehicles for drug delivery applications.^{1, 326, 327} Our research group has reported on the synthesis of derivatives of PEO-*b*-PCL with pendent functional groups on the PCL block that may provide structurally flexible and biodegradable means for nano-drug and gene delivery.^{1, 43, 139, 316} The main objective of this study was to investigate the effect of the chemistry of the core-forming PCL based block on the physicochemical and biological stability of micellar carrier under *in vitro* conditions mimicking that of *in vivo* environment upon micellar intravenous administration. To this end, a series of diblock copolymers composed of PEO as the shell forming block and, either PCL, PCL containing pendent benzyl carboxylate, or pendent carboxyl groups, as the core forming block were synthesized. The degree of polymerization of the core-forming block was varied in all three structures. The effect of the polymerization degree of the core-forming block as well as the chemistry of the pendent group on the physicochemical and biological stability of self-associated structures was assessed in the next step. In general, an increase in the hydrophobicity of the core-forming block was shown to enhance the physicochemical stability of formed polymeric micelles resulting in a reduction in CMC, micellar aggregation, dissociation and hydrolytic degradation rate. This was evident by analyzing the results with respect to changes in two factors in the structure of micelle-forming block copolymers: chemical structure of the pendent group and degree of polymerization of the PCL backbone.

A change in the chemistry of the pendent group on PCL to more hydrophobic structures was proved to have a stabilizing effect on the physicochemical characteristics of resulting polymeric micelles. In the case of PEO-*b*-PBCL, the presence of aromatic groups

on the PCL block was more effective in decreasing the CMC, than increasing the degree of polymerization. This may be due to the presence of other intermolecular interactions in the core, such as π - π stacking interactions between benzyl groups in the micellar core.^{43, 54} Among different micelles under study, the ones formed from PEO-*b*-PCCL, i.e., polymers with hydrophilic carboxyl pendent groups, were found to be the least stable ones. PEO₁₁₄-*b*-PCCL₄₆ micelles started showing higher polydispersity by day 30 of incubation whereas PEO₁₁₄-*b*-PCCL₁₉ and PEO₁₁₄-*b*-PCCL₃₀ micelles were found to dissociate completely within day 15 of incubation in buffer. The dissociation of PEO₁₁₄-*b*-PCCL₁₉ and PEO₁₁₄-*b*-PCCL₃₀ micelles can be due to the rapid degradation of the core imposed by the introduction of hydrophilic carboxyl groups within the micellar core. On the other hand, at the tested pH of 7.4, the COOH groups on the PCCL backbone are expected to be partially ionized. This can lead to repulsive forces between similarly charged COO⁻ groups, enforcing micellar dissociation. For the PEO₁₁₄-*b*-PCCL₄₆ micelles, the apparent increase in average PDI may reflect the swelling of micelles at 30 day incubation period and initiation of the micellar dissociation process at a later time point compared to PEO₁₁₄-*b*-PCCL₁₉ and PEO₁₁₄-*b*-PCCL₃₀ micelles. Micellar swelling can be attributed to the water attraction by COOH groups within the micellar core and/or repulsion of partially ionized carboxyl groups, i.e., COO⁻, formed following buffer penetration to the micellar core (Figure 2.8).^{45, 55} Introduction of COOH groups to the PCL core led to a decrease in the thermodynamic stability of the micelles as measured by the CMC, as well. The significant increase in CMC can be attributed to the substitution of hydrophilic groups in the core-forming block thus leading to a lower tendency for micellar self-association.⁴³ Introduction of hydrophilic carboxyl groups to the PCL core also led to a decrease in the kinetic stability as measured by

an increase in dissociation rate of micelles when incubated with SDS solutions. SDS has the ability to destabilize micelles as well as suppress the formation of micelles. The hydrophobic tail of SDS can be adsorbed onto the hydrophobic block of the micelles. Electrostatic repulsions between the charged anionic heads of SDS can lead to the dissociation of micelles in the system.³²⁸ Another mechanism is that the SDS can interact with the hydrophobic and hydrophilic groups of the block copolymer unimers to form charged complexes thereby depleting the copolymer unimers in the system. This would shift the unimer \leftrightarrow micelle equilibrium to the left thus increasing the CMC and destabilizing and suppressing the formation of micelles.³²⁹ Inclusion of COOH groups in the poly(ester) structure in PCCL also increased the degradation rate of this segment. The PCL and PBCL blocks have shown comparable degradation rate at the time frame and conditions of the study.

An increase in the degree of polymerization of the core forming block in case of PEO-*b*-PBCL and PEO-*b*-PCL led to an increase in the stability of self-associated structures. This is seen from the results that as the degree of polymerization of the core increases, the CMC decreases.⁵⁴ This can lead to a lower concentration of unimers that can bridge between the micellar structures in the solution. An increase in the degree of polymerization of the core forming block resulted in improved stability after addition of SDS reflecting a better resistance against dissociation for those micelles. Similar results were found by Leroux *et al.*³²² It should be noted however, that the encapsulation of a drug into the micelles can change the thermodynamic and kinetic stability of the micelles depending on the physicochemical properties of the drug.

Previous reports have proposed two stage degradation mechanisms for PEO-*b*-poly(ester) micelles with slow interfacial erosion first occurring at the core-shell interface

known as the swelling effect. During this stage, some of the degraded poly(ester) fragments cannot diffuse through into the aqueous phase thus maintaining the integrity of the micelles. This was followed by formation of caves and channels which leads to rapid degradation in the core in the second stage.^{45, 55} For PEO-*b*-PCL micelles, hydrolytic degradation via hydrolysis of the ester bonds has been studied extensively and has been reported to be the major route of degradation for poly(ester)s including PCL.^{36, 45, 47, 55, 57} In our study, PEO-*b*-PCL and PEO-*b*-PBCL micelles maintained their size integrity over the 100 days of incubation similar to first stage of degradation. According to previously published paper,³³⁰ a chemical shift of 4.23 ppm in the ¹H NMR for PEO-*b*-PCL is for the CH₂ group of the PEG at the interface indicating that it is connected to the hydrophilic - hydrophobic interface ester group. In our study, the peak intensity of this group remained constant during the time of the study for both PEO-*b*-PCL and PEO-*b*-PBCL (Figure S4 and S5) indicating that the micelles were still in their first stage of degradation. Hence, from the results of our ¹H NMR data on degradation, it seems that both PEO-*b*-PCL and PEO-*b*-PBCL micelles did not reach the second stage of degradation during the incubation period. In contrast, PEO-*b*-PCCL micelles showed rapid degradation of core and loss of integrity of micelles during the incubation period.

The degradation study for PEO-*b*-PCL and PEO-*b*-PBCL showed micelles with higher degree of polymerization to have slower degradation. This might also be due to the fact that by increasing the block length, the total hydrophobicity of the micelle itself should increase which would make it difficult for water to penetrate the core of the micelles. However, in the case of PEO-*b*-PCCL micelles, increasing the degree of polymerization of

the core led to higher degradation rate which is due to the higher number of –COOH groups leading to accelerated hydrolysis.

The biological stability of polymeric micelles in terms of protein adsorption decreased as a result of increase in the hydrophobicity of the core-forming block. Interaction with serum proteins is one of the factors that influence the fate of drug delivery vehicles like liposomes,¹⁵⁹ nanoparticles,³³¹ and micelles¹⁴⁸ in the body. Different techniques were employed to study the interaction of protein with micelles. Previous studies^{160, 161, 317} have been carried out using bovine serum albumin (BSA) as a model protein. Although albumin is the most abundant protein in the plasma, there are other proteins which can cause increased adsorption and can affect the stability of micellar systems in the plasma. Hence, in this manuscript interaction of protein with micelles was studied in the presence of serum (FBS). In general, protein adsorption showed an increasing trend as the hydrophobicity of the block copolymer increased^{44, 156} which may be due to the fact that as the molecular weight and hydrophobicity of the core is increased, the PEO chain is unable to provide complete coverage of the core. Another explanation to this phenomenon was provided by D'Addio *et al.*,³³² who stated that a lower MW hydrophobic block (or less bulky ones) will occupy a smaller surface area at the hydrophobic interface resulting in a more compressed, dense PEG layer, thus, providing better protection.

Finally, the effect of core-forming block in PEO-*b*-PCL based block copolymers on their *in vitro* DC mediated immunogenicity was assessed. DCs are best known for their roles in host resistance and immunogenicity. They are the most professional antigen presenting cells (APCs) and are the ‘sentries’ of the body. DCs initiate an immune response which is associated with their maturation, migration, and communication with other immune

cells. Located in most of the tissues, immature DCs capture and process foreign antigens leading to their maturation which is followed by release of various cytokines and upregulation of various factors. Upregulation of both CD40 and CD86 markers greatly enhances the antigen presenting capabilities of DCs and their ability to activate T cells. Also, mature DCs release large amounts of cytokines like IL-12 which can stimulate a Th1 response.^{205, 257, 318} Bacterial products like LPS are pathogenic and are used as positive controls to stimulate the maturation of DCs.^{318, 319, 333} From the results, it can be seen that all the micelles show similar upregulation of CD40, and CD86 and secretion of IL-12 when compared with untreated DCs. However, this level was statistically and biologically not significant when compared with untreated DCs. Hence, we can conclude that all the micellar groups had no significant immune activity and have a good biocompatibility with DCs after 24 hrs incubation.

2.5 Conclusion

The chemical structure of the core forming block in polymeric micelles formed based on functionalized PCL cores was found to affect the physicochemical and biological stability of polymeric micelles significantly. Polymeric micelles with free carboxyl groups on the PCL core (abbreviated as PEO-*b*-PCCL here) showed decreased thermodynamic and kinetic stability compared to the original PEO-*b*-PCL, but adsorbed less serum proteins. On the other hand, polymeric micelles formed from PEO-*b*-PBCL which contain a pendent benzyl carboxylate groups on PCL were found to be more stable than their PEO-*b*-PCL counterparts in terms of micellar dissociation, degradation and aggregation tendency, but adsorbed more proteins when exposed to serum. All block copolymers under study were found to be non-

immunogenic to DCs. In conclusion, the results indicate how modifications in the micellar core can be used as a tool in fine-tuning the physicochemical and biological stability of polymeric micelles.

2.6 Acknowledgements

This study was supported by a grant from the Natural Sciences and Engineering Research Council of Canada (NSERC). S.M.G. was supported by the Alberta Innovates Health Solutions Graduate Studentship, Alberta Cancer Foundation Graduate Studentship and the J.N. Tata Trust Scholarship. The authors thank Mr. Vishwanatha Somayaji, Faculty of Pharmacy and Pharmaceutical Sciences, University of Alberta for assistance with ^1H NMR analysis; the Flow Cytometry Lab in Department of Experimental Oncology at Cross Cancer Institute for assistance with flow cytometry; and the Advanced Microscopy Facility (AMF), Department of Biological Sciences, University of Alberta for assistance with TEM analysis.

Chapter Three

Traceable Polymeric Micelles for Breast Cancer Targeting

The data in this chapter will be submitted as a manuscript titled
Traceable Peptide Modified PEO-b-PCL based Micelles for Breast Cancer Targeting

**Shyam M. Garg¹, Mohammad Reza Vakili¹, Rania Soudy¹, Kate Agopsowicz³, Igor
Paiva¹, Amir Soleimani¹, Mary Hitt³, Kamaljit Kaur^{1,4}, Afsaneh Lavasanifar^{1,2}**

¹Faculty of Pharmacy and Pharmaceutical Sciences, University of Alberta, Edmonton, AB

²Department of Chemical and Materials Engineering, Faculty of Engineering, University of
Alberta, Edmonton, AB

³Department of Oncology, Faculty of Medicine and Dentistry, University of Alberta,
Edmonton, Alberta, Canada, T6E 2E1

⁴Chapman University School of Pharmacy (CUSP), Harry and Diane Rinker Health Science
Campus, Chapman University, Irvine, CA, 92618-1908, USA

3.1 Introduction

Breast cancer is the most common cancer in women worldwide.³³⁴ Traditional chemotherapy is still the treatment of choice for breast cancer. Chemotherapeutic agents are systemically administered without any means of restricting drug exposure to tumor cells. As a result, healthy tissues get equally exposed to the powerful chemo-toxic agents, leading to detrimental side effects in cancer patients. Side effects of chemotherapy will not only reduce the quality of life in cancer patients, but also force clinicians to use suboptimal doses of the drug leading to cancer reoccurrence. Targeted cancer therapy through the use of properly designed nanocarriers of conventional chemotherapeutics is suggested as an alternative approach to deliver sufficient amounts of chemotherapeutic drugs to tumors while minimizing drug exposure and damage to normal tissues.^{335, 336}

Proper design, development and optimization of nanocarrier structure for the purpose of tumor targeted drug delivery is a challenging and cumbersome task. In this context, development of traceable nanocarriers that can be imaged in live animals, is being pursued to facilitate the optimization of the nanocarrier structure for tumor targeted delivery. Such carriers can also be further developed for use in personalization of cancer therapy, detection of cancer progress and/or treatment monitoring in patients.^{101, 106}

Nanocarriers are believed to preferentially accumulate in solid tumors passively as a result of enhanced permeation and retention (EPR) effect in tumors. In this context, chemical modifications in the structure of nano-carrier leading to changes in their size, rate and extent of biological elimination, and/or uptake by non-target cells/tissue have been utilized to maximize the passive accumulation of nanocarriers in solid tumors.³³⁷⁻³³⁹ Furthermore, modification of the surface of a nanocarrier with a targeting ligand at an appropriate density

can be used to enhance the specific homing of nanocarriers and delivery of their cargo to tumor cells.^{102, 340}

Self-assembled nanostructures from poly(ethylene oxide)-*b*-poly(ester)s such as poly(ethylene oxide)-*b*-poly(ϵ -caprolactone) (PEO-*b*-PCL),³⁰⁸⁻³¹¹ poly(ethylene oxide)-*b*-poly(lactide) (PEO-*b*-PLA),^{312, 313} and poly(ethylene oxide)-*b*-poly(lactide-co-glycolide) (PEO-*b*-PLGA)^{122, 314} have been the subject of tremendous interest for drug solubilization and targeted drug delivery in cancer.³⁴¹ The increasing interest in the use of these structures is due to their biocompatibility, biodegradability and safe history of use in human.^{47, 315} Despite a long history of use in research and development as drug delivery systems, information on the effect of different structural features of PEO-*b*-poly(ester) based nanocarriers on their biodistribution and tumor targeting properties in live animals is limited.^{102, 105, 342, 343}

Previously our research group has reported on the development of novel PEO-*b*-poly(ester) based block copolymers through introduction of pendant benzyl carboxylate groups to the PCL segment of PEO-*b*-PCL leading to the production of PEO-*b*-poly(α -benzyl carboxylate- ϵ -caprolactone) (PEO-*b*-PBCL).⁴³ This modification was found to increase the kinetic and thermodynamic stability, and decrease the rate of degradation of polymeric micelles, *in vitro*.³⁰⁷ The effect of this modification on the *in vivo* fate of developed nanocarriers was unknown; however. The objective of this study was to develop traceable PEO-*b*-PCL and PEO-*b*-PBCL based nano-carriers through chemical conjugation of a near infrared dye (NIR) to their core-forming block for live imaging of nanocarriers in tumor bearing animal models. The NIR labeling provided means to assess the effect of nano-carrier core structure and shell modification with tumor targeting ligands on the extent and kinetics of nanocarrier tumor accumulation in an orthotopic breast cancer mouse model.

3.2 Experimental Section

3.2.1 Materials

Methoxy-polyethylene oxide (PEO) (average molecular weight of 5000 g/mol) and cholera toxin was purchased from Sigma (St. Louis, MO). ϵ -Caprolactone was purchased from Lancaster Synthesis (UK). α -Benzyl carboxylate- ϵ -caprolactone monomer was synthesized by Alberta Research Chemicals Inc (Edmonton, AB) according to a previously published procedure.⁴³ α -Propargyl carboxylate- ϵ -caprolactone (PCC) monomer was synthesized according to a previously published procedure.³¹⁶ Stannous octoate was purchased from MP Biomedicals Inc. (Germany). Cy5.5-azide was purchased from Lumiprobe (Hallandale Beach, FL). Cell culture media MEM, fetal bovine serum (FBS), sodium pyruvate, L-glutamine, non-essential amino acids, and penicillin-streptomycin-fungizone (Anti-Anti) were purchased from GIBCO, Life Technologies Inc. (Burlington, ON, Canada). MEGM media kit was purchased from Lonza (Basel, Switzerland). Peptide P18-4 was synthesized according to a previously published procedure.¹⁹² 2014S Teklad Global 14% protein rodent maintenance diet was purchased from Harlan Labs (Indianapolis, IN). Spectra/por dialysis tubing (MWCO - 3.5 kDa) was purchased from Spectrum Laboratories (Rancho Dominguez, CA). Dry toluene was prepared by refluxing under H_2SO_4 . All other chemicals were reagent grade.

3.2.2 Cell line

The luciferase expressing human breast cancer cell line MDA-MB-231 (clone D3H2LN) was purchased from Caliper Life Sciences (Woodbridge, ON, Canada). The

MDA-MB-231-luc-D3H2LN cells were grown in MEM media supplemented with 10% FBS, 1mM sodium pyruvate, 0.1 mM non-essential amino acids (NEAA), 2 mM L-glutamine, 100 IU/mL penicillin, 100 µg/mL streptomycin, and 0.25 µg/mL fungizone at 37 °C in 5% CO₂ atmosphere. The human mammary cell line MCF10A was purchased from ATCC (Manassas, VA). The MCF10A cells were grown in MEGM media kit supplemented with 100 ng/mL cholera toxin at 37 °C in 5% CO₂ atmosphere.

3.2.3 Synthesis of Cy5.5 Conjugated Block Copolymers

Block copolymers of PEO-*b*-PCL and PEO-*b*-PBCL were synthesized by ring-opening polymerization of ε-caprolactone (0.1 g) or α-benzyl carboxylate-ε-caprolactone (0.2 g), respectively, using methoxy-PEO (MW: 5000 g/mol) (0.5 g) as initiator and stannous octoate as catalyst according to a method described previously.^{43, 308, 320}

Block copolymers of PEO-*b*-PCL or PEO-*b*-PBCL were end capped with α-propargyl carboxylate-ε-caprolactone (PCC) using stannous octoate as catalyst. Briefly, PEO-*b*-PCL (0.1 g) and PCC (0.014 g) or, PEO-*b*-PBCL (0.1 g) and PCC (0.012 g) were added to a 25 mL round-bottom flask previously filled with 5 mL dry toluene under constant stirring. Stannous octoate (0.010 equiv of monomer) was added to the flask. The flask was then refluxed for 30 h. The reaction was terminated by cooling the product to room temperature. The product was then precipitated in hexane and the supernatant was discarded. The final product was washed with ether and was dried under vacuum for further use.

Near-infrared fluorophore (NIRF) Cy5.5-azide was conjugated to the terminal alkyne of PCC in PEO-*b*-PCL-PCC or PEO-*b*-PBCL-PCC using Huisgens 1,3-dipolar cycloaddition

(azide-alkyne click chemistry) reaction. Briefly, 10 μmol PEO-*b*-PCL-PCC (68 mg) or PEO-*b*-PBCL-PCC (75 mg) was dissolved under constant stirring in a 10 mL round-bottom flask containing 2 mL degassed DMSO. Cy5.5 azide (1 μmol ; 0.7 mg) was dissolved in 400 μL DMSO and added to the mixture under constant stirring followed by addition of ascorbic acid (0.5 μmol ; 0.1 mg) previously dissolved in 100 μL water. The flask was then degassed with argon for about 30 s. 10 mM Cu-TBTA Complex solution (0.5 μmol ; 60 μL) was finally added followed by degassing for 30 s using argon. The reaction mixture was sealed and incubated with stirring at room temperature in the dark for 16 h. Argon was flushed through the sealed vial at 4 h and 8 h time-points. After incubation, the mixture was separated from the non-reacted dye by dialysis against DMSO for 24 h followed by dialysis against water for 24 h to remove the DMSO, and then lyophilized.

3.2.4 Synthesis of P18-4 Modified Block Copolymers

Acetal-PEO-*b*-PCL and acetal-PEO-*b*-PBCL were synthesized according to a previously published procedure.¹⁹¹ P18-4-attached PEO-*b*-PCL or PEO-*b*-PBCL were synthesized from acetal-PEO-*b*-PCL or acetal-PEO-*b*-PBCL according to a previously published procedure.^{102, 198} P18-4 peptide was conjugated to the micelles at a P18-4:polymer molar ratio of 1:5. The resulting micellar solution was dialyzed against distilled water and lyophilized.

3.2.5 Characterization of Synthesized Block Copolymers

The number-average molecular weight of PEO-*b*-PCL and PEO-*b*-PBCL block copolymers was determined from the ^1H NMR spectrum of the block copolymers in CDCl_3 at 600 MHz (Bruker Avance III spectrometer, Bruker BioSpin Corporation, Billerica, MA) by comparing the peak intensity of PEO ($-\text{CH}_2\text{CH}_2\text{O}-$, $\delta = 3.65$ ppm) to that of PCL or PBCL backbone ($-\text{OCH}_2-$, $\delta = 4.05$ ppm), considering a 5000 g/mol molecular weight for PEO.

The number-average molecular weight of PEO-*b*-PCL-PCC and PEO-*b*-PBCL-PCC block copolymers was determined from the ^1H NMR spectrum of the block copolymers in CDCl_3 at 600 MHz by comparing the peak intensity of PEO ($-\text{CH}_2\text{CH}_2\text{O}-$, $\delta = 3.65$ ppm) to that of PCC side-group ($-\text{OCH}_2-$, $\delta = 4.75$ ppm), considering a 5000 g/mol molecular weight for PEO.

The conjugation efficiency of cy5.5 to PEO-*b*-PCL-PCC and PEO-*b*-PBCL-PCC was determined by fluorescence spectrophotometer using a SpectraMax M4 microplate reader (Molecular Devices, Sunnyvale, CA), measuring the excitation at 673 nm and emission at 707 nm as described the manufacturer. The conjugation efficiency of P18-4 peptide to acetal-PEO-*b*-PCL and acetal-PEO-*b*-PBCL micelles was determined by reverse-phase HPLC according to a previously published procedure.^{102, 198}

3.2.6 Preparation and Characterization of Block Copolymer Micelles

Cy5.5-loaded PEO-*b*-PCL or PEO-*b*-PBCL block copolymer micelles were prepared through formation of mixed micelles by a co-solvent evaporation method as described previously.^{43, 308} Briefly, either PEO-*b*-PCL (18.0 mg) and PEO-*b*-PCL-PCC-cy5.5 (2.0 mg)

or PEO-*b*-PBCL (18.9 mg) and PEO-*b*-PBCL-PCC-cy5.5 (1.1 mg) were mixed and dissolved in THF (0.4 mL). The solution was added to 4 mL of doubly distilled water in a drop-wise manner under moderate stirring at room temperature, followed by evaporation of THF under vacuum. The prepared micellar solution was then centrifuged to remove any aggregates. The concentration of cy5.5 dye in the micelles was 0.4 µg/mg of the polymer.

Cy5.5-loaded PEO-*b*-PCL or PEO-*b*-PBCL block copolymer micelles with P18-4 peptide modification on their surface were prepared by co-solvent evaporation method as described above. For peptide density of 0.1 mol/mol of the polymer, mixed micelles were prepared using either PEO-*b*-PCL (9.0 mg), P18-4-PEO-*b*-PCL (9.0 mg), and PEO-*b*-PCL-PCC-cy5.5 (2.0 mg); or PEO-*b*-PBCL (9.4 mg), P18-4-PEO-*b*-PBCL (9.4 mg), and PEO-*b*-PBCL-PCC-cy5.5 (1.1 mg). For peptide density of 0.2 mol/mol of the polymer, mixed micelles were prepared using either P18-4-PEO-*b*-PCL (18.0 mg), and PEO-*b*-PCL-PCC-cy5.5 (2.0 mg); or P18-4-PEO-*b*-PBCL (18.9 mg), and PEO-*b*-PBCL-PCC-cy5.5 (1.1 mg). Polymeric micelles with low peptide density of 0.1 mol/mol of the polymer were termed as P18-4(L)-PEO-*b*-PCL or P18-4(L)-PEO-*b*-PBCL, where the 'L' stands for low density. In the case of polymeric micelles having high peptide density of 0.2 mol/mol of the polymer, they were termed as P18-4(H)-PEO-*b*-PCL or P18-4(H)-PEO-*b*-PBCL, where the 'H' stands for high density. The concentration of cy5.5 dye in the P18-4 decorated micelles was 0.4 µg/mg of the polymer.

The size and size distribution of micelles were measured by dynamic light scattering (DLS) using a commercial Zetasizer Nano-ZS (Malvern Instruments, Worcestershire, UK). All DLS measurements were made at 25.0 ± 0.1 °C with a 173° scattering angle. The samples were dissolved with deionized water and centrifuged prior to analysis. For this

measurement, plain PEO-*b*-PCL-PCC or PEO-*b*-PBCL-PCC were used in the preparation of micelles, instead of PEO-*b*-PCL-PCC-cy5.5 or PEO-*b*-PBCL-PCC-cy5.5, respectively. This is because the excitation and emission spectra of cy5.5 would interfere with the He-Ne 633 nm laser of the Zetasizer Nano-ZS.

The morphology of the micelles was investigated by transmission electron microscopy (TEM) using a Morgagni TEM (Field Emission Inc., Hillsboro, OR) with Gatan digital camera (Gatan, Pleasanton, CA) according to a method described previously.³⁰⁷ Images were obtained at a magnification of 110,000X at 75 kV.

The CMC of the polymeric micelles was determined using fluorescence spectroscopy. Briefly, solutions of Cy5.5-loaded unmodified or P18-4 decorated PEO-*b*-PCL or PEO-*b*-PBCL micelles having concentrations ranging from 400-0.2 $\mu\text{g}/\text{mL}$ were prepared in 96-well opaque plates. The intensity of light emitted at 707 nm after excitation at 673 nm was measured by fluorescence spectroscopy at 25 °C using a fluorescence spectrophotometer.

Kinetic stability of the micellar formulations was evaluated after incubation with a destabilizing agent, sodium dodecyl sulfate (SDS) according to previously published method.^{307, 322} Briefly, micellar stock solutions of PEO-*b*-PCL, PEO-*b*-PBCL, P18-4(L)-PEO-*b*-PCL, or P18-4(L)-PEO-*b*-PBCL having concentrations of 3 mg/mL were mixed with aqueous stock solution of SDS (20 mg/mL) at a ratio of 2:1 v/v (micelle:SDS). Samples were analyzed at predetermined time intervals by DLS for intensity distribution as well as polydispersity index (PDI).

3.2.7 *In Vitro* Cell Uptake Study using Flow Cytometry

Cellular uptake of conjugated cy5.5 in different micellar formulations was quantified using flow cytometry. MDA-MB-231-luc-D3H2LN cells or MCF10A cells were seeded into 24-well plates at densities of 1×10^5 cells/well and incubated at 37 °C for 24 h until they are 70% confluent. Free cy5.5 and micelles of PEO-*b*-PCL, PEO-*b*-PBCL, P18-4(L)-PEO-*b*-PCL, P18-4(L)-PEO-*b*-PBCL, P18-4(H)-PEO-*b*-PCL, P18-4(H)-PEO-*b*-PBCL at a concentration of 0.2 µg/mL of cy5.5 (equivalent to 0.5 mg/mL of micellar solution) were added to the wells in triplicate and incubated with cells for 4 and 24 h at 37 °C. For the competition experiments, MDA-MB-231-luc-D3H2LN cells were pre-incubated with excess free p18-4 peptide (1 mg/mL) for 30 min and then incubated with the above mentioned formulations for 24 h at 37 °C according to a previously described method.¹⁹³ After the incubation period, cells were washed three times with cold PBS and trypsinized. A 4% paraformaldehyde in PBS solution was added to fix the cells and the cy5.5 uptake was acquired on a BD FACSCalibur™ flow cytometer (BD Biosciences, Franklin Lakes, NJ). The cell-associated cy5.5 was excited using a red-diode laser (635 nm) and the FL4 channel (656 - 667 nm) was used to detect the cell-associated fluorescence. The data was analyzed with FCS Express™ software (De Novo Software, Los Angeles, CA).

3.2.8 *In Vitro* Cell Uptake Study using Confocal Microscopy

Confocal microscopy was used to assess the uptake of conjugated cy5.5 in different micellar formulations in MDA-MB-231-luc-D3H2LN cells. Cells were seeded into 12-well plates containing round cover slips (0.2 mm thickness) at densities of 2×10^4 cells/well and

incubated at 37 °C for 24 h until they are 20% confluent. Free cy5.5 and micelles of PEO-*b*-PCL, PEO-*b*-PBCL, P18-4(L)-PEO-*b*-PCL, P18-4(L)-PEO-*b*-PBCL, P18-4(H)-PEO-*b*-PCL, and P18-4(H)-PEO-*b*-PBCL at a concentration of 0.2 µg/mL of cy5.5 (equivalent to 0.5 mg/mL of micellar solution) were added to the wells in triplicate and incubated with cells 24 h at 37 °C. After the incubation period, cells were washed three times with cold PBS and fixed for 10 m using 4% paraformaldehyde in PBS solution. The cover-slips were removed and were inverted on a slide with a drop of mounting media containing DAPI. The slides were allowed to cure in the dark for 24 h. Uptake of cy5.5 in cells was visualized by a Zeiss LSM 710 confocal microscope (Carl Zeiss Microscope systems, Jena, Germany) using blue (Ex: 405 nm; Em: 410-500 nm) and red (Ex: 633 nm; Em: 633-744 nm) filters with 20× magnification. The images were analyzed using Zen 2012 software (Carl Zeiss Microscope systems, Jena, Germany).

3.2.9 Animal Models

Female athymic NIH-III mice were purchased from Charles River (Wilmington, MA). All experiments were performed using 4-6 week old female mice. All animal studies were conducted in accordance with the guidelines of the Canadian Council on Animal Care (CCAC) with approval from the Animal Care and Use Committee (ACUC) of the University of Alberta (Edmonton, AB, Canada). Mice were kept on the 2014S Teklad Global 14% protein rodent maintenance diet which is low on chlorophyll to minimize fluorescence from food. To establish the orthotopic mammary fat pad tumor model, mice were randomly assigned into five groups of six mice per group. Mice were injected with 2×10^6 MDA-MB-

231-luc-D3H2LN cells in 50 μ L solution of 50% Matrigel Basement Membrane Matrix (BD Biosciences, Franklin Lakes, NJ), into the left abdominal mammary fat pad.³⁴⁴ The mice were used when the tumors reached a size of 600 mm³ (3 weeks after injection). Animals were monitored daily according to previously reported method.¹⁹³

3.2.10 *In Vivo* Imaging and Tissue Biodistribution

Animals were treated with micellar solutions of cy5.5-loaded PEO-*b*-PCL, PEO-*b*-PBCL, P18-4(L)-PEO-*b*-PCL, and P18-4(L)-PEO-*b*-PBCL at concentrations of 250 mg/kg of body weight (equivalent to 0.1 mg/kg of free cy5.5³⁴⁵) by IV injection through the tail vein. At various time-points of 4, 24, 48, and 72 h, mice were imaged for fluorescence and bioluminescence using the IVIS Spectrum Preclinical *In Vivo* Imaging System (PerkinElmer, Waltham, MA). For bioluminescence imaging, luciferin potassium salt (150 mg/kg) in DPBS was injected sc into the neck 15 m prior to imaging. For *in vivo* fluorescence imaging, animals were imaged for 0.5 s, 10 bin, level B at an excitation and emission wavelength of 680 nm and 720 nm respectively. Spectral unmixing was used to analyze the images and remove traces of autofluorescence. For bioluminescence imaging, animals were imaged for 0.5 s, 10 bin, level B.

At 48 h and 72 h time-points, three mice were randomly selected from each group and injected with luciferin potassium salt (150 mg/kg) sc into the neck prior to euthanasia. After euthanasia, tumors and other organs (liver, lung, kidneys, heart, spleen, and brain) were excised and soaked in a 12-well plate containing luciferin (300 μ g/mL) prior to imaging. The organs were imaged for fluorescence and bioluminescence using the IVIS Spectrum

Preclinical *In Vivo* Imaging System. For *ex vivo* fluorescence imaging, animals were imaged for 0.5 s, 10 bin, level C at an excitation and emission wavelength of 680 nm and 720 nm respectively. For bioluminescence imaging, animals were imaged for 0.5 s, 10 bin, level C.

3.2.11 Statistics

Compiled data were presented as means \pm standard deviation (SD) or mean \pm standard error mean (SEM). Where feasible, the data were analyzed for statistical significance using unpaired student's t-test, or one-way analysis of variance (ANOVA) followed by Tukey's post test as noted in the results section. The level of significance was set at $\alpha \leq 0.05$.

3.3 Results

3.3.1 Labeling of PEO-*b*-PCL and PEO-*b*-PBCL with NIR dye

The block copolymers have been characterized in Table 3.1. Labeling of PEO-*b*-PCL and PEO-*b*-PBCL block copolymers with NIR dye was accomplished in three steps (Scheme 3.1): first, PEO-*b*-PCL and PEO-*b*-PBCL were synthesized by ring-opening polymerization of ϵ -caprolactone and α -benzyl carboxylate- ϵ -caprolactone monomer, respectively, in the presence of methoxy PEO.⁴³ The molecular weights of PEO-*b*-PCL and PEO-*b*-PBCL were confirmed by ¹H NMR (Figure 3.1) and were found to be 6290 and 7700 g/mol, respectively. The degree of polymerization (DP) of the core-forming block was calculated as 11 for both PEO-*b*-PCL and PEO-*b*-PBCL. In the second step, α -propargyl carboxylate- ϵ -caprolactone (PCC) was conjugated to the PEO-*b*-PCL and PEO-*b*-PBCL end. Conjugation of PCC to

PEO-*b*-PCL or PEO-*b*-PBCL led to chain cleavage of the PCL or PBCL block resulting in a decrease in the DP of the core-forming block from 11 to 7 (Figure 3.1). Finally, Cy5.5 azide was conjugated to the PCC part of PEO-*b*-PCL-PCC or PEO-*b*-PBCL-PCC via copper-catalyzed azide-alkyne cyclo-addition (CuAAC) click chemistry reaction. The terminal alkyne group of PCC reacted with the terminal azide group of cy5.5 azide to form a 1,3-triazole ring. Cu(I) acts as a catalyst for the reaction. Cu(I) is prepared in situ by the addition of Cu(II) TBTA Complex, and ascorbic acid, which acts as a reducing agent and reduces Cu(II) to Cu(I).⁸⁶ The average molar conjugation efficiency of cy5.5 to the block copolymers was 56.9 % and 76.1 % for PEO-*b*-PCL-PCC-cy5.5 and PEO-*b*-PBCL-PCC-cy5.5, respectively (Table 3.1). PEO-*b*-PBCL showed significantly higher conjugation efficiency of cy5.5 than PEO-*b*-PCL ($P < 0.5$; student's *t*-test). P18-4 was successfully conjugated to the PEO end of Acetal-PEO-*b*-PCL or Acetal-PEO-*b*-PBCL with an average molar conjugation of 20.1 % and 20.5 %, respectively, as confirmed by HPLC (Scheme 3.2 and Table 3.1).^{102,}

190

Table 3.1 Characteristics of prepared block copolymers

Block Copolymer ^a	M_n (g/mol) ^b	Dye conjugation (molar % \pm SD) ^c	Dye conjugation efficiency (molar % \pm SD) ^c	P18-4 conjugation (molar % \pm SD) ^d	P18-4 conjugation efficiency (molar %) ^d
PEO ₁₁₄ - <i>b</i> -PCL ₁₁	6290	-	-	-	-
PEO ₁₁₄ - <i>b</i> -PBCL ₁₁	7700	-	-	-	-
PEO ₁₁₄ - <i>b</i> -PCL ₇ -PCC _{1.1} -cy5.5	6520	4.90 \pm 0.12	56.89 \pm 1.35	-	-
PEO ₁₁₄ - <i>b</i> -PBCL ₇ -PCC _{0.9} -cy5.5	7220	7.68 \pm 0.54*	76.12 \pm 5.40*	-	-
P18-4-PEO ₁₂₇ - <i>b</i> -PCL ₈	7570	-	-	20.09 \pm 0.09	100
P18-4-PEO ₁₂₇ - <i>b</i> -PBCL ₈	8710	-	-	20.45 \pm 0.68	100

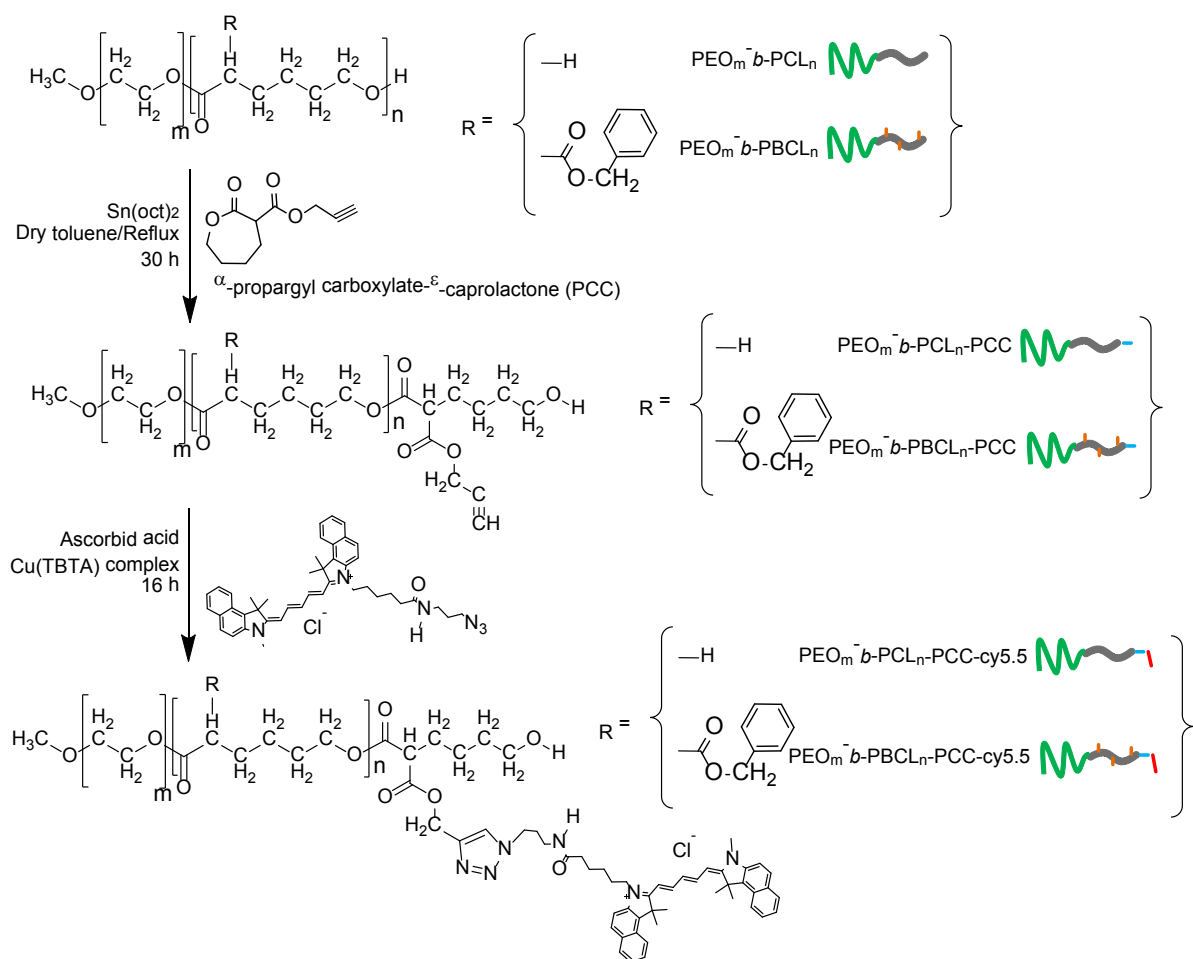
^a The number shown in the subscript indicates the polymerization degree of each block determined by ¹H NMR spectroscopy.

^b Number-average molecular weight measured by ¹H NMR.

^c Dye conjugation and conjugation efficiency as calculated by fluorescence spectroscopy.

^d P18-4 peptide conjugation and conjugation efficiency as calculated by HPLC.

* Signifies significant difference between the groups ($P < 0.05$; Student's *t*-test).



Scheme 3.1 Synthetic scheme for the preparation of PEO-*b*-PCL-PCC-cy5.5 and PEO-*b*-PBCL-PCC-cy5.5

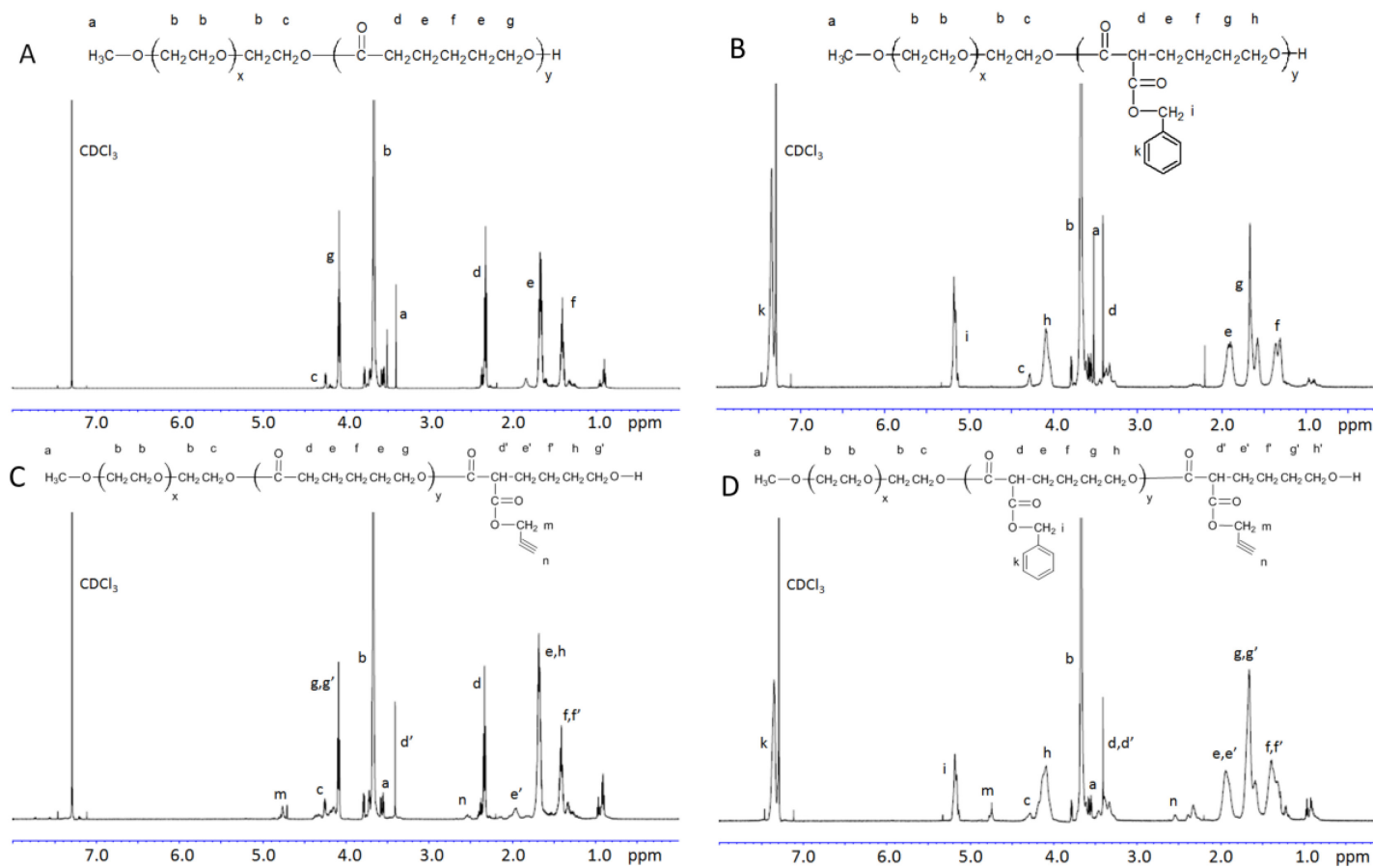


Figure 3.1 ^1H NMR spectrum of (A) PEO-*b*-PCL, (B) PEO-*b*-PBCL, (C) PEO-*b*-PCL-PCC, and (D) PEO-*b*-PBCL-PCC in CDCl_3 and peak assignments.

3.3.2 Preparation of NIR labeled micelles

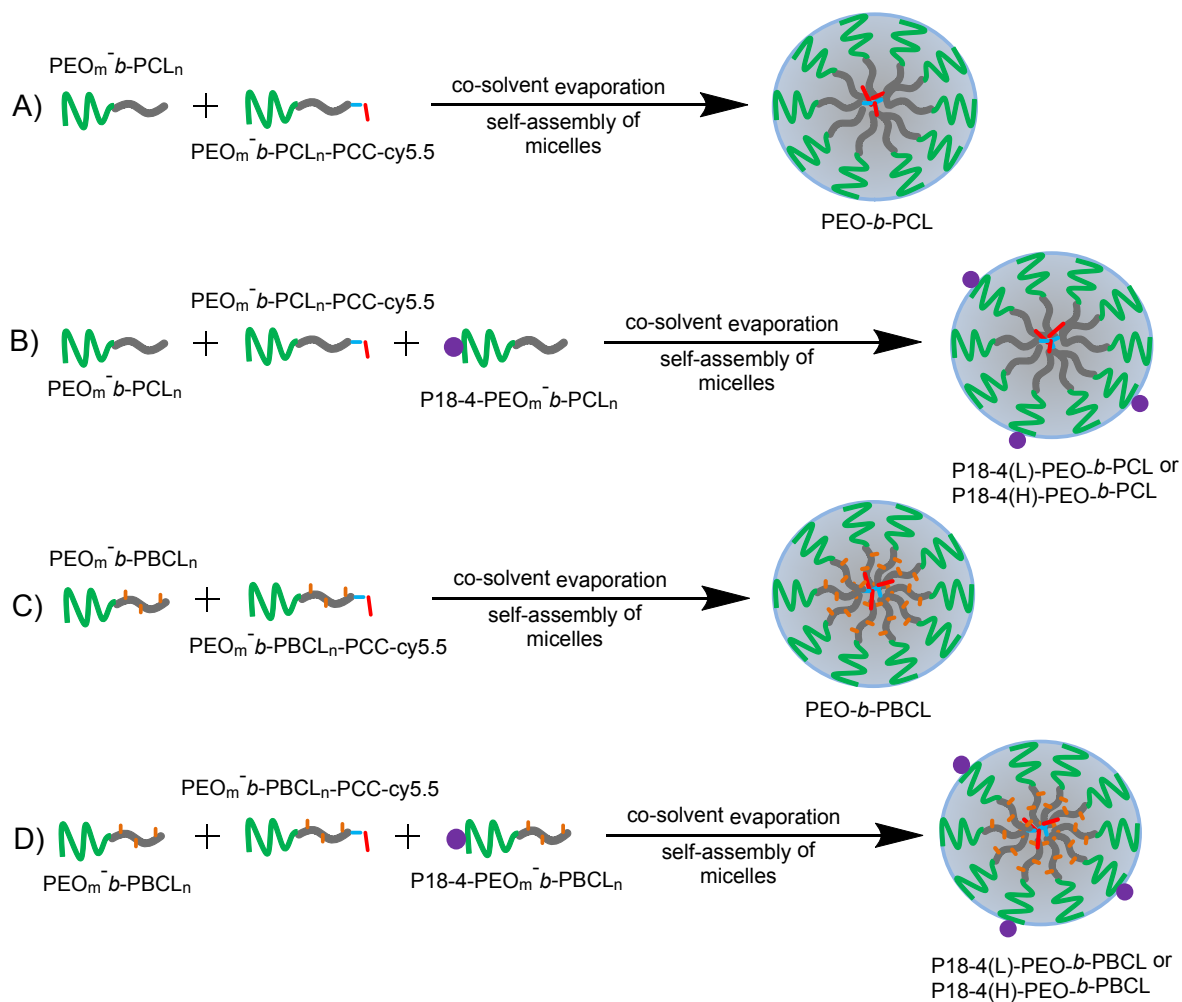
Synthesized block copolymers were assembled to polymeric micelles containing cy5.5 by a co-solvent evaporation method through preparation of mixed micelles (Scheme 3.3).^{43, 308} The characteristics of prepared polymeric micelles are listed in Table 3.2. The average size of micelles formed from PCL containing block copolymers is significantly higher ($P < 0.05$; Students' *t*-test) compared to micelles formed from PBCL containing block copolymers. Similar results were seen in the case of PDI. The average size of micelles also showed a significant increase ($P < 0.05$; one-way ANOVA) as the P18-4 peptide was attached and its density was increased.

TEM was used to study the morphology of the micelles (Figure 3.2). All micelles formed from PBCL containing block copolymers showed a spherical morphology with clear boundary. In the case of micelles formed from PCL containing block copolymers, PEO-*b*-PCL and P18-4(L)-PEO-*b*-PCL showed a mixture of spherical and worm-shaped morphology with clear boundary. In the case of P18-4(H)-PEO-*b*-PCL micelles, large spherical morphology is seen without clear boundary indicating the possibility of aggregate formation.

The CMC of the block copolymers was determined by fluorescence spectroscopy using the intensity values of emitted light as a function of block copolymer concentration (Table 3.2). As the block copolymer forms micelles, the cy5.5 dye enters the core thus showing a decrease in the intensity of emitted light (quenching). The concentration at which the slope of the graph of emission v/s concentration starts to decrease is termed as the CMC. Micelles formed from PBCL containing block copolymers exhibited a 7-fold decrease in

CMC when compared with those formed from PCL containing block copolymers similar to previous findings.³⁰⁷ Attachment of P18-4 peptide to the micellar surface or change in its density did not significantly change ($P > 0.05$; one-way ANOVA) in the CMC of the micelles. One thing to note is that at the highest concentration of 400 $\mu\text{g/mL}$ of the polymer, the intensity of emitted light from all micellar systems was similar to each other ($P < 0.05$; one-way ANOVA, Tukey's post test) indicating that all the micellar systems showed similar quenching of the cy5.5 dye.

The kinetic stability of micelles was studied using DLS after the addition of a destabilizing agent, SDS. Figure 3.3 shows the % intensity of the micellar peak for PEO-*b*-PCL and PEO-*b*-PBCL micelles over time in the presence of SDS. PEO-*b*-PCL micelles, unmodified or modified with 10 mol % P18-4 peptide showed a significant decrease in the signal intensity of the micellar peak to ~50 % and ~21 %, respectively, within 24 hrs of incubation. PEO-*b*-PBCL micelles, on the other hand, whether modified with P18-4 or not, showed a signal intensity of ≥ 90 % throughout the 72 h incubation. Hence, attachment of benzyl carboxylate to the micellar core, resulted in improved stability against SDS. This was in line with previously published results from our lab.³⁰⁷ P18-4 modification of both PEO-*b*-PCL and PEO-*b*-PBCL micelles, however, led to a decrease in the stability of the micelles when incubated with SDS.



Scheme 3.3 Synthetic Scheme for the preparation of cy5.5 loaded (A) $\text{PEO-}b\text{-PCL}$, (B) P18-4 decorated $\text{PEO-}b\text{-PCL}$, (C) $\text{PEO-}b\text{-PBCL}$, and (D) P18-4 decorated $\text{PEO-}b\text{-PBCL}$ micelles.

Table 3.2 Characteristics of prepared block copolymer micelles

Block Copolymer ^a	P18-4 density in micelles (mol/mol) ^b	Average micellar size \pm SD (nm) ^c	PDI \pm SD ^d	CMC \pm SD (μ M) ^e
PEO ₁₁₄ - <i>b</i> -PCL ₁₁	-	148.5 \pm 13.6	0.499 \pm 0.051	3.40 \pm 0.28
PEO ₁₁₄ - <i>b</i> -PBCL ₁₁	-	30.2 \pm 0.4*	0.184 \pm 0.009*	0.49 \pm 0.07*
P18-4(L)-PEO ₁₂₇ - <i>b</i> -PCL ₈	0.1	110.0 \pm 11.8	0.831 \pm 0.158	3.71 \pm 0.39
P18-4(L)-PEO ₁₂₇ - <i>b</i> -PBCL ₈	0.1	40.4 \pm 0.4*	0.302 \pm 0.019*	0.77 \pm 0.02*
P18-4(H)-PEO ₁₂₇ - <i>b</i> -PCL ₈	0.2	318.4 \pm 89.7	0.422 \pm 0.063	4.22 \pm 0.73
P18-4(H)-PEO ₁₂₇ - <i>b</i> -PBCL ₈	0.2	52.2 \pm 0.8*	0.293 \pm 0.022*	1.18 \pm 0.40*

^a The number shown in the subscript indicates the polymerization degree of each block determined by ¹H NMR spectroscopy; L = low density of peptide on polymer, and H = high density of peptide on polymer.

^b Density of peptide in polymeric micelles expressed as the mole of peptide per mole of polymer.

^c Average micellar size estimated by DLS technique ($n = 3$).

^d Average polydispersity index (PDI) of micellar size distribution ($n = 3$).

^e Measured from the onset of a decrease in the slope of the intensity of emission of cy5.5 as a function of concentration of block copolymer ($n = 3$).

* Significantly different from its corresponding micelle containing PCL ($P < 0.05$; Student's *t*-test).

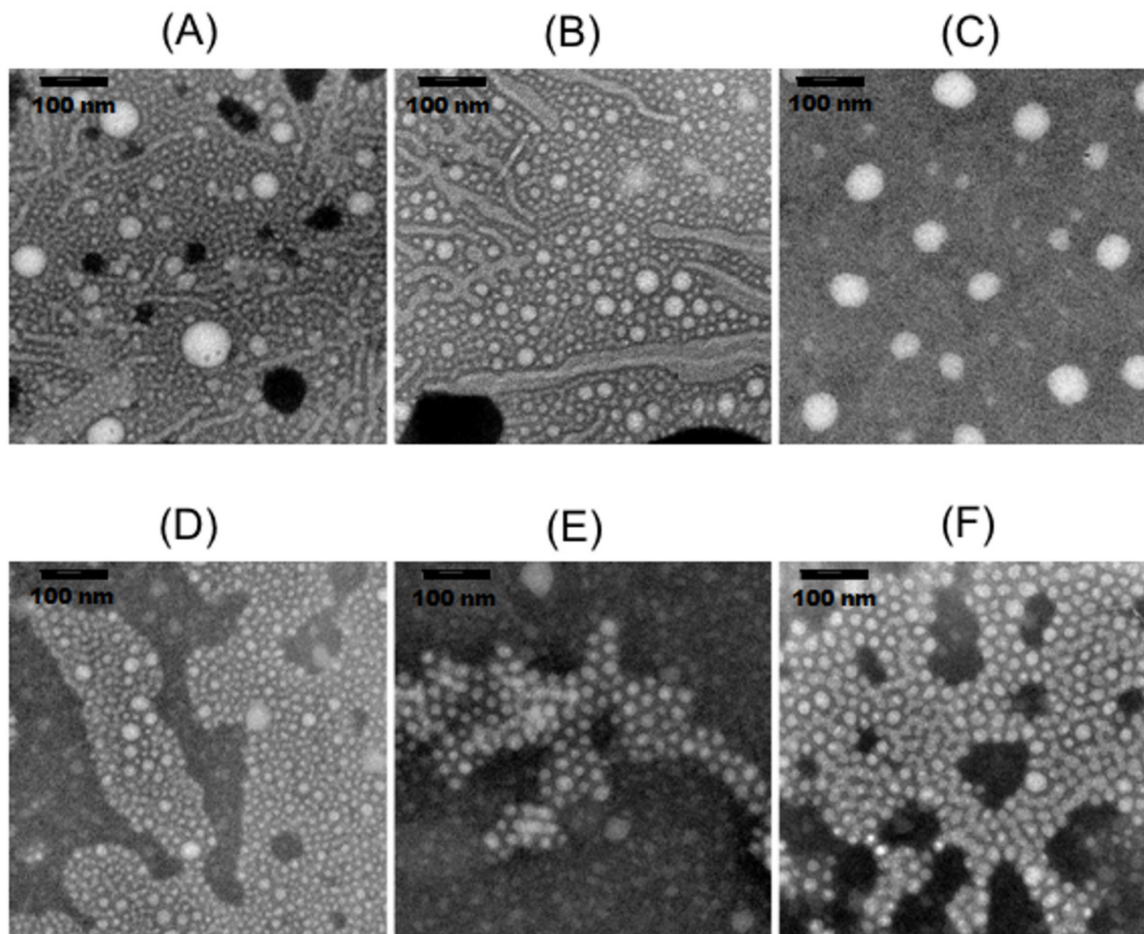


Figure 3.2 TEM picture of (A) PEO-*b*-PCL, (B) P18-4(L)-PEO-*b*-PCL, (C) P18-4(H)-PEO-*b*-PCL, (D) PEO-*b*-PBCL, (E) P18-4(L)-PEO-*b*-PBCL, and (F) P18-4(H)-PEO-*b*-PBCL block copolymer micelles (110,000X). The bar in the top left corner of each image indicates a scale of 100 nm.

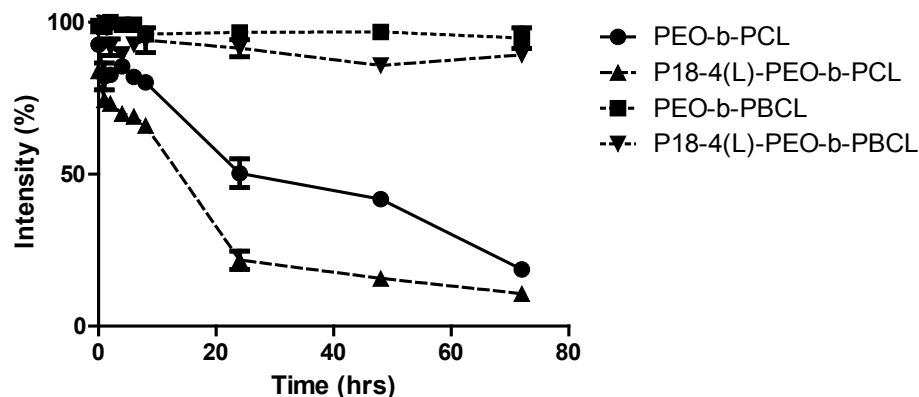


Figure 3.3 Percentage intensity of (A) PEO-*b*-PCL, (B) P18-4(L)-PEO-*b*-PCL, (C) PEO-*b*-PBCL, and (D) P18-4(L)-PEO-*b*-PBCL micellar peak (2 mg/mL) as a function of time in the presence of SDS (6.7 mg/mL). Each point represents mean \pm SD ($n = 3$).

3.3.3 *In Vitro* Cell uptake Study

The uptake of cy5.5-loaded polymeric micelles was determined in MDA-MB-231-luc-D3H2LN breast cancer cells using flow cytometry. Figure 3.4A represents the uptake of free cy5.5, cy5.5-loaded unmodified PEO-*b*-PCL and PEO-*b*-PBCL micelles, and different densities of P18-4 peptide decorated PEO-*b*-PCL and PEO-*b*-PBCL micelles, in MDA-MB-231-luc-D3H2LN cells at 4 h and 24 h, respectively. As seen in Figure 3.4A and Figure 3.5A, peptide modification, even at low density, significantly increased the cellular association ($P < 0.05$; Students' *t*-test) of both PEO-*b*-PCL and PEO-*b*-PBCL micelles. After 24 h incubation, PEO-*b*-PCL and PEO-*b*-PBCL micelles presenting 10 mol % of P18-4 peptide demonstrated 1.7-fold and 1.3-fold greater cellular association (Figure 3.4A) than unmodified micelles, respectively. In the case of PEO-*b*-PCL and PEO-*b*-PBCL micelles

presenting 20 mol % of P18-4 peptide, cellular association increased by 2.0-fold and 1.2-fold, when compared to unmodified micelles, respectively. Although both the unmodified PEO-*b*-PCL and PEO-*b*-PBCL micelles showed similar uptake ($P > 0.05$; Students' *t*-test) by MDA-MB-231-luc-D3H2LN cells at 4 h, PEO-*b*-PCL micelles exhibited a significantly higher cellular association ($P < 0.05$; unpaired students' *t*-test) than PEO-*b*-PBCL at 24 h. P18-4 modification of PEO-*b*-PCL micelles however, significantly increased their uptake ($P > 0.05$; Students' *t*-test) at both 4 h and 24 h, when compared with P18-4 decorated PEO-*b*-PBCL micelles.

The uptake of cy5.5-loaded polymeric micelles was also determined in MCF10A mammary epithelial cells as seen in Figure 3.4B and Figure 3.5B. In the case of MCF10A cells, after 24 h incubation, cellular association of PEO-*b*-PCL and PEO-*b*-PBCL micelles presenting 10 mol % of P18-4 peptide demonstrated 1.4-fold and 1.1-fold greater cellular association than unmodified micelles, respectively (Figure 3.4B). This was lower than the cellular association seen by these micelles in MDA-MB-231-luc-D3H2LN breast cancer cells. However, in the case of PEO-*b*-PCL and PEO-*b*-PBCL micelles presenting 20 mol % of P18-4 peptide, cellular association increased by 2.9-fold and 1.6-fold, respectively, which was more than 2.0-fold and 1.2-fold, seen in the breast cancer cells (Figure 3.4B). This indicated a higher cellular association for PEO-*b*-PCL and PEO-*b*-PBCL micelles modified with 20 mol % of P18-4 peptide in MCF10A cells when compared with MDA-MB-231-luc-D3H2LN cells.

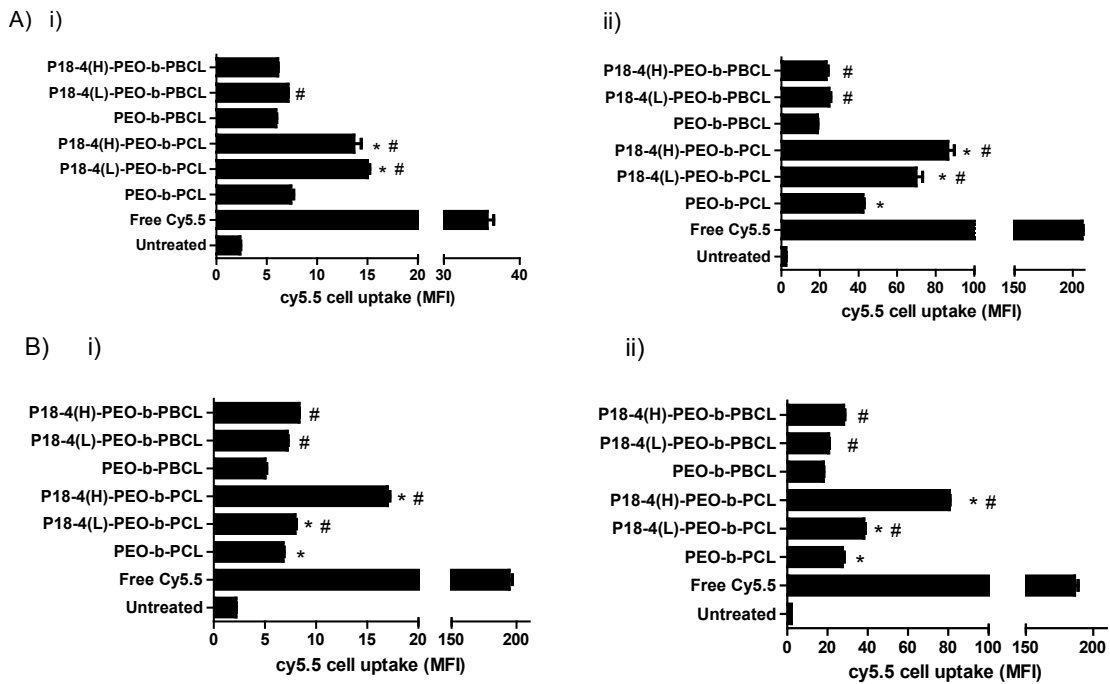


Figure 3.4 Cellular uptake of cy5.5-loaded micelles by A) MDA-MB-231-luc-D3H2LN and B) MCF10A cells. The bar graphs give the mean fluorescence intensity (MFI) of the cells after (i) 4 h and (ii) 24 h exposure to micellar groups. The data are the mean \pm SEM ($n=3$). *Significant difference between PEO-*b*-PCL and PEO-*b*-PBCL, or P18-4-PEO-*b*-PCL and P18-4-PEO-*b*-PBCL ($P < 0.05$), #Significant difference between PEO-*b*-PCL and P18-4-PEO-*b*-PCL, or PEO-*b*-PBCL and P18-4-PEO-*b*-PBCL ($P < 0.05$; unpaired Students' *t*-test, $\alpha = 0.05$).

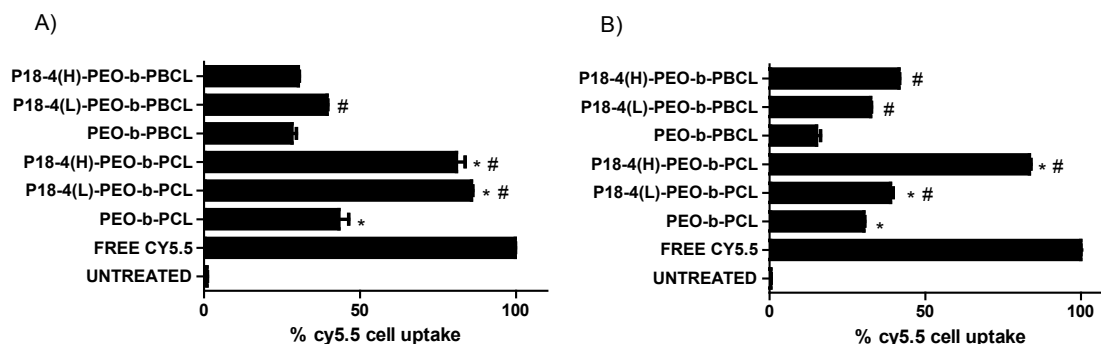


Figure 3.5 Cellular uptake of cy5.5-loaded micelles by A) MDA-MB-231-luc-D3H2LN and B) MCF10A cells. The bar graphs give the % cy5.5 positive cells after 4 h exposure to micellar groups. The data are the mean \pm SEM ($n=3$). *Significant difference between PEO-*b*-PCL and PEO-*b*-PBCL, or P18-4-PEO-*b*-PCL and P18-4-PEO-*b*-PBCL ($P < 0.05$), #Significant difference between PEO-*b*-PCL and P18-4-PEO-*b*-PCL, or PEO-*b*-PBCL and P18-4-PEO-*b*-PBCL ($P < 0.05$; unpaired Students' *t*-test, $\alpha = 0.05$).

To explore whether the increased cell uptake in MDA-MB-231-luc-D3H2LN cells is due to the presence of receptor for the P18-4 peptide, competition study was carried out, in which cells were pre-treated with excess P18-4 peptide before incubating the cells for 24 h with PCL and PBCL containing micellar formulations. As seen in Figure 3.6, presence of excess free P18-4 peptide significantly reduced the cellular association ($P < 0.05$; unpaired students' *t*-test) of PEO-*b*-PCL and PEO-*b*-PBCL micelles presenting 10 mol % of P18-4 peptide. However, presence of excess free P18-4 peptide did not affect the cellular association ($P > 0.05$; unpaired students' *t*-test) of PEO-*b*-PCL and PEO-*b*-PBCL micelles presenting 20 mol % of P18-4 peptide.

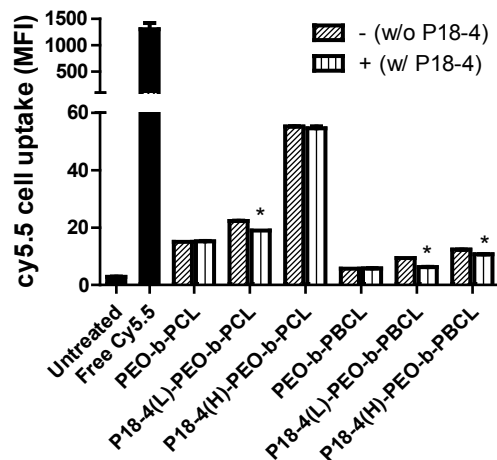
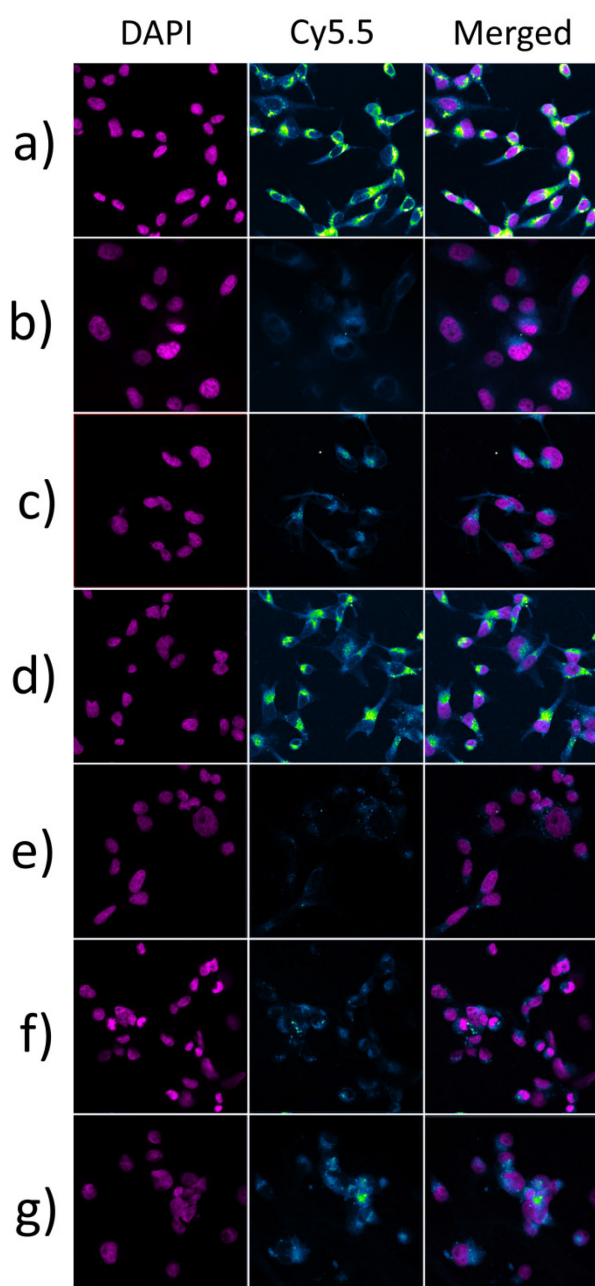


Figure 3.6 Cellular uptake of cy5.5-loaded micelles by MDA-MB-231-luc-D3H2LN cells with (+) or without (-) pre-treatment with excess of free P18-4 peptide. The bar graphs give the mean fluorescence intensity (MFI) of the cells after 24 h exposure to micellar groups. The data are the mean \pm SEM ($n=3$). *Significantly different from its counterpart without (-) free peptide ($P < 0.05$, unpaired Students' t -test).

The uptake of cy5.5-loaded polymeric micelles was also determined in MDA-MB-231-luc-D3H2LN breast cancer cells using confocal microscopy after 24 h incubation. As seen in Figure 3.7, peptide modification increased intracellular fluorescence of cy5.5-loaded PEO-*b*-PCL and PEO-*b*-PBCL micelles in the cytoplasm. Both PEO-*b*-PCL and PEO-*b*-PBCL micelles presenting 20 mol % of P18-4 peptide, showed strongest fluorescence when compared with their unmodified counterparts or counterparts presenting 10 mol % of P18-4 peptide. Also, PEO-*b*-PCL micelles, with or without P18-4 modification showed stronger cy5.5 fluorescence in cells when compared to PEO-*b*-PBCL micelles. These observations were in line with our previous findings and data of flow cytometry studies (Figure 3.4).



Cy5.5 scale bar

Figure 3.7 Cellular distribution of cy5.5-loaded micelles by confocal microscopy. Cellular uptake of (a) Free cy5.5, (b) PEO-*b*-PCL, (c) P18-4(L)-PEO-*b*-PCL, (d) P18-4(H)-PEO-*b*-PCL, (e) PEO-*b*-PBCL, (f) P18-4(L)-PEO-*b*-PBCL, and (g) P18-4(H)-PEO-*b*-PBCL micelles by MDA-MB-231-luc-D3H2LN cells using confocal microscopy after 24 h incubation. Images represent nuclear stain DAPI (pink) alone, cy5.5 (see scale bar - blue - low; yellow - high) alone, and merged together.

3.3.4 *In vivo* body distribution and tumor-targeting ability of polymeric micelles in orthotopic breast cancer model

As seen in Figure 3.7, the bioluminescence signal can be seen only at the site of injection i.e. left mammary fat pad, indicating that this study did not show any signs of metastasis to any organs during the timeline of this study. As seen in Figure 3.9, plain PEO-*b*-PCL micelles, started accumulating in the liver, tumor, and neck (presumably the cervical lymph nodes) within 4 h post-injection. After 24 h post-injection, these micelles started showing higher accumulation in tumor along with increased accumulation in liver and neck. Dorsal images showed uptake of plain PEO-*b*-PCL micelles in the kidneys and spleen. Peptide modified PEO-*b*-PCL micelles showed similar pattern of distribution in the mice except that they only showed uptake in kidneys upon dorsal assessment and no accumulation in spleen. Similar results were seen for the ventral images after 48 h, with decrease in fluorescence in both liver and tumors 72 h post-injection. Dorsal images showed increased fluorescence in kidneys for both PEO-*b*-PCL micelles at 48 h and 72 h, which perhaps points to elimination of PEO-*b*-PCL polymers from this organ at later time points.

In the case of PEO-*b*-PBCL micelles, unmodified micelles show accumulation primarily in the tumor with strong fluorescence signals throughout the body whereas PEO-*b*-PBCL micelles modified with 10 mol % P18-4 peptide showed uptake primarily in the tumor with weak fluorescent signals throughout the body, 4 h post-injection (Figure 3.9). After 24 h post-injection, ventral images showed unmodified PEO-*b*-PBCL micelles primarily in the tumor with weaker fluorescence signals throughout the body. In the case of PEO-*b*-PBCL micelles modified with P18-4 peptide, fluorescent signals were primarily at the tumor site.

Ventral images at 48 and 72 h for both, unmodified and 10 mol % P18-4 peptide modified PEO-*b*-PBCL micelles, showed similar results of strong fluorescent signals primarily from the tumor site. Dorsal images (Figure 3.9) at 24, 48, and 72 h time-points showed strong fluorescent signals from the tumor site at locations that are seen in the dorsal images of bioluminescence (Figure 3.8).

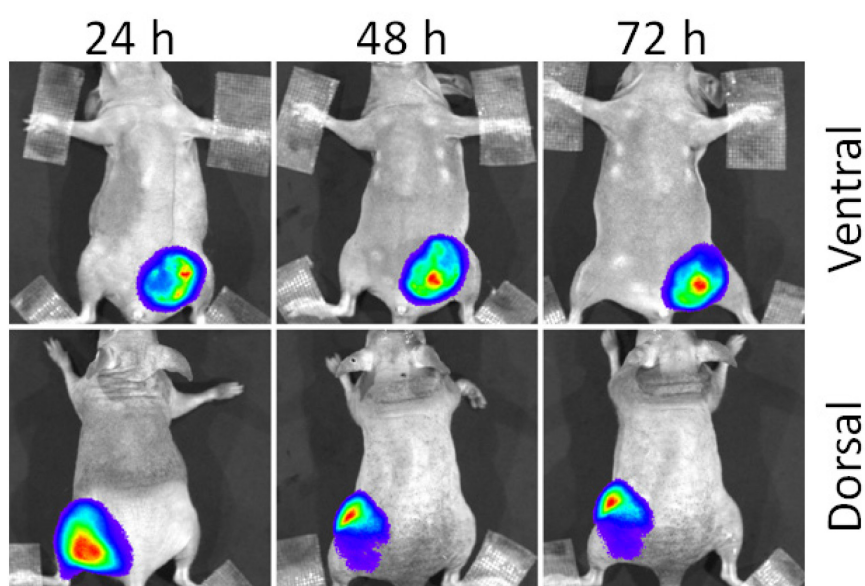


Figure 3.8 Evaluation of orthotopic breast tumor model. *In vivo* bioluminescence imaging of MDA-MB-231-luc-D3H2LN cells at 24 h, 48 h, and 72 h after intravenous administration of cy5.5-loaded micelles ($n = 30$). Images show ventral and dorsal photographs. Each time-point represent image of one mouse from a group of thirty mice.

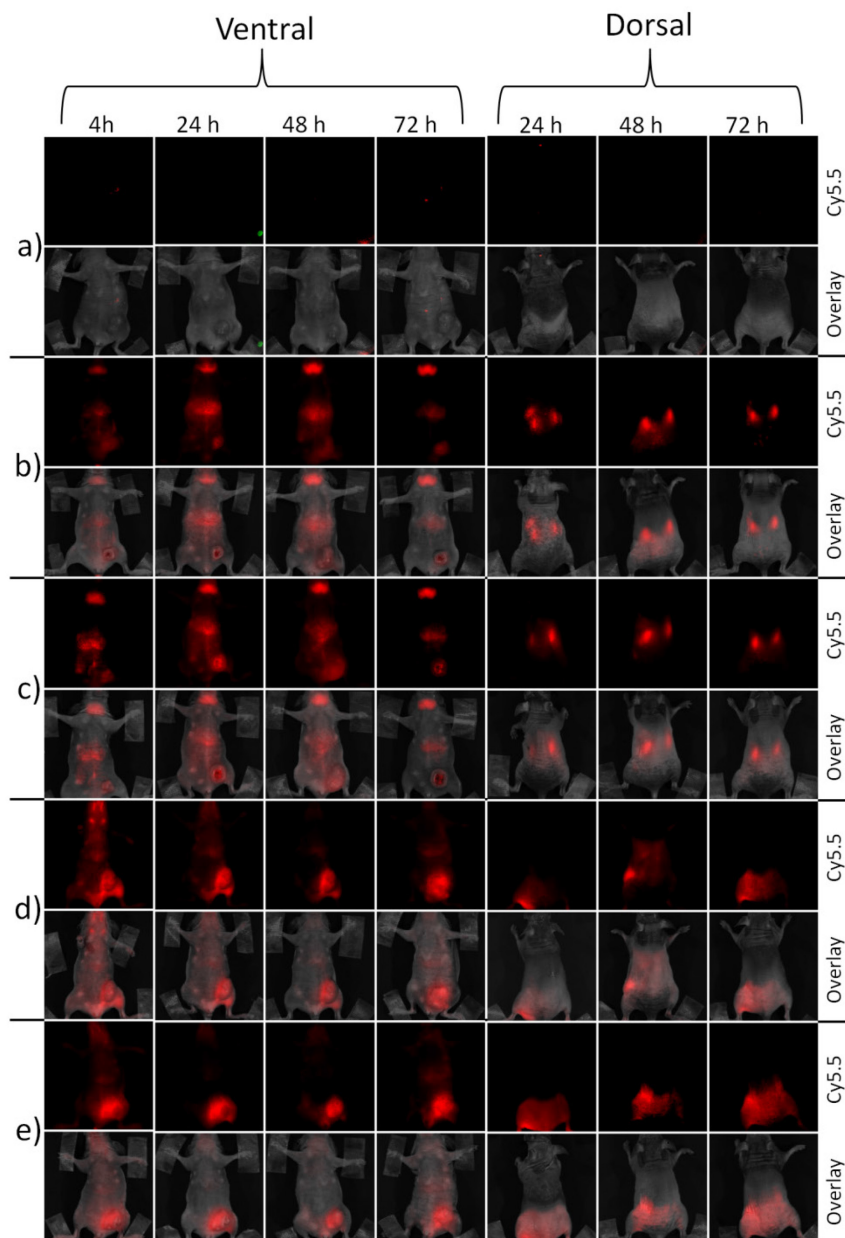


Figure 3.9 *In vivo* biodistribution and tumor accumulation of cy5.5-loaded micelles. *In vivo* NIR imaging of (a) untreated; and cy5.5-labeled (b) PEO-*b*-PCL, (c) P18-4(L)-PEO-*b*-PCL, (d) PEO-*b*-PBCL, and (e) P18-4(L)-PEO-*b*-PBCL micelles at 4 h, 24 h, 48 h, and 72 h after intravenous administration of cy5.5-loaded micelles ($n = 6$). Images show ventral and dorsal photographs. Each time-point represents image of one mouse from a group of six mice.

As seen in Figure 3.10, comparing the average radiant efficiency in the tumor from the *in vivo* images at various time-points, showed that the P18-4 modified micelles exhibited higher accumulation in the tumor at the earlier time-points. In the case of PEO-*b*-PCL micelles, P18-4 modified micelles showed a significantly higher accumulation in the tumor site 4 h after injection when compared to their unmodified counterparts ($P < 0.05$; Student's *t*-test). At later time-points, the average radiant efficiency has significantly decreased and is similar for both plain and P18-4 modified PEO-*b*-PCL micelles. This decrease in the fluorescent intensity maybe due to clearance into the kidneys and liver as seen in Figure 3.9.

In the case of PEO-*b*-PBCL micelles, P18-4 modified micelles showed a significantly higher accumulation in the tumor site 4 and 24 h after injection when compared to their unmodified counterparts ($P < 0.05$; Student's *t*-test). For P18-4 modified PEO-*b*-PBCL micelles, the average radiant efficiency in the tumor reaches maximum at 24 and 48 h post-injection after which it starts to decrease by 72 h. In the case of plain PEO-*b*-PBCL micelles, the average radiant efficiency shows an increasing trend from 4 - 72 h reaching a value similar to the maximum average radiant efficiency of P18-4 modified PEO-*b*-PBCL micelles, only after 72 h.

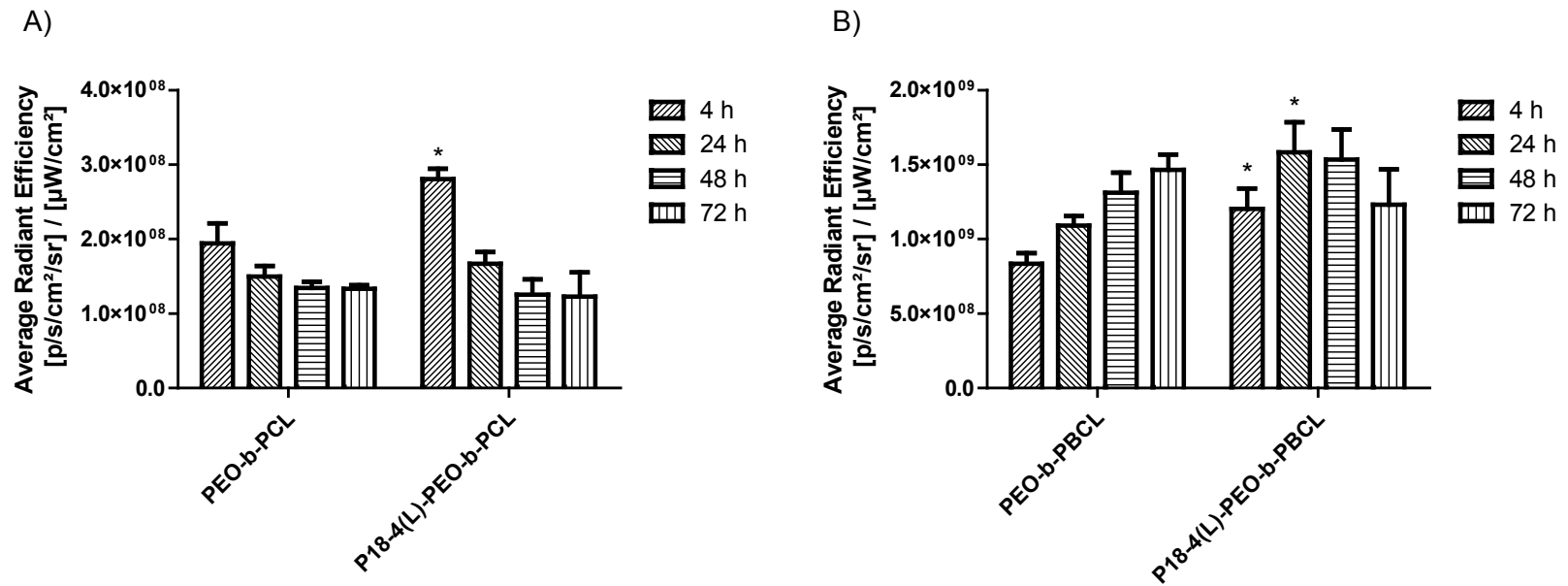


Figure 3.10 Average radiant efficiency in tumor of plain and P18-4 modified A) PEO-*b*-PCL, and B) PEO-*b*-PBCL micelles at 4 h, 24 h, 48 h, and 72 h after intravenous administration of cy5.5-loaded micelles ($n = 3-6$). The bar graphs are the mean \pm SEM ($n=3-6$). *Significantly different from its plain counterpart ($P < 0.05$, unpaired Students' *t*-test).

3.3.5 *Ex vivo* distribution and tumor-targeting ability of polymeric micelles in orthotopic breast cancer model

Fluorescence from cy5.5 was used to image the biodistribution of PEO-*b*-PCL and PEO-*b*-PBCL micelles *ex vivo*. As seen in Figure 3.11, bioluminescence signals were seen only from the tumor thus confirming the findings of the *in vivo* imaging (Figure 3.8), that there were no signs of metastasis in the major organs under the time-line of this study. As seen in Figure 3.11, both plain and P18-4 peptide modified PEO-*b*-PCL micelles, showed increased fluorescence primarily in the kidneys compared to other organs indicating clearance through kidneys within 72 h. This was similar to the results seen during *in vivo* imaging (Figure 3.9). Both plain and peptide modified PEO-*b*-PBCL micelles on the other hand, showed increased fluorescence signals from the liver and tumors similar to that seen *in vivo*.

Figure 3.12 gives the average radiant efficiency in the tumor and various organs at both 48 h and 72 h. The average radiant efficiency of the tumor is significantly higher ($P < 0.05$; one-way ANOVA) for PEO-*b*-PBCL micelles, whether unmodified or modified with P18-4 peptide, when compared with PEO-*b*-PCL micelles. P18-4 modification however, did not significantly increase ($P > 0.05$; one-way ANOVA) the average radiant efficiency of the tumor at both 48 h and 72 h when compared to plain micelles. This was similar to the results of 48 and 72 h seen in the average radiant efficiency in the tumor from the *in vivo* images (Figure 3.10). PEO-*b*-PBCL micelles, whether unmodified or modified with P18-4 peptide, showed a significantly higher ($P < 0.05$; one-way ANOVA) average radiant efficiency in heart, liver, lung, and spleen, and a significantly lower ($P < 0.05$; one-way ANOVA) average

radiant efficiency in kidney when compared with their PEO-*b*-PCL counterparts at 48 h time-point. The higher average radiant efficiency in the kidneys indicated faster clearance for PEO-*b*-PCL micelles. Similar results were also seen after 72 h, but were not significant for some groups. P18-4 modification, however, did not significantly change ($P > 0.05$; one-way ANOVA) the average radiant efficiency in most organs when compared to plain micelles. It was however, successful in significantly decreasing ($P < 0.05$; one-way ANOVA) the average radiant efficiency in the spleen for PEO-*b*-PBCL micelles at both 48 and 72 h, and the average radiant efficiency in the heart for PEO-*b*-PCL micelles at 48 h when compared with its unmodified counterpart. It is to note that although the average radiant efficiency can be used to compare the distribution in any organ amongst the different groups, it is not advisable to use the average radiant efficiency to compare the distribution amongst different organs for each group separately. The reason for this is that the organs are not perfused leading to the possibility of attenuation of the emitted light by hemoglobin. Hemoglobin has a secondary absorption peak between 550 nm to 600 nm. Even though NIR probes like cy5.5 have their absorption and emission maxima at longer wavelengths, some amount of emitted light would still be attenuated.³⁴⁶

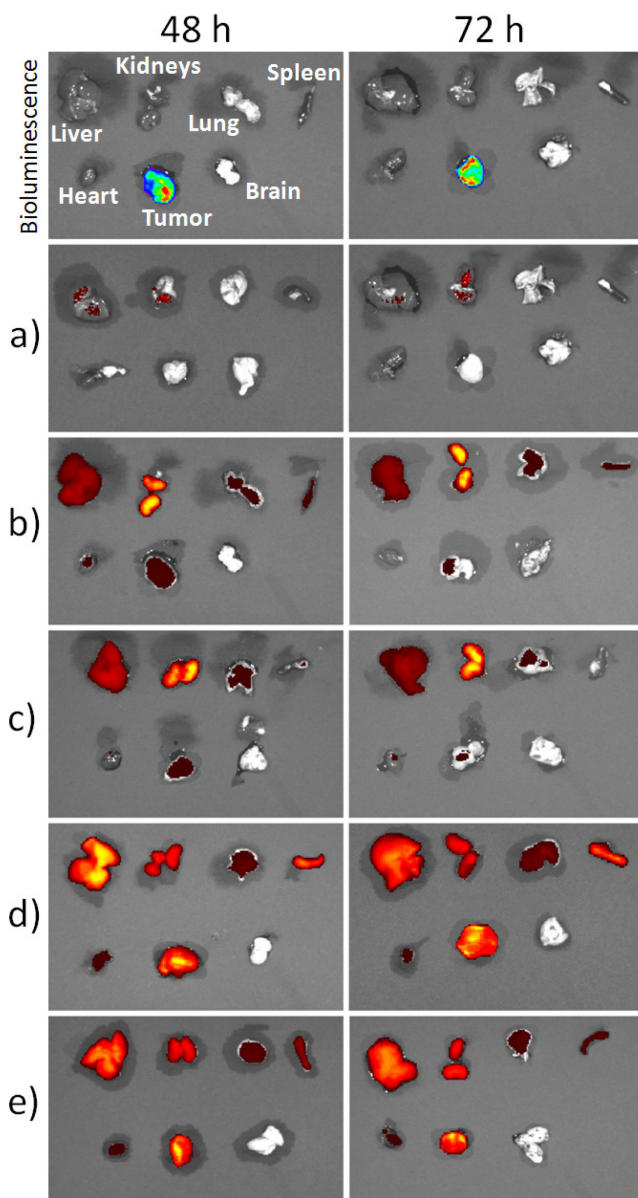


Figure 3.11 *In vivo* biodistribution and tumor accumulation of cy5.5-loaded micelles. *Ex vivo* bioluminescence imaging (top-most image) and NIR imaging of (a) untreated, and cy5.5-loaded (b) PEO-*b*-PCL, (c) P18-4(L)-PEO-*b*-PCL, (d) PEO-*b*-PBCL, and (e) P18-4(L)-PEO-*b*-PBCL micelles at 48 h and 72 h after intravenous administration of cy5.5-loaded micelles ($n = 3$). Images show (clockwise from top left corner) liver, kidneys, lungs, spleen, brain, tumor, and heart. Each time-point represents image of one mouse from a group of three mice.

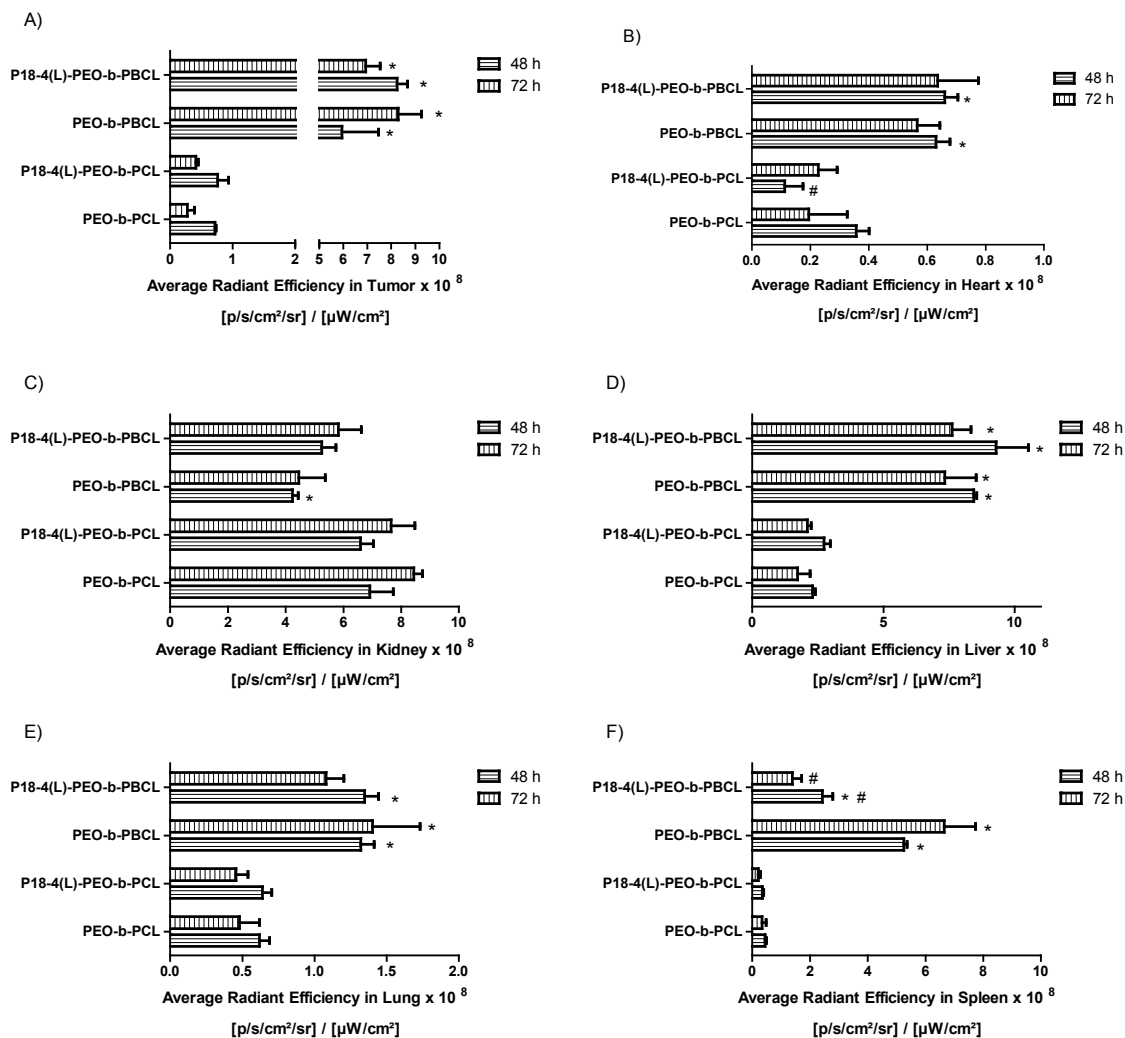


Figure 3.12 *In vivo* biodistribution and tumor accumulation of cy5.5-loaded micelles. (A) Average radiant efficiency of cy5.5 fluorescence in A) tumor, B) heart, C) kidney, D) liver, E) lung, and F) spleen at 48 h and 72 h after intravenous administration of cy5.5-loaded PEO-*b*-PCL, P18-4(L)-PEO-*b*-PCL, PEO-*b*-PBCL, and P18-4(L)-PEO-*b*-PBCL micelles ($n = 3$). *Significant difference between core forming block i.e. PBCL and PCL ($P < 0.05$). #Significant difference between plain and P18-4 modified micelles ($P < 0.05$, one-way ANOVA, Tukey's post test).

3.4 Discussion

The main objective of our study was to develop traceable polymeric micellar carriers that can be used to image the biodistribution of micelles in live animals and by doing so, assess the effect of different modifications in the structure of these nanocarriers on their tumor accumulation. For this purpose, we have chemically conjugated a near infra-red probe (NIR), i.e., cy5.5, to the end of PEO-*b*-PCL and PEO-*b*-PBCL micellar carriers and assessed the effect of pendent group chemistry on the distribution of formed nano-carriers in an orthotopic breast tumor model *in vivo*. We have then modified the surface of the two nanocarrier with novel breast cancer targeting peptide ligands and assessed the effect of this modification on micellar biodistribution. NIR dyes have absorption and emission spectra at wavelengths of 700-1000 nm, and are better suitable for optical imaging since at this wavelength most biological tissues exhibit low scattering and minimal absorption thus enabling deeper tissue penetration and imaging.^{101, 102} In the case of block copolymer micelles, these NIR probes can either be conjugated to the hydrophilic shell of the micellar system,¹⁰⁵ or encapsulated¹⁰⁴ or conjugated^{53, 102} to the hydrophobic core.^{103, 106} However, conjugating to the hydrophilic shell can change the interaction of the micellar system with the proteins of the complement system thus leading to early removal by MPS. Physical encapsulation of NIR probe into the hydrophobic core can also lead to release of the probe from the micellar system. To the best of our knowledge this is the first report on the development of NIR labelled PEO-*b*-PCL and PEO-*b*-PBCL through chemical conjugation of NIR dye to the core of these nanocarrier and their tumor targeting ligand modified counterparts.

Our study was conducted on PEO-*b*-PCL and PEO-*b*-PBCL micelles with similar DP of 114 for the PEO block and 8-11 for the PCL/PBCL block. We chose to use a similar DP of the core-forming block in both polymers to eliminate the possibility of hydrophobic block length contribution to our observations. The Cy5.5 labeled PEO-*b*-PCL and PEO-*b*-PBCL polymers were then mixed with either plain or P18-4 modified PEO-*b*-PCL and PEO-*b*-PBCL polymers, respectively to achieve NIR labeled micelles. Characterization studies of the mixed micelles show a significantly higher size for PEO-*b*-PCL micelles when compared to their PEO-*b*-PBCL counterparts as measured by DLS (Table 3.2). This might reflect the presence of worm shaped micelles along with spherical micelles for PEO-*b*-PCL (Figure 3.2). Previous literature suggested the formation of worm-like micelles, to begin at PCL/PEO molecular weight fractions higher than 2.5 in PEO-*b*-PCL micelles.³⁴⁷ Formation of spherical micelles, on the other hand, has been documented at PCL/PEO molecular weight fractions as low as 0.5. The PCL/PEO molecular weight fraction in our case however, was 0.25.^{307, 348} Morphology at such low PCL/PEO molecular weight fractions have not been reported previously and further investigation needs to be carried out to find the reason for this change in shape from spherical morphology. The conjugation of Cy.5.5 dye might have contributed to this observation.

In line with previous findings we have seen a higher thermodynamic stability for PEO-*b*-PBCL micelles compared to PEO-*b*-PCL ones as evidenced by lower CMC of PEO-*b*-PBCL micelles at similar degrees of polymerization for the hydrophobic block (Table 3.2). The high thermodynamic stability of the polymeric micelles is an important factor determining the stability of polymeric micelles in the biological system.^{54, 307} Presence of aromatic groups on the PCL block also led to an increase in the kinetic stability as measured

by a decrease in the rate of dissociation of micelles when incubated with SDS (Figure 3.3). This may be due to the π - π stacking of the benzyl carboxylate groups in PEO-*b*-PBCL micelles leading to resistance towards dissociation.³⁰⁷

Surface modification with P18-4 peptide did not affect the thermodynamic stability of micelles, it did however, decrease the kinetic stability of the micelles when incubated with SDS. Coupling of peptide P18-4 to polymeric micelles facilitated their uptake in MDA-MB-231 breast cancer cells. P18-4 is a stable derivative of the p160 peptide which is known to have a high affinity for breast cancer cells compared to noncancerous cells. Although the receptor for both these peptides is unknown, they can be internalized by cells thereby delivering the nanocarriers inside the cancer cells.^{192, 349} Increasing the peptide density of P18-4 significantly increased the cellular uptake of cy5.5-loaded micelles in MDA-MB-231 cells using flow cytometry and confocal microscopy (Figure 3.4, Figure 3.5, and Figure 3.7). These results were similar to those seen previously for P18-4 modified liposomes and p160 modified micelles.^{193, 350} Presence of excess free P18-4 peptide significantly reduced the uptake of PEO-*b*-PCL and PEO-*b*-PBCL micelles modified with 10 mol % P18-4 peptide pointing to the involvement of receptor mediated endocytosis in the uptake of P18-4 decorated micelles via the receptor for the P18-4 peptide (Figure 3.6). Similar results were seen previously for the P18-4 peptide in MDA-MB-435 cells.^{192, 193} However, at higher peptide density of 20 mol %, presence of free P18-4 peptide did not affect the uptake of both PEO-*b*-PCL and PEO-*b*-PBCL micelles. This may be due to the possibility of non-specific cell uptake at higher peptide densities. Similar results were seen in MCF10A cell line where P18-4 modification of 10 mol % exhibited a lower cellular association than in MDA-MB-231 cells however, P18-4 modification of 20 mol % resulted in significantly higher cellular

uptake pointing to the possibility of non-specific cell uptake. These results were also seen previously for high density P18-4 modified liposomes in MCF10A cells.¹⁹³

PEO-*b*-PCL micelles showed significantly higher uptake in MDA-MB-231 breast cancer cells compared to PEO-*b*-PBCL. One possible reason for the higher uptake in case of PEO-*b*-PCL micelles might be the presence of worm shape micelles in this population.³⁵¹ As the cy5.5 dye quenches once inside the micellar core, another possible reason for the higher MFI for PEO-*b*-PCL micelles (Figure 3.4) can be due to their lower thermodynamic and kinetic stability, which might have led to their dissociation inside the cell, thus de-quenching the cy5.5 dye showing higher fluorescence when compared to PEO-*b*-PBCL micelles. However, in our case, this does not look like a possible reason since we not only saw an increase in the MFI for PEO-*b*-PCL micelles, but also an increase in the % cy5.5 positive cells for PEO-*b*-PCL micelles when compared to PEO-*b*-PBCL micelles (Figure 3.5), indicating that the PEO-*b*-PCL micelles, indeed show a higher uptake into the MDA-MB-231 breast cancer cells.

In vivo biodistribution studies were carried out in an orthotopic breast tumor animal model. Orthotopic tumor models are more representative of a primary tumor with respect to tumor site and metastasis when compared to s.c. tumor models which are commonly used for screening various anti-cancer drugs in mice.³⁵² The organ environment has been found to influence the response of tumors to chemotherapy. A previous study has shown that the response to doxorubicin can be highly varied depending on the site of the tumor with 80% inhibition in growth at the s.c. site whereas only 40% inhibition in tumor growth at the orthotopic site.³⁵³ Thus orthotopic models are necessary for a more accurate analysis of

tumor growth and treatment. To follow the growth of the tumor and also track any possible metastasis in major organs, MDA-MB-231 cells expressing firefly luciferase were used.

Both PEO-*b*-PCL and PEO-*b*-PBCL micelles showed fluorescence in liver, spleen, and kidneys indicating their recognition by the organs of the MPS along with renal clearance in kidney, respectively (Figure 3.12). Plain and P18-4 modified PEO-*b*-PCL micelles showed higher accumulation in kidneys indicating faster renal clearance compared to their PEO-*b*-PBCL counterparts. Since glomerular filtration, which is the first step in renal clearance is highly size-selective and the PEO-*b*-PCL micelles had a size of 100 nm and above which is higher than the threshold for renal clearance,³⁵⁴ it is most likely that the PEO-*b*-PCL micelles dissociated in the serum leading to their faster clearance. This is possible due to their lower thermodynamic and kinetic stability. PEO-*b*-PBCL micelles, on the other hand, showed better stability both *in vitro* and *in vivo* which might be due to the rigidity of the core.³⁵¹ PEO-*b*-PBCL micelles showed significantly higher accumulation into the heart, liver, lungs, and spleen, but lower accumulation into the kidneys, when compared to PEO-*b*-PCL micelles (Figure 3.12), indicating that the higher accumulation into the other organs may not be due to the higher uptake of PEO-*b*-PBCL micelles to these organs but rather due to the faster clearance of PEO-*b*-PCL micelles through the kidneys.

P18-4 modification of micelles resulted in more rapid accumulation into the tumor site. Owing to the small size of the PEO-*b*-PBCL micelles, plain micelles can quickly diffuse out of the vasculature into the tumor tissue through the large endothelial gaps. However, due to their small size, they are less likely to be retained at the tumor site since they can easily diffuse out of the tumor tissue back into the vasculature.³⁵⁵ P18-4 modified micelles, however, can interact with the P18-4 receptors over-expressed on the cancer cells thus being

retained in the tumor tissue leading to more rapid accumulation. Previous studies using RGD modified nanocarriers showed more rapid accumulation in tumor sites compared to plain nanocarriers. However, RGD is also over-expressed in the tumor endothelium and the rapid accumulation for the RGD modified carriers may be due to the uptake of these targeted nanocarriers in the tumor endothelium rather than by retention in the tumor cells.³⁵⁶

P18-4 modification of micelles at low density did not alter the biodistribution into other organs. Previous studies have shown that high densities of peptides on the nanocarrier surface can lead to an abnormal uptake by the MPS organs like spleen and liver resulting in faster clearance from the body.^{357, 358} Since our results did not show any increased accumulation in the spleen or kidney after P18-4 modification, this indicated that the density used for modification was apt. In fact, P18-4 modified PEO-*b*-PBCL micelles showed lower accumulation in the spleen.

3.5 Conclusion

In general, aromatic substitution of PEO-*b*-PCL improved the thermodynamic and kinetic stability of the micelles, leading to a better accumulation of the nanocarrier in primary breast tumors in an orthotopic mouse tumor model. Modification of polymeric micelles with a novel breast tumor targeting peptide ligand, improved rapid homing of nanocarriers in primary breast tumors in mice, irrespective of the core structure. The results of this study demonstrated the tremendous potential of developed traceable nano-carriers, particularly those based on PEO-*b*-PBCL and their P18-4 modified counterparts for targeted therapy of breast cancer. The results also point to the potential of the NIR-labeling chemistry

in studying the biodistribution of other PEO-*b*-poly(ester) based nanocarriers and as possible contrast agents for diagnosis of breast tumors in the future.

3.6 Acknowledgements

This study was supported by a grant from Canadian Institution of Health Research (CIHR). S.M.G. was supported by the Alberta Innovates Health Solutions Graduate Studentship and the Honorary Dissertation Fellowship. We thank Mr. Vishwanatha Somayaji, Faculty of Pharmacy and Pharmaceutical Sciences, University of Alberta for assistance with ¹H NMR analysis; the Flow Cytometry Lab in Department of Experimental Oncology at Cross Cancer Institute for assistance with flow cytometry; the Microscopy Lab in Department of Experimental Oncology at Cross Cancer Institute for assistance with confocal microscopy; the Advanced Microscopy Facility (AMF), Department of Biological Sciences, University of Alberta for assistance with TEM analysis; Mr. Dan McGinn, Department of Oncology, University of Alberta, for assistance with IV (tail-vein) injections; and Ms. Nicole Favis, Department of Immunology, University of Alberta for assistance with the animal facility.

Chapter Four
**Application of Click Chemistry in the Preparation of Poly(ethylene oxide)-
block-poly(ϵ -caprolactone) with Hydrolysable Crosslinks in the Micellar
Core**

A version of this chapter has been published in

Macromolecules 2011, 44, 2058-2066

Shyam M Garg¹, Xiao-Bing Xiong¹, Changhai Lu¹, Afsaneh Lavasanifar^{1,2}

¹Faculty of Pharmacy and Pharmaceutical Sciences, University of Alberta, Edmonton, AB

²Department of Chemical and Materials Engineering, Faculty of Engineering, University of
Alberta, Edmonton, AB

Reprinted with permission from Reference.³¹⁶ Copyright (2011) American Chemical Society

4.1 Introduction

Over the last few decades, block copolymers have emerged as an interesting class of biomaterials due to their versatile applications in pharmaceutical science and drug delivery. Of particular interest are amphiphilic block copolymers which self-assemble into polymeric micelles with core-shell architectures above the critical micelle concentration (CMC). Polymeric micelles are currently under investigation as nano-delivery systems for depot drug release and targeted drug delivery.¹⁶⁻¹⁸ The use of polymeric micelles for the mentioned applications, however, has been hampered by the poor *in vivo* stability of most micellar structures upon administration to systemic circulation, which leads to micellar dissociation and premature release of encapsulated drugs.

Considerable research has focused on increasing the stability of polymeric micelles by preventing their dissociation in the extreme dilution conditions of the blood stream upon intravenous administration. Some of the strategies currently under study for the stabilization of polymeric micelles include chemical modification of the hydrophobic block,^{42, 359, 360} introduction of crystallinity or stereocomplex formation,^{322, 361} covalent attachment of hydrophobic drug,^{362, 363} formation of glassy core,³⁶⁴ and crosslinking of the micellar core or shell. Crosslinked micelles can stay in the micellar form at concentrations below CMC of their block copolymer; thus avoiding rapid drug release.^{71, 365-367} Crosslinks are preferred to degrade in response to internal or external stimuli ensuring the release of incorporated drug in the vicinity of cellular or molecular drug targets and at the same time result in the biological elimination of the colloidal carrier after drug release.

One of the earliest examples of crosslinking of the micellar shell was reported by Wooley and coworkers in 1996.¹⁶⁶ Since then, this strategy has been investigated by many

other groups.^{169, 176, 368-370} Core-crosslinking was first reported by Tuzar and coworkers in 1979⁷⁶ and 1982⁷⁷ in which poly(styrene/butadiene/styrene) micelles with cores consisting of polybutadiene blocks were stabilized by UV radiation in the presence of a photo-initiator. Similar strategies involving crosslinking of the hydrophobic core by either thermal,³⁹ photo-induced polymerization,^{40, 72} or conventional chemical reactions in the micellar core have been carried out.^{39, 40, 46, 72, 74, 75, 371, 372} More recently, a doxorubicin methacrylamide derivative bearing a hydrolytically sensitive hydrazone linker was covalently incorporated into the crosslinked core of polymeric micelles composed of mPEO-*b*-poly[N-(2-hydroxypropyl)methacrylamide-lactate] diblock copolymers by free radical polymerization.³⁷³ However most of these strategies included harsh conditions during the procedures and have other disadvantages. For example, photo-crosslinkable materials are conventionally unstable when exposed to light.³⁷⁴ Besides, high temperatures during thermal polymerization can cause decomposition of the incorporated biomolecules.

Click chemistry has emerged as a highly efficient technique, providing attractive possibilities for the synthesis of polymers with different architectures. It offers advantages including ambient reaction conditions, quantitative yields, easily obtained starting materials, and in particular high specificity which make the reaction doable for molecules bearing extra functional groups avoiding the need for the protection/deprotection reactions.⁸¹⁻⁸⁴ In 2001, Sharpless and coworkers⁸² introduced the concept of click chemistry reactions of which the Cu(I)-catalyzed Huisgen 1,3-dipolar cycloaddition reaction between terminal alkynes and azides is one of the most popular and commonly used click reaction.^{86, 87} In previous studies, click chemistry has been used to prepare shell as well as core-crosslinked micelles.^{81, 88, 89, 177}

In this article, we report a unique strategy leading to the introduction of hydrolysable crosslinks to the core of poly(ethylene oxide)-*block*-poly(ϵ -caprolactone) (PEO-*b*-PCL) micelles using click chemistry. Copolymers of PEO-*b*-PCL have been extensively explored in drug delivery. In our research group both the core and shell block of PEO-*b*-PCL micelles have been engineered to achieve depot or targeted drug and siRNA delivery.^{43, 111, 121, 139, 190, 191, 198, 201, 301-303} Here we report the successful synthesis and characterization of core-crosslinked PEO-*b*-PCL micelles by click chemistry. Toward this, block copolymers of PEO-*b*-PCL having pendent propargyl carboxylate groups on PCL block, i.e. PEO-*b*-PPCL were synthesized via ring-opening polymerization of α -propargyl carboxylate ϵ -caprolactone (PCL) using PEO as the initiator. Consequently, the block copolymer self-associated into micelles in aqueous solution. The micelle core was then crosslinked via reaction between the azide group of tetraethylene glycol (bis)azide reagent and the alkyne group on the PPCL block in the presence of copper catalysts at room temperature. The formation of crosslinked micelles were confirmed and characterized by ¹H NMR and IR spectroscopy, transmission electron microscopy (TEM), X-ray photoelectron spectroscopy (XPS) and dynamic light scattering (DLS). The encapsulation and *in vitro* release of paclitaxel (PTX) in crosslinked micelles was compared to these properties for micelles without crosslinks. The results from this study points to the enhanced stability of crosslinked micelles in diluted conditions without any negative impact on the encapsulation and *in vitro* release of PTX in the presence of crosslinks.

To the best of our knowledge, this is the first paper that reports the use of click chemistry to develop core-crosslinked polymeric micelles which contain biocompatible PEO “crosslinks” that are attached to the poly(ester) core of polymeric micelles via “degradable”

ester bonds. This is also the first report on the application of click chemistry to prepare core-crosslinked micelles made up of highly used PEO-*b*-PCL diblock copolymers.

4.2 Experimental Section

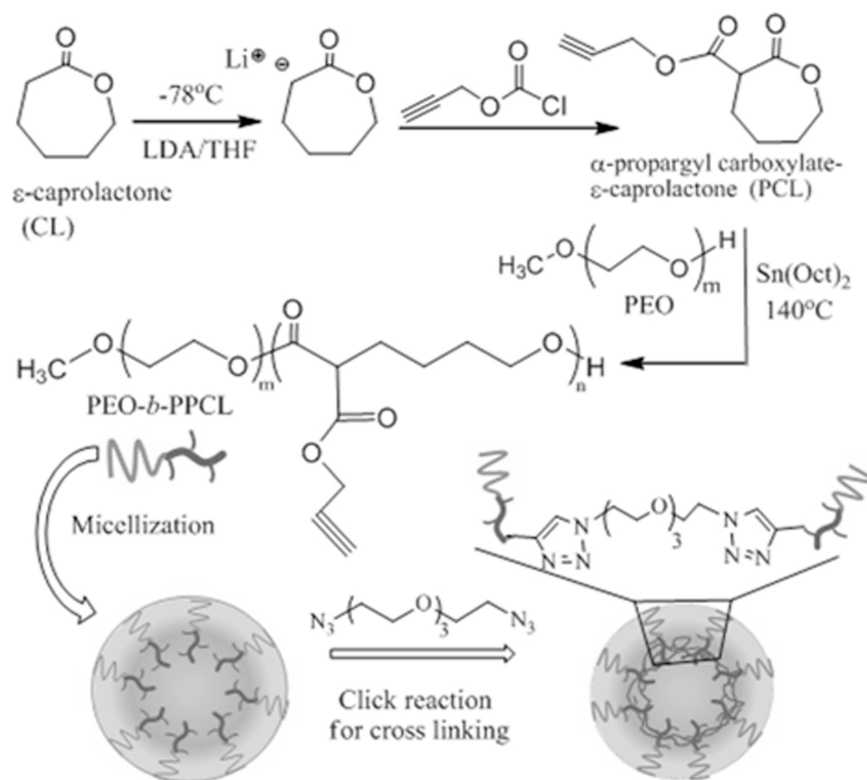
4.2.1 Materials.

Methoxy-polyethylene oxide (PEO) (average molecular weight of 5000 g/mol), diisopropylamine (99%), propargyl chloroformate, sodium (in kerosin), butyllithium (Bu-Li) in hexane (2.5 M solution), tetraethylene glycol ditosylate, and bovine serum albumin (BSA) powder were purchased from Sigma (St. Louis, MO). Paclitaxel (purity > 99.5) was purchased from LC Laboratories (Woburn, MA, USA). ϵ -Caprolactone was purchased from Lancaster Synthesis (UK). Stannous octoate was purchased from MP Biomedicals Inc. (Germany). All other chemicals were reagent grade. Tetraethylene glycol (bis)azide was synthesized from tetraethylene glycol ditosylate and sodium azide according to literature procedures and confirmed by ^1H NMR.³⁷⁵

4.2.2 Synthesis of α -Propargyl Carboxylate- ϵ -Caprolactone.

The method used for the synthesis of α -propargyl carboxylate- ϵ -caprolactone is shown in Scheme 1. Briefly, Bu-Li (24 mL) in hexane was slowly added to dry diisopropylamine (8.4 mL) in 50 mL of dry THF in a three-neck round-bottomed flask at -30 °C under vigorous stirring with continuous argon supply. The solution was cooled to -78 °C. ϵ -Caprolactone (3.42 g) was dissolved in 10 mL of dry THF and added to the above mentioned mixture slowly and the reaction was allowed to continue for 45 m. Propargyl

chloroformate (3.55 g) was added and the temperature was allowed to rise to 0 °C. The reaction was allowed to continue for 2 hours and was quenched with 5 mL of saturated ammonium chloride solution. The reaction mixture was diluted with water and extracted with ethyl acetate (110 mL). The combined extracts were dried over Na₂SO₄ and evaporated. The dark yellowish oily crude mixture was purified twice over a silica gel column, and the purity of the compound was confirmed with thin-layer chromatography (TLC) using hexane:ethyl acetate (2:1) as the mobile phase. The chemical structure was analyzed by ¹H NMR, ¹³C NMR, and IR.



Scheme 4.1 Synthetic scheme for the preparation of core-crosslinked micelles.

4.2.3 Synthesis of PEO-*block*-Poly(α -Propargyl Carboxylate- ϵ -Caprolactone) (PEO-*b*-PPCL).

Block copolymers of PEO-*b*-PPCL were synthesized by ring-opening polymerization of α -propargyl carboxylate- ϵ -caprolactone using PEO as initiator and stannous octoate as catalyst (Scheme 1). Briefly, PEO (M_w : 5000 g/mol) (1.5 g), α -propargyl carboxylate- ϵ -caprolactone (1.5 g), and stannous octoate (0.002 equiv of monomer) were added to a 10 mL previously flamed ampoule, nitrogen purged and sealed under vacuum. The polymerization reaction was allowed to proceed for 4 h at 140 °C in oven. The reaction was terminated by cooling the product to room temperature. The ^1H NMR spectrum of α -propargyl carboxylate- ϵ -caprolactone bearing block copolymer in CDCl_3 at 300 MHz was used to assess the conversion of α -propargyl carboxylate- ϵ -caprolactone monomer to PPCL comparing the intensity of -O-CH₂ ($\delta = 4.25$ ppm) related peak for α -propargyl carboxylate- ϵ -caprolactone monomer to the intensity of the same protons for PPCL ($\delta = 4.05$ ppm). The number-average molecular weight of PEO-*b*-PPCL was determined from the ^1H NMR spectrum comparing peak intensity of PEO (-CH₂CH₂O-, $\delta = 3.65$ ppm) to that of PPCL (-C \equiv CH, $\delta = 2.55$ ppm), considering a 5000 g/mol molecular weight for PEO. The IR spectrum was obtained by dissolving the block copolymers in dichloromethane and preparing a thin film on NaCl disk.

The polydispersity of prepared block copolymer was assessed by gel permeation chromatography (GPC). Briefly, 20 μL of polymer solution (20 mg/mL in THF) was manually injected into a 7.8 \times 300 mm Styragel HMW 6E column (Waters Inc. Milford, MA) which was attached to an HP 1100 pump. The column was eluted with 1 mL/min THF.

The elution pattern was detected by refractive index (model 410; Waters Inc.) and dynamic light scattering detectors (PD 2000 DLS; Precision Detectors, Franklin, MA) using polystyrene standard of two molecular weights (M_w) (9580 and 13700 g/mol).

4.2.4 Micelle Formation and Core-Crosslinking.

First, micellization was achieved by solvent evaporation method. Briefly, the synthesized block copolymer of PEO-*b*-PPCL (60 mg) was dissolved in acetone (1 mL). This solution was added to 6 mL of doubly distilled water in a drop-wise manner under moderate stirring at room temperature, followed by the evaporation of acetone under vacuum. The prepared micellar solution was then centrifuged to remove any aggregates.

Micellar solution of block copolymers was crosslinked using the Huisgens 1,3-dipolar cycloaddition (azide-alkyne Click chemistry) reaction.^{86, 87} Briefly, to the prepared PEO-*b*-PPCL micelle solutions tetraethylene glycol (bis)azide (15.86 mg; 0.065 mmol) was added under vigorous stirring, followed by the addition of sodium ascorbate (2.57 mg; 0.013 mmol) and copper sulphate (0.21 mg; 0.0013 mmol). The reaction mixture was stirred for 16 h and then purified by dialysis against water and freeze-dried. The resulted polymer was subjected to ^1H NMR and IR analysis. The schematic representation of the preparation method for core-crosslinked micelles is shown in Scheme 1.

4.2.5 Characterization of Micelles.

The particle size and distribution of prepared micelles were estimated by DLS using Malvern Zetasizer 3000 at a polymer concentration of 10 mg/mL in water at 25 °C.

Morphology of the micelles was investigated by TEM. An aqueous droplet of micellar solution (20 μ L) with a polymer concentration of 1-2 mg/mL was placed on a copper-coated grid. The grid was held horizontally for 20 s to allow the colloidal aggregates to settle. A drop of 2% solution of phototungstic acid (PTA) in PBS (pH = 7) was then added to provide the negative stain. After 1 min, the excess fluid was removed by filter paper. The samples were then air-dried and loaded into a Hitachi H 700 transmission electron microscope. Images were obtained at a magnification of 18000X at 75 kV.

A change in the fluorescence excitation spectra of the hydrophobic pyrene in the presence of varied concentrations of PEO-*b*-PPCL was used to measure the critical micellar concentration (CMC) of the prepared block copolymer according to a method described previously.³⁷⁶ The fluorescence spectra were recorded using a Varian Cary Eclipse Fluorescence Spectrophotometer (Victoria, Australia). Emission wavelength and excitation/emission slit were set at 390 and 5 nm, respectively. The intensity ratio of peaks at 338 nm to those at 333 nm was plotted against the logarithm of copolymer concentration. The CMC was measured from a sharp rise in intensity ratios (I_{338}/I_{333}) at the onset of micellization.

X-ray photoelectron spectroscopy (XPS) measurements were conducted on freeze-dried sample of crosslinked micelles using an Axis-165 spectrometer (Kratos Analytical Inc, USA) with a monochromatic Al K α X-ray source at 1486.6 eV. The analyzer was operated in constant resolution mode at a pass energy of 20 eV and charge referencing was accomplished by setting the C 1s line of adventitious hydrocarbon on the specimen surface at 284.8 eV.

4.2.6 Evaluation of Protein Adsorption on Micelles.

Measurement of the amount of protein adsorbed on the surface of the micelles was carried out according to a method described previously.¹⁴⁸ Briefly, non-crosslinked and crosslinked micellar solutions (8 mg/mL) were mixed with equal volume of BSA solution (45 g BSA/L in 0.01 M PBS) and incubated for 4 h at 37 °C. Micellar solutions with equal volume of PBS were used as control and incubated for 4 h at 37 °C. After incubation, solution samples of 20 µL were injected into a gel permeation chromatography (GPC) system with a hydrogel column (Waters Inc., Milford, MA) at 25 °C. The elution pattern was detected at 35 °C by light scattering detector (model 410, Waters Inc.). 0.01 M PBS (pH 7.4) (1 mL/min) was used as eluent. Eluate containing the micellar fraction was collected and the concentration of protein in the eluate was measured using the Bio-Rad Protein assay (Bio-Rad, Hercules, CA).

4.2.7 Preparation of PTX loaded Micelles.

Encapsulation of PTX in non-crosslinked PEO-*b*-PPCL was accomplished as reported before.^{111, 377} Briefly, the block copolymer and PTX were both dissolved in N-N-dimethyl formamide (DMF) as the organic solvent. This solution was added to water in a drop-wise manner followed by dialysis of the solution against water to remove DMF. For PTX loading in crosslinked micelles, two different methods were used. In the first method (method I), PTX, PEO-*b*-PPCL and the crosslinking agent (tetraethylene glycol (bis)azide) were all added to DMF and this solution was added to water containing sodium ascorbate and CuSO₄. In the second method (method II), PTX encapsulated micelles were prepared as

described above. The crosslinking agent and other reagents were then added to micellar aqueous solution. The applied drug to polymer weight ratio was 20 for all formulations. After dialysis, the solution was centrifuged at $11,600 \times g$ for 5 min to remove any precipitate, and an aliquot (100 μL) of the micellar solution was diluted with acetonitrile. The solution was analyzed for PTX content using HPLC. Reversed phase chromatography was carried out using a Varian Prostar 210 HPLC system equipped with a Microsorb-MV 5 μm C18-100 Å column (4.6 mm \times 250 mm), and Varian 335 Photodiode Array HPLC detector (Varian Inc., Australia). 20 μL of sample was injected in a gradient elution using 0.1% trifluoroacetic acid aqueous solution and acetonitrile at a flow rate of 1.0 mL/min at room temperature. The proportion of acetonitrile was 40% at time 0 and increased with elution time up to 100% within 15 min.^{111, 378} The detection was performed at 227 nm. The level of PTX loading (w/w %) and encapsulation efficiency was calculated using the following equations:

$$\text{PTX loading (\%)} = \frac{\text{amount of physically loaded PTX in mg}}{\text{amount of copolymer in mg}} \times 100 \%$$

$$\text{Encapsulation efficiency (\%)} = \frac{\text{amount of physically loaded PTX in mg}}{\text{amount of PTX added in mg}} \times 100\%$$

4.2.8 Release of PTX from Polymeric Micelles.

Release of PTX from non-crosslinked and crosslinked micelles was determined in 0.01 M phosphate buffer (pH 7.4) containing 2M sodium salicylate at 37 °C.^{111, 379, 380} The experiment was initiated by the addition of free or micellar PTX solution to the buffer. The PTX loaded non-crosslinked and crosslinked micelles were prepared at 20 $\mu\text{g/mL}$ PTX

concentration according to the previous mentioned method. Then, 10 mL (containing 200 µg PTX) of the micellar solutions were transferred into a dialysis bag (Spectraphor, M_w cutoff 3500 g/mol). The dialysis bags were placed into 500 mL of 0.01 M phosphate buffer (pH 7.4). The release study was performed at 37 °C in a Julabo SW 22 shaking water bath (Germany). At selected time intervals the whole release media was replaced with fresh one and aliquots of 200 µL were withdrawn from the inside of the dialysis bag for HPLC analysis. The amount of PTX released was calculated by subtracting the amount of PTX remained in the dialysis bag from the initially added PTX. The release profiles were compared using similarity factor, f_2 , and the profiles were considered significantly different if $f_2 < 50$.³⁸¹

$$f_2 = 50 \times \log \left(\left[1 + \left(\frac{1}{n} \right) \sum_{j=1}^n |R_j - T_j|^2 \right]^{-0.5} \times 100 \right)$$

Where n is the sampling number, R_j and T_j are the percent released of the reference and test formulations at each time point j .

4.3 Results and Discussion

4.3.1 Synthesis and Characterization of Block Copolymers.

Block copolymers of PEO-*b*-PPCL were developed by ring-opening polymerization of α -propargyl carboxylate- ϵ -caprolactone monomer using PEO as initiator and stannous octoate as catalyst.³⁰⁸ Our research group and others have previously reported on the preparation of substituted lactone monomers such as α -benzyl carboxylate- ϵ -caprolactone,⁴³ α -propargyl- δ -valerolactone,³⁸² α -allyl- δ -valerolactone,³⁸³ α -propargyl- ϵ -caprolactone,^{384, 385}

and α -iodo- ϵ -caprolactone.³⁸⁶ For this purpose, anionic activation of ϵ -caprolactone monomer was performed using freshly prepared non-nucleophilic strong base LDA to extract a methylene proton from α -position ($-\text{CH}_2-\text{C}=\text{O}$). The generated lithium carbanion was then quenched with propargyl chloroformate to obtain α -propargyl carboxylate- ϵ -caprolactone (Scheme 1).³⁸⁷ After column chromatography, α -propargyl carboxylate- ϵ -caprolactone was isolated as a slightly yellow thick oily liquid. The product produced a single spot at R_f value of 0.37 in TLC. The yield of reaction was 49.2%. The structure was confirmed by combined analysis of ^1H NMR and IR. In 300 MHz ^1H NMR spectroscopy in CDCl_3 , corresponding proton peaks were observed at δ : 1.20-2.20 (m, 6H); δ : 2.50 (s, 1H); δ : 3.75 (d, 1H); δ : 4.15-4.40 (m, 2H); δ : 4.70-4.85 (q, 2H) (Figure 4.1A). The peak at 3.75 ppm for α -propargyl carboxylate- ϵ -caprolactone, which corresponds to a single proton instead of two protons of ϵ -caprolactone monomer, indicates the successful substitution of the propargyl carboxylate on ϵ -caprolactone at the α -position. The presence of two negative peaks for carbonyl at 168.10 and 171.38 ppm and the generation of a new characteristic positive peak at 50.65 ppm in the ^{13}C NMR spectrum also confirm the chemical structure of the reaction product (Figure 4.2). The presence of strong peak in the IR spectrum (Figure 4.1B) at 1725 cm^{-1} corresponds to the carbonyl groups in lactone and propargyl carboxylate. The presence of strong peak at 3270 cm^{-1} and weak peak at 2120 cm^{-1} corresponds to the alkyne group in the monomer.

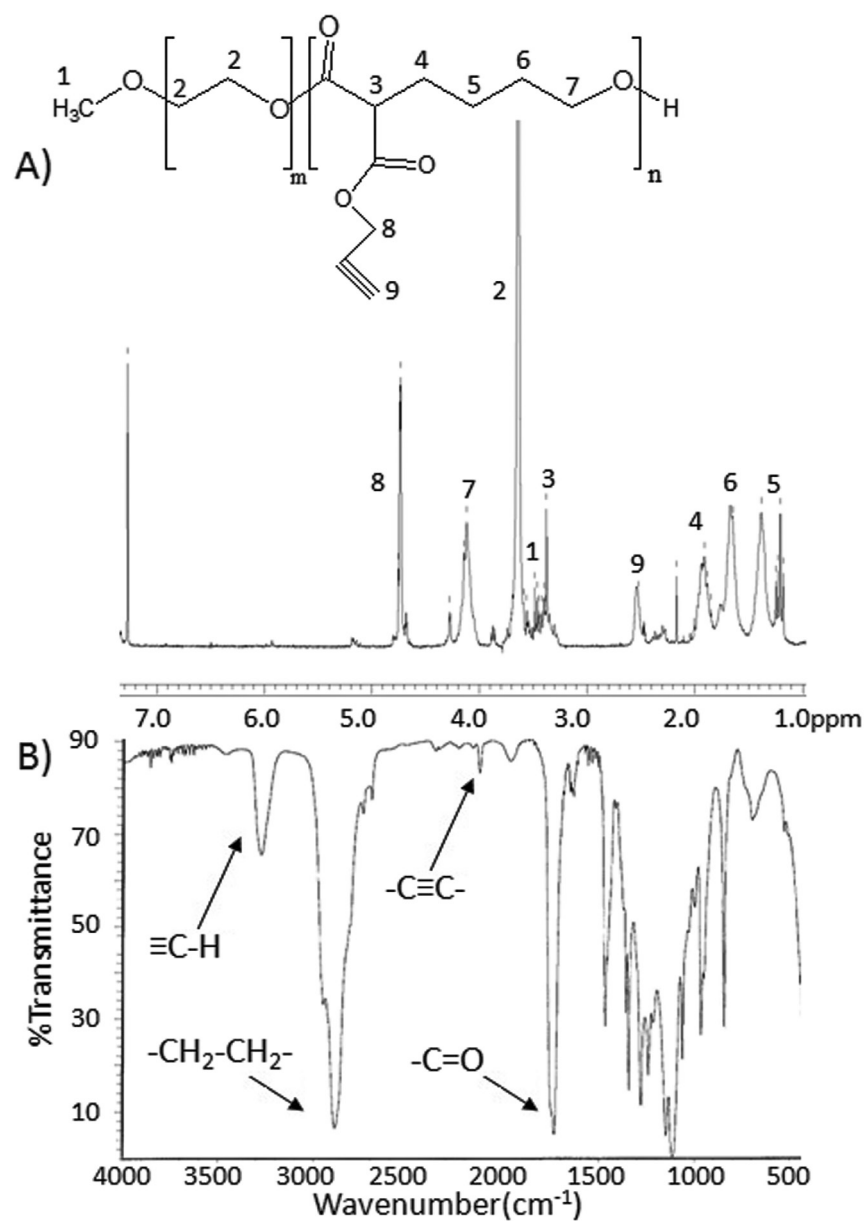


Figure 4.1 (A) ^1H NMR spectrum of α -propargyl carboxylate- ϵ -caprolactone (substituted monomer) in CDCl_3 and peak assignments. (B) IR spectrum of α -propargyl carboxylate- ϵ -caprolactone. Arrow indicates the presence of characteristic groups.

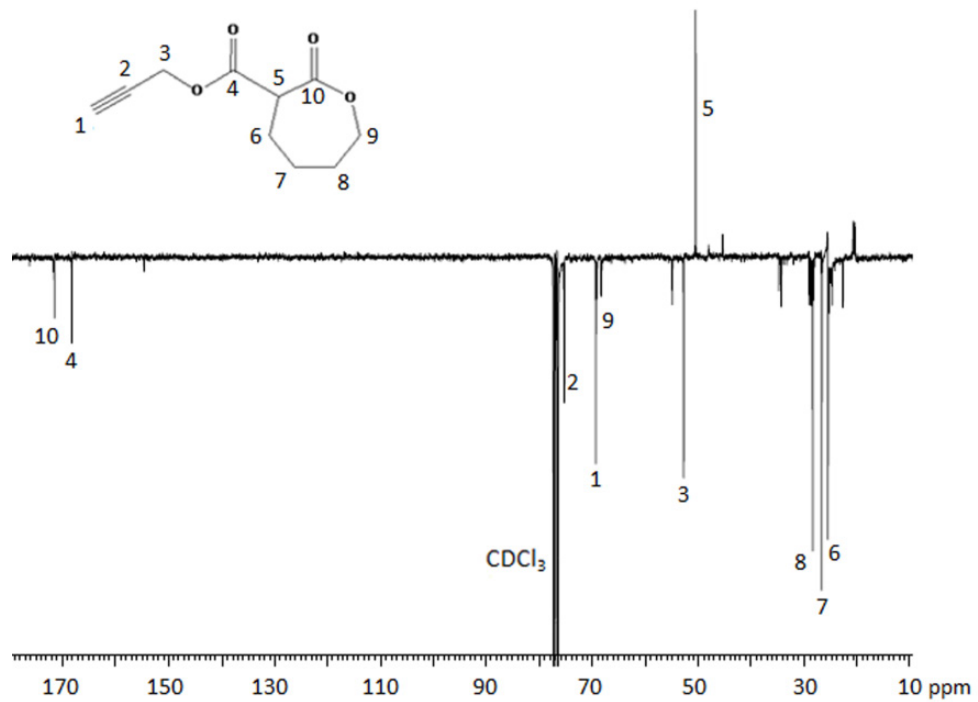


Figure 4.2 ^{13}C NMR spectrum of α -propargyl carboxylate- ϵ -caprolactone (substituted monomer) in CDCl_3 and peak assignments.

In 300 MHz ^1H NMR spectroscopy conducted on PEO-*b*-PPCL in CDCl_3 corresponding proton peaks for the product were observed at δ : 1.20-2.15 (m, 6H); δ : 2.50 (s, 1H); δ : 3.30-3.45 (s, 3H; m, 1H); δ : 3.65 (s, 4H); δ : 4.05-4.25 (m, 2H); δ : 4.75 (s, 2H) (Figure 4.3A). The presence of peaks at 2.50 and 4.75 ppm, which are due to the alkyne and methylene protons of the propargyl carboxylate group, respectively, confirms the polymerization of α -propargyl carboxylate- ϵ -caprolactone and the presence of alkyne groups in the structure of block copolymer. Furthermore, the characteristic downfield shift of the methylene protons ($-\text{OCH}_2-$ of α -propargyl carboxylate- ϵ -caprolactone) from 4.30 to 4.15 and $\text{O}=\text{C}-\text{CH}-$ proton from 3.75 to 3.30 in the ^1H NMR spectra (Figure 4.1A and 4.3A) strongly indicates the ring-opening polymerization of the monomer and formation of block copolymers. The characteristic terminal alkyne peak at 3270 cm^{-1} and the $-\text{C}\equiv\text{C}-$ peak at 2120 cm^{-1} in the IR spectrum of PEO-*b*-PPCL indicates the presence of terminal alkyne group in the block copolymer (Figure 4.3B).

The molecular weight of prepared PEO-*b*-PPCL block copolymer, measured by comparing the peak intensities of four methylene protons of PEO (δ : 3.65) and one alkyne proton of PPCL (δ : 2.50) in the ^1H NMR spectrum, was calculated to be 8800 g/mol (equal to a degree of α -propargyl carboxylate- ϵ -caprolactone polymerization of 19 i.e. PEO₁₁₄-*b*-PPCL₁₉). The resulting block copolymer showed a broad polydispersity ($M_w/M_n = 1.50$) when measured by GPC analysis.

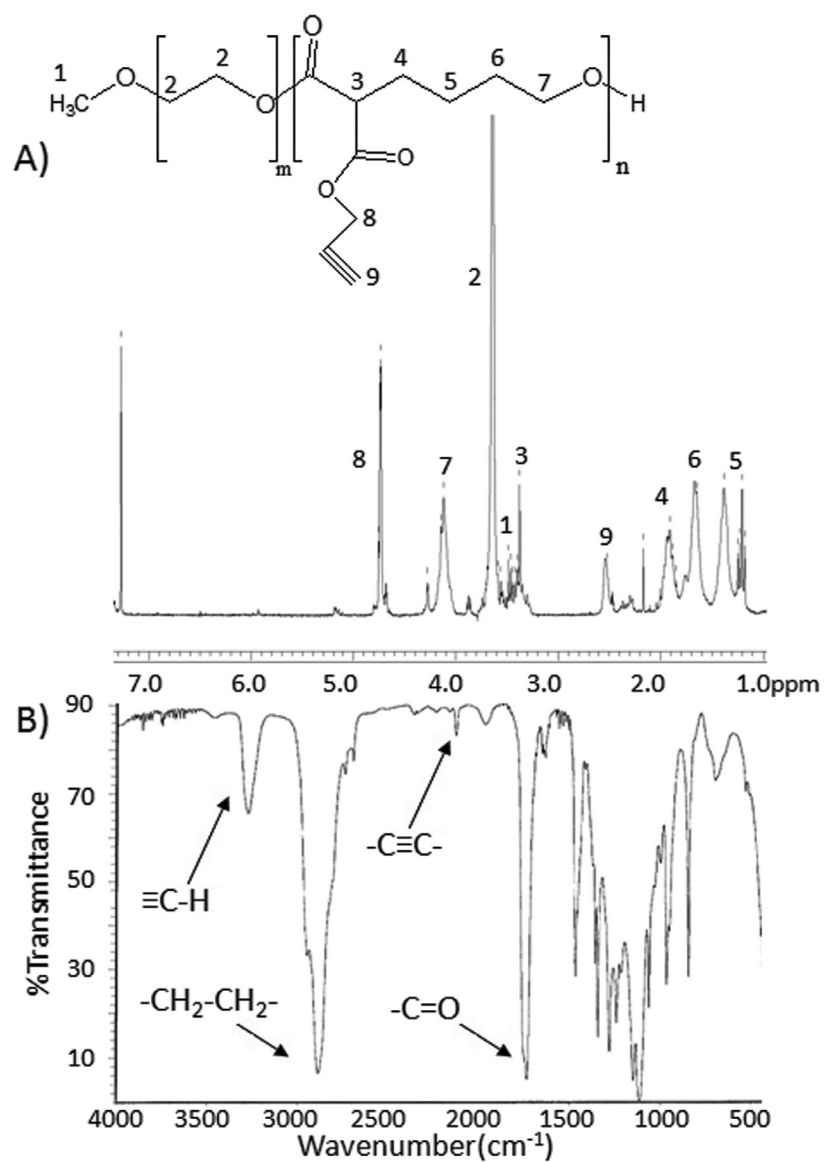


Figure 4.3 (A) ^1H NMR spectrum of PEO-*b*-PPCL in CDCl_3 and peak assignments. (B) IR spectrum of PEO-*b*-PPCL.

4.3.2 Micellization of Block Copolymers and Core-Crosslinking.

Synthesized block copolymers were assembled to polymeric micelles by a co-solvent evaporation method as described previously.^{43, 308} In order to prevent the disassembly of micelles in the high dilution conditions of the blood stream, the dissociation of the micellar core must be prevented. This can be achieved by crosslinking the micelles at the core which has proven to be an effective method in the past.^{39, 40, 72} Crosslinking of the PPCL core was carried out using bifunctional tetraethylene glycol bis(azide) via copper-catalyzed azide-alkyne cycloaddition (CuAAC) click chemistry reaction which has been previously used for the preparation of block copolymers or polyesters with various functional groups.^{388, 389}

The presence of terminal alkyne group and azide group is necessary for the Cu(I)-catalyzed Huisgen 1,3-dipolar cycloaddition reaction to take place. Cu(I) acts as a catalyst for the reaction. Cu(I) is prepared in-situ by addition of Cu(II) CuSO₄, and ascorbic acid, which acts as a reducing agent, and reduces Cu(II) to Cu(I).⁸⁶ Preparation of crosslinked micelles by this method has several major advantages to those previously reported: The reaction is known to be carried out under ambient conditions and is highly specific. The Cu(I), ascorbic acid, and unreacted azide can be removed by dialysis after completion of the reaction. Finally, this method provides means for the introduction of crosslinks at desired density through potentially degradable ester bonds to the poly(ester) core of micelles ensuring ultimate removal of the micellar carrier from the biological system upon degradation.

The size and morphology of the micelles were studied by DLS and TEM (Figure 4.4). The average diameter for micelles was shown to decrease from 97.9 ± 0.6 nm for non-

crosslinked micelles to 82.6 ± 0.3 nm for crosslinked micelles. The micellar population showed a similar distribution in both cases (PI=0.43). The decrease in size can be a result of the packing at the core due to covalent bond formations. The TEM picture for both micelles shows the formation of true spherical-shaped colloidal particles having a clear boundary (Figure 4.4A and 4.4B). The average diameter in the dry state based on TEM images was shown to decrease from 19.5 nm for non-crosslinked micelles to 15.4 nm for crosslinked micelles, which shows a similar trend to the DLS data. The difference in size measured by these two methods (97.9 vs. 19.5 nm for non-crosslinked micelles and 82.6 vs. 15.4 nm for crosslinked micelles) is attributed to the acquirement of the TEM images under a dry state as opposed to DLS that measures particles in a hydrated state in aqueous solutions.^{111, 390, 391}

To further verify the success of core-crosslinking, equal volume of acetone was added to a 500 $\mu\text{g/mL}$ micellar solution. DLS measurements were performed to compare the stability of the crosslinked and non-crosslinked micelles (Figure 4.4C and 4.4D). The crosslinked micelles did not dissolve in acetone thus confirming crosslinking of the core.³⁹² The average size and polydispersity of the crosslinked micelles were slightly larger in acetone which can be due to swelling of the core of the crosslinked micelles as a result of being penetrated by solvent molecules in this case acetone.^{46, 372} The non-crosslinked micelles however, dissociated and did not give any reading on the DLS. Samples maintained at 25 °C were analyzed by DLS after 21 days (data not shown). The crosslinked micelles still maintained their nanostructure as opposed to the non-crosslinked micelles, but with slightly larger size. This further verifies the stability of the core-crosslinked micelles.

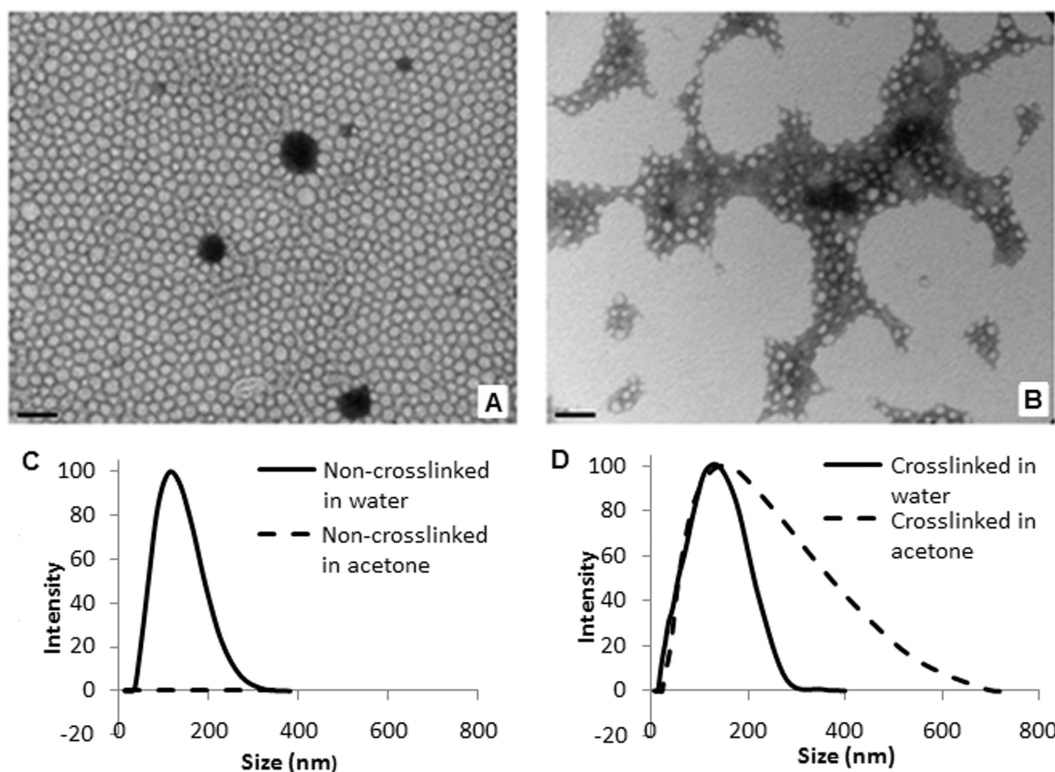


Figure 4.4 TEM picture of A) non-crosslinked micelles and B) crosslinked micelles (magnification 18000X). Particle size distribution of C) non-crosslinked micelles and D) crosslinked micelles by DLS in water and in acetone.

^1H NMR spectroscopy was performed on the freeze-dried micelles in CDCl_3 (Figure 4.5). CDCl_3 is a good solvent for the PEO-*b*-PPCL block copolymer. The signal for the hydrophobic PCL block is clearly visible in the non-crosslinked micelles (1.20-2.00 ppm) (Figure 4.5A). However, the signal has weakened considerably in case of the crosslinked micelles (Figure 4.5B). Since the PCL segment is present in the interior of the micelle, the covalent bond formed while crosslinking results in the rigidity of the hydrophobic core and maintenance of micellar structure in organic solvents like CDCl_3 . Since the solvent is unable

to penetrate the interior, the signal corresponding to the intensity of the PCL block at the interior is weakened due to lack of mobility of core segments.³⁷² This confirms the stability of crosslinked micelles over the non-crosslinked micelles.

The IR spectrum confirmed that click chemistry reaction has taken place (Figure 4.6). The absence of peaks at 3270 cm^{-1} and weak peak at 2120 cm^{-1} corresponding to the alkyne group in the PPCL core along with the appearance of sharp peak at 810 cm^{-1} corresponding to =C-H bending (characteristic of tri-substituted alkene) indicates the reaction of alkyne and azide groups in the PPCL core and diazide crosslinker producing the triazole ring.

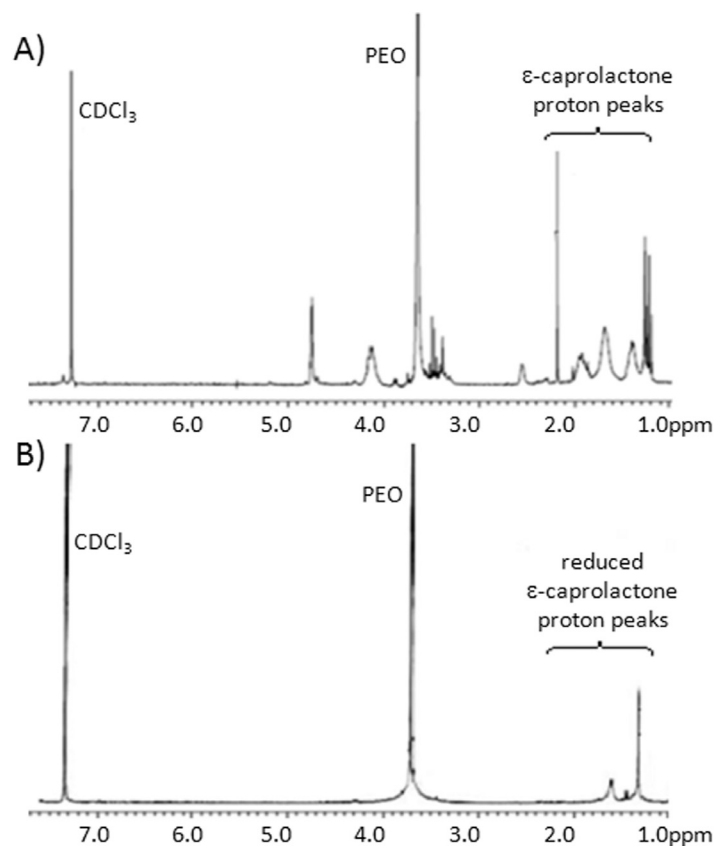


Figure 4.5 ^1H NMR spectrum and peak assignments of (A) non-crosslinked micelles and (B) crosslinked micelles in CDCl_3 .

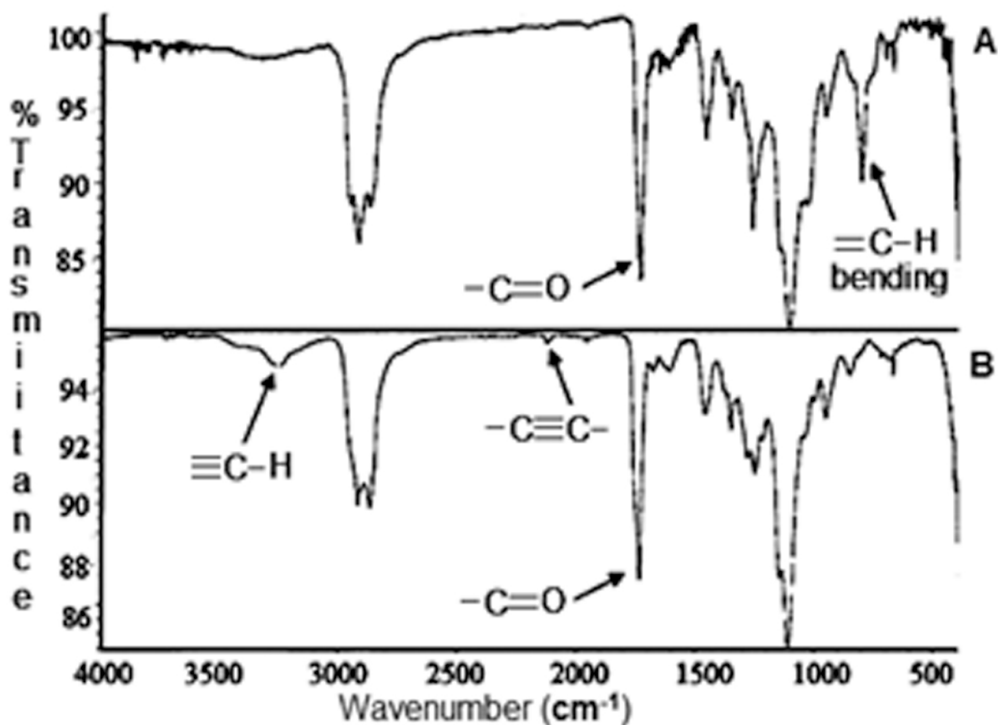


Figure 4.6 IR spectrum of (A) crosslinked micelles and (B) non-crosslinked micelles.

The elemental analysis by XPS is showed in Table 4.1. The mass concentration of Nitrogen in the sample calculated by XPS was found to be 3.65 %. Figure 4.7 shows a broad N1s peak near 400 eV. By multipeak fitting, the peak can be separated into two peaks at 399.9 and 401.4 eV, which corresponds to the triazole ring. The absence of a peak at ~405 eV indicates the absence of azide group in the sample.³⁹³⁻³⁹⁵ This indicates the removal of any excess azide from the crosslinked micelles. In addition, XPS revealed an extremely small Cu2p peak denoting the presence of residual Cu²⁺ ions, with a mass concentration of 0.20 % in the crosslinked micelles. This indicates that Cu ion could not be completely removed from the sample which may be due to the fact that the dialysis was not carried out in the presence of 0.02M ethylenediaminetetraacetic acid disodium (EDTA).³⁹³

Table 4.1 Elemental analysis by XPS giving atomic and mass concentrations (%) of the following elements.

Peak	Atomic Concentration (%)	Mass Concentration (%)
C 1s	69.87	63.20
O 1s	25.66	30.93
N 1s	3.46	3.65
Cu 2p	0.04	0.20

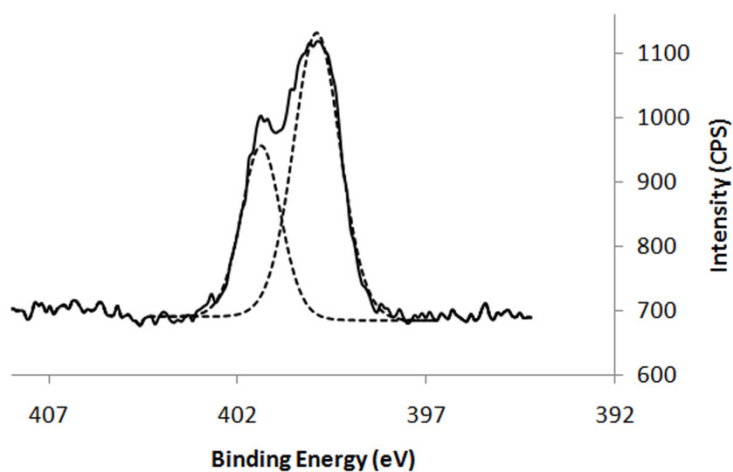


Figure 4.7 XPS spectrum of nitrogen (N 1s) in core-crosslinked micellar sample. The dotted line indicates the use of peak fitting software to identify two peaks within the N 1s spectrum.

The CMC of PEO-*b*-PPCL block copolymer was determined by fluorescence spectroscopy using pyrene as the fluorescent probe. Pyrene is a strong hydrophobic probe with very low water solubility. Because of its hydrophobicity, it preferentially partitions into the hydrophobic domain of the micellar core at concentrations above CMC, resulting in a change in its photophysical properties. This property is used to measure the CMC of block copolymers. A sharp rise in intensity ratio of peaks at 338 nm to those at 333 nm from the excitation spectra of pyrene indicates the onset of micellization. Using this method, the average CMC of PEO₁₁₄-*b*-PPCL₁₉ block copolymer was found to be $0.305 \pm 0.025 \mu\text{M}$. This value was found to be higher than that obtained for PEO₁₁₄-*b*-PBCL₁₉ ($0.182 \mu\text{M}$; previously carried out in our laboratory).⁴³ The increase in the CMC of PEO₁₁₄-*b*-PPCL₁₉ compared to PEO₁₁₄-*b*-PBCL₁₉ is attributed to the lower hydrophobicity of the core-forming block in PEO-*b*-PPCL. With regards to crosslinked micelles, the concept of CMC is not applicable as they have a covalently attached micellar structure and hence the CMC assessment for crosslinked micelles was not carried out.³⁹²

4.3.3 Protein Adsorption on Micelles.

Interaction with serum proteins is one of the factors that influence the fate of drug delivery vehicles like liposomes,¹⁵⁹ nanoparticles,³³¹ and micelles¹⁴⁸ in the body. The amount of protein adsorbed on the surface of the non-crosslinked and crosslinked micelles after incubation in a BSA solution prepared at physiological concentration was assessed according to a previously published method using gel permeation chromatography for the separation of BSA adsorbed micelles from free BSA followed by Bio-Rad protein assay on the eluted

sample containing BSA adsorbed micelles.^{148, 159} As shown in Figure 4.8A, crosslinked micelles were found to elute from the column at 7-10 min. Non-crosslinked micelles were found to have similar elution profile as crosslinked micelles (data not shown). The elution time of BSA was found to be 10-12 min. After incubation for 4 h with BSA, the elution peak for crosslinked and non-crosslinked micelles remained the same. The protein binding values for crosslinked and non-crosslinked micelles were 12.6 ± 0.7 and 19.1 ± 1.4 μg BSA/mg of micelles ($n = 3$), respectively. Both crosslinked and non-crosslinked micelles showed insignificant adsorption of BSA suggesting that the hydrophilic PEO block provides sufficient coverage of the hydrophobic core of the micelles.¹⁴⁸ Crosslinking of the micelles, however, was shown to have caused a significant decrease ($p < 0.05$) in the adsorption of proteins on the micellar surface. This can be due to the fact that the core of crosslinked micelles is in a fixed and more compact state when compared to non-crosslinked micelles. This may result in a higher density and extension of the PEO chains in the micellar shell leading to a better steric effect by the hydrophilic shell in case of crosslinked micelles. Also, the crosslinking block (tetraethylene glycol) is hydrophilic in nature which might be decreasing the hydrophobicity of the core/shell interface region leading to less protein adsorption. These results imply better *in vivo* stability of crosslinked micelles as compared to non-crosslinked micelles in terms of preventing protein adsorption and further opsonization in the biological system.

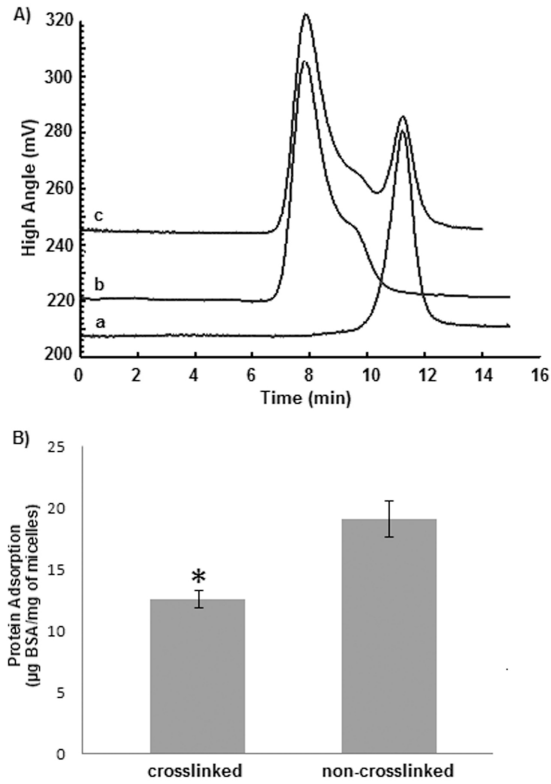


Figure 4.8 A) Gel permeation chromatogram of a) BSA solution, b) crosslinked micelles, and c) mixture of crosslinked micelles and BSA after incubation at 37 °C for 4 h; B) Protein adsorption of crosslinked and non-crosslinked micelles ($\mu\text{g BSA}/\text{mg of micelles}$) ($n = 3$).

4.3.4 Preparation and Characterization of Polymeric Micelles Containing Physically Encapsulated PTX.

A maximum PTX solubility of 20.99 $\mu\text{g/mL}$ was achieved with non-crosslinked PEO-*b*-PPCL micelles (Table 4.2). The PTX encapsulation for the PEO-*b*-PPCL micelles was lower than that obtained by PEO-*b*-PCL micelles,¹¹¹ which may be due to an increase in the rigidity of the core with propargyl side chain in PEO-*b*-PPCL micelles and/or the presence of shorter hydrophobic backbone in PEO-*b*-PPCL micelles studied here.

Table 4.2 Characteristics of PTX loaded copolymer micelles when DMF was used as the solvent for micellization ($n = 3$)

Micelles	PTX loading content (%) \pm SD		Encapsulation efficiency(%)	Average diameter (nm) (empty)	Average diameter (nm) (PTX loaded)	PDI ^a	PTX released after 72 hrs (%) ^b
	PTX/polymer (mol%)	PTX/polymer (wt%)					
Non-crosslinked	9.37 \pm 0.13	0.92 \pm 0.01	18.34 \pm 0.25	57.1 \pm 0.6	56.9 \pm 0.3	0.41	75.17 \pm 4.43
Crosslinked	9.60 \pm 0.12	0.94 \pm 0.01	18.80 \pm 0.23	57.5 \pm 0.5	56.4 \pm 0.4	0.38	72.20 \pm 2.01

^a Polydispersity index of micellar size distribution.

^b Release study was performed in phosphate buffer (pH 7.4) containing 2M sodium salicylate

For PTX loading in crosslinked micelles, better solubility was achieved when the crosslinking agent was added in DMF containing polymer and drug (method I, PTX solubility of 21.48 $\mu\text{g/mL}$) as opposed to the method in which crosslinking agent was added to micellar solution of drug in water (method II, PTX solubility of 1.66 $\mu\text{g/mL}$). This may be due to leaking out of the PTX from the micellar core during the crosslinking step after the preparation of non-crosslinked micelles. Drug loading was expected to decrease in core-

crosslinked micelles as a result of a reduction in the free-volume of the micellar core however this was not the case for the crosslinked micelles prepared by method I.

The results of assessments on the *in vitro* release of PTX from non-crosslinked and crosslinked micelles, and free PTX in phosphate buffer (pH 7.4, 0.01 M) containing 2M sodium salicylate at 37 °C is illustrated in Figure 4.9. The maximum concentration of PTX in the medium was 0.4 µg/mL, while the solubility of PTX in 2M sodium salicylate medium was 333.1 µg/mL,³⁸⁰ thus sink conditions were respected in the release study condition. Free PTX was released from the dialysis bag at a rapid rate, which means that the transfer of PTX through dialysis membrane to buffer solution is not a restricting factor and the release of PTX from the micellar formulation is the rate limiting step in the process. Both non-crosslinked and crosslinked micelles showed much slower release profiles when compared to free PTX. Owing to a decrease in free volume in the micellar core as a result of crosslinking, we expected to see a slower release of PTX from the core-crosslinked micelles. In reality; however, the release profile of PTX at concentrations above the CMC of polymers was similar for both structures. Similar release profiles of PTX between non-crosslinked and crosslinked micelles were also seen in studies carried out previously by Kissel and group.⁴⁶ This could be due to the fact that although the core is stabilized by core-crosslinking, the drug is easily diffusible from the micellar structure. The observation may also imply the localization of PTX in core/shell interface rather than the micellar core in micellar structure. Further investigations are needed to define the possible reason behind this observation. Even without a difference in release, the stabilization of micelles by crosslinking is expected to lead to lower rate and extent of drug release *in vivo* because dissociation of micellar structure is now prevented by crosslinking. This hypothesis is under further investigation in our

research group through *in vivo* studies comparing the pharmacokinetics of PTX formulated using crosslinked and non-crosslinked micelles.

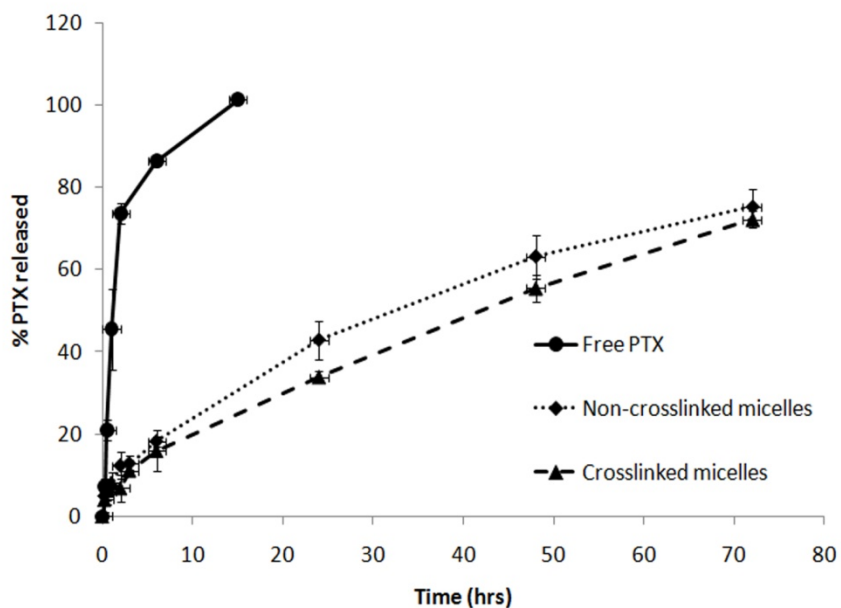


Figure 4.9 *In vitro* release profile of physically encapsulated PTX from different micellar formulations in phosphate buffer (pH 7.4) containing 2M sodium salicylate at 37 °C. Each point represents mean \pm SD (n = 3).

4.4 Conclusion

Diblock copolymers of poly(ethylene oxide) and terminal alkyne bearing α -propargyl carboxylate- ϵ -caprolactone were successfully synthesized via ring-opening polymerization. The process of self-association of block copolymer to micelles was followed by crosslinking of the core using bifunctional tetraethylene glycol bis(azide) via the Cu(I)-catalyzed 1,3-Huisgen cycloaddition click reaction. The crosslinked micelles were characterized by ^1H

NMR and IR spectroscopy, XPS, DLS, and TEM which confirmed the formation of stable crosslinked micelles by the mentioned procedures. Protein adsorption study revealed low adsorption of BSA on crosslinked micelles implying better *in vivo* stability of these structures against opsonization. The crosslinking did not influence the size distribution, loading and *in vitro* release of PTX from the micelles significantly. Overall, the results points to the suitability of prepared core-crosslinked polymeric micelles for use as more stable nano-delivery vehicles.

4.5 Acknowledgement

This study was supported by a grant from the Natural Sciences and Engineering Research Council of Canada (NSERC). S.G. was supported by the Alberta Cancer Foundation Graduate Studentship and the J.N. Tata Trust Scholarship.

Chapter Five

Self-associating Poly(ethylene oxide)-*block*-poly(ϵ -caprolactone (PEO-*b*-PCL) Drug Conjugates for the Delivery of STAT3 Inhibitor JSI-124: Application in Cancer Immunotherapy

The data in this chapter will be submitted as part of a manuscript titled

Self-associating Poly(ethylene oxide)-*block*-poly(ϵ -caprolactone (PEO-*b*-PCL) Drug Conjugates for Tumor Targeted Delivery of STAT3 Inhibitor JSI-124: Implications for Application in Cancer Immunotherapy

Shyam M Garg¹, Mohammad Reza Vakili¹, Afsaneh Lavasanifar^{1,2}

¹Faculty of Pharmacy and Pharmaceutical Sciences, University of Alberta, Edmonton, AB

²Department of Chemical and Materials Engineering, Faculty of Engineering, University of Alberta, Edmonton, AB

5.1 Introduction

Signal transducer and activator of transcription 3 (STAT3) is a transcription factor responsible for relaying biological information from the cell surface into the nucleus, for activation of gene expression in many different cells.³⁹⁶ Constitutive activation of STAT3 is found to play a major role in the progression of various cancers, including melanoma, by modulating expression of genes involved in cell proliferation, survival, angiogenesis, and metastasis. Activation of STAT3 also induces the release of various immunosuppressive tumor-derived factors in the tumor microenvironment such as IL-10 and VEGF.^{227, 397-399} Recent evidence suggests these factors activate STAT3 in various immune cells including dendritic cells (DCs) in the tumor microenvironment. In DCs, activated STAT3 has been linked to abnormal differentiation and inhibition of maturation/activation in response to various stimuli, thus suppressing their ability to create an effective anti-tumor immune response.^{219, 227, 232} Multiple lines of evidence suggest that inhibition of STAT3 activation in tumor cells and DCs can result in tumor regression directly and can modulate bystander anti-cancer immune responses.^{226, 228, 229, 231, 255, 256, 400, 401}

JSI-124 has been the subject of several studies as a potent inhibitor of the JAK/STAT3 pathway both in tumor cells as well as immunosuppressed DCs.^{226, 231, 249, 255-258} JSI-124 is shown to have direct anti-cancer activity on tumor cells that over-express activated STAT3.^{249, 261, 402} It can also activate the anti-tumor immune response by inhibiting the tumor-induced activated STAT3 in DCs, *in vitro*.^{226, 228, 231, 257}

Despite high potency of JSI-124 in inhibition of STAT3 activation in both, tumor cells and immune suppressed DCs, its use in pre-clinical and clinical models has been limited because of the poor water solubility of JSI-124, as well as its non-specificity for tumor cells

and/or tumor microenvironment. In this context, development of formulations that can effectively solubilize JSI-124, avoid its distribution to normal cells where STAT3 expression is vital, and direct it towards tumor and its microenvironment is of great interest.

Our research group has previously reported on the development of polymeric micellar formulations of JSI-124 that were successful in increasing its water solubility while maintaining its cytotoxicity towards B16 melanoma cells. The developed polymeric micellar formulations, however, were unable to significantly sustain the release of JSI-124 *in vitro* under sink condition.^{261, 301} For tumor targeted drug delivery following intravenous administration of the nanocarrier, the delivery system is required to keep the encapsulated drug inside under sink conditions mimicking that of plasma. In the current study, we report on the successful conjugation of JSI-124 to pendent COOH groups of self-associating poly(ethylene oxide)-*block*-poly(α -carboxylate- ϵ -caprolactone) (PEO-*b*-PCCL) in order to achieve a nano-carrier for solubilisation and passive targeting of JSI-124 to tumor cells and tumor associated DCs following intravenous administration.

5.2 Experimental Section

5.2.1 Materials

Methoxy-poly(ethylene oxide) (PEO) (average molecular weight of 5000 g/mol), palladium on charcoal, oxalyl chloride, lipopolysaccharide (LPS) and bovine serum albumin (BSA) powder were purchased from Sigma (St. Louis, MO). α -Benzyl carboxylate- ϵ -caprolactone monomer was synthesized by Alberta Research Chemicals Inc (Edmonton, AB) according to a previously published procedure.⁴³ Stannous octoate was purchased from MP

Biomedicals Inc. (Santa Ana, CA). Cell culture media RPMI 1640, fetal bovine serum (FBS), and penicillin-streptomycin-L-glutamine were purchased from GIBCO, Life Technologies Inc. (Carlsbad, CA). Murine interleukin-12 (IL-12) p70, IL-2, IL-6, transforming growth factor- β 1 (TGF- β 1), interferon- γ (IFN- γ) ELISA (enzyme-linked immunosorbent assay) Ready-SET-Go® kits, Fluorescein isothiocyanate (FITC) conjugated anti-mouse CD-86 (B7-2) (GL7) mAb, Phycoerythrin-Cy5 (PE-Cy5) conjugated anti-mouse CD40 mAb, and purified anti-mouse CD16/CD32 (Fc γ -III/II receptor) were purchased from e-Biosciences (San Diego, CA). JSI-124 was purchased from ABCR GmbH and Co. KG (Karlsruhe, Germany). Recombinant murine granulocyte-macrophage colony-stimulating factor (GM-CSF) was purchased from Peprotech (Rocky Hill, NJ). Anti-p-STAT3 antibody and its respective isotype control were purchased from Santa Cruz Biotechnology (Dallas, TX). CpG (ODN#1826) was obtained from InvivoGen (San Diego, CA). All other chemicals were reagent grade.

5.2.2 Mice

C57Bl/6 mice and BALB/c mice were purchased from Charles River Laboratories (Wilmington, MA). All experiments were performed using 6 - 12 week old female mice. All experiments were performed in accordance with the University of Alberta guidelines for the care and use of laboratory animals.

5.2.3 Cell line

The murine melanoma cancer cell line B16.F10 of C57BL/6 origin was obtained from American Type Culture Collection (ATCC) (Manassas, VA). The B16 cells were grown in RPMI-1640 supplemented with 10% FBS, 2 mM L-glutamine and 100 IU/mL penicillin/streptomycin at 37 °C in 5% CO₂ atmosphere.

5.2.4 Synthesis of PEO-*b*-poly(α -JSI-124-carboxylate- ϵ -caprolactone) (PEO-*b*-P(CL-JSI-124))

The polymer-JSI-124 conjugate was prepared in three steps. First, block copolymers of PEO-*b*-poly(α -benzyl carboxylate- ϵ -caprolactone) (PEO-*b*-PBCL) were synthesized by ring-opening polymerization of α -benzyl carboxylate- ϵ -caprolactone using methoxy-PEO as initiator and stannous octoate as catalyst according to published procedures.^{308, 320} Briefly, methoxy PEO (MW: 5000 g/mol) (1 g), α -benzyl carboxylate- ϵ -caprolactone (1 g), and stannous octoate (0.002 equiv of monomer) were added to a 10 mL previously flamed ampoule and sealed under vacuum. The polymerization reaction was allowed to proceed for 4h at 140 °C in oven. The reaction was terminated by cooling the product to room temperature.

In the second step, block copolymers of PEO-*b*-poly(α -carboxyl- ϵ -caprolactone) (PEO-*b*-PCCL) were synthesized by catalytic debenzoylation of PEO-*b*-PBCL in the presence of H₂ to obtain PEO-*b*-PCCL according to a method described previously with slight modifications.⁴³ Briefly, a solution of PEO-*b*-PBCL (1g in 50 mL dry THF) was placed into a cylindrical flask. Palladium on charcoal (300 mg) was dispersed in the solution. The

mixture was stirred vigorously with a magnetic stirrer under the continuous supply of hydrogen gas for 12 h at room temperature. The reaction mixture was centrifuged at $11,600 \times g$ to remove the catalyst. The supernatant was collected, condensed under reduced pressure and precipitated in hexane and washed with diethyl ether. The final product was dried under vacuum for further use.

For the conjugation of JSI-124 to PEO-*b*-PCCL, block copolymer containing pendent COOH groups on the PCCL backbone, PEO-*b*-PCCL (100 mg, 0.2 mmol of COOH) was dissolved in 10 mL of dry dichloromethane in a 25 mL round-bottom flask fixed with a drierite stopper. The flask was cooled using dry ice, oxalyl chloride (30 mg, 0.2 mmol) was added with constant stirring to the reaction mixture and allowed to dissolve. Then two drops of dimethyl formamide were added after which the color of the reaction mixture turned yellow. The progress of the reaction was checked by the removal of HCl gas during the reaction using a pH paper. After the reaction mixture was stirred for 24 hrs, dichloromethane was removed under vacuum and the resulting crude polymer was washed twice with dry hexane to remove excess oxalyl chloride. The crude polymer was then re-dissolved in dry dichloromethane and excess triethylamine (0.1 mL) was added. The flask was cooled in dry ice and a solution of JSI-124 (10 mg, 0.02 mmol) in dry dichloromethane was added with constant stirring and the reaction was stirred overnight. Evaporation of the reaction mixture gave a residue that was dissolved in toluene and centrifuged at $11,600 \times g$ to remove other by-products. The supernatant was then precipitated in hexane and washed with ether to remove any unreacted JSI-124. PEO-*b*-P(CL-JSI-124) was then dried in vacuum to a bright yellow solid for further use. TLC analysis of the conjugate compared to free drug using ethyl acetate as the mobile phase and vanillin/phosphoric acid as a JSI-124 indicator confirmed the

conjugation of JSI-124 to PEO-*b*-PCCL and the absence of free JSI-124 in the purified product.^{257, 403} To further confirm the absence of free JSI-124 in the drug-polymer conjugate, PEO-*b*-P(CL-JSI-124) was dissolved in 1:4 methanol:chloroform and analyzed by liquid chromatography/mass spectrometry (LC-MS) for the presence of free JSI-124. A Waters Micromass ZQ 4000 spectrometer, coupled to a Waters 2795 separations module with an autosampler (Milford, MA) was used for LC-MS analysis. No peak corresponding to the molecular ion of JSI-124 was observed in the SIR chromatogram of PEO-*b*-P(CL-JSI-124), indicating the absence of free drug in the conjugate. PEO-*b*-P(CL-JSI-124) was further characterized by ¹H NMR using deuterated chloroform (CDCl₃) as the solvent and tetramethylsilane as an internal reference.

5.2.5 Characterization of PEO-*b*-P(CL-JSI-124)

The JSI-124 content in the conjugate was calculated by gradient reversed phase HPLC method described previously.⁴⁰⁴ A μ Bondapak (Waters Corp., United States) C18 analytical column (10 μ m 3.9 \times 300 mm) was used. Gradient elution was performed at a flow rate of 1 mL/min using a Varian Prostar 210 HPLC System. Detection was performed at 230 nm using a Varian 335 detector (Varian Inc., Australia). The mobile phase consisted of acetonitrile (solution A) and water (solution B). The mobile phase was programmed as follows: (1) 0 - 35 min linear gradient from 20% A to 40% A (2) 35 - 40 min linear gradient from 40% A to 20% A (3) hold for 5 min at 20% A. The column temperature was 25 °C and the injection volume was 20 μ L. The concentration of unreacted JSI-124 was calculated based on a calibration curve for the peak height of known concentrations of JSI-124 in

acetonitrile. The amount of conjugated JSI-124 was calculated by subtracting the amount of unreacted JSI-124 from the initial JSI-124 added to the reaction, and was expressed as percentage by weight of the polymer. Conjugation reaction with JSI-124 in the absence of PEO-*b*-PCCL was used as the control. Conjugation of JSI-124 was also measured by ¹H NMR spectrum by comparing the peak intensity of JSI-124 (-CH=, $\delta = 5.5\text{--}7.1$ ppm) to that of PEO (-CH₂CH₂O-, $\delta = 3.65$ ppm).

5.2.6 Self Assembly of PEO-*b*-P(CL-JSI-124) and characterization of assembled structures

Self-assembly of PEO-*b*-P(CL-JSI-124) was accomplished by solvent evaporation method. The block copolymer (3 mg) was dissolved in acetone (0.5 mL). This solution was added to doubly distilled water (3 mL) in a drop-wise manner under moderate stirring at room temperature, followed by the evaporation of acetone under vacuum. The prepared micellar solution was then centrifuged at $11,600 \times g$ for 5 min to remove any precipitate.

The Z-average particle diameter and size distribution of prepared micelles were estimated by dynamic light scattering (DLS) using a commercial Zetasizer Nano-ZS (Malvern Instruments, Worcestershire, UK). All DLS measurements were made at 25.0 ± 0.1 °C with a 173° scattering angle. The samples were prepared in deionized water at a concentration of 1 mg/mL of polymer and centrifuged prior to analysis.

The CMC of polymeric micelles was determined using light scattering according to a previously published procedure.¹²⁰ Briefly, micellar solutions of PEO-*b*-P(CL-JSI-124) and PEO-*b*-PCCL, having concentrations ranging from 800-0.20 $\mu\text{g/mL}$ were prepared in a black

opaque 96-well plate. Light scattering was measured by a fluorescence spectrophotometer using a SpectraMax M4 microplate reader (Molecular Devices, Sunnyvale, CA), with excitation and emission wavelengths set at 450 nm. The average intensity of scattered light from three measurements was plotted against the logarithm of copolymer concentration. The CMC was measured from a sharp rise in intensity of scattered light at the onset of micellization.

To measure the stability of the JSI-124 conjugation, PEO-*b*-P(CL-JSI-124) or free JSI-124 were dissolved in ethanol and then suspended in a formic acid solution at pH=2.0 at a concentration of 0.5 mg/mL (such that final concentration of ethanol was 20% in the solution). The mixture was incubated in water bath at 37 °C for 24 h. After incubation the solution was centrifuged, but no precipitation was observed. The level of free JSI-124 in the supernatant was measured by LC-MS method as described previously.⁴⁰⁵

5.2.7 Release of JSI-124 from PEO-*b*-P(CL-JSI-124)

To assess the release profile of JSI-124 from the block copolymer conjugate, PEO-*b*-P(CL-JSI-124) was dissolved in ethanol, and then suspended in deionized water at a concentration of 0.5 mg/mL (such that final concentration of ethanol is 20% in the solution). The solution was then aliquoted into 8 samples of 1 mL in microcentrifuge tubes. The samples were incubated in a Julabo SW 22 shaking water bath (Seelbach, Germany) at 37 °C. At predetermined time intervals, the supernatant of one sample was collected by centrifugation ($11,600 \times g$ for 10 min) and analyzed for the level of released JSI-124 by LC-MS.

Release of free JSI-124 or JSI-124 physically encapsulated into PEO-*b*-PCCL micelles was assessed in deionized water at 37 °C according to a previous method with slight modification.³¹⁶ Free or micellar JSI-124 (5 mL solution containing 1 mg JSI-124) was prepared and transferred to a dialysis bag (MWCO - 3.5 kDa). The dialysis bag was placed in 500 mL of deionized water and release study was performed in a shaking water bath at 37 °C. At selected time intervals, the release media was replaced, and aliquots of 200 uL were withdrawn from the inside of the dialysis bag and analyzed by LC-MS. The release profiles were compared using similarity factor, f_2 , and the profiles were considered significantly different if $f_2 < 50$.³⁸¹

$$f_2 = 50 \times \log \left(\left[1 + \left(\frac{1}{n} \right) \sum_{j=1}^n |R_j - T_j|^2 \right]^{-0.5} \times 100 \right)$$

Where n is the sampling number, R_j and T_j are the percent released of the reference and test formulations at each time point j .

5.2.8 Generation of bone marrow derived dendritic cells (BMDCs)

DC primary cultures were generated from murine bone marrow precursors from femurs of C57Bl/6 mice in complete media in the presence of GM-CSF as described previously with minor modifications.³²³ Briefly, femurs were removed and purified from surrounding tissue. Both ends of the intact bone were cut with scissors and the bone marrow was flushed with sterile PBS using an insulin syringe. Leukocytes were triturated and filtered through a nylon screen (40 μ m cell strainer) to obtain a single cell suspension. Bone marrow leukocytes were washed and 2×10^6 cells were seeded in 100 mm non-treated cell culture

dishes with 10 mL DC complete medium (RPMI-1640 with penicillin-streptomycin-L-glutamine, 10 % heat-inactivated FBS supplemented with 20 ng/mL of GM-CSF). At day 3, another 10 mL complete medium was added to the plates. At day 6, 10 mL of culture media was replaced with 10 mL fresh complete medium. At day 7, the cells were ready for use. The purity of the DC population on day 7 was found to be between 70 and 75% based on flow cytometric analysis of the expression of CD11c on the semi-adherent and non-adherent cell populations.

5.2.9 Cell viability studies

The cytotoxicity of free JSI-124 and PEO-*b*-P(CL-JSI-124) micelles against murine B16.F10 cancer cells and BMDCs was monitored using 3-(4,5-dimethylthiazol-2-yl)-2,5-diphenyl tetrazolium bromide (MTT) assay.⁴⁰⁶ B16 cells were seeded at a density of 5000 cells/well in a 96-well plate and grown in RPMI-1640 supplemented with 10% FBS, 2 mM L-glutamine and 100 IU/mL penicillin/streptomycin at 37 °C in 5% CO₂ atmosphere. After 24 h incubation, the cells were treated with different concentrations of free JSI-124 or PEO-*b*-P(CL-JSI-124) micelles and incubated for 24 and 48 h. Untreated cells were used as control. After incubation, 20 µL MTT solution (5 mg/mL sterile-filtered solution in PBS) was added to each well and the plates were re-incubated for 4 h. The residual MTT solution was removed from the wells, and the formazan crystals were dissolved in 150 µL DMSO and cell viability was determined by measuring the optical absorbance at 570 nm using a Power Wave X 340 microplate reader (Bio-Tek Instruments, Inc., USA). The mean and the standard deviation of cell viability for each treatment was determined by converting to the percentage

of viable cells relative to the control. The IC₅₀ was calculated from the plot of the % of viable cells vs. log JSI-124 concentration.

In case of BMDCs, cells were seeded on day 6 (Section 5.2.8) at a density of 8000 cells/well in a 96-well plate. After 24 h incubation, the cells were treated with different concentrations of free JSI-124 or PEO-*b*-P(CL-JSI-124) micelles and incubated for 24 h. Untreated cells were used as control. After incubation, 20 μ L MTT solution (5 mg/mL sterile-filtered solution in PBS) was added to each well and the plates were re-incubated for 4 h. The plates were then centrifuged at $600 \times g$ for 5 min and the residual MTT solution was removed from the wells. The formazan crystals were dissolved in 150 μ L DMSO and cell viability and IC₅₀ were determined according to the method above. The selectivity index (SI) was defined as the ratio of the measured IC₅₀ in BMDCs to the IC₅₀ in B16.F10 cells.

5.2.10 Cell cycle analysis

Cell cycle of B16 cells treated with JSI-124 was analyzed by flow cytometry using propidium iodide according to the manufacturer's instructions. Briefly, B16 cells were seeded at a density of 3×10^5 cells/well in a 6-well plate and grown in RPMI-1640 supplemented with 10% FBS, 2 mM L-glutamine and 100 IU/mL penicillin/streptomycin at 37 °C in 5% CO₂ atmosphere. After 24-48 h incubation (60% confluency), the cells were treated with different concentrations of free JSI-124 or PEO-*b*-P(CL-JSI-124) micelles (5-20 μ M) and incubated for 24 or 48 h. Untreated cells were used as control. After incubation, the cells were trypsinized, washed with PBS, and then fixed with ice-cold 70% ethanol for 30 min at 4 °C. After two washes with PBS, cells were stained with propidium iodide

(FxCycle™PI/RNase Staining Solution, Molecular Probes) for 30 min in the dark. DNA content was acquired on a BD FACSCalibur flow cytometer (BD Biosciences, Franklin Lakes, NJ) and analyzed using BD Cell-Quest software.

5.2.11 Generation of tumor-induced immunosuppressed DCs

Tumor-induced immunosuppressed DCs were generated according to a method described previously with some modifications.²⁵⁷ Bone marrow leukocytes were obtained from C57BL/6 mice according to the method described in section 5.2.8 above. 2×10^6 cells were seeded in 100 mm non-treated cell culture dishes with 10 mL of a 1:1 mixture of DC complete medium (RPMI-1640 with penicillin-streptomycin-L-glutamine, 10 % heat-inactivated FBS supplemented with 20 ng/mL of GM-CSF), and conditioned media from B16 cells. At day 3, another 10 mL of the mixture was added to the plates. At day 6, 10 mL of culture media was replaced with 10 mL fresh 1:1 mixture of DC complete medium and conditioned media. At day 7, the cells were ready for use. To make B16 conditioned media, B16 cells were grown in 75 cm² culture flasks containing RPMI-1640 supplemented with 10% FBS, 2 mM L-glutamine and 100 IU/mL penicillin/streptomycin at 37 °C in 5% CO₂ for 48 h. The supernatants were then collected, filtered, supplemented with 20 ng/mL of GM-CSF and used in the experiments.

5.2.12 Analysis of p-STAT3 level by flow cytometry

Intracellular staining of p-STAT3 (phosphorylated STAT3) of B16 cells or DCs was done using PE labeled-anti-pSTAT3 antibody or isotype control according to a previous

method with modifications.²⁵⁷ Briefly, B16 cells were seeded at a density of 3×10^5 cells/well in a 6-well plate and grown in RPMI-1640 supplemented with 10% FBS, 2 mM L-glutamine and 100 IU/mL penicillin/streptomycin at 37 °C in 5% CO₂ atmosphere. After 24-48 h incubation (60% confluency), the cells were treated with different concentrations of free JSI-124 or PEO-*b*-P(CL-JSI-124) micelles (1-20 μM) and incubated for 24 or 48 h. Untreated cells and empty PEO-*b*-PCCL micelles were used as control. After incubation, the cells were trypsinized, washed with PBS, and then fixed with paraformaldehyde (4% paraformaldehyde solution in PBS) at 37 °C for 15 min. After two washes, the cells were permeabilized using ice-cold 90% methanol and incubated for 30 min at -20° C. Intracellular staining was then performed according to the manufacturer's instructions. Cells were washed twice and then blocked for 10 min with incubation buffer (0.5% w/v bovine serum albumin (BSA) in PBS) followed by staining with PE labeled-anti-pSTAT3 antibody or isotype control (2 μg/10⁶ cells) for 60 min at room temperature. Cells were washed twice with incubation buffer and examined on a BD FACSCalibur flow cytometer. Ten thousand cells were counted with logarithmic settings. Results were analyzed using FCS Express software (De Novo Software, Los Angeles, CA).

In the case of BMDCs, tumor-induced immunosuppressed DCs were prepared according to the method described in section 5.2.11 above. On day 6, the cells were transferred to 6-well plates at a density of 3×10^5 cells/well and grown in 1:1 mixture of DC complete medium and conditioned media. BMDCs grown in DC complete medium without conditioned media was used as control. On day 7, cells were treated with different concentrations of free JSI-124 or PEO-*b*-P(CL-JSI-124) micelles (0.5-2 μM) and incubated for 24 or 48 h. Untreated cells were used as control. After incubation, the non-adherent and

semi-adherent cells were collected, and then analyzed for p-STAT3 level according to the procedure described above.

5.2.13 Assessment of the functional characteristics of DCs by flow cytometry and ELISA

Tumor-induced immunosuppressed DCs were obtained according to the method described in section 5.2.11 above and treated with free JSI-124 or PEO-*b*-P(CL-JSI-124) (200 nM) on day 6 of their culture. After 12 hrs incubation (on day 7), cells were treated with 100 ng/mL of lipopolysaccharide (LPS) or PBS. BMDCs grown in DC complete medium without conditioned media and treated on day 7 with 100 ng/mL of lipopolysaccharide (LPS) or PBS were used as control. After 24 h treatment, cells were harvested and the supernatant was collected and stored in -20 °C until further use. The cells were then washed twice with sterile PBS. Cell suspensions consisting of 5×10^5 cells/100 μ L were prepared in FACS buffer (PBS containing 2% FBS) and incubated with anti-mouse CD16/CD32 mAb to block Fc γ receptors for 15 min before incubating with anti-CD86 with FITC-conjugated secondary antibody, or anti-CD40 with PE-Cy5-conjugated secondary antibody for 30 min. The cells were then washed twice with FACS buffer. The samples were acquired on a BD FACSCalibur flow cytometer and the data was analyzed with FCS Express software.

The previously collected supernatants were analyzed for the level of IL-12, IL-6, and TGF- β 1 by ELISA using the commercially available ELISA kits in a 96-well microplate according to the manufacturer's instructions. The samples were analyzed using a microplate reader Powerwave with KC Junior Software (BioTek, Winooski, VT) at OD of 450 nm. The

minimum detection level of the cytokines were: IL-12, 15 pg/mL; IL-6, 4 pg/mL; and TGF- β 1, 8 pg/mL.

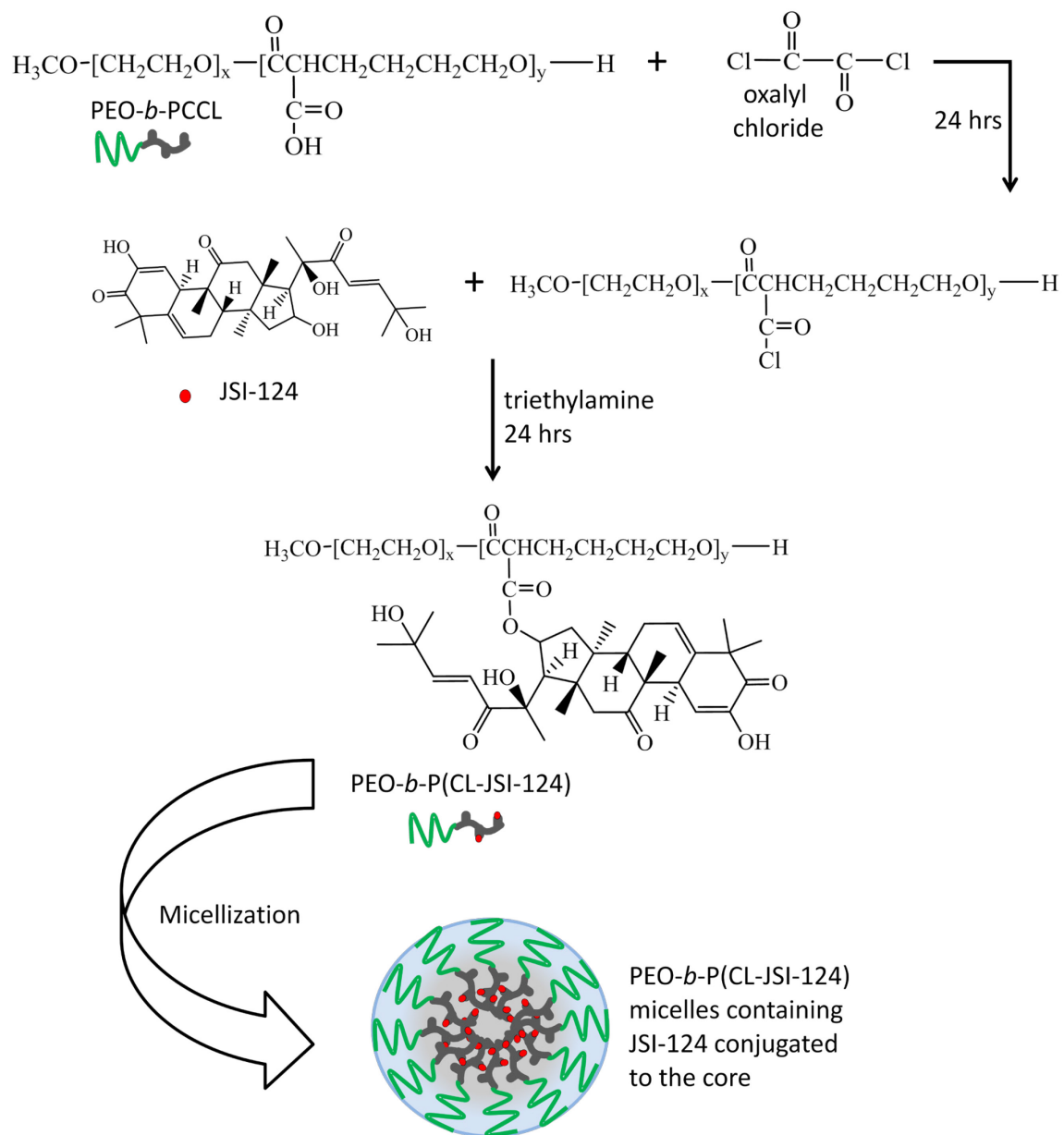
5.2.14 Assessment of the functional characteristics of DCs by MLR

Tumor-induced immunosuppressed DCs were obtained according to the method described in section 5.2.11 above and treated with free JSI-124 or PEO-*b*-P(CL-JSI-124) (500-1000 nM) on day 6 of their culture. After 12 hrs incubation (on day 7), cells were treated with 250 ng/mL of CpG ODN or PBS. BMDCs grown in DC complete medium without conditioned media and treated on day 7 with 250 ng/mL of CpG ODN or PBS were used as control. After 24 h treatment, cells were harvested, washed, and irradiated (2000 rads). CD4⁺ T-cells were isolated from the spleen of Balb/c mice using the EasySep mouse CD4⁺ T-cell enrichment kit (Stem Cell Technologies, Vancouver, BC). The irradiated DCs were co-cultured with CD4⁺ T-cells (1:5, 1:10, and 1:20 ratio) for 72 h in a 96-well plate. The plate was then centrifuged at 1000 \times g for 5 min and the supernatant was analyzed for IL-2, and IFN- γ by ELISA using the commercially available ELISA kits according to the manufacturer's instructions. The samples were analyzed using a microplate reader Powerwave with KC Junior Software (BioTek, Winooski, VT) at OD of 450 nm. The minimum detection level of the cytokines were: IL-2, 2 pg/mL; and IFN- γ , 15 pg/mL.

5.3 Results

5.3.1 Synthesis and characterization of PEO-*b*-P(CL-JSI-124) block copolymer

The conversion of α -benzyl carboxylate- ϵ -caprolactone monomer to its respective copolymer, i.e., PEO-*b*-PBCL, and its catalytic hydrogenolysis to PEO-*b*-PCCL was confirmed by ^1H NMR as reported before (Figure 5.1B).^{43, 308} The degree of polymerization (DP) of the PCCL block was found to be 20 by ^1H NMR, i.e. PEO₁₁₄-*b*-PCCL₂₀. JSI-124 was conjugated to PEO-*b*-PCCL by forming an ester bond between the hydroxyl group of JSI-124 and the pendent carboxyl groups of PEO-*b*-PCCL (Scheme 1). Conjugation of JSI-124 to PEO-*b*-PCCL led to chain cleavage of the PCCL block resulting in a decrease in the DP of the PCCL block from 20 to 16. The successful conjugation of JSI-124 to PEO-*b*-PCCL was confirmed by a combination of TLC, ^1H NMR, and HPLC (Figure 5.1). No spot for free JSI-124 has been visualized in the TLC for the PEO-*b*-P(CL-JSI-124) (Figure 5.1F). Whereas in the ^1H NMR spectra of PEO-*b*-P(CL-JSI-124), on the other hand, characteristic peaks of PEO-*b*-PCCL and JSI-124 were observed (Figure 5.1C). Also, in the HPLC chromatogram of PEO-*b*-P(CL-JSI-124) block copolymer, no peak for free JSI-124 was observed (Figure 5.1E). Together, the results of TLC, ^1H NMR, and HPLC provide strong evidence for the conjugation of JSI-124 to PEO-*b*-PCCL and efficient removal of free JSI-124 after the purification step.



Scheme 5.1 Synthetic scheme for the preparation of PEO-*b*-P(CL-JSI-124) block copolymer micelles.

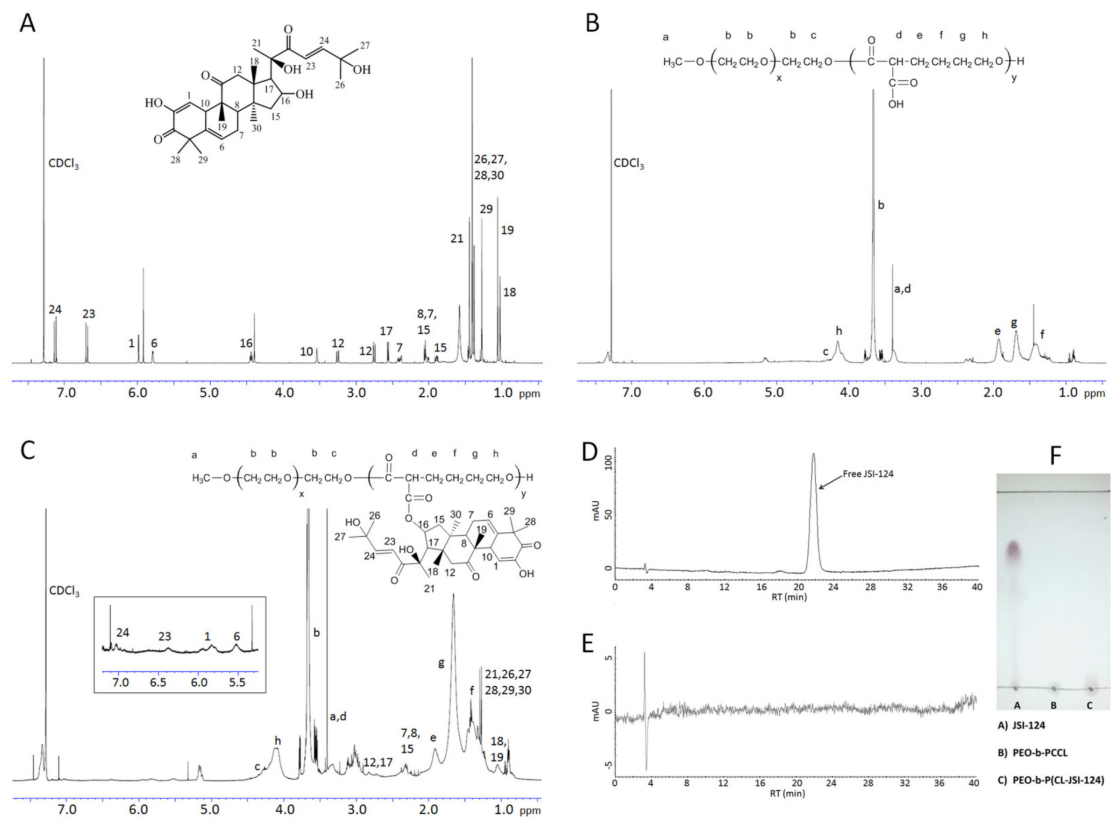


Figure 5.1 Characterization of PEO-*b*-P(CL-JSI-124). ¹H NMR spectrum of A) JSI-124, B) PEO-*b*-PCCL, and C) PEO-*b*-P(CL-JSI-124) in CDCl₃; HPLC Chromatogram of D) Free JSI-124 and E) PEO-*b*-P(CL-JSI-124); F) TLC analysis of free JSI-124, PEO-*b*-PCCL, and PEO-*b*-P(CL-JSI-124).

The content of JSI-124 in the conjugate was calculated by determining the amount of unreacted JSI-124 after the conjugation reaction by HPLC. Conjugation reaction with JSI-124 in the absence of PEO-*b*-PCCL was used as the control. The level of JSI-124 conjugation was calculated to be 8.89% w/w of the polymer, on average, based on HPLC results. The content of JSI-124 in the conjugate was also calculated by ¹H NMR by comparing the peak intensity of JSI-124 (-CH=, $\delta = 5.5\text{--}7.1$ ppm) to that of PEO (-CH₂CH₂O-, $\delta = 3.65$ ppm) and was found to be ~8.75% w/w of the polymer. The substitution level of JSI-124 on PEO-*b*-P(CL-JSI-124) was ~8.1% (moles JSI-124/moles monomer). This corresponds to 1.3 JSI-124 molecules per PEO₁₁₄-*b*-P(CL-JSI-124)₁₆ chain on average, i.e. PEO₁₁₄-*b*-P(CL-JSI-124)_{16-1.3}. The conjugation efficiency of the reaction was 88.9% w/w, on average.

5.3.2 Characterization of PEO-*b*-P(CL-JSI-124) micelles

Synthesized block copolymers were assembled to polymeric micelles by a cosolvent evaporation method as previously described.^{43, 308} The average hydrodynamic diameter and polydispersity of PEO-*b*-P(CL-JSI-124) was 41.42 ± 0.78 nm and 0.357 ± 0.025 as determined by DLS technique, respectively (Table 5.1). This was smaller than the size of PEO-*b*-PCCL micelles formed through a similar assembly process.

The CMC of PEO-*b*-PCCL, and PEO-*b*-P(CL-JSI-124) in aqueous media as determined by light scattering method is shown in Table 5.1. PEO-*b*-P(CL-JSI-124) conjugate showed significantly lower CMC than PEO-*b*-PCCL block copolymer, which is

attributed to an increase in the hydrophobicity of the core forming block upon JSI-124 conjugation.¹¹¹

Table 5.1 Characteristics of prepared block copolymers and block copolymer micelles

Block Copolymer ^a	M_n (g/mol) ^b	Polydispersity (M_w/M_n) ^c	Average micellar size \pm SD (nm) ^d	PDI \pm SD ^e	CMC \pm SD (μ M) ^f
PEO- <i>b</i> -PCCL	8020	1.938	70.7 \pm 0.50	0.305 \pm 0.003	9.055 \pm 0.213
PEO- <i>b</i> -P(CL-JSI-124)	8280	1.400	41.4 \pm 0.78*	0.357 \pm 0.025	5.073 \pm 0.276*

^a The number shown in the subscript indicates the polymerization degree of each block determined by ¹H NMR spectroscopy

^b Number-average molecular weight measured by ¹H NMR

^c Polydispersity index measured by GPC

^d Average micellar size estimated by the DLS technique ($n = 3$).

^e Polydispersity index (PDI) of micellar size distribution estimated by DLS technique ($n = 3$)

^f Measured from the onset of rise in the intensity values of scattered light as a function of concentration of block copolymer ($n = 3$)

*Indicates statistical significance between PEO-*b*-P(CL-JSI-124) and PEO-*b*-PCCL (student's *t*-test; $P < 0.05$)

The ester bond between PEO-*b*-PCCL and JSI-124 in the conjugate was found to be highly stable to acid hydrolysis when PEO-*b*-P(CL-JSI-124) was suspended in a formic acid solution at pH=2 for 24 h. The level of JSI-124 released from the conjugate was 2.52 % \pm 0.01 under this condition. Incubation in free formic acid for 48 and 72 h; however, resulted in the degradation of free JSI-124. Hence, the amount of JSI-124 released from the conjugate in acidic condition could not be accurately calculated at longer incubation times.

5.3.3 Release of JSI-124 from PEO-*b*-P(CL-JSI-124)

PEO-*b*-P(CL-JSI-124) showed an extremely slow release profile of JSI-124 which was significantly different from free JSI-124 or physically encapsulated JSI-124 ($f_2 < 50$). The JSI-124 conjugate followed a biphasic release pattern with an initial release of 5.3% of

JSI-124 within the first 7 days followed by an extremely slow release of 6.1% of conjugated JSI-124 within 28 days (Figure 5.2). For free JSI-124, however, > 93 % of the drug was released to the media within 4 h, implying the existence of sink condition in the study. Similar burst release results profile was also seen in the case of JSI-124 physically encapsulated in PEO-*b*-PCCL micelles.

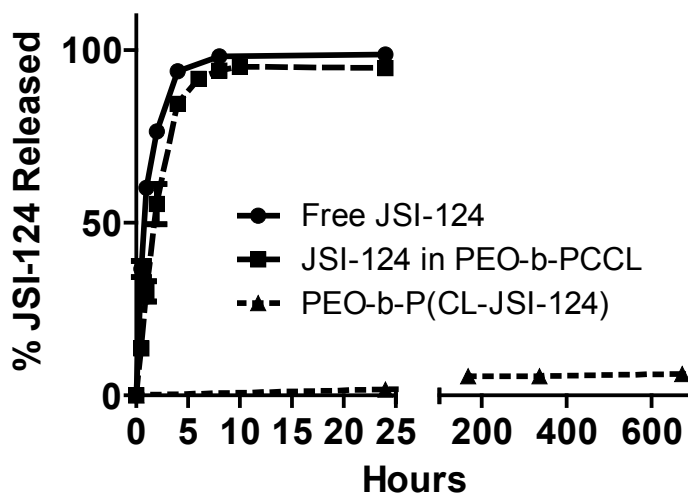
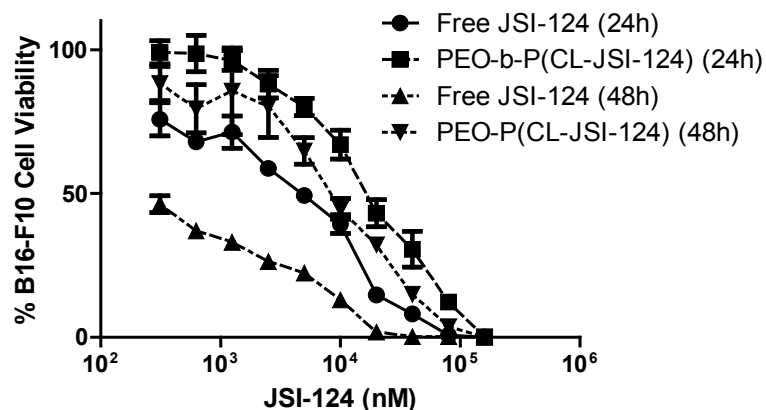


Figure 5.2 *In vitro* release profile of JSI-124 from PEO-*b*-PCCL or PEO-*b*-P(CL-JSI-124) micelles in phosphate buffer (pH 7.4) at 37 °C. Each point represents mean \pm SD ($n = 3$).

5.3.4 Cell viability studies

The anti-cancer activity of free JSI-124, and PEO-*b*-P(CL-JSI-124) against murine B16-F10 melanoma cell lines using MTT assay is shown in Figure 5.3. Treatment of B16 cells with increasing concentrations of free or conjugated JSI-124 resulted in a significant loss of cell viability at both 24 and 48 h. PEO-*b*-P(CL-JSI-124) showed about ~3 times less cytotoxicity than free JSI-124 as judged by the IC₅₀ values after 24 h. PEO-*b*-PCCL did not show any noticeable cytotoxicity and resulted in a cell viability of 89.4% ± 2.7 at concentrations equivalent to the highest concentrations for PEO-*b*-P(CL-JSI-124).

A



B

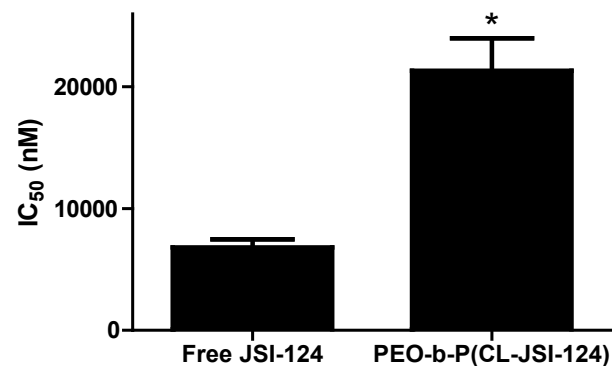


Figure 5.3 Assessment of the anticancer activity of PEO-*b*-P(CL-JSI-124) micelles against B16 melanoma cell line. A) *In vitro* anticancer activity of free JSI-124 and PEO-*b*-P(CL-JSI-124) against B16 melanoma cell line after 24 and 48 h incubation. B16 cells were treated with different concentrations of free or conjugated JSI-124. After 24 and 48 h incubation, cell viability was estimated by MTT assay and expressed as percentage of untreated controls. Each point represents mean \pm SD ($n = 6$). B) Estimation of relative IC₅₀ of free JSI-124 and PEO-*b*-P(CL-JSI-124) against B16 melanoma cell line after 24 h incubation. Each bar represents mean \pm SD ($n = 6$). *Indicates statistically different from free JSI-124 ($P < 0.05$; Student's *t*-test).

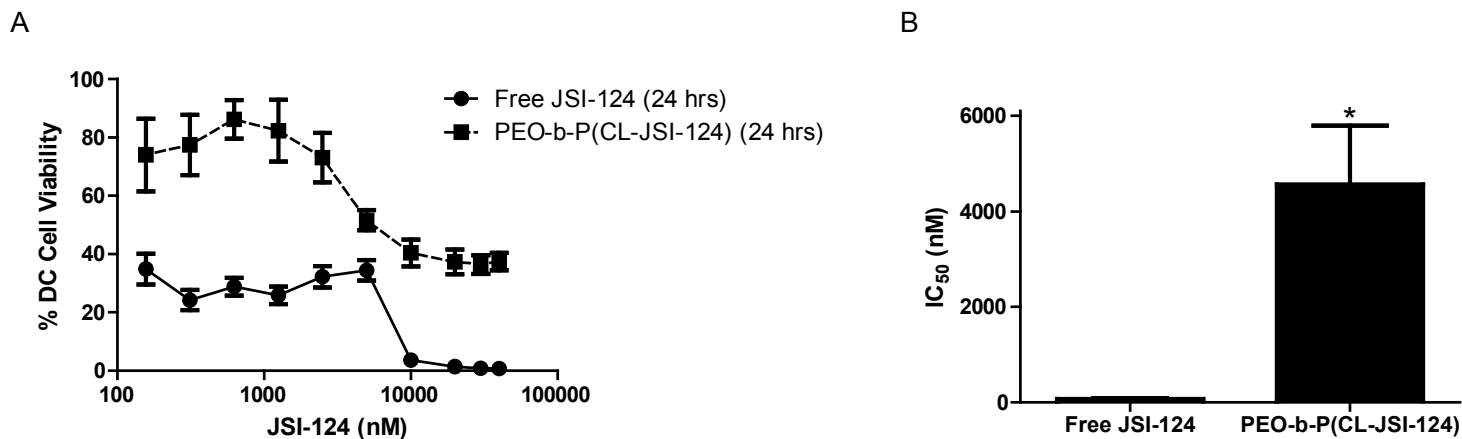


Figure 5.4 Assessment of the cytotoxicity of PEO-*b*-P(CL-JSI-124) micelles to BMDCs. A) *In vitro* cytotoxicity of free JSI-124 and PEO-*b*-P(CL-JSI-124) to BMDCs after 24 h incubation. BMDCs were treated with different concentrations of free or conjugated JSI-124. After 24 h incubation, cell viability was estimated by MTT assay and expressed as percentage of untreated controls. Each point represents mean \pm SD ($n = 6$). B) Estimation of the relative IC₅₀ of free JSI-124 and PEO-*b*-P(CL-JSI-124) against BMDCs after 24 h incubation. Each bar represents mean \pm SD ($n = 6$). *Indicates statistically different from free JSI-124 ($P < 0.05$; Student's *t*-test).

The cytotoxicity of free JSI-124, and PEO-*b*-P(CL-JSI-124) was also studied against BMDCs using MTT assay as shown in Figure 5.4. Treatment of BMDCs with increasing concentrations of free or conjugated JSI-124 resulted in a significant loss of cell viability after 24 h. PEO-*b*-P(CL-JSI-124) showed significantly less cytotoxicity than free JSI-124. At an equivalent concentration of 40 μ M JSI-124 for PEO-*b*-P(CL-JSI-124), 40% viable BMDCs were present. For free JSI-124, BMDCs reached 40 % viability at concentrations as low as 0.15 μ M. In the case of BMDCs, the relative IC₅₀ of PEO-*b*-P(CL-JSI-124) was ~63 times higher than free JSI-124 after 24 h incubation. Both, free JSI-124 and PEO-*b*-P(CL-JSI-124) were more cytotoxic to BMDCs than B16 cells showing lower IC₅₀s in BMDCs. However, the selectivity index of conjugated JSI-124 for B16 cells was ~20-fold higher than that of free drug. (Figure 5.5)

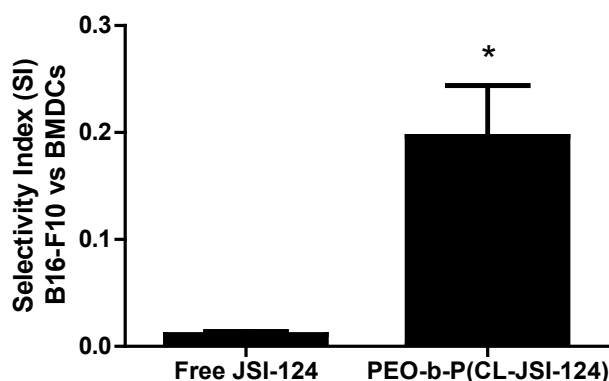


Figure 5.5 Selectivity index (SI) of free JSI-124 and PEO-*b*-P(CL-JSI-124) micelles by B16-F10 cells vs. BMDCs. Each bar represents mean \pm SD ($n = 6$). *Indicates statistically different from free JSI-124 ($P < 0.05$; Student's *t*-test).

5.3.5 Cell cycle analysis

STAT3 plays a key role in the regulation of cell cycle since it controls several genes associated with cell cycle progression.^{398, 407} JSI-124 has been previously shown to inhibit cell growth, at least in part, via cell-cycle arrest in the G2/M phase for other cancer cell lines.⁴⁰⁸⁻⁴¹⁰ Similar results were seen for murine B16 melanoma cells. Treatment with both, JSI-124 or PEO-*b*-P(CL-JSI-124), led to cell-cycle arrest in the G2/M phase followed by apoptosis (sub G0/G1) as seen in Figure 5.6. The percentage of B16 cells in the G2/M phase increased from 13.9 % for untreated B16 cells to 33.6 % and 18.9 %, after 24 h treatment with 5 μ M of free JSI-124 or PEO-*b*-P(CL-JSI-124), respectively. The percentage of cells in the sub G0/G1 phase increased from 5.3 % for untreated B16 cells to 29.9 % and 13.6 %, after 24 h treatment with 20 μ M of free JSI-124 or PEO-*b*-P(CL-JSI-124), respectively. PEO-*b*-P(CL-JSI-124) was less effective in terms of cell cycle arrest in the G2/M phase and apoptosis (sub G0/G1) than free JSI-124 at similar concentrations. The percentage of cells in the G2/M phase and sub G0/G1 phase after 48 h treatment with 5 μ M of free JSI-124, was similar to that for 20 μ M of PEO-*b*-P(CL-JSI-124) implying a 4-fold decrease in the potency of drug in terms of B16 cell cycle arrest as a result of polymer conjugation.

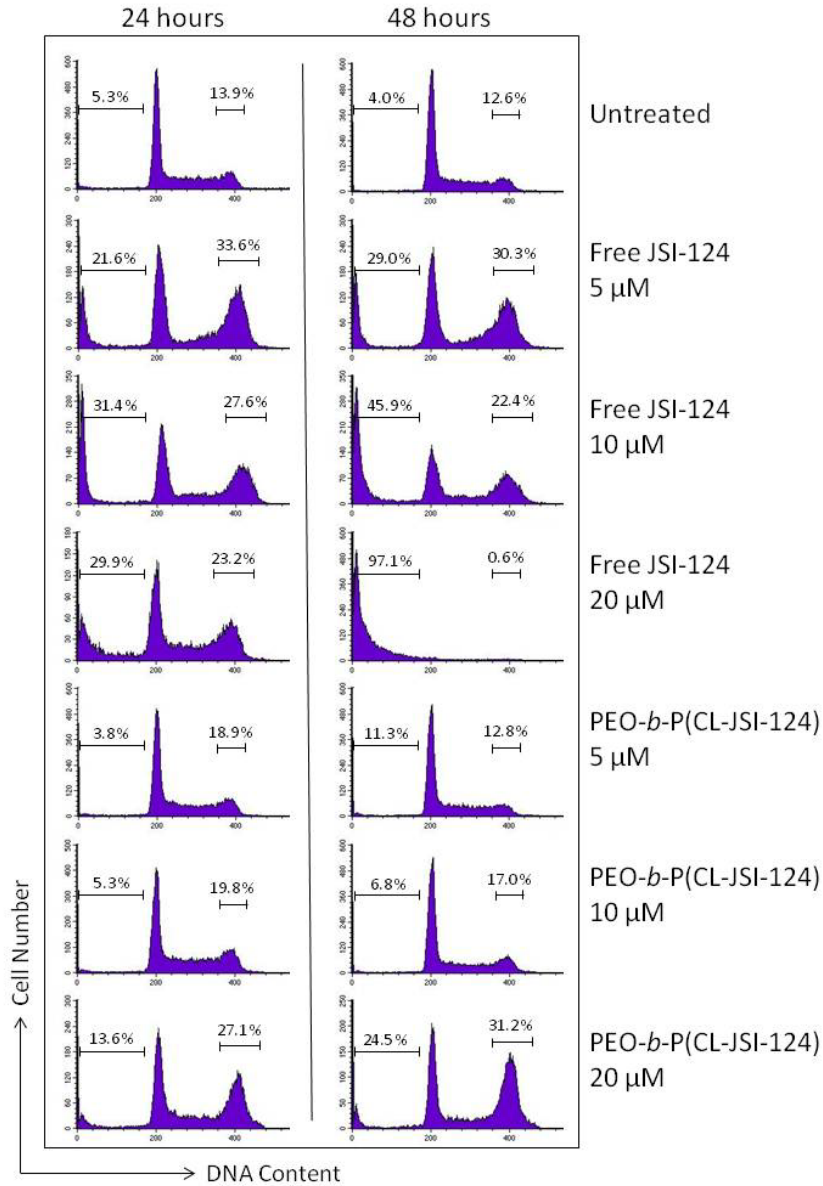


Figure 5.6 Representative cell cycle analysis of B16 cells exposed to free or conjugated JSI-124. JSI-124 causes accumulation of B16 cells in G₂/M phase and apoptosis (sub G₀/G₁) in a dose-dependent manner. Cells were treated with the indicated concentrations of JSI-124 for 24 and 48 h, after which the cells were subjected cell cycle analysis using a flow cytometer. The data represents one out of three independent experiments which showed similar results.

5.3.6 STAT3 inhibitory activity

The STAT3 inhibitory activity of free JSI-124, and PEO-*b*-P(CL-JSI-124) against murine B16-F10 melanoma cell line is shown in Figure 5.7. Treatment of B16 cells with increasing concentrations of free or conjugated JSI-124 resulted in a significant suppression of p-STAT3 levels at 24 and 48 h treatment. The level of p-STAT3 down-regulation for free JSI-124 at a concentration of 5 μ M was similar to that of PEO-*b*-P(CL-JSI-124) at 20 μ M ($p > 0.05$, one-way ANOVA; Tukey's post-hoc test) implying a 4 times less potency in terms of inhibition of STAT3 activation for the conjugated versus free drug. Free JSI-124 concentrations at 10 and 20 μ M resulted in significant cell death leading to inaccurate readings. Empty PEO-*b*-PCCL micelles however, showed no significant decrease in the level of p-STAT3 indicating that the STAT3 inhibitory activity was due to JSI-124 and not due to the PEO-*b*-PCCL block copolymer itself.

In the case of BMDCs; however, PEO-*b*-P(CL-JSI-124) was found to be more potent than free JSI-124 in suppressing p-STAT3 levels after treatment for 24 hrs (Figure 5.8). Treatment of BMDCs with conjugated JSI-124 at concentrations of 100, 500, 1000, and 2000 nM for 24 h suppressed p-STAT3 positive cells to 34.2, 28.4, 23.3, and 13.7 %, respectively as compared to 53.9, 70.1, 60.1, and 54.0 % in the case of free JSI-124. Treatment with 1 μ M of free JSI-124 or PEO-*b*-P(CL-JSI-124) resulted in a \sim 1.8-fold and \sim 1.3 fold decrease in % p-STAT3 positive B16 cells, as compared to a \sim 1.5-fold and 3.8-fold decrease in % p-STAT3 positive BMDCs, respectively, pointing to better p-STAT3 inhibitory activity for polymer-JSI-124 conjugates in BMDCs compared to free drug. Empty PEO-*b*-PCCL micelles however, showed no significant decrease in the level of p-STAT3 compared to

B16/DC indicating that the STAT3 inhibitory activity was due to JSI-124 and not due to the PEO-*b*-PCCL block copolymer itself.

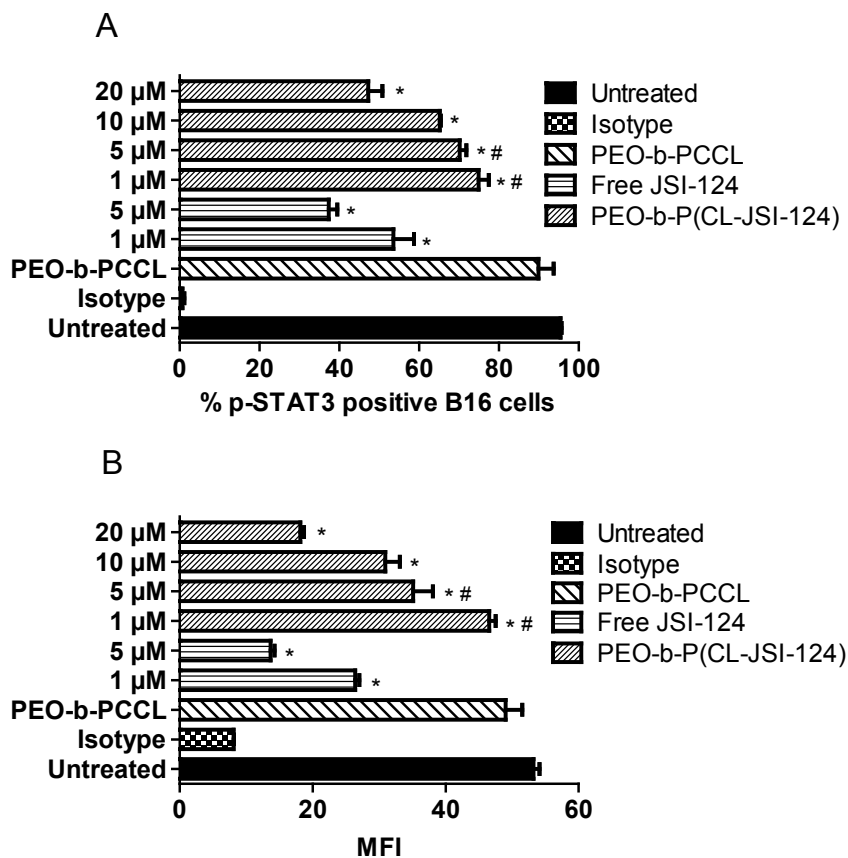


Figure 5.7 Assessment of the p-STAT3 inhibitory activity of PEO-*b*-P(CL-JSI-124) in B16 melanoma cells. A) % p-STAT3 positive and B) MFI of B16 cells treated with different concentrations of free or conjugated JSI-124 after 24 h incubation. Each bar represents mean \pm SD ($n = 3$). *Indicates statistically different from untreated group ($P < 0.05$; one-way ANOVA with Tukey's post-hoc test). #Indicates statistically different from free JSI-124 at similar concentration ($P < 0.05$; one-way ANOVA with Tukey's post-hoc test).

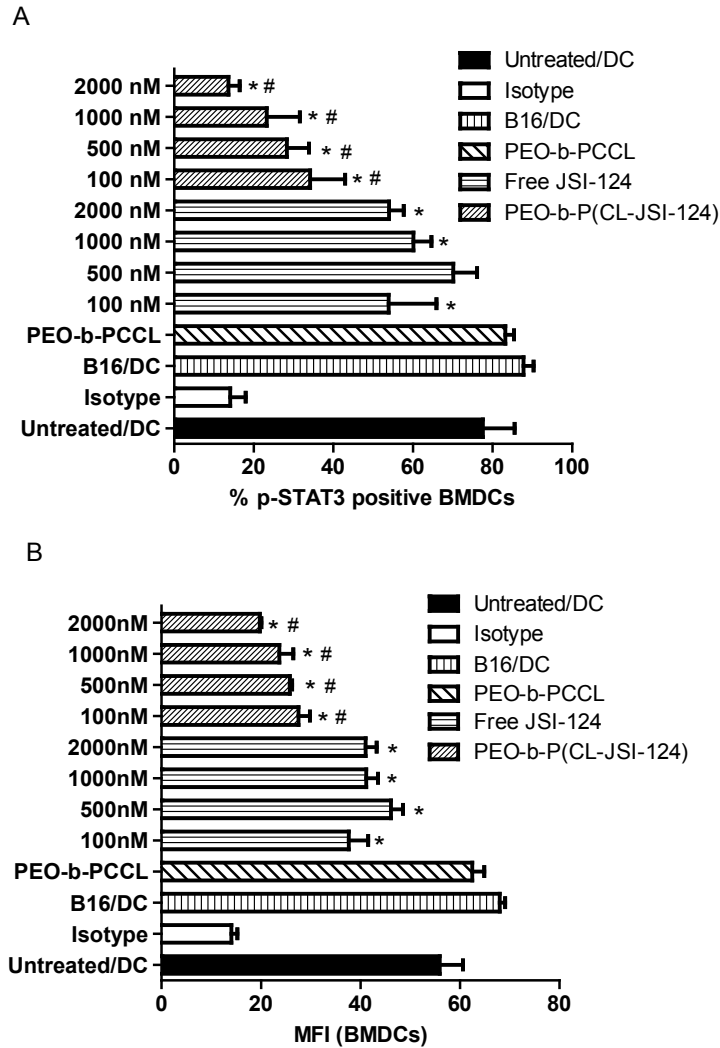


Figure 5.8 Assessment of the p-STAT3 inhibitory activity of PEO-*b*-P(CL-JSI-124) in BMDCs. A) % p-STAT3 positive and B) MFI of BMDCs treated with different concentrations of free or conjugated JSI-124 after 24 h incubation. Each bar represents mean \pm SD ($n=3$). *Indicates statistically different from untreated group ($P < 0.05$; one-way ANOVA with Tukey's post-hoc test). #Indicates statistically different from free JSI-124 at similar concentration ($P < 0.05$; one-way ANOVA with Tukey's post-hoc test).

5.3.7 Immunomodulatory effects of JSI-124 and its polymer conjugate on B16 tumor induced immune-suppressed BMDCs

In contrast to untreated BMDCs, the BMDCs pretreated with B16 tumor supernatant, showed decrease in the expression of maturation markers, i.e., CD40 and CD86, and secretion of IL-12 following LPS exposure ($P < 0.05$, one way ANOVA; Tukey's post-hoc test) (Figure 5.9A, B, and C). Both, free and conjugated JSI-124 were able to reverse the suppressive effects of tumor on CD86 expression in LPS exposed BMDCs ($P < 0.05$, one-way ANOVA; Tukey's post-hoc test). No significant difference in CD40 expression was observed for the same treatment groups, however ($P > 0.05$, one-way ANOVA; Tukey's post-hoc test).

IL-12 is produced by mature DCs and plays an important role in Th1 immune responses by augmenting IFN- γ production.⁴¹¹ Treatment with conjugated JSI-124 significantly increased the secretion of IL-12 from tumor suppressed BDMCs in the presence of LPS ($P < 0.05$, one-way ANOVA; Tukey's post-hoc test). On the other hand, treatment with free JSI-124 significantly decreased the secretion of IL-12 in the same treatment groups ($P < 0.05$, one-way ANOVA; Tukey's post-hoc test). The results points to the Th1 polarized immune-stimulating effects of polymer-JSI-124 conjugate in tumor suppressed BMDCs. Interestingly, this effect was only seen for the JSI-124 conjugate and not the free drug.

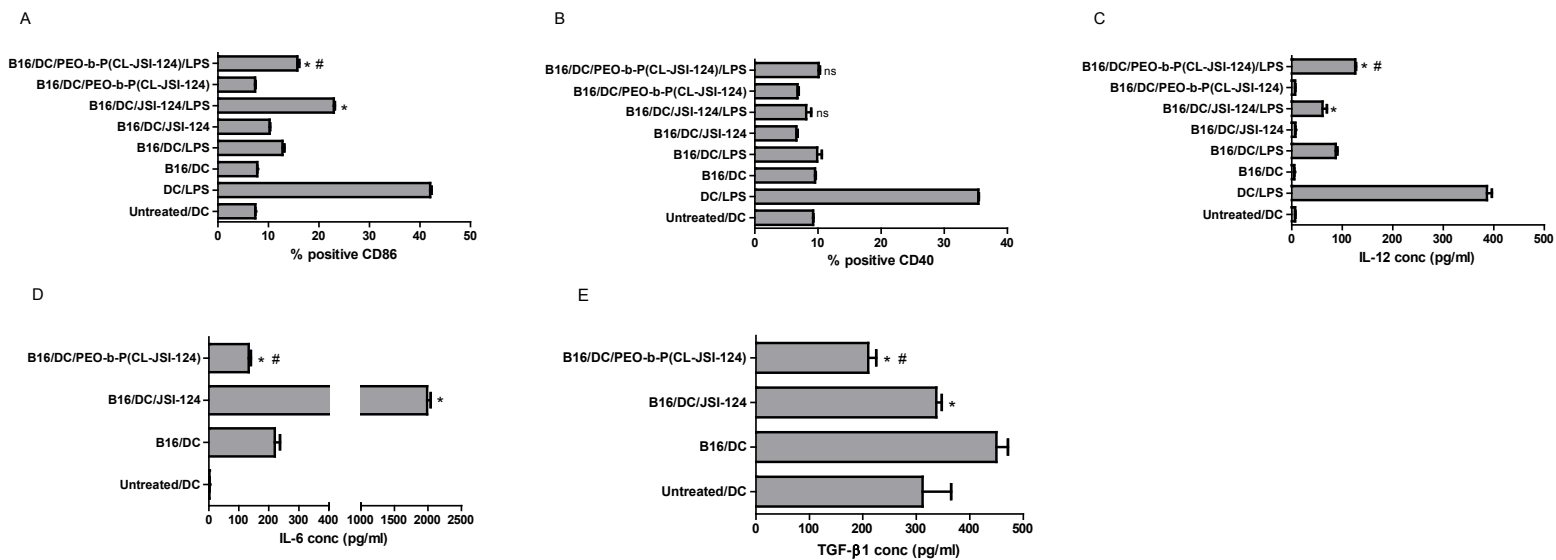


Figure 5.9 The effects of JSI-124 and PEO-*b*-P(CL-JSI-124) on the maturation and activation of B16 tumor induced immune-suppressed BMDCs. BMDCs treated with B16 tumor supernatant were incubated with different formulations for 24 h and analyzed by flow cytometry for upregulation of A) CD86 and B) CD40, and by ELISA for secretion of C) IL-12. D) IL-6, and E) TGF-β1. Each bar represents mean ± SD ($n=3$). For (A), (B), and (C), *Indicates statistically different from B16/DC/LPS ($P < 0.05$). ^{ns}Indicates statistically not different from B16/DC/LPS ($P > 0.05$). #Indicates statistically different from corresponding free JSI-124 group ($P < 0.05$; one-way ANOVA with Tukey's post-test). For (D) and (E), *Indicates statistically different from B16/DC ($P < 0.05$). #Indicates statistically different from corresponding free JSI-124 group ($P < 0.05$; one-way ANOVA with Tukey's post-test).

IL-6 mediates inflammation and its increased secretion has found to play a role in the pathogenesis of many cancers.⁴¹² Treatment of untreated BMDCs with B16 tumor supernatant shows increased secretion of IL-6 as seen in Figure 5.9D. Treatment of immune-suppressed BMDCs with PEO-*b*-P(CL-JSI-124) was able to reverse the effect of tumor and resulted in a 1.7-fold reduction in IL-6 secretion from immunosuppressed BMDCs ($P < 0.05$, one-way ANOVA; Tukey's post-hoc test). Free JSI-124, however, increased secretion of IL-6 further to what was seen for tumor suppressed BMDCs ($P < 0.05$, one-way ANOVA; Tukey's post-hoc test).

TGF- β 1 has been found to play a role in immune suppression by polarizing T cell responses towards Th2 phenotype. Its over-expression is shown to play a role in tumor progression.⁴¹² Treatment of BMDCs with B16 tumor supernatant was found to increase secretion of TGF- β 1 (Figure 5.9E). Treatment of tumor-suppressed BMDCs (B16/DC) with free or conjugated JSI-124, reversed this effect and significantly reduced the secretion of TGF- β 1 ($P < 0.05$, one-way ANOVA; Tukey's post-hoc test). This effect of conjugated JSI-124 in decreasing TGF- β 1 secretion from BMDCs was significantly more than free drug ($P < 0.05$, one-way ANOVA; Tukey's post-hoc test).

The functional effects of JSI-124 and its polymer conjugate on the reversal of tumor induced immunosuppression in BMDCs were assessed by MLR study. BMDCs treated with B16 tumor supernatant were found to be dysfunctional in stimulating T-cells even in the presence of CPG as evidenced by a reduction in the IL-2 and IFN- γ production (Figure 5.10). IL-2 is a major cytokine produced by T cells in a primary response, facilitating their differentiation into one of the two types of effector cells.⁴¹³ PEO-*b*-P(CL-JSI-124) at a concentration of 1000 nM was able to significantly reverse the suppressive effect of tumor

supernatant in terms of the IL-2 production in the presence of CPG at both BMDC:T-cell ratios of 1:10 and 1:20 ($P < 0.05$, one-way ANOVA). In contrast, free JSI-124 at both concentrations did not significantly increase the production of IL-2 from T-cells ($P > 0.05$, one-way ANOVA) (Figure 5.10A and B).

Over-expression of IFN- γ promotes Th1 differentiation of CD4⁺ T-cells and plays an important role in coordinating tumor immune responses.⁴¹⁴ Compared to tumor immunosuppressed BMDCs treated with CPG alone, Immunosuppressed BMDCs treated with CPG + PEO-*b*-P(CL-JSI-124) (500 and 1000 nM) showed significant increase in IFN- γ production upon exposure to T cells at 1:10 cell ratios ($P < 0.05$, one-way ANOVA) by 2.3-fold and 3.3-fold, respectively. In the case of BMDC:T-cell ratios of 1:20, PEO-*b*-P(CL-JSI-124) at 1000 nM concentration was effective in increasing the expression of IFN- γ by 1.9-fold ($P < 0.05$, one-way ANOVA). In contrast, free JSI-124 at both concentrations did not significantly increase the IFN- γ production from T-cells exposed to tumor immunosuppressed BMDCs.

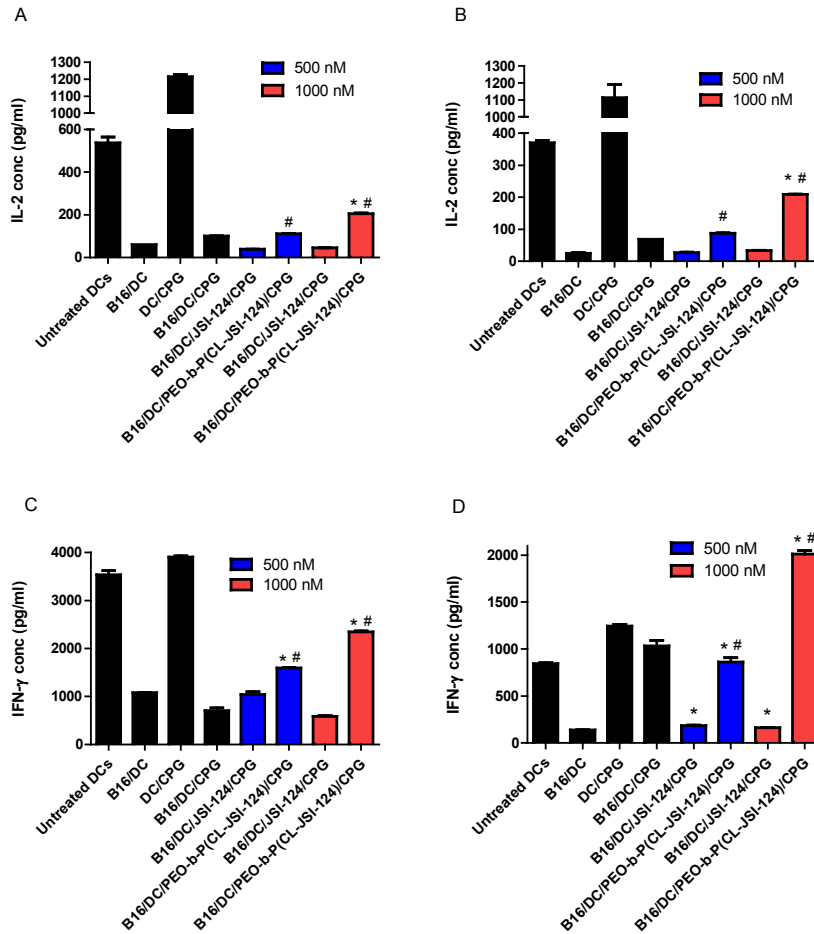


Figure 5.10 The effects of JSI-124 and PEO-*b*-P(CL-JSI-124) on the function of B16 tumor induced immune-suppressed BMDCs in activating T-cells. BMDCs treated with B16 tumor supernatant were incubated with different formulations for 24 h and then co-cultured with CD4⁺ T-cells in DC:T-cell ratios of 1:10 and 1:20 and analyzed by ELISA for secretion of A) IL-2 (1:10), B) IL-2 (1:20), C) IFN- γ (1:10), and D) IFN- γ (1:20). Each bar represents mean \pm SD ($n=3$). *Indicates statistically different from B16/DC/CPG ($P < 0.05$). #Indicates statistically different from corresponding free JSI-124 group ($P < 0.05$; one-way ANOVA with Tukey's post-test).

5.4 Discussion

Constitutive activation of STAT3 is a major contributor to tumor cell proliferation, survival, invasion, and angiogenesis, and cancer immune evasion in many cancers.^{397, 415} STAT3 activation is implicated in tumor cell immune evasion through two mechanisms; first, by the inhibition of pro-inflammatory cytokines and chemokines which are important to enhance the antigen-presenting capacity of dendritic cells; and second, by release of certain tumor-derived soluble factors which increase the activation of STAT3 in DCs.²²⁵ Hyperactivation of STAT3 in DCs has found to suppress myeloid differentiation into DCs, inhibit DC functional maturation and induce the activation of tolerogenic DCs.^{227-229, 231, 232} Inhibition of DC maturation inhibits their ability to induce T-cell activation whereas activation of tolerogenic DCs can induce the activation of T_{reg} cells which further inhibit the function of DCs and effector T-cells.²³⁴ Therefore, inhibition of STAT3 in tumor cells as well as tumor associated DCs is expected to result in direct inhibition of tumor proliferation and metastasis, and by-stander effect in modulating the immunosuppressive micro-environment of tumor in favor of anti-cancer immune response, respectively.^{219, 231, 257, 401} STAT3 activation is, however, also essential for regular function of several vital cells including keratinocytes, embryonic stem cells, mammary and thymic epithelium, sensory and motor neurons, neutrophils, macrophages and pancreatic β cells.⁴¹⁶⁻⁴¹⁹ Therefore, selective inhibition of STAT3 function in tumor and tumor microenvironment is of particular interest.

The main objective of this research is to develop a nano-delivery system for tumor targeted delivery of STAT3 inhibitors as means to enhance anti-cancer immune responses. JSI-124 is a potent JAK-STAT3 inhibitor, and a member of the cucurbitacin family of compounds. It has been studied extensively for its direct anti-tumor activity and effects in

enhancing anti-cancer immunity in several human and murine models.^{226, 227, 231, 249, 255-258} Our research group has previously reported on the development of polymeric micellar formulations that were successful in increasing the solubility of JSI-124 and maintaining its cytotoxicity towards B16 melanoma cells, but were unable to significantly hold on their encapsulated JSI-124 for a long time, *in vitro*.^{261, 301} To enhance the properties of JSI-124 nanodelivery systems in this regard, we pursued chemical conjugation of JSI-124 to the micellar core in self-associating PEO-*b*-PCCL through an ester linkage. Previously, our research group has successfully conjugated JSI-124 to PLGA nanoparticles for delivery of JSI-124 to immunosuppressed DCs.²⁵⁷ PLGA nanoparticles can be naturally taken up by DCs through phagocytosis due to their larger size and unprotected surface,⁴²⁰ however, the size of developed PLGA particles was larger than what is required for passive drug targeting to the tumor. Polymeric micelles, on the other hand, have the ideal size (i.e., ~ 100 nm) for preferential accumulation in the tumor via the enhanced permeability and retention (EPR) effect⁴²¹ where they can be taken up by tumor cells and tumor-associated DCs (Evidence for the uptake of polymeric micelles by DCs is provided in appendix C).

PEO-*b*-P(CL-JSI-124) micelles exhibited a decrease in CMC when compared with PEO-*b*-PCCL micelles which clearly indicates that the introduction of hydrophobic JSI-124 makes self-association of the block copolymers thermodynamically more favorable.^{111, 307} PEO-*b*-P(CL-JSI-124) also exhibited a smaller size as compared to PEO-*b*-PCCL even after the introduction of a bulky JSI-124 substituent. This might be due to increased hydrogen bonding between the -COOH group of PCCL and the -OH group of JSI-124 resulting in increased packing of the block copolymer chains in the core.

Free JSI-124 was released from the dialysis bag rapidly within 6 h indicating that the transfer of JSI-124 from the dialysis bag to the buffer solution is not a restricting factor. Hence, the release of JSI-124 from the micelles is the rate-limiting step in the process. Release of free JSI-124 from PEO-*b*-P(CL-JSI-124) was very slow, pointing to the stability of ester linkage between COOH group on the polymer backbone and the drug. This observation is in line with previous findings on paclitaxel conjugated PEO-*b*-PCCL where 5.0 % drug release after 3 days was observed.^{45, 55}

In general, in *in vitro* biological studies, we observed contrasting effects between comparative effects of free and conjugated JSI-124 in B16 versus tumor suppressed BMDCs. Constitutively activated STAT3 in B16 melanoma cells is a major contributor in their growth, survival, and resistance to apoptosis.³⁹⁹ Inhibition of STAT3 activation by small molecules like JSI-124 can lead to apoptosis of B16 melanoma cells.^{256, 257, 261} Conjugation of JSI-124 to PEO-*b*-PCCL decreased its cytotoxicity against B16 melanoma cells by 3-folds. The lower potency of the drug-polymer conjugate is either caused by slow release of free drug from the conjugate in tumor cells and/or the activity of the polymer-drug conjugate at lower potency itself. Free JSI-124 is taken up quickly by diffusion process, whereas polymeric micellar JSI-124 conjugates were either expected to release the drug in the acidic extracellular tumor environment followed by diffusion of the free drug to the tumor cells, or the polymeric micelles are taken up by endocytosis by tumor cells and then release of the drug in the acidic environment of the endosome.⁴²² Our studies; however, has shown that the bond between PEO-*b*-PCCL and JSI-124 in the conjugate was very stable to acid hydrolysis. Similar to cytotoxicity studies, conjugation of JSI-124 to PEO-*b*-PCCL showed a significant decrease in the cell-cycle arrest in the G2/M phase for B16 melanoma cells when compared

with free JSI-124, perhaps as a result of slow uptake and/or release of JSI-124 from the micelles.

In the case of BMDCs, conjugation of JSI-124 to PEO-*b*-PCCL led to a 63-fold decrease in the cytotoxicity of JSI-124 to BMDCs. The significantly lower cytotoxicity of PEO-*b*-P(CL-JSI-124) in BMDCs compared to free drug may reflect the slow uptake of polymeric-JSI-124 micelles due to the protective effect of the PEG shell.^{307, 423}

The activity of polymer-JSI-124 conjugate in rescuing the tumor suppressed BMDCs to the favorable immune-active state was shown to be higher than the free drug in several *ex vivo* studies performed here. Constitutive activation of STAT3 in tumors like B16 melanoma promotes the release of soluble tumor-derived factors like IL-10, IL-6, M-CSF, and VEGF into the tumor microenvironment. Interaction of cytokines with cytokine receptors indirectly activates STAT3 by first activating receptor-associated tyrosine kinases like JAK which then activates STAT3. Growth factors, on the other hand, can interact with growth factor receptor to either directly activate STAT3 through intrinsic tyrosine kinase activity or indirectly via activation of JAK.^{219, 424} This leads to upregulation of STAT3 expression in DCs which suppresses their immune activity against cancer.^{225, 227, 229} Similar to previous literature, our studies showed that exposure of BMDCs to tumor-conditioned media from B16 melanoma cells resulted in increased activation of STAT3 and expression of pSTAT3 in BMDCs. As expected, treatment of BMDCs pre-exposed to tumor supernatant with JSI-124, reduced the p-STAT3 expression (MFI) and the percentage of p-STAT3 positive cells. Interestingly, compared to the free drug, polymer conjugated JSI-124 decreased the p-STAT3 expression and the percentage of pSTAT3 positive BMDCs further by 2- and 4-folds, respectively. The reason for increased effect of polymer conjugated JSI-124 versus free drug on the inhibition

of p-STAT3 expression in tumor suppressed BMDCs is not clear and needs further investigation.

Previous studies have shown that up-regulation of STAT3 in DCs as a result of exposure to tumor supernatant, inhibit their differentiation into mature DCs even in the presence of TLR ligands like LPS or CPG.^{227, 231, 232, 425} Tumor suppressed BMDCs were also unable to efficiently stimulate T-cell proliferation, or show Th1-dependent immune responses reflected by IFN- γ production by CD4+ T-cells⁴²⁶ even in the presence of immune adjuvants.^{226, 231, 257} In line with previous reports, in our studies, exposure of BMDCs to tumor-conditioned media from B16 melanoma cells resulted in a decrease in the expression of co-stimulatory molecules like CD86, CD40, and secretion of IL-12, as well as a decrease in the secretion of IFN- γ and IL-2 by CD4+ T-cells. Exposure to free and conjugated JSI-124 reversed the effect of tumor supernatant on DCs with regards to CD86 expression, but no effect on CD40 expression was observed. PEO-*b*-P(CL-JSI-124) was able to show better up-regulation of IL-12 by tumor suppressed BMDCs compared to free drug. PEO-*b*-P(CL-JSI-124) also improved production of IFN- γ by CD4+ T-cells in the presence of TLR ligand when compared to free JSI-124. These observations are in line with the improved STAT3 inhibitory activity of PEO-*b*-P(CL-JSI-124) compared to free drug in tumor suppressed BMDCs. IL-12 is mainly produced by BMDCs promoting Th1 differentiation of CD4+ T-cells and production of IFN- γ .⁴¹² TGF- β 1 is a cytokine known to regulate multiple physiological events. In cancer cells, it has found to promote invasion and metastasis,⁴¹² whereas in BMDCs, it inhibits activation and maturation of immature DCs and can affect the trafficking of mature DCs into lymph nodes.⁴²⁷ There has been evidence of cross-talk between TGF- β 1 and STAT3 in both cancer cells and DCs^{428, 429, 430} In our study, inhibition

of STAT3 in BMDCs by JSI-124 and its polymer conjugate resulted in down-regulation of TGF- β 1. In line with previous results, conjugated JSI-124 showed better down-regulation of TGF- β 1 compared to free JSI-124.

Another cytokine IL-6, has found to play a role in the pathogenesis of many cancers.⁴¹² IL-6 has also shown to play a major role in maintaining immature DCs and interference with their ability to mount Th1-type immune responses.⁴³¹ In our studies, PEO-*b*-P(CL-JSI-124) was able to down-regulate IL-6 production by tumor suppressed BMDCs. This was in contrast with free JSI-124 which exhibited upregulation of IL-6 production by BMDCs.

Both, IFN- γ and IL-2, are cytokines produced by Th1 cells that play an important role in coordinating immune responses against cancer.^{414, 432} IFN- γ has shown to regulate the anti-tumor activity of IL-12 and IL-2. IL-2 has previously been shown to play an important role in creating an effective immune response in patients suffering from metastatic melanoma.⁴¹² Hence, up-regulation of both IL-2 and IFN- γ by CD4+ T-cells when treated with PEO-*b*-P(CL-JSI-124) indicates the development of a Th1 immune response against cancer which is required for cancer rejection. Free JSI-124, on the other hand, showed a decreased secretion of IL-2, IFN- γ , and IL-12 indicating a lack of Th1 immune response against cancer. The reason for this opposing effect by free versus conjugated JSI-124 in tumor suppressed BDMCs is not clear and needs further investigation.

5.5 Conclusion

JSI-124 was successfully conjugated in to the core of PEO-*b*-PCL based block copolymer micelles to generate an efficient nanocarrier for JSI-124 having sustained release

properties. Conjugation of JSI-124 to PEO-*b*-PCCL was found to maintain its STAT3 inhibitory activity in B16 melanoma cells at a lower potency, *in vitro*. This approach, however, increased the STAT3 inhibitor activity of JSI-124 in immune suppressed BMDCs and also improved their function in initiating a Th1 immune response when compared to free JSI-124. These findings point to the potential of polymeric micelles based on PEO-*b*-PCL for efficient delivery of STAT3 inhibitor, JSI-124 to the tumor cells and tumor-suppressed DCs in the tumor microenvironment. The results also point to the potential of these nanocarriers in improving the efficacy of cancer immunotherapy in the future.

5.6 Acknowledgements

This study was supported by a grant from CIHR and Alberta Cancer Foundation. S.M.G. was supported by the Alberta Innovates Health Solutions Graduate Studentship, Alberta Cancer Foundation Graduate Studentship, and the J.N. Tata Trust Scholarship. We thank Mr. Vishwanatha Somayaji, Faculty of Pharmacy and Pharmaceutical Sciences, University of Alberta for assistance with ¹H NMR analysis; the Flow Cytometry Lab in Department of Experimental Oncology at Cross Cancer Institute for assistance with flow cytometry; and Dr. Ommoleila Molavi, Faculty of Pharmacy, Tabriz University of Medical Sciences, Iran for assistance with T-cell removal and isolation from BALB/c mice.

Chapter Six
**Modification of the Core/Shell Structure in Poly(ethylene oxide)-*block*-
poly(ϵ -caprolactone-*graft*-spermine) Micellar siRNA for MCL-1 Gene
Silencing in Tumor Xenografts**

The data in this chapter will be submitted as part of a manuscript titled
**Modification of the core/shell structure in poly(ethylene oxide)-*b*-poly(ϵ -caprolactone-*g*-
spermine) micellar siRNA for MCL-1 gene silencing in cancer cells and tumor
xenografts**

**Shyam M Garg^{1*}, Arash Falamarzian^{1*}, Mohammad Reza Vakili¹, Hamidreza
Montazeri Aliabadi³, Hasan Uludağ^{1,2}, Afsaneh Lavasanifar^{1,2}**

¹Faculty of Pharmacy and Pharmaceutical Sciences, University of Alberta, Edmonton, AB

²Department of Chemical and Materials Engineering, Faculty of Engineering, University of
Alberta, Edmonton, AB

³Department of Biomedical and Pharmaceutical Sciences, School of Pharmacy, Chapman
University, Irvine, CA 92618

6.1 Introduction

Despite great promise of gene silencing entities like siRNA, translation of this approach to clinical practice particularly following systemic administration has been challenging. This is mostly due to the instability of siRNA and other gene silencing materials in plasma, poor distribution in diseased tissue and inadequate access to their molecular targets within the target cells. Several delivery systems developed to address these issues, are mostly successful in siRNA delivery *in vitro* or following localized *in vivo* administration.^{271, 299, 300} Success in the targeted delivery of siRNA following systemic administration has been limited mostly because of the non-specific toxicity imposed by the siRNA carrier, uptake by the reticuloendothelial system, insufficient stability in blood, and/or lack of specific interaction and distribution in the target tissue and cells.²⁸¹

Amphiphilic block copolymers with poly(ethylene oxide) (PEO) as the shell-forming block and polyesters like poly(ϵ -caprolactone) (PCL),^{308, 309} poly(lactide) (PLA),³¹³ or poly(lactide-*co*-glycolide) (PLGA)^{122, 314} as the core-forming block have shown tremendous potential in drug delivery.^{1, 16} This is due to the biocompatibility of PEO and polyesters as well as the biodegradability of polyesters, making them safe for human administration.⁴⁷ However, the lack of cationic moieties in PEO-polyester block copolymers limits their use in siRNA delivery. Our research group has previously reported on the development of a biodegradable and biocompatible siRNA delivery system based on self-associating PEO-*b*-PCL block copolymers bearing spermine (SP) on the α -carbons of ϵ -caprolactone in the PCL block. The PEO-*b*-P(CL-*g*-SP) micelles were able to protect siRNA from degradation by serum nucleases, be taken up by cancer cells and effectively down-regulate *MDR-1* through delivery of its siRNA leading to significant decrease in the expression of P-glycoprotein in

MDA-MB-435 cells.¹³⁹ Further modification of PEO-*b*-P(CL-*g*-SP) micellar shell with cancer targeting and cell penetrating peptides, i.e., RGD4C and TAT, respectively, increased the transfection efficiency of the MDR-1 siRNA, *in vitro*.²⁰¹ Systemic administration of RGD4C modified PEO-*b*-P(CL-*g*-SP) enhanced the localization of siRNA in tumor in an MDA-MB-435 xenograft model pointing to the potential of this nanocarrier for siRNA delivery following systemic administration.¹⁰²

Hydrophobic or lipid modification of polymeric complexes has previously been pursued as a method in improving the efficacy of non-viral gene delivery vectors. Lipid modification is expected to enhance the interaction between the polymer/siRNA complexes and the hydrophobic domains of the plasma membrane facilitating cell uptake.^{246, 433} For instance, cholesteryl modification of linear branched polyethyleneimine (PEI) has significantly enhanced cellular uptake and also decreased the toxicity of the linear PEI-cholesterol/pDNA and branched PEI-cholesterol/anti-EGFP siRNA complexes in B16-F0 murine melanoma cells and enhanced green fluorescent protein (EGFP) gene expressing BHK-IR780 cancer cells, respectively. The studies suggested the improved transfection and reduced toxicity to be due to the sequestering of charged secondary amines on PEI by cholesterol.⁴³⁴⁻⁴³⁶ In another study, Wang *et. al.* showed efficient transfection of Bcl-2 siRNA in MDA-MB-231 breast cancer cells by core/shell nanoparticles containing amine groups modified by up to 40 % of cholesterol.⁴³⁷ The role of cholesteryl moiety could not be specifically assessed because control studies with unmodified nanoparticles were not included. In previous studies from our lab, we have modified the spermine groups of PEO-*b*-P(CL-*g*-SP) micelles with different levels of cholesterol substitution. A cholesteryl

substitution of 40% on SP was optimal to improve the siRNA delivery and silencing of myeloid cell leukemia-1 (MCL-1) mRNA in human MDA-MB-435 cancer cells *in vitro*.²⁴⁷

In the current study, we modified 40% of the spermine groups of PEO-*b*-P(CL-*g*-SP) micelles with cholesterol and studied the effect of this approach in plain and/or RGD4C modified micelles on siRNA delivery and silencing of (MCL-1) mRNA in human MDA-MB-435 tumor models, *in vivo*.

Myeloid cell leukemia-1 (MCL-1) is an anti-apoptotic member of the Bcl-2 family of proteins, which maintains survival of cells by inhibiting cytochrome c release via binding and sequestering pro-apoptotic Bcl-2 proteins.^{266, 269-271} Up-regulation of MCL-1 is implicated in cancer survival in a variety of human hematological^{266, 272} as well as solid cancers.^{268,273} Down-regulation of MCL-1, on the other hand, is implicated in the induction of apoptosis.²⁶⁴ Many synthetic and natural chemicals were shown to inhibit MCL-1 expression either at pre- or post-transcription stages. This includes cyclin-dependent kinase inhibitors like flavopiridol,²⁷⁴ tyrosine kinase inhibitors like sorafenib,²⁷³ and STAT3 inhibitors like resveratrol.²⁷⁵ However, these compounds lack specificity for MCL-1 and affect multiple molecular targets.²⁶⁴ Specific inhibitors of MCL-1 are divided to two classes of compounds: BH3 mimetics and gene-silencing treatments. BH3 mimetics like Obatoclax and Bim₅2A can antagonize the interaction of MCL-1 with pro-apoptotic proteins.^{264, 268, 276, 277} However, many of these compounds have shown to cause nonspecific cytotoxicity by damaging mitochondria.²⁶⁸ An alternative and more specific approach is down-regulation of MCL-1 expression through the use of gene silencing entities like antisense oligonucleotides⁴³⁸ or siRNA.

In previous studies, knockdown of MCL-1 using siRNA in resistant melanoma cells is shown to sensitize these cells towards Fas-mediated apoptosis.⁴³⁹ Modugno et. al. tested 44 solid cancer cell lines with MCL-1 siRNA and found silencing of MCL-1 expression to induce apoptosis in 30% of the tested cell lines.²⁶⁸ Suppression of MCL-1 via siRNA in hepatocellular carcinoma cells also sensitized these chemoresistant cells towards chemotherapeutic drugs.⁴⁴⁰ Previous studies of MCL-1 silencing in MDA-MB-435 have shown that PEI-linoleic acid (PEI-LA) complexes with 18 nM MCL-1 siRNA at siRNA:polymer ratios (w/w) of 1:8 were able to decrease the MCL-1 mRNA expression by ~80% and also reduced cell viability by up to ~50% *in vitro*. *In vivo* studies in MDA-MB-435 xenografts showed a ~35% decrease in MCL-1 mRNA expression and delayed tumor growth after intratumoral injections with PEI-LA/MCL-1 siRNA complexes, however, after intraperitoneal injections, MCL-1 mRNA expression decreased by ~20% but did not result in any significant tumor retardation.⁴⁴¹

6.2 Experimental Section

6.2.1 Materials

Ethylene oxide, 3,3-diethoxy-1-propanol (DEP), naphthalene, methoxy polyethylene oxide (Mw 5000 Da), N,N-dicyclohexyl carbodiimide (DCC), N-hydroxysuccinimide (NHS), spermine, cholesteryl chloroformate, and anhydrous dimethylsulfoxide (DMSO) were obtained from Sigma (St. Louis, MO). α -Benzyl carboxylate- ϵ -caprolactone monomer was synthesized by Alberta Research Chemicals Inc (Edmonton, AB) according to a previously published procedure.⁴³ Stannous octoate was purchased from MP Biomedicals

Inc. (Eschwege, Germany). Acetone, THF and DMF were obtained from Caledon Laboratories Ltd. (Ontario, Canada). RGD4C (KACDCRGDCFCG, MW 1273.9) was purchased from Anaspec Inc. (Torrence, CA). All other chemicals were reagent grade. Cell culture media RPMI 1640, penicillin-streptomycin-glutamine, fetal bovine serum, HEPES buffer solution (1M) and trypsin/ethylenediaminetetraacetate (EDTA) were purchased from GIBCO, Invitrogen Corp (USA). The scrambled siRNA used as control was supplied from Ambion (catalog number: AM4636). The Silencer siRNA against MCL-1 was purchased from Qiagen (catalog numbers: SI02781205, sequence: CGCCGAAUUCAUUAUUUATT).

6.2.2 Cell lines

The wild-type MDA-MB-435 (MDA-MB-435 WT) cells were originally obtained as a gift from the laboratory of Dr. Robert Clark (Georgetown University, USA). MDA-MB-435 WT cells were cultured in RPMI 1640 media supplemented with 10% FBS, 100 U/mL penicillin, and 100 mg/mL streptomycin in 37 °C and 5% CO₂. Cell cultures were considered confluent when a monolayer of cells covered more than 80% of the flask surface. To propagate the cells, a monolayer was washed with sterile PBS, and subsequently incubated with 0.25% trypsin/EDTA for 3 min at 37 °C. The suspended cells were centrifuged at 500×g for 5 min, and were re-suspended in the medium after removal of the supernatant. The suspended cells were sub-cultured at 10% of the original count.

6.2.3 Synthesis of Cholesteryl Substituted PEO-*b*-P(CL-*g*-SP) Block Copolymers

Methoxy-poly(ethylene oxide)-*b*-poly(ϵ -caprolactone-*g*-N-(spermine)-cholesteryl carboxylate) (PEO-*b*-P(CL-*g*-SP-Chol)) were prepared as described previously.²⁴⁷ Spermine was conjugated to PEO-*b*-PCCL forming Methoxy-poly(ethylene oxide)-*block*-poly(ϵ -caprolactone-*g*-N-(spermine)) (PEO-*b*-P(CL-*g*-SP)) according to a previously published procedure with slight modification.¹³⁹ Briefly, PEO-*b*-PCCL (200 mg, \sim 0.01 mmol) was dissolved in 10 mL of dry THF. After addition of DCC and NHS in THF, the solution was stirred for 2 h until a precipitate was formed. The precipitate was removed by filtration. THF was removed under vacuum. The remaining solid product was dissolved in DMF. Spermine was dissolved in DMF and added drop-wise to the polymer solution. The reaction proceeded for another 24 h under stirring at room temperature. The resulting solution was centrifuged to remove the precipitate. The resulting solution was then dialyzed (molecular weight cut-off of 3500 Da) extensively against DMF (24 h) and then water (7 h). The polymer solution was then freeze-dried for further use. After purification, the synthesis of PEO-*b*-P(CL-*g*-SP) was confirmed by ¹H NMR (Bruker Avance III spectrometer, Bruker BioSpin Corporation, Billerica, MA). The spermine substitution level of the synthesized copolymer was estimated based on peak intensity ratio of the methylene protons from polyamine (-CH₂-NH-) and PEO (-CH₂CH₂O-). The degree of polymerization was estimated based on peak intensity ratio of proton from PCL (-OCH₂- proton, δ = 4.1 ppm) to the intensity of specific peak in PEO ((-CH₂CH₂O-) proton, δ = 3.65 ppm).

PEO-*b*-P(CL-*g*-SP-Chol) was synthesized by attaching pendant cholesteryl groups to the polyamine section of PEO-*b*-P(CL-*g*-SP). Briefly, a solution of 0.3 g of PEO-*b*-P(CL-*g*-

SP) in 6 mL dried DMF was placed in a round bottom flask under argon atmosphere. This flask was cooled down to 0 °C by an ice-water bath. A solution of cholesteryl chloroformate (0.074 g) in 6 mL of dry DMF was added dropwise to previous solution over a period of 45 s. The reaction was left for 24 h at room temperature under argon atmosphere. Finally, the resulting solution was poured into a large amount of ether to precipitate the product. The separated solid product was completely washed by ether and dried under vacuum. The degree of polymerization of poly (ϵ -caprolactone) (PCL) backbone after reaction with cholesteryl chloroformate was estimated as described for PEO-*b*-P(CL-*g*-SP). Cholesteryl substitution level was estimated by comparing the peak intensity of (-CH₃ proton, δ = 0.9 ppm) cholesteryl moiety to the intensity of specific peak in PEO ((-CH₂CH₂O-) proton, δ = 3.65 ppm) (Table 6.1).

6.2.4 Synthesis of RGD4C-PEO-*b*-PCCL with pendant N,N-dimethyldipropylentriamine (DP) (RGD4C-PEO-*b*-P(CL-*g*-DP))

For *in vivo* studies, acetal-PEO-*b*-PCCL was synthesized according to a previously reported method.¹⁹¹ Acetal-PEO-*b*-P(CL-*g*-DP) was synthesized from acetal-PEO-*b*-PCCL as reported previously.¹³⁹ RGD4C-attached PEO-*b*-P(CL-*g*-DP) was synthesized from acetal-PEO-*b*-P(CL-*g*-DP) according a method reported previously with slight modification.^{102, 198} RGD4C was conjugated to the micelles at an RGD4C:polymer molar ratio of 1:5. The conjugation efficiency of RGD4C peptide to polymeric micelles was determined by a reverse gradient HPLC method as described previously (Table 6.1).^{102, 198} The resulting micellar solution was dialyzed against distilled water and lyophilized.

6.2.5 Preparation of polymeric micellar siRNA complexes for *in vivo* study

Preparation of micellar siRNA complex compositions are shown in Table 6.2. For intratumoral injections, 200 μM solution of scrambled or MCL-1 siRNA in RNase free water was added to HEPES solution in an eppendorf tube. PEO-*b*-P(CL-*g*-SP) or PEO-*b*-P(CL-*g*-SP-Chol) was prepared as a solution of 20 mg/mL in HEPES buffer and added to the siRNA solution in HEPES such that the final concentration of siRNA or polymer in 50 μL of HEPES is 10 μg and 160 μg , respectively. The solution is allowed to incubate for 20 m before injection. For intravenous injection, 200 μM solution of MCL-1 siRNA in RNase free water was added to a solution of dextrose in an eppendorf tube. PEO-*b*-P(CL-*g*-SP) or PEO-*b*-P(CL-*g*-SP-Chol) was prepared as a solution of 20 mg/mL in RNase free water and added to the siRNA solution. Acetal-PEO-*b*-P(CL-*g*-DP) or RGD4C-PEO-*b*-P(CL-*g*-DP) was prepared as a solution of 40 mg/mL in RNase free water and added to the siRNA solution. The final concentration in 100 μL of 5% dextrose solution was 40 μg of MCL-1 siRNA, 640 μg of PEO-*b*-P(CL-*g*-SP) or PEO-*b*-P(CL-*g*-SP-Chol), and 1280 μg of acetal-PEO-*b*-P(CL-*g*-DP) or RGD4C-PEO-*b*-P(CL-*g*-DP).

6.2.6 Animal models

Female athymic NCr nude mice (NCRNU-F) were purchased from Taconic Biosciences Inc. (Hudson, NY). All experiments were performed using 4 to 6 week old female mice. All animal studies were conducted in accordance with the guidelines of the Canadian Council on Animal Care (CCAC) with approval from the Animal Care and Use

Committee (ACUC) of the University of Alberta (Edmonton, AB, Canada). To establish the tumor model, mice were randomly assigned into five groups of six mice per group. Mice were inoculated with 2×10^6 MDA-MB-435 WT cells in a volume of 50 μ L PBS injected s.c. in the right rear flank. The mice were used when the tumors reached a size of 100 mm³ (10 days after injection).

6.2.7 *In vivo* activity of MCL-1 siRNA micelles after intratumoral and intravenous injection

The composition of treatment groups for the test samples for intratumoral and intravenous injections is shown in Table 6.2. For intratumoral injections, mice bearing tumors were injected with 50 μ L HEPES, 10 μ g scrambled or MCL-1 siRNA loaded SCR-SP micelles, MCL-SP micelles, SCR-SP-Chol micelles, or MCL-SP-Chol micelles (Table 6.2). For intravenous injections, mice bearing tumors were injected via tail vein with 100 μ L dextrose, 40 μ g MCL-1 siRNA loaded NON-SP micelles, NON-SP-Chol micelles, RGD-SP micelles, and RGD-SP-Chol micelles (Table 6.2). For both experiments, treatment was given every third day for three doses (days 4, 7, and 10). Mice were monitored daily according to previously reported method.¹⁹³ Tumor size was measured on days 0, 4, 7, 10, and 13 with a caliper and mean \pm SEM of relative tumor volume in each group was calculated using the formula: tumor volume = $0.4LW^2$ (L is the long diameter and W is the short diameter of the tumor); and plotted as a function of time according to previously reported method.¹⁹³ Tumors were excised on day 13 and stored in RNeasy lysis solution (Life Technologies, Burlington, ON) at -20 °C until further analysis.

Real time (RT) PCR was carried out on the excised tumors from both experiments to determine MCL-1 knock-down at the mRNA level. Tumors were homogenized and total RNA was extracted using RNeasy spin columns (Qiagen) according to the manufacturer's recommendations. cDNA was synthesized and real time PCR was performed on a StepOnePlus™ RT-PCR system (Applied Biosystems) with β -Actin as the endogenous housekeeping gene and the specific MCL-1 primers according to the procedure described above. Each sample was measured in triplicate.

To study the safety of the micellar complexes after intravenous administration, mice were monitored for their weights and tissues (liver, spleen, and kidneys) were excised for histological examination on day 13 and stored in 10% neutral buffered formalin until further use. For histological examination, the stored tissues were embedded in paraffin. Slices of 2- μ m thickness were cut, deparaffinized, hydrated, and stained with hematoxylin-eosin. Each slide was assigned a code number before being sent for microscopic assessment. The microscopic assessments were performed by a qualified veterinary pathologist, Dr. P.N. Nation, DVM, PhD, DACVP from the Animal Pathology Services (APS) Ltd. The assessor, who was blinded to the treatment groups and to the nature of the study design, was asked to look for qualitative evidence of microscopic changes consistent with tissue toxicity. Tissues of three mice from each group were randomly chosen for histological examination.

6.2.8 Statistics

Compiled data were presented as mean \pm standard error mean (SEM). Where feasible, the data were analyzed for statistical significance using unpaired student's *t*-test, or one-way

analysis of variance (ANOVA) followed by Tukey's post hoc test as noted in the results section. The level of significance was set at $\alpha \leq 0.05$.

6.3 Results

6.3.1 Synthesis and Characterization of PEO-*b*-P(CL-*g*-SP-Chol)

The PEO-*b*-P(CL-*g*-SP) with cholesteryl substitution on the SP groups, i.e., PEO-*b*-P(CL-*g*-SP-Chol), was synthesized through reaction of PEO-*b*-P(CL-*g*-SP) with cholesteryl chloroformate. The final structure of copolymers was confirmed by ¹H NMR as reported previously.²⁴⁷ Based on those results, the degree of polymerization of PCL block was calculated to be 16. For PEO-*b*-P(CL-*g*-SP) copolymer, the number of spermines on the PCL block was determined to be 6. In other words approximately 40 % of carboxyl groups were substituted with spermine. On average, the substitution level of cholesteryl group on the SP was also around 40 % (i.e. 2.4 out of 6 spermines) (Table 6.1). This polymer is shown as PEO₁₁₄-*b*-P(CL-*g*-SP-Chol)_{16-6-2.4} where 15-6-2.4 subscript refers to the degree of caprolactone polymerization, the number of conjugated spermine groups and the number of cholesteryl substituted spermines, respectively.

Table 6.1 Characteristics of polymers used in the study

No.	Polymer abbreviate	MWt ^a (g/mol)	Polyamine substitution (% mol caprolactone in PCCL) ^a	Cholesteryl substitution (% mol caprolactone in PCCL) ^a	RGD4C substitution (% mol polymer) ^b
I	PEO- <i>b</i> -P(CL- <i>g</i> -SP)	8750	38	None	None
II	PEO- <i>b</i> -P(CL- <i>g</i> -SP-Chol)	9700	38	15	None
III	acetal-PEO- <i>b</i> -P(CL- <i>g</i> -DP)	9350	42	None	None
IV	RGD4C-PEO- <i>b</i> -P(CL- <i>g</i> -DP)	10600	42	None	10

^aDetermined by ¹H NMR; ^bDetermined by HPLC

Table 6.2 Polymer compositions for the preparation of siRNA micellar complexes for *in vivo* study.

Micelle compositions used for intratumoral injection		Micelle compositions used for intravenous injection	
Polymer composition	Composition ratio (W:W) ^a	Polymer composition	Composition ratio (W:W) ^a
SCR-SP micelles	I:V (16:1)	plain-SP micelles	I:III:VI (16:32:1)
MCL-SP micelles	I:VI (16:1)	plain-SP-Chol micelles	II:III:VI (16:32:1)
SCR-SP-Chol micelles	II:V (16:1)	RGD-SP micelles	I:IV:VI (16:32:1)
MCL-SP-Chol micelles	II:VI (16:1)	RGD-SP-Chol micelles	II:IV:VI (16:32:1)

^a(I) PEO-*b*-P(CL-*g*-SP), (II) PEO-*b*-P(CL-*g*-SP-Chol), (III) acetal-PEO-*b*-P(CL-*g*-DP), (IV) RGD4C-PEO-*b*-P(CL-*g*-DP), (V) Scrambled siRNA, (VI) MCL-1 siRNA

6.3.2 *In vivo* activity of MCL-1 siRNA micelles following intratumoral injection

The *in vivo* activity of MCL-1 siRNA complexed with PEO-*b*-P(CL-*g*-SP) and PEO-*b*-P(CL-*g*-SP-Chol) following intratumoral injections was assessed in MDA-MB-435 WT s.c xenografts in nude mice. As shown in Figure 6.1A, the level of MCL-1 mRNA expression after treatment with MCL-SP-Chol micelles was reduced by ~38 % compared to untreated control group and SCR-SP-Chol micelles, which showed no decrease in MCL-1 mRNA expression (unpaired student's *t*-test, $P < 0.05$). MCL-SP micelles were effective in reducing MCL-1 mRNA expression by ~31 % compared to untreated control group and SCR-SP micelles which showed no decrease in MCL-1 mRNA expression (unpaired student's *t*-test, $P < 0.05$). The difference in down-regulation of MCL-1 mRNA by MCL-SP-Chol micelles was not statistically significant from that of MCL-SP micelles (unpaired student's *t*-test, $P > 0.05$).

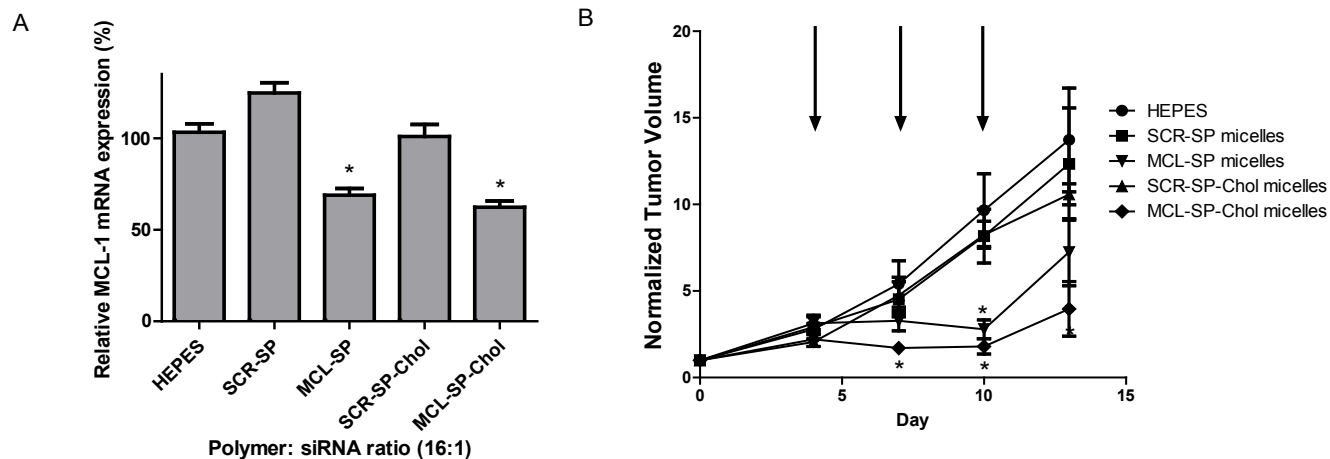


Figure 6.1 *In vivo* MCL-1 siRNA activity in nude mice bearing MDA-MB-435 WT xenograft treated with three intratumoral injections of polymer/siRNA formulations or HEPES. A) Relative MCL-1 mRNA expression in MDA-MB-435 WT xenograft after treatment with polymer/siRNA formulations or HEPES. Values are relative to untreated control. The data are presented as mean \pm SEM (n = 4-5). *Significantly different from its corresponding scrambled siRNA group (unpaired student's *t*-test, $P < 0.05$). B) Normalized tumor volume of MDA-MB-435 WT xenograft after treatment with polymer/siRNA formulations or HEPES. Each point represents mean \pm SEM (n = 4-5). Arrow indicates onset of intratumoral injection. *Significantly different from its corresponding scrambled siRNA group or HEPES (unpaired student's *t*-test, $P < 0.05$); #Significantly different from its corresponding group without cholesteryl modification (unpaired student's *t*-test, $P < 0.05$).

To evaluate the effect of *MCL-1* silencing at mRNA level on tumor growth, tumor volumes were measured on day 0, 4, 7, 10, and 13. In general, both MCL-SP-Chol and MCL-SP micelles were able to retard the growth of the tumor up to Day 10 following which the tumor started to grow again (Figure 6.1B). Similar results were seen previously by Aliabadi et.al. using lipid-modified PEI/MCL-1 siRNA complexes.⁴⁴¹ This might be due to the compensating effect of other anti-apoptotic factors in the treated cells at this point. On day 13, although MCL-SP micelles showed a 1.9-fold decrease in tumor volume, this decrease in tumor volume was statistically not significant from SCR-SP micelles (unpaired student's *t*-test, $P > 0.05$). MCL-SP-Chol, on the other hand, showed a 3.46-fold decrease in tumor volume on day 13 which was significantly different from that of SCR-SP-Chol micelles and the untreated group (unpaired student's *t*-test; $P < 0.05$). Although treatment with MCL-SP-Chol micelles resulted in a significant decrease in tumor volume compared to untreated group on day 7, 10, and 13, this decrease in tumor volume was not significantly different from MCL-SP micelles (unpaired student's *t*-test; $P > 0.05$).

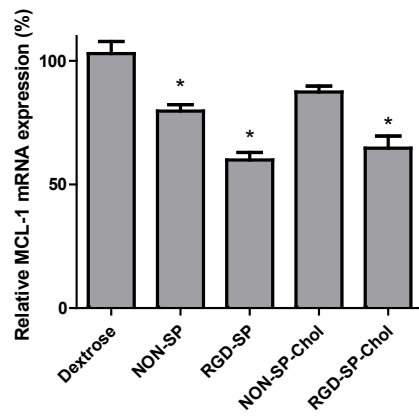
6.3.3 *In vivo* activity of RGD4C-functionalized versus plain MCL-1 siRNA micelles after intravenous injection

The *in vivo* activity of RGD4C-modified MCL-1 siRNA micelles of PEO-*b*-P(CL-*g*-SP) and PEO-*b*-P(CL-*g*-SP-Chol) following intravenous injection was assessed in MDA-MB-435 WT subcutaneous xenografts in nude mice and compared to that for their plain (unmodified) micellar counterparts. The choice of RGD4C modified micellar siRNA as test groups in this study was based on our previous results which has shown high accumulation

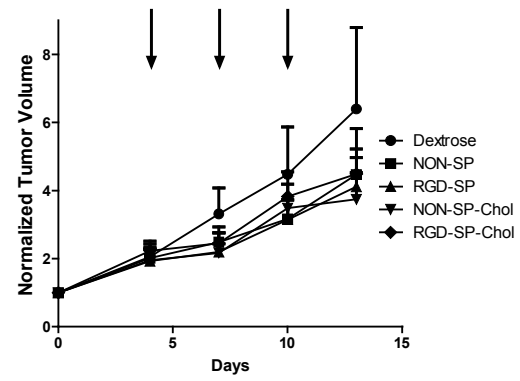
and targeting of RGD4C modified PEO-*b*-P(CL-*g*-SP) micelles in the same tumor model following intravenous administration.¹⁰² The composition of test treatment groups in this study is summarized in Table 6.1 and Table 6.2. The general safety of formulations was also assessed by monitoring animal behavior, movement and body weight during the study.

In general, RGD4C modification of polymeric micellar siRNA complexes, was shown to enhance the silencing activity of complexed siRNA in MDA-MB-435 xenografts following intravenous injection. Cholesterol modification of the core, however, did not affect the silencing activity of complexed siRNA following intravenous administration under the same conditions. As shown in Figure 6.2A, the level of MCL-1 mRNA expression after treatment with RGD-SP-Chol micelles was reduced by ~36 % compared to untreated control group (unpaired student's *t*-test, $P < 0.05$). This level of MCL-1 mRNA knockdown was significantly different from plain-SP-chol micelles which showed only ~12 % decrease in MCL-1 mRNA expression (unpaired student's *t*-test, $P < 0.05$). RGD-SP micelles were effective in reducing MCL-1 mRNA expression by ~40 % compared to untreated control group (unpaired student's *t*-test, $P < 0.05$). This level of MCL-1 mRNA knockdown was significantly different from identical plain-SP micelles which showed ~20 % decrease in MCL-1 mRNA expression (unpaired student's *t*-test, $P < 0.05$). Both RGD-SP-Chol and plain-SP-Chol micelles showed similar MCL-1 mRNA knockdown when compared to RGD-SP and plain-SP micelles (unpaired student's *t*-test, $P < 0.05$) indicating that cholesterol modification of PEO-*b*-P(CL-*g*-SP) had no effect on the MCL-1 knockdown after systemic delivery. This was similar to results seen after intratumoral injection but different from what we observed *in vitro*.

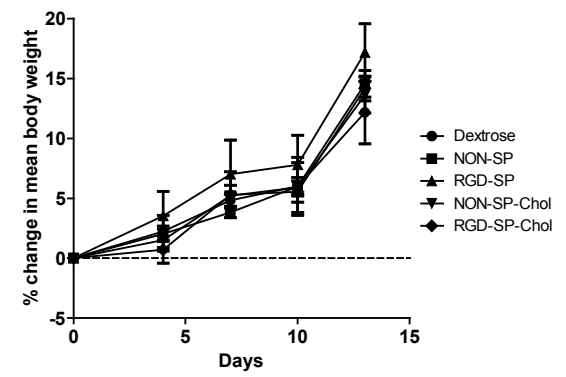
A



B



C



D

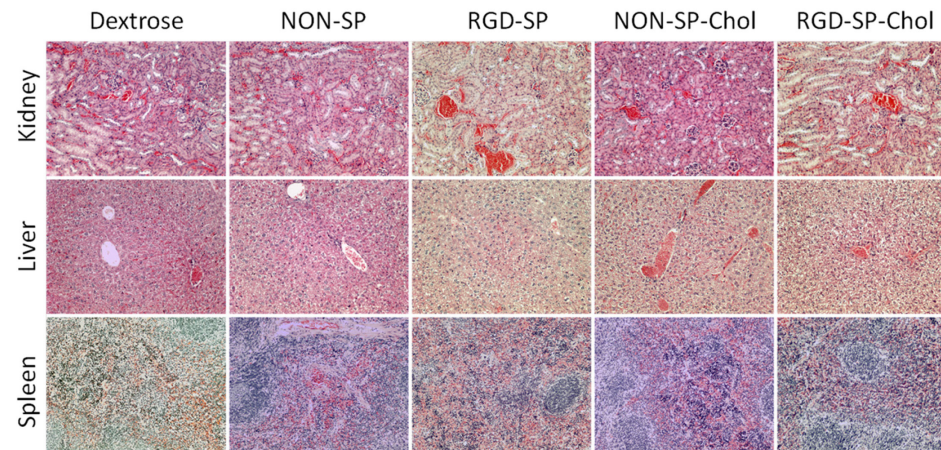


Figure 6.2 *In vivo* MCL-1 siRNA activity in nude mice bearing MDA-MB-435 WT xenograft treated with three intravenous injections of polymer/siRNA formulations or dextrose. A) Relative MCL-1 mRNA expression in MDA-MB-435 WT xenograft after treatment with polymer/siRNA formulations or dextrose. Values are relative to untreated control. The data are presented as mean \pm SEM (n = 3-5). B) Normalized tumor volume of MDA-MB-435 WT xenograft after treatment with polymer/siRNA formulations or dextrose. Each point represents mean \pm SEM (n = 3-5). Arrow indicates onset of intravenous injection. C) Percentage change in mean animal body weight after treatment with polymer/siRNA formulations or dextrose. Each point represents mean \pm SEM (n = 3-5). *Significantly different from untreated group/dextrose (unpaired student's *t*-test, $P < 0.05$); #Significantly different from its corresponding group without cholesteryl modification (unpaired student's *t*-test, $P < 0.05$) D) Microscopic histology images of the spleen, liver, and kidney cortex stained with haematoxylin and eosin at 100X. Each image is representative of one mouse from a group of 3.

Mice treated with polymer/MCL-1 siRNA complexes with or without RGD4C functionalization at the surface showed retardation in tumor growth rate when compared to the control group treated with dextrose 5 %, however the relative tumor volumes of the treated test groups were not significantly different from the control group (unpaired student's *t*-test, $P > 0.05$). On day 13, RGD-SP and RGD-SP-Chol micelles showed a 1.55-fold and 1.44-fold decrease in tumor volume, as compared to 1.43-fold and 1.71-fold decrease shown by plain-SP and plain-SP-Chol micelles, respectively (Figure 6.2B).

To determine the safety of the different MCL-1 siRNA/polymer complexes administered in the study, mice were monitored for their weight during the study, and histopathological examination of the kidney, spleen, and liver tissues after H&E staining was performed on the mice at the end of the study. The weight of the animals increased during the study indicating that the mice tolerated the regimen well (Figure 6.2C). The organs of most mice in the treatment groups were microscopically normal (Figure 6.2D). One mouse each from plain-SP and RGD-SP micelles group had minimal hyperplasia of the lymphoid germinal centers. This, however, is a normal physiological reaction of the spleen, and as there was no particular group associated pattern, it was concluded not to be related to the formulations. All formulations were found to have no adverse anatomic effects on the mice during the duration of this study.

6.4 Discussion

Advancement of siRNA technology for use in preclinical cancer models and clinic has been slow due to the difficulty in the safe and effective delivery of siRNA to cancer cells following systemic administration.⁴⁴² Our research group has previously reported on the

preparation of a siRNA delivery system for use in cancer targeted siRNA delivery following intravenous administration. This delivery system is based on PEO-*b*-PCL block copolymers bearing polycations like spermine (SP)^{102, 139} on the α -carbon of ϵ -caprolactone in the PCL block for siRNA complexation. The PEO-*b*-P(CL-*g*-SP) is shown to complex siRNA effectively and protect it against degradation in serum and silence the expression of P-glycoprotein in human cancer cells leading to their sensitization to chemotherapeutics.¹³⁹ We have also used the RGD4C peptide as ligand to modify the surface of PEO-*b*-P(CL-*g*-SP) micelles,^{102, 201} or separately, have also modified the SP group on the PCL backbone of PEO-*b*-P(CL-*g*-SP) with cholesterol moieties.²⁴⁷ RGD4C modification led to a reduction in the required dose of siRNA for gene silencing and also improved the accumulation of polymeric micelles in MDA-MB-435 tumor,^{102, 201} whereas cholesteryl modification led to improved delivery of MCL-1 siRNA into MDA-MB-435 cells translating into efficient down-regulation of MCL-1 mRNA and subsequent cell death *in vitro*.²⁴⁷ In the current study, we investigated the effect of cholesteryl modification of SP groups of PEO-*b*-P(CL-*g*-SP) on siRNA delivery and silencing activity by plain or RGD4C modified micelles in *in vivo* cancer models. Cholesterol modification of SP was hypothesized to lead to improvements in gene silencing and therapeutic activity of developed polymeric micellar siRNA delivery system after local or systemic administration.

Intratumoral injection of MCL-1 siRNA complexed with PEO-*b*-P(CL-*g*-SP) and PEO-*b*-P(CL-*g*-SP-Chol) produced similar trends to *in vitro* results in terms of MCL-1 mRNA down-regulation, with MCL-1 siRNA complexes of PEO-*b*-P(CL-*g*-SP-Chol) showing slightly better downregulation of MCL-1 mRNA over PEO-*b*-P(CL-*g*-SP) complexes, but the difference was not statistically significant. In line with the decreased

expression of MCL-1 mRNA by polymeric micellar MCL-1 siRNA complexes, a decrease in the rate of tumor growth rate was also observed. However, again the slight better inhibition of tumor growth by the siRNA complexes with PEO-*b*-P(CL-*g*-SP-Chol) over PEO-*b*-P(CL-*g*-SP) complexes was statistically insignificant. The rate of tumor growth inhibition by MCL-1 siRNA delivery was reduced after the 3rd injection of siRNA complexes by both polymeric micellar siRNA delivery systems, particularly that of PEO-*b*-P(CL-*g*-SP) formulations. This may reflect a compensating effect by other anti-apoptotic factors for the down-regulation of MCL-1.

Following systemic administration, cholesterol modification of the core in PEO-*b*-P(CL-*g*-SP) did not impact the gene silencing or therapeutic activity of MCL-1 siRNA complexes in tumor xenografts. But the RGD4C modification of the micellar shell did improve the silencing activity of the polymeric micellar siRNA delivery systems for both PEO-*b*-P(CL-*g*-SP-Chol) and PEO-*b*-P(CL-*g*-SP) in tumor xenografts. This is perhaps due to increased accumulation of RGD4C-coated micelles in MDA-MB-435 tumors, in which $\alpha_v\beta_3$ integrins is overexpressed,⁴⁴³⁻⁴⁴⁵ as shown in our previous study.¹⁰² The down-regulation of MCL-1 mRNA in tumor xenografts following intravenous administration of MCL-1 siRNA complexes with RGD4C modified micelles was not sufficient to cause significant inhibition of tumor growth when compared to control animals, however. Higher MCL-1 mRNA silencing (> 40 %) might be required to see any measurable difference in inhibition of MDA-MB-435 tumor growth. One interesting observation was that although intravenous administration of the RGD4C modified polymer:siRNA complexes showed a similar downregulation of MCL-1 mRNA expression when compared to that after intratumoral administration of complexes; a similar reduction in tumor volume for the two routes of

administration was not observed. The reason behind this is unknown but there could be a possibility of increased cytotoxicity upon injection directly to the tumor site, when the delivery system is in direct and more uniform contact with tumor cells. This is in contrast to RGD modified micelles that may be sequestered by tumor vasculature cells or other non-cancerous cells of the tumor. Another possibility is the slight difference in the composition of polymeric micellar siRNA administered either by intratumoral or iv routes. The micellar construct used for iv administration contains 32 parts of PEO-*b*-P(CL-*g*-DP) (to which the RGD4C is attached). However, PEO-*b*-P(CL-*g*-DP) is more cytotoxic and less efficient in siRNA delivery when compared to PEO-*b*-P(CL-*g*-SP).¹³⁹ The reason for this observation needs to be investigated further.

The treatments did not have any adverse impact on the activity level and mean body weight of the animals. Also, histopathological examination of the kidney, spleen, and liver tissues did not show any toxicity confirming the safety of the siRNA and the selected delivery system in the mouse model employed. These results points to the relative safety of the siRNA complexes following intravenous injection.

6.5 Conclusion

In this study, we demonstrated that the therapeutic efficacy of both PEO-*b*-P(CL-*g*-SP) and PEO-*b*-P(CL-*g*-SP-Chol) in nude mice bearing MDA-MB-435 xenograft showed significant improvements in silencing of MCL-1 mRNA and tumor volume inhibition after intratumoral administration. This trend was not observed following intravenous administration of the cholesterol modified and unmodified siRNA micellar complexes. Surface modification of polymeric micellar siRNA with RGD4C, however, resulted in

improved MCL-1 mRNA silencing activity of both micellar complexes in tumor xenografts after systemic administration. Our results also demonstrated the safety of PEO-*b*-P(CL-*g*-SP) based micelles for systemic siRNA administration. However, our results showed that cholesteryl substitution of PEO-*b*-P(CL-*g*-SP) did not improve the activity of polymeric micellar siRNA in nude mice bearing MDA-MB-435 xenograft in silencing of MCL-1 mRNA. Following MCL-1 silencing by around 30-40 % upon intratumoral injection of polymeric micellar MCL-1 siRNA, inhibition in tumor xenograft growth was observed up to 10 days, but the tumor resumed more rapid growth after this time point, despite MCL-1 silencing. The level of MCL-1 silencing in tumor seemed not to be sufficient to impose significant inhibition of tumor growth following intravenous administration of MCL-1 siRNA complexes, however. Even though the cholesteryl modification did not improve the activity of polymeric micellar siRNA *in vivo*, the results point to the potential of surface modification with RGD4C in improving the efficacy of these nanocarriers in siRNA delivery after systemic administration.

6.6 Acknowledgements

This study was supported by a grant from the Alberta Cancer Foundation (ACF) and the Canadian Institute of Health Research (CIHR). S.M.G. was supported by the Alberta Innovates Health Solutions (AIHS) Graduate Studentship, ACF Graduate Studentship and the J.N. Tata Trust Scholarship. We thank Mr. Dan McGinn, Department of Oncology, University of Alberta, for assistance with IV injections; Ms. Suellen Lamb, Department of Medical Microbiology and Immunology, University of Alberta, for assistance with tissue

processing and slide preparation for histopathological studies; and Dr. P.N. Nation, Animal Pathology Services (APS) Ltd., for assistance with histopathological analysis.

Chapter Seven
General Discussion, Conclusion, and Future Directions

7.1 General Discussion

Nanotechnology has shown immense promise in the field of cancer diagnosis and therapy. It has provided solutions to the problems of solubility, degradation, biocompatibility, toxicity, and bioavailability of various anti-cancer drugs. In this area, lipid-based nanocarriers like liposomes have shown great advancement with several formulations in clinical trials or in the market.⁴⁴⁶ However, liposomes lack the chemical flexibility in their structure making it difficult to develop versatile formulations for multiple therapeutic entities. Besides, liposomal carriers can show leakage of entrapped drug and instability during storage.⁴⁴⁷ Polymeric micelles, on the other hand, are showing increased attention due to their chemical flexibility which enables them to be optimized for the delivery of various therapeutic or diagnostic agents for cancer therapy. Our goal in this thesis was to take advantage of this chemical flexibility of polymeric micelles in developing chemotherapeutic, immunotherapeutic, and gene silencing strategies to fight cancer.

In the first two chapters of this thesis (Chapter 2 and 3) our goal was to modify the core of PEO-*b*-PCL block copolymers with pendant groups of different polarity and explore the effect of this structural modification on the thermodynamic and kinetic stability, degradation, biocompatibility, and immunogenicity of the generated polymeric micelles, as well as their passive accumulation in orthotopic breast tumors. To this end, we synthesized a series of diblock copolymers composed of PEO-*b*-PCL, PEO-*b*-PBCL (PCL containing pendent benzyl carboxylate), or PEO-*b*-PCCL (PCL containing pendent carboxyl). The degree of polymerization of the core-forming block was varied in all three structures (Chapter 2). An increase in the degree of polymerization of the core forming block is known to increase the thermodynamic and kinetic stability of polymeric micelles.⁵⁴ However,

attaching a pendant group was found to have a more profound effect in affecting the thermodynamic and kinetic stability of the micelles. For PEO-*b*-PBCL, the presence of benzyl group gave rise to π - π stacking interactions increasing the stability further, whereas the presence of hydrophilic carboxyl group in the case of PEO-*b*-PCCL decreased the thermodynamic and kinetic stability further (Table 2.1 and Figure 2.4).^{43, 54}

Since the *in vivo* fate of this modification was unknown, we developed traceable PEO-*b*-PCL and PEO-*b*-PBCL based nano-carriers through chemical conjugation of a near infrared dye (NIR) to their core-forming block for live imaging of nanocarriers in orthotopic breast tumor bearing animal models (Chapter 3). Conjugating the NIR probe to the micellar core can prevent the probe from releasing from the micellar system as might happen after physical encapsulation,¹⁰⁴ or from interacting with the proteins of the complement system as can be possible after conjugating to the hydrophilic shell.¹⁰⁵ PEO-*b*-PCL micelles showed higher accumulation in kidneys indicating faster renal clearance compared to their PEO-*b*-PBCL counterparts (Figure 3.11 and 3.12). Since glomerular filtration is highly size-selective and the PEO-*b*-PCL micelles had a size which is higher than the threshold for renal clearance,³⁵⁴ it is likely that the PEO-*b*-PCL micelles dissociated in the serum, owing to their lower thermodynamic and kinetic stability, leading to their faster clearance. PEO-*b*-PBCL micelles, on the other hand, showed higher uptake into the tumor (Figure 3.10). PEO-*b*-PBCL micelles also showed higher accumulation in the MPS organs such as liver and spleen when compared to PEO-*b*-PCL though (Figure 3.11 and 3.12).

We further modified the micellar surface with the breast cancer targeting peptide, P18-4. P18-4 is a stable derivative of p160 peptide which has shown exceptional proteolytic stability, and upto 3.5-fold higher uptake in breast cancer cell lines MDA-MB-231, MDA-

MB-435, and MCF-7.¹⁹² Modification with P18-4 maintained the thermodynamic stability of the micelles but decreased their kinetic stability. P18-4 modification of micelles resulted in an increase in tumor associated NIR signal particularly in early detection time points (Figure 3.10). This perhaps reflects a better accumulation of both PEO-*b*-PCL and PEO-*b*-PBCL at the tumor site following P18-4 surface modification. The observation can be attributed to enhanced interaction of peptide modified micellar carrier with cancer cells in tumor or their internalization, which will prevent the diffusion of the nanocarrier out of the tumor site at early time points.³⁵⁵ At later time points the tumor accumulation of plain and targeted nanocarriers became similar for both nanocarriers. This could reflect the saturation of receptors accessible to the nanocarrier at the tumor site or due to the decrease in kinetic stability of the nanocarrier after modification with P18-4.

In order to further increase the thermodynamic stability of the micelles, we aimed at crosslinking the core of PEO-*b*-PCL micelles via degradable crosslinks using click chemistry (Chapter 4). Crosslinking of the core and shell using click chemistry has been studied extensively,^{81, 88, 89, 177} however, the presence of degradable crosslinks in the PEO-*b*-PCL micellar core ensures their removal from the biological system upon degradation. Core crosslinked PEO-*b*-PCL micelles did not lose their micellar structure even after dissolving in acetone, indicating their improved thermodynamic stability (Figure 4.4).³⁹² Crosslinking however, did not slow down the release profile of both PTX (Figure 4.9) and JSI-124 (Appendix A). This was previously observed in the case of PTX after core-crosslinking.⁴⁶ Polymeric micellar formulations of JSI-124, based on PEO-*b*-PCL have been developed, however, they were unable to significantly sustain the release of JSI-124 *in vitro* under sink

condition (Appendix A).^{261, 301} This observation may imply the localization of JSI-124 in core/shell interface rather than the micellar core.

JSI-124 is a potent JAK-STAT3 inhibitor, and a member of the cucurbitacin family of compounds. It has been studied extensively for its direct anti-tumor activity and effects in enhancing anti-cancer immunity in several human and murine models.^{226, 227, 231, 249, 255-258} Constitutive activation of STAT3 has been implicated in cancer progression,^{397, 415} and immune evasion, whereby it can inhibit DC functional maturation and induce the activation of tolerogenic DCs.^{227-229, 231, 232} However, STAT3 activation is, also essential for regular function of several vital cells.⁴¹⁶⁻⁴¹⁹ Therefore, sustaining the premature release of JSI-124 for selective inhibition of STAT3 function in tumor and tumor microenvironment is important. With this in mind, our goal was to conjugate JSI-124 to the core of PEO-*b*-PCCL micelles through an ester linkage (Chapter 5). The ester linkage was expected to be cleaved in the acidic pH of the endosomal compartment after carrier internalization leading to drug release and activation.

Conjugation of JSI-124 to the micellar core slowed down the release considerably (Figure 5.2), pointing to the stability of ester linkage between COOH group on the polymer backbone and the drug. This observation is in line with previous findings on PTX conjugated PEO-*b*-PCCL.^{45, 55} As expected, conjugation of JSI-124 to PEO-*b*-PCCL decreased its STAT3 inhibitory activity against B16 melanoma cells (Figure 5.7). This was anticipated since the stability of the ester linkage between JSI-124 and the polymer backbone can lead to slow release of free drug from the conjugate in tumor cells. However, the activity of the polymer-JSI-124 conjugate in rescuing the tumor suppressed BMDCs to the favorable immune-active state was higher than the free drug in several *ex vivo* studies performed

(Figure 5.9 and 5.10). Even though the conjugate was less cytotoxic to BMDCs, which we thought might be because of the slow uptake of polymeric-JSI-124 micelles due to the protective effect of the PEG shell,^{307, 423} the polymeric-JSI-124 micelles were able to show improved STAT3 inhibitory activity in tumor-exposed BMDCs (Figure 5.8) and also upregulated the production of IL-2 and IFN- γ by CD4⁺ T-cells in the presence of TLR ligand when compared to free JSI-124 (Figure 5.10). Both, IFN- γ and IL-2, are cytokines produced by Th1 cells that play an important role in coordinating immune responses against cancer.^{414, 432} IFN- γ can regulate the anti-tumor activity of IL-12 and IL-2, whereas, IL-2 can play an important role in creating an effective immune response in patients suffering from metastatic melanoma.⁴¹² Hence, upregulation of both IL-2 and IFN- γ by CD4⁺ T-cells when treated with the polymer-JSI-124 micelles indicates the development of a Th1 immune response against cancer which is required for cancer rejection. The reason for improved activity of JSI-polymer conjugate versus free drug in tumor exposed and immune-suppressed BMDCs is not clear and might be related to difference in cell trafficking between free and conjugated drug in DCs.

In the last chapter (Chapter 6), our efforts were shifted toward development of lipid-based PEO-*b*-PCL nanocarriers for localized or systemic siRNA delivery. siRNA can be used to silence any specific gene, however advancement of this technology has been slow due to the difficulty in the safe and effective delivery of siRNA to cancer cells following systemic administration.⁴⁴² Previous approaches using either lipids or cationic polymers for siRNA delivery have been adopted. In this chapter, we have taken advantage of both, lipids and cationic polymers, to design cholesteryl-modified cationic nanocarriers of PEO-*b*-P(CL-*g*-SP) and explore their ability to silence MCL-1 gene following either local or systemic

administration. MCL-1 is an anti-apoptotic member of the Bcl-2 family of proteins,²⁶⁹ whose upregulation has found to play a role in cancer survival and is found to be over-expressed in a variety of cancers.^{266, 268, 272, 273} Down-regulation of MCL-1 has been found to induce apoptosis²⁶⁴ and can be a potential target in the treatment of a number of cancer cell types.

In previous studies, PEO-*b*-P(CL-*g*-SP) showed great promise in encapsulating siRNA, protecting it against degradation in serum, and silencing the expression of P-glycoprotein in human cancer cells leading to their sensitization to chemotherapeutics.¹³⁹ In further studies, RGD4C was used to modify the surface of PEO-*b*-P(CL-*g*-SP) micelles,^{102, 201} or separately, cholesterol was used to modify the SP group on the PCL backbone of PEO-*b*-P(CL-*g*-SP).²⁴⁷ RGD4C modification improved the accumulation of polymeric micelles in MDA-MB-435 tumor following systemic administration,^{102, 201} whereas cholesteryl modification led to improved delivery of MCL-1 siRNA into MDA-MB-435 cells translating into efficient down-regulation of MCL-1 mRNA and subsequent cell death *in vitro*.²⁴⁷ Seeing this, we investigated the effect of RGD4C modification in the shell and cholesteryl modification of SP groups in the PEO-*b*-P(CL-*g*-SP) core on MCL-1 siRNA delivery and silencing activity in *in vivo* cancer models. Cholesteryl modification did not improve the gene silencing or therapeutic activity of MCL-1 siRNA complexes in tumor xenografts when compared to PEO-*b*-P(CL-*g*-SP), however, both showed significant improvements in silencing of MCL-1 mRNA and tumor volume inhibition after intratumoral administration (Figure 6.1). RGD4C modification of the micellar shell did improve the silencing activity of the polymeric micellar siRNA delivery systems for both PEO-*b*-P(CL-*g*-SP-Chol) and PEO-*b*-P(CL-*g*-SP) which might be due to increased interaction with $\alpha_v\beta_3$ integrins over-expressed on MDA-MB-435 (Figure 6.2).⁴⁴³⁻⁴⁴⁵ However, this improved silencing activity

was not sufficient to cause significant inhibition of tumor growth which might be because higher MCL-1 silencing is required to see any measurable difference in inhibition of MDA-MB-435 tumor growth (Figure 6.2). This was surprising given the fact that, at a similar level of MCL-1 silencing upon intratumoral administration of MCL-1 siRNA complexes, significant inhibition of tumor had been observed (Figure 6.1). This may be attributed to the un-uniform distribution of the siRNA complexes within the tumor mass following iv administration. The siRNA complexes, however, did not show any signs of toxicity in kidney, liver, and spleen pointing to the relative safety of the siRNA complexes following intravenous injection (Figure 6.2).

7.2 Conclusion

The flexibility of the micelle forming platform based on PEO and modified PCL can be used to produce versatile excipients for targeted delivery of drugs or siRNA to the tumor site. The feasibility of this approach has been shown in this thesis. In this context, PEO-*b*-PCL block copolymers were modified in their core with pendant benzyl carboxylate (PEO-*b*-PBCL) or carboxyl (PEO-*b*-PCCL) groups. Incorporation of pendant benzyl carboxylate group (PEO-*b*-PBCL) enhanced the thermodynamic and kinetic stability of the micelles leading to increased passive tumor accumulation of these micelles in orthotopic breast tumors. Crosslinking of the core further enhanced the thermodynamic stability of these micelles, but failed to sustain the release of PTX and JSI-124. For this, JSI-124 was conjugated to the core of PEO-*b*-PCL based micelles which sustained the release of the drug. The polymer-JSI-124 conjugate maintained its STAT3 inhibitory activity against B16 melanoma cells and improved its activity in immune suppressed BMDCs and also improved

their function in initiating a Th1 immune response when compared to free JSI-124. In the case of MCL-1 siRNA delivery, cholesteryl modification of PEO-*b*-P(CL-*g*-SP) did not have any effect on MCL-1 silencing or tumor growth inhibition when compared to PEO-*b*-P(CL-*g*-SP) after local or systemic administration.

PEO-*b*-PCL based micelles were also modified on their shell with targeting peptides. Modification of the shell with P18-4 peptide resulted in a rapid accumulation of both PEO-*b*-PCL and PEO-*b*-PBCL micelles in orthotopic breast tumors after intravenous administration, whereas modification of PEO-*b*-P(CL-*g*-SP) and PEO-*b*-P(CL-*g*-SP-Chol) micellar shell with RGD4C peptide led to improved MCL-1 silencing in MDA-MB-435 tumors after systemic administration.

The potential use of these modifications is immense. Modification in the core/shell structure with hydrophobic or hydrophilic substitutions can be used to fine-tune the stability, biodistribution and uptake of the nanocarriers into tumors. At the same time, modifications with an NIR probe can be used as a system for investigating the biodistribution of other nanocarriers, with potential use as a diagnostic agent in the future for detection of tumors. Further modification of the core with a drug like JSI-124 has excellent potential in increasing the efficacy of cancer immunotherapy whereas cholesteryl modification can be used as a safe tool to study the silencing of various genes both *in vitro* and *in vivo*. Overall, the results of our studies point to the excellent chemical flexibility of these PEO-*b*-PCL based nanocarriers.

7.3 Future Studies

In this thesis, we explored the chemical flexibility of the core/shell of PEO-*b*-PCL based nanocarriers. Future development of these carriers may constitute several paths. Based on the improved passive tumor accumulation of PEO-*b*-PBCL micelles in primary breast tumors, we might think of selecting this nanocarrier for delivery of various drugs or drug combinations in addition to the NIR probe to primary breast tumors. The breast tumor growth inhibition will be tracked using bioluminescence. P18-4 modification would further be carried out to confirm if the rapid accumulation would lead to better tumor inhibition in primary tumor models. Another approach we are considering is to study the effect of the pendant benzyl carboxylate group on the passive tumor accumulation in metastatic breast tumor models using the NIR probe. A metastatic model for the luciferase expressing MDA-MB-231 cancer cells already exists in order to study this approach. Depending on the results of this study, we might think of selecting the appropriate nanocarrier for delivery of drugs or a combination of drugs in a metastatic breast cancer model. Finally, based on our current protocol of conjugating the NIR probe to the core of PEO-*b*-PBCL and PEO-*b*-PCL based micelles, we might use this approach in the future to conjugate the probe to other nanocarriers developed by our research group in order to study their biodistribution in various tumor models.

Looking at the success of the *in vitro* results of the polymer-JSI-124 conjugate in improving its STAT3 inhibitory activity, and function in initiating an immune response, in immune suppressed BMDCs; we are now thinking of seeing the direct anti-cancer activity and immune modulation of the polymer-JSI-124 conjugate in B16 melanoma s.c. xenografts after intratumoral injections *in vivo*. Our research group has previously shown an improved

immunomodulatory and anticancer effect for CPG and free JSI-124 in B16 melanoma mouse tumor model after intratumoral injection.²⁵⁵ A similar study comparing the polymer-JSI-124 conjugate with free JSI-124 would be the next logical step in this approach.

Since silencing of only MCL-1 was not completely effective in tumor growth inhibition, we might now look at considering other siRNA combinations along with MCL-1 using PEO-*b*-P(CL-*g*-SP) modified with RGD4C on the surface against MDA-MB-435 WT and resistant tumors. Previous studies have been carried out with PEI-lipid based polymeric nanocarriers for delivery of MCL-1 siRNA in combination with ribosomal protein S6 kinase siRNA, or with P-gp and survivin siRNA.^{271, 441} We might look at using PEO-*b*-P(CL-*g*-SP) nanocarriers modified with RGD4C for delivery of multiple siRNA combinations, or siRNA combinations with drugs like DOX to MDA-MB-435 WT and resistant tumors.

References

1. Xiong, X. B.; Falamarzian, A.; Garg, S. M.; Lavasanifar, A. Engineering of amphiphilic block copolymers for polymeric micellar drug and gene delivery. *J. Control. Release* 2011, 155, 248-61.
2. Farokhzad, O. C.; Langer, R. Impact of nanotechnology on drug delivery. *ACS Nano* 2009, 3, 16-20.
3. Shi, J.; Votruba, A. R.; Farokhzad, O. C.; Langer, R. Nanotechnology in drug delivery and tissue engineering: from discovery to applications. *Nano Lett* 2010, 10, 3223-30.
4. Balzani, V. Nanoscience and nanotechnology: a personal view of a chemist. *Small* 2005, 1, 278-83.
5. Park, K. Nanotechnology: What it can do for drug delivery. *Journal of controlled release : official journal of the Controlled Release Society* 2007, 120, 1-3.
6. Bangham, A. D.; Horne, R. W. Negative Staining of Phospholipids and Their Structural Modification by Surface-Active Agents as Observed in the Electron Microscope. *J Mol Biol* 1964, 8, 660-8.
7. Bangham, A. D.; Standish, M. M.; Watkins, J. C. Diffusion of univalent ions across the lamellae of swollen phospholipids. *J Mol Biol* 1965, 13, 238-52.
8. Langer, R.; Folkman, J. Polymers for the sustained release of proteins and other macromolecules. *Nature* 1976, 263, 797-800.
9. Yatvin, M. B.; Kreutz, W.; Horwitz, B. A.; Shinitzky, M. pH-sensitive liposomes: possible clinical implications. *Science* 1980, 210, 1253-5.
10. Leserman, L. D.; Barbet, J.; Kourilsky, F.; Weinstein, J. N. Targeting to cells of fluorescent liposomes covalently coupled with monoclonal antibody or protein A. *Nature* 1980, 288, 602-4.
11. Wicki, A.; Witzigmann, D.; Balasubramanian, V.; Huwyler, J. Nanomedicine in cancer therapy: challenges, opportunities, and clinical applications. *J Control Release* 2015, 200, 138-57.
12. Friberg, S.; Nystrom, A. M. Nanotechnology in the war against cancer: new arms against an old enemy - a clinical view. *Future Oncol* 2015, 11, 1961-75.
13. CANSIM Table 102-0561 - Leading causes of death, total population, by age group and sex, Canada, annual. Canada, S., Ed. 2011.
14. Gharpure, K. M.; Wu, S. Y.; Li, C.; Lopez-Berestein, G.; Sood, A. K. Nanotechnology: Future of Oncotherapy. *Clin Cancer Res* 2015, 21, 3121-30.
15. Palekar-Shanbhag, P.; Jog, S. V.; Chogale, M. M.; Gaikwad, S. S. Theranostics for cancer therapy. *Curr Drug Deliv* 2013, 10, 357-62.
16. Adams, M. L.; Lavasanifar, A.; Kwon, G. S. Amphiphilic block copolymers for drug delivery. *J. Pharm. Sci.* 2003, 92, 1343-55.
17. Mahmud, A.; Xiong, X. B.; Aliabadi, H. M.; Lavasanifar, A. Polymeric micelles for drug targeting. *J. Drug Target.* 2007, 15, 553-84.
18. Rapoport, N. Physical stimuli-responsive polymeric micelles for anti-cancer drug delivery. *Prog Polym Sci* 2007, 32, 962-990.

19. Aliabadi, H. M.; Lavasanifar, A. Polymeric micelles for drug delivery. *Expert Opin. Drug Deliv.* 2006, 3, 139-62.
20. Kataoka, K.; Kwon, G. S.; Yokoyama, M.; Okano, T.; Sakurai, Y. Block-Copolymer Micelles as Vehicles for Drug Delivery. *Journal of Controlled Release* 1993, 24, 119-132.
21. Kwon, G. K.; Forrest, M. L. Amphiphilic block copolymer micelles for nanoscale drug delivery. *Drug Development Research* 2006, 67, 15-22.
22. Sutton, D.; Nasongkla, N.; Blanco, E.; Gao, J. Functionalized micellar systems for cancer targeted drug delivery. *Pharm. Res.* 2007, 24, 1029-46.
23. Kim, S.; Shi, Y.; Kim, J. Y.; Park, K.; Cheng, J. X. Overcoming the barriers in micellar drug delivery: loading efficiency, in vivo stability, and micelle-cell interaction. *Expert Opin. Drug Deliv.* 2010, 7, 49-62.
24. Lu, Y.; Park, K. Polymeric micelles and alternative nanonized delivery vehicles for poorly soluble drugs. *Int J Pharm* 2013, 453, 198-214.
25. Cabral, H.; Kataoka, K. Progress of drug-loaded polymeric micelles into clinical studies. *Journal of Controlled Release* 2014, 190, 465-476.
26. Nippon Kayaku Co. Ltd. A Phase III Study of NK105 in Patients With Breast Cancer. In: ClinicalTrials.gov [Internet]. Bethesda (MD): National Library of Medicine (US). <https://clinicaltrials.gov/ct2/show/NCT01644890>.
27. Nippon Kayaku Co. Ltd. A Study of NK012 in Patients With Relapsed Small Cell Lung Cancer. In: ClinicalTrials.gov [Internet]. Bethesda (MD): National Library of Medicine (US). <https://clinicaltrials.gov/ct2/show/NCT00951613>.
28. Nippon Kayaku Co. Ltd. A Study of NK012 in Patients With Advanced, Metastatic Triple Negative Breast Cancer. In: ClinicalTrials.gov [Internet]. Bethesda (MD): National Library of Medicine (US). <https://clinicaltrials.gov/ct2/show/NCT00951054>.
29. Nanocarrier Co. Ltd. Combination Therapy With NC-6004 and Gemcitabine in Advanced Solid Tumors or Non-Small Cell Lung Cancer. In: ClinicalTrials.gov [Internet]. Bethesda (MD): National Library of Medicine (US). <https://clinicaltrials.gov/ct2/show/NCT02240238>.
30. Orient Europharma Co. Ltd. Combination Therapy With NC-6004 and Gemcitabine Versus Gemcitabine Alone in Pancreatic Cancer. In: ClinicalTrials.gov [Internet]. Bethesda (MD): National Library of Medicine (US). <https://clinicaltrials.gov/ct2/show/NCT02043288>.
31. Samyang Biopharmaceuticals Corporation. Evaluate the Efficacy and Safety of Genexol®-PM Compared to Genexol® in Recurrent or Metastatic Breast Cancer. In: ClinicalTrials.gov [Internet]. Bethesda (MD): National Library of Medicine (US). <https://clinicaltrials.gov/ct2/show/NCT00876486>.
32. Seoul National University Hospital. Efficacy Study of Genexol-PM and Cisplatin in Locally Advanced Head and Neck Cancer. In: ClinicalTrials.gov [Internet]. Bethesda (MD): National Library of Medicine (US). <https://clinicaltrials.gov/ct2/show/NCT01689194>.
33. M.D. Anderson Cancer Center. A Phase I Dose-Escalation and Pharmacokinetic Study of NC-4016 in Patients With Advanced Solid Tumors or Lymphoma. In: ClinicalTrials.gov [Internet]. Bethesda (MD): National Library of Medicine (US). <https://clinicaltrials.gov/ct2/show/NCT01999491>.
34. Chen, H.; Kim, S.; He, W.; Wang, H.; Low, P. S.; Park, K.; Cheng, J. X. Fast release of lipophilic agents from circulating PEG-PDLLA micelles revealed by in vivo forster resonance energy transfer imaging. *Langmuir* 2008, 24, 5213-7.

35. Savic, R.; Azzam, T.; Eisenberg, A.; Maysinger, D. Assessment of the integrity of poly(ϵ -caprolactone)-*b*-poly(ethylene oxide) micelles under biological conditions: a fluorogenic-based approach. *Langmuir* 2006, 22, 3570-8.
36. Muratov, A.; Baulin, V. A. Degradation versus Self-Assembly of Block Co-polymer Micelles. *Langmuir* 2012, 28, 3071-3076.
37. Adams, M. L.; Kwon, G. S. The effects of acyl chain length on the micelle properties of poly(ethylene oxide)-block-poly(N-hexyl-L-aspartamide)-acyl conjugates. *J Biomater Sci Polym Ed* 2002, 13, 991-1006.
38. Adams, M. L.; Kwon, G. S. Relative aggregation state and hemolytic activity of amphotericin B encapsulated by poly(ethylene oxide)-block-poly(N-hexyl-L-aspartamide)-acyl conjugate micelles: effects of acyl chain length. *J. Control. Release* 2003, 87, 23-32.
39. Iijima, M.; Nagasaki, Y.; Okada, T.; Kato, M.; Kataoka, K. Core-polymerized reactive micelles from heterotelechelic amphiphilic block copolymers. *Macromolecules* 1999, 32, 1140-1146.
40. Jiang, J. Q.; Qi, B.; Lepage, M.; Zhao, Y. Polymer micelles stabilization on demand through reversible photo-cross-linking. *Macromolecules* 2007, 40, 790-792.
41. Kim, S. H.; Tan, J. P.; Nederberg, F.; Fukushima, K.; Colson, J.; Yang, C.; Nelson, A.; Yang, Y. Y.; Hedrick, J. L. Hydrogen bonding-enhanced micelle assemblies for drug delivery. *Biomaterials* 2010, 31, 8063-71.
42. Lavasanifar, A.; Samuel, J.; Kwon, G. S. The effect of alkyl core structure on micellar properties of poly(ethylene oxide)-block-poly(L-aspartamide) derivatives. *Colloids Surf. B Biointerfaces* 2001, 22, 115-126.
43. Mahmud, A.; Xiong, X.; Lavasanifar, A. Novel Self-Associating Poly(ethylene oxide)-*block*-(ϵ -caprolactone) Block Copolymers with Functional Side Groups on the Polyester Block for Drug Delivery. *Macromolecules* 2006, 39, 9419-9428.
44. Masayuki, Y.; Kwon, G. S.; Teruo, O.; Yasuhisa, S.; Mayumi, N.; Kazunori, K. Influencing factors on in vitro micelle stability of adriamycin-block copolymer conjugates. *Journal of Controlled Release* 1994, 28, 59-65.
45. Shen, C.; Guo, S.; Lu, C. Degradation behaviors of monomethoxy poly(ethylene glycol)-*b*-poly(ϵ -caprolactone) nanoparticles in aqueous solution. *Polym Advan Technol* 2008, 19, 66-72.
46. Shuai, X. T.; Merdan, T.; Schaper, A. K.; Xi, F.; Kissel, T. Core-cross-linked polymeric micelles as paclitaxel carriers. *Bioconjugate Chem* 2004, 15, 441-448.
47. Yang, L.; El Ghzaoui, A.; Li, S. In vitro degradation behavior of poly(lactide)-poly(ethylene glycol) block copolymer micelles in aqueous solution. *Int. J. Pharm.* 2010, 400, 96-103.
48. Van Domeselaar, G. H.; Kwon, G. S.; Andrew, L. C.; Wishart, D. S. Application of solid phase peptide synthesis to engineering PEO-peptide block copolymers for drug delivery. *Colloids and Surfaces B: Biointerfaces* 2003, 30, 323-334.
49. Kabanov, A. V.; Lemieux, P.; Vinogradov, S.; Alakhov, V. Pluronic block copolymers: novel functional molecules for gene therapy. *Adv Drug Deliv Rev* 2002, 54, 223-33.
50. Kabanov, A. V.; Batrakova, E. V.; Alakhov, V. Y. Pluronic block copolymers as novel polymer therapeutics for drug and gene delivery. *J Control Release* 2002, 82, 189-212.

51. Kim, S. Y.; Ha, J. C.; Lee, Y. M. Poly(ethylene oxide)-poly(propylene oxide)-poly(ethylene oxide)/poly(epsilon-caprolactone) (PCL) amphiphilic block copolymeric nanospheres. II. Thermo-responsive drug release behaviors. *J Control Release* 2000, 65, 345-58.
52. Ha, J. C.; Kim, S. Y.; Lee, Y. M. Poly(ethylene oxide)-poly(propylene oxide)-poly(ethylene oxide) (Pluronic)/poly(epsilon-caprolactone) (PCL) amphiphilic block copolymeric nanospheres. I. Preparation and characterization. *J Control Release* 1999, 62, 381-92.
53. Cho, H. K.; Cho, K. S.; Cho, J. H.; Choi, S. W.; Kim, J. H.; Cheong, I. W. Synthesis and characterization of PEO-PCL-PEO triblock copolymers: Effects of the PCL chain length on the physical property of W1/O/W2 multiple emulsions. *Colloids and Surfaces B: Biointerfaces* 2008, 65, 61-68.
54. Owen, S. C.; Chan, D. P. Y.; Shoichet, M. S. Polymeric micelle stability. *Nano Today* 2012, 7, 53-65.
55. Hu, Y.; Zhang, L.; Cao, Y.; Ge, H.; Jiang, X.; Yang, C. Degradation behavior of poly(epsilon-caprolactone)-b-poly(ethylene glycol)-b-poly(epsilon-caprolactone) micelles in aqueous solution. *Biomacromolecules* 2004, 5, 1756-62.
56. Hu, Y.; Jiang, Z.; Chen, R.; Wu, W.; Jiang, X. Degradation and degradation-induced re-assembly of PVP-PCL micelles. *Biomacromolecules* 2010, 11, 481-8.
57. Carstens, M. G.; van Nostrum, C. F.; Verrijck, R.; de Leede, L. G.; Crommelin, D. J.; Hennink, W. E. A mechanistic study on the chemical and enzymatic degradation of PEG-Oligo(epsilon-caprolactone) micelles. *J. Pharm. Sci.* 2008, 97, 506-18.
58. Salaam, L. E.; Dean, D.; Bray, T. L. In vitro degradation behavior of biodegradable 4-star micelles. *Polymer* 2006, 47, 310-318.
59. Li, S. M.; Chen, X. H.; Gross, R. A.; McCarthy, S. P. Hydrolytic degradation of PCL/PEO copolymers in alkaline media. *J. Mater. Sci. Mater. Med.* 2000, 11, 227-33.
60. Li, S.; Garreau, H.; Pauvert, B.; McGrath, J.; Toniolo, A.; Vert, M. Enzymatic degradation of block copolymers prepared from epsilon-caprolactone and poly(ethylene glycol). *Biomacromolecules* 2002, 3, 525-30.
61. Venkatraman, S. S.; Jie, P.; Min, F.; Freddy, B. Y.; Leong-Huat, G. Micelle-like nanoparticles of PLA-PEG-PLA triblock copolymer as chemotherapeutic carrier. *Int J Pharm* 2005, 298, 219-32.
62. Han, D.; Tong, X.; Zhao, Y. Fast Photodegradable Block Copolymer Micelles for Burst Release. *Macromolecules* 2011, 44, 437-439.
63. Han, D.; Tong, X.; Zhao, Y. Block copolymer micelles with a dual-stimuli-responsive core for fast or slow degradation. *Langmuir* 2012, 28, 2327-31.
64. Diezi, T. A.; Bae, Y.; Kwon, G. S. Enhanced stability of PEG-block-poly(N-hexyl stearate l-aspartamide) micelles in the presence of serum proteins. *Mol. Pharm.* 2010, 7, 1355-60.
65. Gao, Z.; Lukyanov, A. N.; Singhal, A.; Torchilin, V. P. Diacyllipid-Polymer Micelles as Nanocarriers for Poorly Soluble Anticancer Drugs. *Nano Letters* 2002, 2, 979-982.
66. Vladimir, P. T. Tumor-Targeted Delivery of Sparingly-Soluble Anti-Cancer Drugs with Polymeric Lipid-Core Immunomicelles. In *Nanotechnology for Cancer Therapy*, CRC Press: 2006; pp 409-420.

67. Lukyanov, A. N.; Gao, Z.; Mazzola, L.; Torchilin, V. P. Polyethylene glycol-diacyl lipid micelles demonstrate increased accumulation in subcutaneous tumors in mice. *Pharm Res* 2002, 19, 1424-9.
68. Harada, A.; Kataoka, K. Formation of Polyion Complex Micelles in an Aqueous Milieu from a Pair of Oppositely-Charged Block Copolymers with Poly(ethylene glycol) Segments. *Macromolecules* 1995, 28, 5294-5299.
69. Kabanov, A. V.; Bronich, T. K.; Kabanov, V. A.; Yu, K.; Eisenberg, A. Soluble Stoichiometric Complexes from Poly(N-ethyl-4-vinylpyridinium) Cations and Poly(ethylene oxide)-block-polymethacrylate Anions. *Macromolecules* 1996, 29, 6797-6802.
70. Gohy, J.-F.; Varshney, S. K.; Antoun, S.; Jérôme, R. Water-Soluble Complexes Formed by Sodium Poly(4-styrenesulfonate) and a Poly(2-vinylpyridinium)-block-poly(ethyleneoxide) Copolymer. *Macromolecules* 2000, 33, 9298-9305.
71. Rosler, A.; Vandermeulen, G. W. M.; Klok, H. A. Advanced drug delivery devices via self-assembly of amphiphilic block copolymers. *Adv Drug Deliver Rev* 2001, 53, 95-108.
72. Kim, J. H.; Emoto, K.; Iijima, M.; Nagasaki, Y.; Aoyagi, T.; Okano, T.; Sakurai, Y.; Kataoka, K. Core-stabilized polymeric micelle as potential drug carrier: Increased solubilization of taxol. *Polym Advan Technol* 1999, 10, 647-654.
73. Lee, B. H.; West, B.; McLemore, R.; Pauken, C.; Vernon, B. L. In-situ injectable physically and chemically gelling NIPAAm-based copolymer system for embolization. *Biomacromolecules* 2006, 7, 2059-2064.
74. Tao, J.; Liu, G. J. Polystyrene-block-poly(2-cinnamoyl ethyl methacrylate) tadpole molecules. *Macromolecules* 1997, 30, 2408-2411.
75. Tao, J.; Liu, G. J.; Ding, J. F.; Yang, M. L. Cross-linked nanospheres of poly(2-cinnamoyl ethyl methacrylate) with immediately attached surface functional groups. *Macromolecules* 1997, 30, 4084-4089.
76. Procházka, K.; Baloch, M. K.; Tuzar, Z. Photochemical stabilization of block copolymer micelles. *Die Makromolekulare Chemie* 1979, 180, 2521-2523.
77. Tuzar, Z.; Bedná, B.; Koák, e.; Kubín, M.; Svobodová, t.; Procházka, K. Stabilization of block copolymer micelles by UV and fast electron radiation. *Die Makromolekulare Chemie* 1982, 183, 399-408.
78. Guo, A.; Liu, G.; Tao, J. Star polymers and nanospheres from cross-linkable diblock copolymers. *Macromolecules* 1996, 29, 2487-2493.
79. Henselwood, F.; Liu, G. Water-soluble nanospheres of poly(2-cinnamoyl ethyl methacrylate)-block-poly(acrylic acid). *Macromolecules* 1997, 30, 488-493.
80. Hoppenbrouwers, E.; Li, Z.; Liu, G. Triblock nanospheres with amphiphilic coronal chains. *Macromolecules* 2003, 36, 876-881.
81. Joralemon, M. J.; O'Reilly, R. K.; Hawker, C. J.; Wooley, K. L. Shell Click-crosslinked (SCC) nanoparticles: A new methodology for synthesis and orthogonal functionalization. *J Am Chem Soc* 2005, 127, 16892-16899.
82. Kolb, H. C.; Finn, M. G.; Sharpless, K. B. Click chemistry: Diverse chemical function from a few good reactions. *Angew Chem Int Edit* 2001, 40, 2004-+.
83. van Dijk, M.; Rijkers, D. T. S.; Liskamp, R. M. J.; van Nostrum, C. F.; Hennink, W. E. Synthesis and Applications of Biomedical and Pharmaceutical Polymers via Click Chemistry Methodologies. *Bioconjugate Chem* 2009, 20, 2001-2016.

84. Lecomte, P.; Riva, R.; Jerome, C. Synthesis of Functionalized Aliphatic Polyesters by the "Click" Copper-Catalyzed Alkyne—Azide Cycloaddition. In *New Smart Materials via Metal Mediated Macromolecular Engineering*, Khosravi, E.; Yagci, Y.; Savelyev, Y., Eds. Springer: Dordrecht, 2009; pp 77-91.
85. Brockway, L. O.; Pauling, L. The Electron-Diffraction Investigation of the Structure of Molecules of Methyl Azide and Carbon Suboxide. *Proceedings of the National Academy of Sciences* 1933, 19, 860-867.
86. Rostovtsev, V. V.; Green, L. G.; Fokin, V. V.; Sharpless, K. B. A stepwise huisgen cycloaddition process: copper(I)-catalyzed regioselective "ligation" of azides and terminal alkynes. *Angew. Chem. Int. Ed. Engl.* 2002, 41, 2596-9.
87. Tornøe, C. W.; Christensen, C.; Meldal, M. Peptidotriazoles on solid phase: [1,2,3]-triazoles by regiospecific copper(I)-catalyzed 1,3-dipolar cycloadditions of terminal alkynes to azides. *Journal of Organic Chemistry* 2002, 67, 3057-64.
88. Jiang, X. Z.; Zhang, J. Y.; Zhou, Y. M.; Xu, J.; Liu, S. Y. Facile preparation of core-crosslinked micelles from azide-containing thermoresponsive double hydrophilic diblock copolymer via click chemistry. *J Polym Sci Pol Chem* 2008, 46, 860-871.
89. O'Reilly, R. K.; Joralemon, M. J.; Hawker, C. J.; Wooley, K. L. Preparation of orthogonally-functionalized core Click cross-linked nanoparticles. *New J Chem* 2007, 31, 718-724.
90. He, J.; Tong, X.; Zhao, Y. Photoresponsive nanogels based on photocontrollable cross-links. *Macromolecules* 2009, 42, 4845-4852.
91. Jin, Q.; Liu, X.; Liu, G.; Ji, J. Fabrication of core or shell reversibly photo cross-linked micelles and nanogels from double responsive water-soluble block copolymers. *Polymer* 2010, 51, 1311-1319.
92. Kakizawa, Y.; Harada, A.; Kataoka, K. Environment-sensitive stabilization of core-shell structured polyion complex micelle by reversible cross-linking of the core through disulfide bond [13]. *J Am Chem Soc* 1999, 121, 11247-11248.
93. Heffernan, M. J.; Murthy, N. Disulfide-crosslinked polyion micelles for delivery of protein therapeutics. *Ann. Biomed. Eng.* 2009, 37, 1993-2002.
94. Torchilin, V. P. PEG-based micelles as carriers of contrast agents for different imaging modalities. *Adv Drug Deliv Rev* 2002, 54, 235-52.
95. Torchilin, V. P.; Frank-Kamenetsky, M. D.; Wolf, G. L. CT visualization of blood pool in rats by using long-circulating, iodine-containing micelles. *Acad Radiol* 1999, 6, 61-5.
96. Ai, H.; Flask, C.; Weinberg, B.; Shuai, X. T.; Pagel, M. D.; Farrell, D.; Duerk, J.; Gao, J. Magnetite-Loaded Polymeric Micelles as Ultrasensitive Magnetic-Resonance Probes. *Advanced Materials* 2005, 17, 1949-1952.
97. Nakamura, E.; Makino, K.; Okano, T.; Yamamoto, T.; Yokoyama, M. A polymeric micelle MRI contrast agent with changeable relaxivity. *J Control Release* 2006, 114, 325-33.
98. Hoang, B.; Lee, H.; Reilly, R. M.; Allen, C. Noninvasive monitoring of the fate of ¹¹¹In-labeled block copolymer micelles by high resolution and high sensitivity microSPECT/CT imaging. *Mol Pharm* 2009, 6, 581-92.
99. Yang, Z.; Zheng, S.; Harrison, W. J.; Harder, J.; Wen, X.; Gelovani, J. G.; Qiao, A.; Li, C. Long-circulating near-infrared fluorescence core-cross-linked polymeric micelles: synthesis, characterization, and dual nuclear/optical imaging. *Biomacromolecules* 2007, 8, 3422-8.

100. Matson, J. B.; Grubbs, R. H. Synthesis of fluorine-18 functionalized nanoparticles for use as in vivo molecular imaging agents. *J Am Chem Soc* 2008, 130, 6731-3.
101. Radoslav, S.; Jinzi, Z.; Christine, A.; Dusica, M. Nanomedicines Coming of Age. In *Polymeric Biomaterials*, CRC Press: 2013; pp 337-368.
102. Xiong, X. B.; Lavasanifar, A. Traceable multifunctional micellar nanocarriers for cancer-targeted co-delivery of MDR-1 siRNA and doxorubicin. *ACS Nano* 2011, 5, 5202-13.
103. Blanco, E.; Kessinger, C. W.; Sumer, B. D.; Gao, J. Multifunctional micellar nanomedicine for cancer therapy. *Exp Biol Med (Maywood)* 2009, 234, 123-31.
104. Rodriguez, V. B.; Henry, S. M.; Hoffman, A. S.; Stayton, P. S.; Li, X.; Pun, S. H. Encapsulation and stabilization of indocyanine green within poly(styrene-alt-maleic anhydride) block-poly(styrene) micelles for near-infrared imaging. *J Biomed Opt* 2008, 13, 014025.
105. Tsai, H. C.; Chang, W. H.; Lo, C. L.; Tsai, C. H.; Chang, C. H.; Ou, T. W.; Yen, T. C.; Hsiue, G. H. Graft and diblock copolymer multifunctional micelles for cancer chemotherapy and imaging. *Biomaterials* 2010, 31, 2293-301.
106. Zhu, X.; Anquillare, E. L. B.; Farokhzad, O. C.; Shi, J. Chapter 22 - Polymer- and Protein-Based Nanotechnologies for Cancer Theranostics. In *Cancer Theranostics*, Chen, X.; Wong, S., Eds. Academic Press: Oxford, 2014; pp 419-436.
107. Cho, H.; Cho, C. S.; Indig, G. L.; Lavasanifar, A.; Vakili, M. R.; Kwon, G. S. Polymeric micelles for apoptosis-targeted optical imaging of cancer and intraoperative surgical guidance. *PLoS One* 2014, 9, e89968.
108. Xiong, C.; Brewer, K.; Song, S.; Zhang, R.; Lu, W.; Wen, X.; Li, C. Peptide-based imaging agents targeting phosphatidylserine for the detection of apoptosis. *J Med Chem* 2011, 54, 1825-35.
109. Kim, D.; Lee, E. S.; Park, K.; Kwon, I. C.; Bae, Y. H. Doxorubicin loaded pH-sensitive micelle: antitumoral efficacy against ovarian A2780/DOXR tumor. *Pharm Res* 2008, 25, 2074-82.
110. Lavasanifar, A.; Samuel, J.; Kwon, G. S. The effect of fatty acid substitution on the in vitro release of amphotericin B from micelles composed of poly(ethylene oxide)-block-poly(N-hexyl stearate-L-aspartamide). *J Control Release* 2002, 79, 165-72.
111. Shahin, M.; Lavasanifar, A. Novel self-associating poly(ethylene oxide)-b-poly(epsilon-caprolactone) based drug conjugates and nano-containers for paclitaxel delivery. *Int. J. Pharm.* 2010, 389, 213-22.
112. Tang, Y.; Liu, S. Y.; Armes, S. P.; Billingham, N. C. Solubilization and controlled release of a hydrophobic drug using novel micelle-forming ABC triblock copolymers. *Biomacromolecules* 2003, 4, 1636-45.
113. Lee, E. S.; Shin, H. J.; Na, K.; Bae, Y. H. Poly(L-histidine)-PEG block copolymer micelles and pH-induced destabilization. *J Control Release* 2003, 90, 363-74.
114. Gillies, E. R.; Jonsson, T. B.; Frechet, J. M. Stimuli-responsive supramolecular assemblies of linear-dendritic copolymers. *J Am Chem Soc* 2004, 126, 11936-43.
115. Bromberg, L. Scaling of Rheological Properties of Hydrogels from Associating Polymers. *Macromolecules* 1998, 31, 6148-6156.
116. Schmolka, I. R. Artificial skin. I. Preparation and properties of pluronic F-127 gels for treatment of burns. *J Biomed Mater Res* 1972, 6, 571-82.

117. Hirano, T.; Klesse, W.; Ringsdorf, H. Polymeric derivatives of activated cyclophosphamide as drug delivery systems in antitumor chemotherapy. Pharmacologically active polymers, 20. *Die Makromolekulare Chemie* 1979, 180, 1125-1131.
118. Hu, X.; Jing, X. Biodegradable amphiphilic polymer-drug conjugate micelles. *Expert Opin Drug Deliv* 2009, 6, 1079-90.
119. Kwon, G.; Suwa, S.; Yokoyama, M.; Okano, T.; Sakurai, Y.; Kataoka, K. Enhanced tumor accumulation and prolonged circulation times of micelle-forming poly (ethylene oxide-aspartate) block copolymer-adriamycin conjugates. *Journal of Controlled Release* 1994, 29, 17-23.
120. Li, Y.; Kwon, G. S. Methotrexate esters of poly(ethylene oxide)-block-poly(2-hydroxyethyl-L-aspartamide). Part I: Effects of the level of methotrexate conjugation on the stability of micelles and on drug release. *Pharm Res* 2000, 17, 607-11.
121. Mahmud, A.; Xiong, X. B.; Lavasanifar, A. Development of novel polymeric micellar drug conjugates and nano-containers with hydrolyzable core structure for doxorubicin delivery. *European Journal of Pharmaceutics and Biopharmaceutics* 2008, 69, 923-934.
122. Yoo, H. S.; Park, T. G. Biodegradable polymeric micelles composed of doxorubicin conjugated PLGA-PEG block copolymer. *J. Control. Release* 2001, 70, 63-70.
123. Gillies, E. R.; Frechet, J. M. A new approach towards acid sensitive copolymer micelles for drug delivery. *Chem Commun (Camb)* 2003, 1640-1.
124. Yoo, H. S.; Lee, E. A.; Park, T. G. Doxorubicin-conjugated biodegradable polymeric micelles having acid-cleavable linkages. *J Control Release* 2002, 82, 17-27.
125. Bae, Y.; Fukushima, S.; Harada, A.; Kataoka, K. Design of Environment-Sensitive Supramolecular Assemblies for Intracellular Drug Delivery: Polymeric Micelles that are Responsive to Intracellular pH Change. *Angewandte Chemie International Edition* 2003, 42, 4640-4643.
126. Ponta, A.; Bae, Y. PEG-poly(amino acid) block copolymer micelles for tunable drug release. *Pharm Res* 2010, 27, 2330-42.
127. Alani, A. W.; Bae, Y.; Rao, D. A.; Kwon, G. S. Polymeric micelles for the pH-dependent controlled, continuous low dose release of paclitaxel. *Biomaterials* 2010, 31, 1765-72.
128. Harada, A.; Togawa, H.; Kataoka, K. Physicochemical properties and nuclease resistance of antisense-oligodeoxynucleotides entrapped in the core of polyion complex micelles composed of poly(ethylene glycol)-poly(L-lysine) block copolymers. *Eur J Pharm Sci* 2001, 13, 35-42.
129. Kakizawa, Y.; Harada, A.; Kataoka, K. Glutathione-sensitive stabilization of block copolymer micelles composed of antisense DNA and thiolated poly(ethylene glycol)-block-poly(L-lysine): a potential carrier for systemic delivery of antisense DNA. *Biomacromolecules* 2001, 2, 491-7.
130. Miyata, K.; Kakizawa, Y.; Nishiyama, N.; Harada, A.; Yamasaki, Y.; Koyama, H.; Kataoka, K. Block cationic polyplexes with regulated densities of charge and disulfide cross-linking directed to enhance gene expression. *J Am Chem Soc* 2004, 126, 2355-61.
131. Meister, A.; Anderson, M. E. Glutathione. *Annu Rev Biochem* 1983, 52, 711-60.

132. Terpstra, M.; Henry, P. G.; Gruetter, R. Measurement of reduced glutathione (GSH) in human brain using LCModel analysis of difference-edited spectra. *Magn Reson Med* 2003, 50, 19-23.
133. Richie, J. P., Jr.; Skowronski, L.; Abraham, P.; Leutzinger, Y. Blood glutathione concentrations in a large-scale human study. *Clin Chem* 1996, 42, 64-70.
134. Behr, J.-P. The Proton Sponge: a Trick to Enter Cells the Viruses Did Not Exploit. *CHIMIA International Journal for Chemistry* 1997, 51, 34-36.
135. Boussif, O.; Lezoualc'h, F.; Zanta, M. A.; Mergny, M. D.; Scherman, D.; Demeneix, B.; Behr, J. P. A versatile vector for gene and oligonucleotide transfer into cells in culture and in vivo: polyethylenimine. *Proc Natl Acad Sci U S A* 1995, 92, 7297-301.
136. Itaka, K.; Kanayama, N.; Nishiyama, N.; Jang, W.-D.; Yamasaki, Y.; Nakamura, K.; Kawaguchi, H.; Kataoka, K. Supramolecular Nanocarrier of siRNA from PEG-Based Block Cationic Carrying Diamine Side Chain with Distinctive pKa Directed To Enhance Intracellular Gene Silencing. *J Am Chem Soc* 2004, 126, 13612-13613.
137. Kanayama, N.; Fukushima, S.; Nishiyama, N.; Itaka, K.; Jang, W. D.; Miyata, K.; Yamasaki, Y.; Chung, U. I.; Kataoka, K. A PEG-based biocompatible block cationic with high buffering capacity for the construction of polyplex micelles showing efficient gene transfer toward primary cells. *ChemMedChem* 2006, 1, 439-44.
138. La, S. B.; Okano, T.; Kataoka, K. Preparation and characterization of the micelle-forming polymeric drug indomethacin-incorporated poly(ethylene oxide)-poly(beta-benzyl L-aspartate) block copolymer micelles. *J Pharm Sci* 1996, 85, 85-90.
139. Xiong, X. B.; Uludağ, H.; Lavasanifar, A. Biodegradable amphiphilic poly(ethylene oxide)-block-polyesters with grafted polyamines as supramolecular nanocarriers for efficient siRNA delivery. *Biomaterials* 2009, 30, 242-253.
140. Kabanov, A.; Zhu, J.; Alakhov, V. Pluronic block copolymers for gene delivery. *Adv Genet* 2005, 53, 231-61.
141. Vinogradov, S.; Batrakova, E.; Li, S.; Kabanov, A. Polyion complex micelles with protein-modified corona for receptor-mediated delivery of oligonucleotides into cells. *Bioconjug Chem* 1999, 10, 851-60.
142. Basu, M. K.; Lala, S. Nanoparticulate Drug Delivery to the Reticuloendothelial System and to Associated Disorders. In *Nanoparticulates as Drug Carriers*, Torchilin, V. P., Ed. Imperial College Press: London, 2006; pp 463-480.
143. Kaminskis, L. M.; Boyd, B. J. *Nanosized Drug Delivery Vectors and the Reticuloendothelial System*. Springer: New York, 2011; p 867.
144. Kim, H. R.; Andrieux, K.; Delomenie, C.; Chacun, H.; Appel, M.; Desmaele, D.; Taran, F.; Georgin, D.; Couvreur, P.; Taverna, M. Analysis of plasma protein adsorption onto PEGylated nanoparticles by complementary methods: 2-DE, CE and Protein Lab-on-chip system. *Electrophoresis* 2007, 28, 2252-61.
145. Lu, J.; Owen, S. C.; Shoichet, M. S. Stability of Self-Assembled Polymeric Micelles in Serum. *Macromolecules* 2011, 44, 6002-6008.
146. Chaudhari, K. R.; Ukawala, M.; Manjappa, A. S.; Kumar, A.; Mundada, P. K.; Mishra, A. K.; Mathur, R.; Monkkonen, J.; Murthy, R. S. Opsonization, biodistribution, cellular uptake and apoptosis study of PEGylated PBCA nanoparticle as potential drug delivery carrier. *Pharm. Res.* 2012, 29, 53-68.

147. Gessner, A.; Lieske, A.; Paulke, B.; Muller, R. Influence of surface charge density on protein adsorption on polymeric nanoparticles: analysis by two-dimensional electrophoresis. *Eur. J. Pharm. Biopharm.* 2002, 54, 165-70.
148. Liu, J.; Zeng, F.; Allen, C. Influence of serum protein on polycarbonate-based copolymer micelles as a delivery system for a hydrophobic anti-cancer agent. *J. Control. Release* 2005, 103, 481-97.
149. Takeuchi, H.; Kojima, H.; Yamamoto, H.; Kawashima, Y. Polymer coating of liposomes with a modified polyvinyl alcohol and their systemic circulation and RES uptake in rats. *J. Control. Release* 2000, 68, 195-205.
150. Guo, S.; Huang, L. Nanoparticles Escaping RES and Endosome: Challenges for siRNA Delivery for Cancer Therapy. *Journal of Nanomaterials* 2011, 2011.
151. Muller, R. H.; Maassen, S.; Weyhers, H.; Mehnert, W. Phagocytic uptake and cytotoxicity of solid lipid nanoparticles (SLN) sterically stabilized with poloxamine 908 and poloxamer 407. *J. Drug Target.* 1996, 4, 161-70.
152. Lacava, L. M.; Lacava, Z. G.; Da Silva, M. F.; Silva, O.; Chaves, S. B.; Azevedo, R. B.; Pelegrini, F.; Gansau, C.; Buske, N.; Sabolovic, D.; Morais, P. C. Magnetic resonance of a dextran-coated magnetic fluid intravenously administered in mice. *Biophys. J.* 2001, 80, 2483-6.
153. Bonfá, A.; Saito, R. S. N.; França, R. F. O.; Fonseca, B. A. L.; Petri, D. F. S. Poly(ethylene glycol) decorated poly(methylmethacrylate) nanoparticles for protein adsorption. *Materials Science and Engineering: C* 2011, 31, 562-566.
154. Unsworth, L. D.; Sheardown, H.; Brash, J. L. Protein Resistance of Surfaces Prepared by Sorption of End-Thiolated Poly(ethylene glycol) to Gold: Effect of Surface Chain Density. *Langmuir* 2005, 21, 1036-1041.
155. Fukai, R.; Dakwa, P. H. R.; Chen, W. Strategies toward biocompatible artificial implants: Grafting of functionalized poly(ethylene glycol)s to poly(ethylene terephthalate) surfaces. *Journal of Polymer Science Part A: Polymer Chemistry* 2004, 42, 5389-5400.
156. Gref, R.; Luck, M.; Quellec, P.; Marchand, M.; Dellacherie, E.; Harnisch, S.; Blunk, T.; Muller, R. H. 'Stealth' corona-core nanoparticles surface modified by polyethylene glycol (PEG): influences of the corona (PEG chain length and surface density) and of the core composition on phagocytic uptake and plasma protein adsorption. *Colloids Surf. B Biointerfaces* 2000, 18, 301-313.
157. Leroux, J.-C.; Gravel, P.; Balant, L.; Volet, B.; Anner, B. M.; Allémann, E.; Doelker, E.; Gurny, R. Internalization of poly(D,L-lactic acid) nanoparticles by isolated human leukocytes and analysis of plasma proteins adsorbed onto the particles. *Journal of Biomedical Materials Research* 1994, 28, 471-481.
158. Price, M. E.; Cornelius, R. M.; Brash, J. L. Protein adsorption to polyethylene glycol modified liposomes from fibrinogen solution and from plasma. *Biochim. Biophys. Acta* 2001, 1512, 191-205.
159. Allen, C.; Dos Santos, N.; Gallagher, R.; Chiu, G. N.; Shu, Y.; Li, W. M.; Johnstone, S. A.; Janoff, A. S.; Mayer, L. D.; Webb, M. S.; Bally, M. B. Controlling the physical behavior and biological performance of liposome formulations through use of surface grafted poly(ethylene glycol). *Biosci. Rep.* 2002, 22, 225-50.

160. Lo, C. L.; Huang, C. K.; Lin, K. M.; Hsiue, G. H. Mixed micelles formed from graft and diblock copolymers for application in intracellular drug delivery. *Biomaterials* 2007, 28, 1225-35.
161. Li, Y.; Pan, S.; Zhang, W.; Du, Z. Novel thermo-sensitive core-shell nanoparticles for targeted paclitaxel delivery. *Nanotechnology* 2009, 20, 065104.
162. Yang, C.; Tan, J. P. K.; Cheng, W.; Attia, A. B. E.; Ting, C. T. Y.; Nelson, A.; Hedrick, J. L.; Yang, Y. Y. Supramolecular nanostructures designed for high cargo loading capacity and kinetic stability. *Nano Today* 2010, 5, 515-523.
163. Kabanov, A. V.; Nazarova, I. R.; Astafieva, I. V.; Batrakova, E. V.; Alakhov, V. Y.; Yaroslavov, A. A.; Kabanov, V. A. Micelle Formation and Solubilization of Fluorescent Probes in Poly(oxyethylene-b-oxypropylene-b-oxyethylene) Solutions. *Macromolecules* 1995, 28, 2303-2314.
164. Cedervall, T.; Lynch, I.; Lindman, S.; Berggård, T.; Thulin, E.; Nilsson, H.; Dawson, K. A.; Linse, S. Understanding the nanoparticle-protein corona using methods to quantify exchange rates and affinities of proteins for nanoparticles. *Proceedings of the National Academy of Sciences* 2007, 104, 2050-2055.
165. Lynch, I.; Cedervall, T.; Lundqvist, M.; Cabaleiro-Lago, C.; Linse, S.; Dawson, K. A. The nanoparticle-protein complex as a biological entity; a complex fluids and surface science challenge for the 21st century. *Advances in Colloid and Interface Science* 2007, 134-135, 167-174.
166. Thurmond, K. B.; Kowalewski, T.; Wooley, K. L. Water-soluble knedel-like structures: The preparation of shell-cross-linked small particles. *J Am Chem Soc* 1996, 118, 7239-7240.
167. Huang, H. Y.; Kowalewski, T.; Remsen, E. E.; Gertzmann, R.; Wooley, K. L. Hydrogel-coated glassy nanospheres: A novel method for the synthesis of shell cross-linked knedels. *J Am Chem Soc* 1997, 119, 11653-11659.
168. Huang, H. Y.; Remsen, E. E.; Wooley, K. L. Amphiphilic core-shell nanospheres obtained by intramicellar shell crosslinking of polymer micelles with poly(ethylene oxide) linkers. *Chem Commun* 1998, 1415-1416.
169. Nystrom, A. M.; Wooley, K. L. Thiol-functionalized shell crosslinked knedel-like (SCK) nanoparticles: A versatile entry for their conjugation with biomacromolecules. *Tetrahedron* 2008, 64, 8543-8552.
170. O'Connor, R. D.; Zhang, Q.; Wooley, K. L.; Schaefer, J. Crystallization of poly(epsilon-caprolactone) under nanoparticle confinement. *Helv Chim Acta* 2002, 85, 3219-3224.
171. Zhang, Q.; Remsen, E. E.; Wooley, K. L. Shell cross-linked nanoparticles containing hydrolytically degradable, crystalline core domains. *J Am Chem Soc* 2000, 122, 3642-3651.
172. Pan, D.; Turner, J. L.; Wooley, K. L. Folic acid-conjugated nanostructured materials designed for cancer cell targeting. *Chem Commun* 2003, 2400-2401.
173. Pan, D. J.; Turner, J. L.; Wooley, K. L. Shell cross-linked nanoparticles designed to target angiogenic blood vessels via alpha(v)beta(3) receptor-ligand interactions. *Macromolecules* 2004, 37, 7109-7115.
174. Wei, H.; Quan, C. Y.; Chang, C.; Zhang, X. Z.; Zhuo, R. X. Preparation of Novel Ferrocene-Based Shell Cross-Linked Thermoresponsive Hybrid Micelles with Antitumor Efficacy. *J Phys Chem B* 2010, 114, 5309-5314.

175. Rodriguez-Hernandez, J.; Babin, J.; Zappone, B.; Lecommandoux, S. Preparation of shell cross-linked nano-objects from hybrid-peptide block copolymers. *Biomacromolecules* 2005, 6, 2213-2220.
176. Butun, V.; Billingham, N. C.; Armes, S. P. Synthesis of shell cross-linked micelles with tunable hydrophilic/hydrophobic cores. *J Am Chem Soc* 1998, 120, 12135-12136.
177. Jiang, X.; Zhang, G.; Narain, R.; Liu, S. Fabrication of two types of shell-cross-linked micelles with "inverted" structures in aqueous solution from schizophrenic water-soluble ABC triblock copolymer via click chemistry. *Langmuir* 2009, 25, 2046-54.
178. Ding, J.; Liu, G. Polystyrene-block-poly(2-cinnamoyl ethyl methacrylate) Nanospheres with Cross-Linked Shells. *Macromolecules* 1998, 31, 6554-6558.
179. Stewart, S.; Liu, G. Hollow nanospheres from polyisoprene-block-poly(2-cinnamoyl ethyl methacrylate)-block-poly(tert-butyl acrylate). *Chemistry of Materials* 1999, 11, 1048-1054.
180. Sugihara, S.; Ito, S.; Irie, S.; Ikeda, I. Synthesis of Thermo-responsive Shell Cross-Linked Micelles via Living Cationic Polymerization and UV Irradiation. *Macromolecules* 2010, 43, 1753-1760.
181. Butun, V.; Wang, X. S.; Banez, M. V. D.; Robinson, K. L.; Billingham, N. C.; Armes, S. P.; Tuzar, Z. Synthesis of shell cross-linked micelles at high solids in aqueous media. *Macromolecules* 2000, 33, 1-3.
182. Fujii, S.; Cai, Y. L.; Weaver, J. V. M.; Armes, S. P. Syntheses of shell cross-linked micelles using acidic ABC triblock copolymers and their application as pH-responsive particulate emulsifiers. *J Am Chem Soc* 2005, 127, 7304-7305.
183. Jiang, X. Z.; Luo, S. Z.; Armes, S. P.; Shi, W. F.; Liu, S. Y. UV irradiation-induced shell cross-linked micelles with pH-responsive cores using ABC triblock copolymers. *Macromolecules* 2006, 39, 5987-5994.
184. Li, Y. T.; Lokitz, B. S.; Armes, S. P.; McCormick, C. L. Synthesis of reversible shell cross-linked micelles for controlled release of bioactive agents. *Macromolecules* 2006, 39, 2726-2728.
185. Koo, A. N.; Lee, H. J.; Kim, S. E.; Chang, J. H.; Park, C.; Kim, C.; Park, J. H.; Lee, S. C. Disulfide-cross-linked PEG-poly(amino acid)s copolymer micelles for glutathione-mediated intracellular drug delivery. *Chem. Commun. (Camb.)* 2008, 6570-2.
186. Sun, J.; Chen, X. S.; Lu, T. C.; Liu, S.; Tian, H. Y.; Guo, Z. P.; Jing, X. B. Formation of reversible shell cross-linked micelles from the biodegradable amphiphilic diblock copolymer poly(L-cysteine)-block-poly(L-lactide). *Langmuir* 2008, 24, 10099-10106.
187. Babin, J.; Lepage, M.; Zhao, Y. "Decoration" of shell cross-linked reverse polymer micelles using ATRP: A new route to stimuli-responsive nanoparticles. *Macromolecules* 2008, 41, 1246-1253.
188. Nasongkla, N.; Shuai, X.; Ai, H.; Weinberg, B. D.; Pink, J.; Boothman, D. A.; Gao, J. cRGD-functionalized polymer micelles for targeted doxorubicin delivery. *Angew Chem Int Ed Engl* 2004, 43, 6323-7.
189. Nasongkla, N.; Bey, E.; Ren, J.; Ai, H.; Khemtong, C.; Guthi, J. S.; Chin, S. F.; Sherry, A. D.; Boothman, D. A.; Gao, J. Multifunctional polymeric micelles as cancer-targeted, MRI-ultrasensitive drug delivery systems. *Nano Lett* 2006, 6, 2427-30.
190. Xiong, X. B.; Mahmud, A.; Uludağ, H.; Lavasanifar, A. Conjugation of arginine-glycine-aspartic acid peptides to poly(ethylene oxide)-b-poly(ϵ -caprolactone) micelles for

- enhanced intracellular drug delivery to metastatic tumor cells. *Biomacromolecules* 2007, 8, 874-884.
191. Xiong, X. B.; Mahmud, A.; Uludağ, H.; Lavasanifar, A. Multifunctional polymeric micelles for enhanced intracellular delivery of doxorubicin to metastatic cancer cells. *Pharmaceutical Research* 2008, 25, 2555-2566.
192. Soudy, R.; Gill, A.; Sprules, T.; Lavasanifar, A.; Kaur, K. Proteolytically stable cancer targeting peptides with high affinity for breast cancer cells. *J. Med. Chem.* 2011, 54, 7523-34.
193. Shahin, M.; Soudy, R.; Aliabadi, H. M.; Kneteman, N.; Kaur, K.; Lavasanifar, A. Engineered breast tumor targeting peptide ligand modified liposomal doxorubicin and the effect of peptide density on anticancer activity. *Biomaterials* 2013, 34, 4089-97.
194. Kursa, M.; Walker, G. F.; Roessler, V.; Ogris, M.; Roedl, W.; Kircheis, R.; Wagner, E. Novel shielded transferrin-polyethylene glycol-polyethylenimine/DNA complexes for systemic tumor-targeted gene transfer. *Bioconjug Chem* 2003, 14, 222-31.
195. Huang, C. K.; Lo, C. L.; Chen, H. H.; Hsiue, G. H. Multifunctional Micelles for Cancer Cell Targeting, Distribution Imaging, and Anticancer Drug Delivery. *Advanced Functional Materials* 2007, 17, 2291-2297.
196. Bae, Y.; Jang, W. D.; Nishiyama, N.; Fukushima, S.; Kataoka, K. Multifunctional polymeric micelles with folate-mediated cancer cell targeting and pH-triggered drug releasing properties for active intracellular drug delivery. *Mol Biosyst* 2005, 1, 242-50.
197. Zhu, L.; Wang, T.; Perche, F.; Taigind, A.; Torchilin, V. P. Enhanced anticancer activity of nanopreparation containing an MMP2-sensitive PEG-drug conjugate and cell-penetrating moiety. *Proc Natl Acad Sci U S A* 2013, 110, 17047-52.
198. Xiong, X. B.; Ma, Z.; Lai, R.; Lavasanifar, A. The therapeutic response to multifunctional polymeric nano-conjugates in the targeted cellular and subcellular delivery of doxorubicin. *Biomaterials* 2010, 31, 757-768.
199. Guillemard, V.; Uri Saragovi, H. Prodrug chemotherapeutics bypass p-glycoprotein resistance and kill tumors in vivo with high efficacy and target-dependent selectivity. *Oncogene* 2004, 23, 3613-21.
200. Lampidis, T. J.; Kolonias, D.; Podona, T.; Israel, M.; Safa, A. R.; Lothstein, L.; Savaraj, N.; Tapiero, H.; Priebe, W. Circumvention of P-GP MDR as a function of anthracycline lipophilicity and charge. *Biochemistry* 1997, 36, 2679-85.
201. Xiong, X. B.; Uludağ, H.; Lavasanifar, A. Virus-mimetic polymeric micelles for targeted siRNA delivery. *Biomaterials* 2010, 31, 5886-5893.
202. Dunn, G. P.; Old, L. J.; Schreiber, R. D. The immunobiology of cancer immunosurveillance and immunoediting. *Immunity* 2004, 21, 137-48.
203. Stewart, T. J.; Smyth, M. J. Improving cancer immunotherapy by targeting tumor-induced immune suppression. *Cancer Metastasis Rev.* 2011, 30, 125-40.
204. Molavi, O. Delivery of STAT3 Inhibitor Cucurbitacins to Tumor by Polymeric Nano-Carriers : Implications in Cancer Chemo- and Immunotherapy. University of Alberta, Edmonton, 2009.
205. Steinman, R. M. The control of immunity and tolerance by dendritic cells. *Pathologie Biologie* 2003, 51, 59-60.
206. Banchereau, J.; Steinman, R. M. Dendritic cells and the control of immunity. *Nature* 1998, 392, 245-52.

207. Lee, H. K.; Iwasaki, A. Innate control of adaptive immunity: dendritic cells and beyond. *Semin. Immunol.* 2007, 19, 48-55.
208. Janeway, C.; Travers, P.; Walport, M.; Shlomchik, M. *Immunobiology: The Immune System in Health and Disease*. 5th ed.; Garland Science: New York, 2001; p 600.
209. Underhill, D. M.; Ozinsky, A. Phagocytosis of microbes: complexity in action. *Annu. Rev. Immunol.* 2002, 20, 825-52.
210. Kim, R.; Emi, M.; Tanabe, K.; Arihiro, K. Potential functional role of plasmacytoid dendritic cells in cancer immunity. *Immunology* 2007, 121, 149-57.
211. Schuster, M.; Nechansky, A.; Kircheis, R. Cancer immunotherapy. *Biotechnology Journal* 2006, 1, 138-147.
212. Dougan, M.; Dranoff, G. Immune therapy for cancer. *Annu. Rev. Immunol.* 2009, 27, 83-117.
213. Topalian, S. L.; Weiner, G. J.; Pardoll, D. M. Cancer immunotherapy comes of age. *J. Clin. Oncol.* 2011, 29, 4828-36.
214. Weiner, G. J. Monoclonal antibody mechanisms of action in cancer. *Immunol. Res.* 2007, 39, 271-8.
215. Acres, B.; Paul, S.; Haegel-Kronenberger, H.; Calmels, B.; Squiban, P. Therapeutic cancer vaccines. *Curr. Opin. Mol. Ther.* 2004, 6, 40-7.
216. Kaufman, H. L.; Disis, M. L. Immune system versus tumor: shifting the balance in favor of DCs and effective immunity. *J. Clin. Invest.* 2004, 113, 664-7.
217. Zou, W. Immunosuppressive networks in the tumour environment and their therapeutic relevance. *Nature Reviews Cancer* 2005, 5, 263-274.
218. Kim, R.; Emi, M.; Tanabe, K. Cancer immunosuppression and autoimmune disease: beyond immunosuppressive networks for tumour immunity. *Immunology* 2006, 119, 254-64.
219. Yu, H.; Kortylewski, M.; Pardoll, D. Crosstalk between cancer and immune cells: role of STAT3 in the tumour microenvironment. *Nat. Rev. Immunol.* 2007, 7, 41-51.
220. Yu, H.; Jove, R. The STATs of cancer--new molecular targets come of age. *Nat. Rev. Cancer* 2004, 4, 97-105.
221. Al Zaid Siddiquee, K.; Turkson, J. STAT3 as a target for inducing apoptosis in solid and hematological tumors. *Cell Res.* 2008, 18, 254-267.
222. National Cancer Institute. <http://www.cancer.gov/> (accessed April 28, 2012).
223. Stewart, C. A.; Trinchieri, G. Reinforcing suppression using regulators: a new link between STAT3, IL-23, and Tregs in tumor immunosuppression. *Cancer Cell* 2009, 15, 81-3.
224. Kortylewski, M.; Jove, R.; Yu, H. Targeting STAT3 affects melanoma on multiple fronts. *Cancer Metastasis Rev* 2005, 24, 315-27.
225. Wang, T.; Niu, G.; Kortylewski, M.; Burdelya, L.; Shain, K.; Zhang, S.; Bhattacharya, R.; Gabilovich, D.; Heller, R.; Coppola, D.; Dalton, W.; Jove, R.; Pardoll, D.; Yu, H. Regulation of the innate and adaptive immune responses by Stat-3 signaling in tumor cells. *Nat Med* 2004, 10, 48-54.
226. Nefedova, Y.; Nagaraj, S.; Rosenbauer, A.; Muro-Cacho, C.; Sebt, S. M.; Gabilovich, D. I. Regulation of dendritic cell differentiation and antitumor immune response in cancer by pharmacologic-selective inhibition of the janus-activated kinase 2/signal transducers and activators of transcription 3 pathway. *Cancer Res* 2005, 65, 9525-35.

227. Gabrilovich, D. A Role for STAT3 in Dendritic Cell Regulation by Tumor-Derived Factors. In *Dendritic Cells in Cancer*, Salter, R. D.; Shurin, M. R., Eds. Springer US: 2009; pp 143-155.
228. Nefedova, Y.; Gabrilovich, D. I. Targeting of Jak/STAT pathway in antigen presenting cells in cancer. *Curr Cancer Drug Targets* 2007, 7, 71-7.
229. Kortylewski, M.; Kujawski, M.; Wang, T.; Wei, S.; Zhang, S.; Pilon-Thomas, S.; Niu, G.; Kay, H.; Mule, J.; Kerr, W. G.; Jove, R.; Pardoll, D.; Yu, H. Inhibiting Stat3 signaling in the hematopoietic system elicits multicomponent antitumor immunity. *Nat Med* 2005, 11, 1314-21.
230. Kusmartsev, S.; Gabrilovich, D. I. Effect of tumor-derived cytokines and growth factors on differentiation and immune suppressive features of myeloid cells in cancer. *Cancer Metastasis Rev* 2006, 25, 323-31.
231. Nefedova, Y.; Cheng, P.; Gilkes, D.; Blaskovich, M.; Beg, A. A.; Sebti, S. M.; Gabrilovich, D. I. Activation of dendritic cells via inhibition of Jak2/STAT3 signaling. *J Immunol* 2005, 175, 4338-46.
232. Nefedova, Y.; Huang, M.; Kusmartsev, S.; Bhattacharya, R.; Cheng, P.; Salup, R.; Jove, R.; Gabrilovich, D. Hyperactivation of STAT3 is involved in abnormal differentiation of dendritic cells in cancer. *J Immunol* 2004, 172, 464-74.
233. Steinman, R. M.; Hawiger, D.; Nussenzweig, M. C. Tolerogenic dendritic cells. *Annu Rev Immunol* 2003, 21, 685-711.
234. Hubert, P.; Jacobs, N.; Caberg, J. H.; Boniver, J.; Delvenne, P. The cross-talk between dendritic and regulatory T cells: good or evil? *J Leukoc Biol* 2007, 82, 781-94.
235. Turkson, J.; Ryan, D.; Kim, J. S.; Zhang, Y.; Chen, Z.; Haura, E.; Laudano, A.; Sebti, S.; Hamilton, A. D.; Jove, R. Phosphotyrosyl peptides block Stat3-mediated DNA binding activity, gene regulation, and cell transformation. *J Biol Chem* 2001, 276, 45443-55.
236. Zhao, M.; Jiang, B.; Gao, F. H. Small molecule inhibitors of STAT3 for cancer therapy. *Curr Med Chem* 2011, 18, 4012-8.
237. Turkson, J.; Zhang, S.; Mora, L. B.; Burns, A.; Sebti, S.; Jove, R. A novel platinum compound inhibits constitutive Stat3 signaling and induces cell cycle arrest and apoptosis of malignant cells. *J Biol Chem* 2005, 280, 32979-88.
238. Turkson, J.; Zhang, S.; Palmer, J.; Kay, H.; Stanko, J.; Mora, L. B.; Sebti, S.; Yu, H.; Jove, R. Inhibition of constitutive signal transducer and activator of transcription 3 activation by novel platinum complexes with potent antitumor activity. *Mol Cancer Ther* 2004, 3, 1533-42.
239. Yue, P.; Turkson, J. Targeting STAT3 in cancer: how successful are we? *Expert Opin Investig Drugs* 2009, 18, 45-56.
240. Song, H.; Wang, R.; Wang, S.; Lin, J. A low-molecular-weight compound discovered through virtual database screening inhibits Stat3 function in breast cancer cells. *Proc Natl Acad Sci U S A* 2005, 102, 4700-5.
241. Fuh, B.; Sobo, M.; Cen, L.; Josiah, D.; Hutzen, B.; Cisek, K.; Bhasin, D.; Regan, N.; Lin, L.; Chan, C.; Caldas, H.; DeAngelis, S.; Li, C.; Li, P. K.; Lin, J. LLL-3 inhibits STAT3 activity, suppresses glioblastoma cell growth and prolongs survival in a mouse glioblastoma model. *Br J Cancer* 2009, 100, 106-12.
242. Siddiquee, K.; Zhang, S.; Guida, W. C.; Blaskovich, M. A.; Greedy, B.; Lawrence, H. R.; Yip, M. L.; Jove, R.; McLaughlin, M. M.; Lawrence, N. J.; Sebti, S. M.; Turkson, J.

- Selective chemical probe inhibitor of Stat3, identified through structure-based virtual screening, induces antitumor activity. *Proc Natl Acad Sci U S A* 2007, 104, 7391-6.
243. Schust, J.; Sperl, B.; Hollis, A.; Mayer, T. U.; Berg, T. Stattic: a small-molecule inhibitor of STAT3 activation and dimerization. *Chem Biol* 2006, 13, 1235-42.
244. Lin, L.; Hutzen, B.; Li, P. K.; Ball, S.; Zuo, M.; DeAngelis, S.; Foust, E.; Sobo, M.; Friedman, L.; Bhasin, D.; Cen, L.; Li, C.; Lin, J. A novel small molecule, LLL12, inhibits STAT3 phosphorylation and activities and exhibits potent growth-suppressive activity in human cancer cells. *Neoplasia* 2010, 12, 39-50.
245. Alshamsan, A.; Hamdy, S.; Haddadi, A.; Samuel, J.; El-Kadi, A. O.; Uludag, H.; Lavasanifar, A. STAT3 Knockdown in B16 Melanoma by siRNA Lipopolyplexes Induces Bystander Immune Response In Vitro and In Vivo. *Transl Oncol* 2011, 4, 178-88.
246. Falamarzian, A.; Aliabadi, H. M.; Molavi, O.; Seubert, J. M.; Lai, R.; Uludag, H.; Lavasanifar, A. Effective down-regulation of signal transducer and activator of transcription 3 (STAT3) by polyplexes of siRNA and lipid-substituted polyethyleneimine for sensitization of breast tumor cells to conventional chemotherapy. *J Biomed Mater Res A* 2014, 102, 3216-28.
247. Falamarzian, A. Lipid modification of polymeric nanocarriers for drug and siRNA delivery. University of Alberta, Edmonton, 2013.
248. Levitzki, A. Tyrosine kinase blockers as novel antiproliferative agents and dissectors of signal transduction. *FASEB J* 1992, 6, 3275-82.
249. Blaskovich, M. A.; Sun, J.; Cantor, A.; Turkson, J.; Jove, R.; Sebt, S. M. Discovery of JSI-124 (cucurbitacin I), a selective Janus kinase/signal transducer and activator of transcription 3 signaling pathway inhibitor with potent antitumor activity against human and murine cancer cells in mice. *Cancer Res* 2003, 63, 1270-9.
250. Ferrajoli, A.; Faderl, S.; Van, Q.; Koch, P.; Harris, D.; Liu, Z.; Hazan-Halevy, I.; Wang, Y.; Kantarjian, H. M.; Priebe, W.; Estrov, Z. WP1066 disrupts Janus kinase-2 and induces caspase-dependent apoptosis in acute myelogenous leukemia cells. *Cancer Res* 2007, 67, 11291-9.
251. Iwamaru, A.; Szymanski, S.; Iwado, E.; Aoki, H.; Yokoyama, T.; Fokt, I.; Hess, K.; Conrad, C.; Madden, T.; Sawaya, R.; Kondo, S.; Priebe, W.; Kondo, Y. A novel inhibitor of the STAT3 pathway induces apoptosis in malignant glioma cells both in vitro and in vivo. *Oncogene* 2007, 26, 2435-44.
252. Pardnani, A.; Hood, J.; Lasho, T.; Levine, R. L.; Martin, M. B.; Noronha, G.; Finke, C.; Mak, C. C.; Mesa, R.; Zhu, H.; Soll, R.; Gilliland, D. G.; Tefferi, A. TG101209, a small molecule JAK2-selective kinase inhibitor potently inhibits myeloproliferative disorder-associated JAK2V617F and MPLW515L/K mutations. *Leukemia* 2007, 21, 1658-68.
253. Kotha, A.; Sekharam, M.; Cilenti, L.; Siddiquee, K.; Khaled, A.; Zervos, A. S.; Carter, B.; Turkson, J.; Jove, R. Resveratrol inhibits Src and Stat3 signaling and induces the apoptosis of malignant cells containing activated Stat3 protein. *Mol Cancer Ther* 2006, 5, 621-9.
254. Nam, S.; Buettner, R.; Turkson, J.; Kim, D.; Cheng, J. Q.; Muehlbeyer, S.; Hippe, F.; Vatter, S.; Merz, K. H.; Eisenbrand, G.; Jove, R. Indirubin derivatives inhibit Stat3 signaling and induce apoptosis in human cancer cells. *Proc Natl Acad Sci U S A* 2005, 102, 5998-6003.

255. Molavi, O.; Ma, Z.; Hamdy, S.; Lai, R.; Lavasanifar, A.; Samuel, J. Synergistic antitumor effects of CpG oligodeoxynucleotide and STAT3 inhibitory agent JSI-124 in a mouse melanoma tumor model. *Immunol Cell Biol* 2008, 86, 506-14.
256. Molavi, O.; Ma, Z.; Hamdy, S.; Lavasanifar, A.; Samuel, J. Immunomodulatory and anticancer effects of intra-tumoral co-delivery of synthetic lipid A adjuvant and STAT3 inhibitor, JSI-124. *Immunopharmacol Immunotoxicol* 2009, 31, 214-21.
257. Molavi, O.; Mahmud, A.; Hamdy, S.; Hung, R. W.; Lai, R.; Samuel, J.; Lavasanifar, A. Development of a poly(D,L-lactic-co-glycolic acid) nanoparticle formulation of STAT3 inhibitor JSI-124: implication for cancer immunotherapy. *Mol. Pharm.* 2010, 7, 364-74.
258. Nefedova, Y. B.; Lyn, D.; Sebt, S. M.; Gibrilovich, D. I. A new selective Jak2/STAT3 pathway inhibitor JSI-124 improves dendritic cells differentiation in cancer. *Cancer Research* 2004, 64, 545-545.
259. Chen, J. C.; Chiu, M. H.; Nie, R. L.; Cordell, G. A.; Qiu, S. X. Cucurbitacins and cucurbitane glycosides: structures and biological activities. *Nat Prod Rep* 2005, 22, 386-99.
260. Shi, X.; Franko, B.; Frantz, C.; Amin, H. M.; Lai, R. JSI-124 (cucurbitacin I) inhibits Janus kinase-3/signal transducer and activator of transcription-3 signalling, downregulates nucleophosmin-anaplastic lymphoma kinase (ALK), and induces apoptosis in ALK-positive anaplastic large cell lymphoma cells. *Br J Haematol* 2006, 135, 26-32.
261. Molavi, O.; Ma, Z.; Mahmud, A.; Alshamsan, A.; Samuel, J.; Lai, R.; Kwon, G. S.; Lavasanifar, A. Polymeric micelles for the solubilization and delivery of STAT3 inhibitor cucurbitacins in solid tumors. *Int J Pharm* 2008, 347, 118-27.
262. Fujita, M.; Zhu, X.; Sasaki, K.; Ueda, R.; Low, K. L.; Pollack, I. F.; Okada, H. Inhibition of STAT3 promotes the efficacy of adoptive transfer therapy using type-1 CTLs by modulation of the immunological microenvironment in a murine intracranial glioma. *J Immunol* 2008, 180, 2089-98.
263. Elmore, S. Apoptosis: a review of programmed cell death. *Toxicol Pathol* 2007, 35, 495-516.
264. Akgul, C. Mcl-1 is a potential therapeutic target in multiple types of cancer. *Cell Mol Life Sci* 2009, 66, 1326-36.
265. Willis, S.; Day, C. L.; Hinds, M. G.; Huang, D. C. The Bcl-2-regulated apoptotic pathway. *J Cell Sci* 2003, 116, 4053-6.
266. Thomas, L. W.; Lam, C.; Edwards, S. W. Mcl-1; the molecular regulation of protein function. *FEBS Lett* 2010, 584, 2981-9.
267. Soini, Y.; Kinnula, V.; Kaarteenaho-Wiik, R.; Kurttila, E.; Linnainmaa, K.; Paakko, P. Apoptosis and expression of apoptosis regulating proteins bcl-2, mcl-1, bcl-X, and bax in malignant mesothelioma. *Clin Cancer Res* 1999, 5, 3508-15.
268. Modugno, M.; Banfi, P.; Gasparri, F.; Borzilleri, R.; Carter, P.; Cornelius, L.; Gottardis, M.; Lee, V.; Mapelli, C.; Naglich, J. G.; Tebben, A.; Vite, G.; Pastori, W.; Albanese, C.; Corti, E.; Ballinari, D.; Galvani, A. Mcl-1 antagonism is a potential therapeutic strategy in a subset of solid cancers. *Exp Cell Res* 2014.
269. Kozopas, K. M.; Yang, T.; Buchan, H. L.; Zhou, P.; Craig, R. W. MCL1, a gene expressed in programmed myeloid cell differentiation, has sequence similarity to BCL2. *Proc Natl Acad Sci U S A* 1993, 90, 3516-20.
270. Adams, K. W.; Cooper, G. M. Rapid turnover of mcl-1 couples translation to cell survival and apoptosis. *J Biol Chem* 2007, 282, 6192-200.

271. Aliabadi, H. M.; Mahdipoor, P.; Uludag, H. Polymeric delivery of siRNA for dual silencing of Mcl-1 and P-glycoprotein and apoptosis induction in drug-resistant breast cancer cells. *Cancer Gene Ther* 2013, 20, 169-77.
272. Le Gouill, S.; Podar, K.; Harousseau, J. L.; Anderson, K. C. Mcl-1 regulation and its role in multiple myeloma. *Cell Cycle* 2004, 3, 1259-62.
273. Ding, Q.; Huo, L.; Yang, J. Y.; Xia, W.; Wei, Y.; Liao, Y.; Chang, C. J.; Yang, Y.; Lai, C. C.; Lee, D. F.; Yen, C. J.; Chen, Y. J.; Hsu, J. M.; Kuo, H. P.; Lin, C. Y.; Tsai, F. J.; Li, L. Y.; Tsai, C. H.; Hung, M. C. Down-regulation of myeloid cell leukemia-1 through inhibiting Erk/Pin 1 pathway by sorafenib facilitates chemosensitization in breast cancer. *Cancer Res* 2008, 68, 6109-17.
274. Mitchell, C.; Yacoub, A.; Hossein, H.; Martin, A. P.; Bareford, M. D.; Eulitt, P.; Yang, C.; Nephew, K. P.; Dent, P. Inhibition of MCL-1 in breast cancer cells promotes cell death in vitro and in vivo. *Cancer Biol Ther* 2010, 10, 903-17.
275. Jazirehi, A. R.; Bonavida, B. Resveratrol modifies the expression of apoptotic regulatory proteins and sensitizes non-Hodgkin's lymphoma and multiple myeloma cell lines to paclitaxel-induced apoptosis. *Mol Cancer Ther* 2004, 3, 71-84.
276. Nguyen, M.; Marcellus, R. C.; Roulston, A.; Watson, M.; Serfass, L.; Murthy Madiraju, S. R.; Goulet, D.; Viallet, J.; Belec, L.; Billot, X.; Acoca, S.; Purisima, E.; Wiegman, A.; Cluse, L.; Johnstone, R. W.; Beauparlant, P.; Shore, G. C. Small molecule obatoclax (GX15-070) antagonizes MCL-1 and overcomes MCL-1-mediated resistance to apoptosis. *Proc Natl Acad Sci U S A* 2007, 104, 19512-7.
277. Lee, E. F.; Czabotar, P. E.; van Delft, M. F.; Michalak, E. M.; Boyle, M. J.; Willis, S. N.; Puthalakath, H.; Bouillet, P.; Colman, P. M.; Huang, D. C.; Fairlie, W. D. A novel BH3 ligand that selectively targets Mcl-1 reveals that apoptosis can proceed without Mcl-1 degradation. *J Cell Biol* 2008, 180, 341-55.
278. Shegokar, R.; Al Shaal, L.; Mishra, P. R. SiRNA delivery: challenges and role of carrier systems. *Pharmazie* 2011, 66, 313-8.
279. Falamarzian, A.; Xiong, X. B.; Uludag, H.; Lavasanifar, A. Polymeric micelles for siRNA delivery. *Journal of Drug Delivery Science and Technology* 2012, 22, 43-54.
280. Tuschl, T.; Zamore, P. D.; Lehmann, R.; Bartel, D. P.; Sharp, P. A. Targeted mRNA degradation by double-stranded RNA in vitro. *Genes Dev* 1999, 13, 3191-7.
281. Leng, Q.; Woodle, M. C.; Lu, P. Y.; Mixson, A. J. Advances in Systemic siRNA Delivery. *Drugs Future* 2009, 34, 721.
282. Wu, H.; Ramachandran, C.; Bielinska, A. U.; Kingzett, K.; Sun, R.; Weiner, N. D.; Roessler, B. J. Topical transfection using plasmid DNA in a water-in-oil nanoemulsion. *Int J Pharm* 2001, 221, 23-34.
283. Chono, S.; Li, S. D.; Conwell, C. C.; Huang, L. An efficient and low immunostimulatory nanoparticle formulation for systemic siRNA delivery to the tumor. *J Control Release* 2008, 131, 64-9.
284. Sato, A.; Takagi, M.; Shimamoto, A.; Kawakami, S.; Hashida, M. Small interfering RNA delivery to the liver by intravenous administration of galactosylated cationic liposomes in mice. *Biomaterials* 2007, 28, 1434-42.
285. Akinc, A.; Zumbuehl, A.; Goldberg, M.; Leshchiner, E. S.; Busini, V.; Hossain, N.; Bacallado, S. A.; Nguyen, D. N.; Fuller, J.; Alvarez, R.; Borodovsky, A.; Borland, T.; Constien, R.; de Fougerolles, A.; Dorkin, J. R.; Narayanannair Jayaprakash, K.; Jayaraman,

- M.; John, M.; Koteliansky, V.; Manoharan, M.; Nechev, L.; Qin, J.; Racie, T.; Raitcheva, D.; Rajeev, K. G.; Sah, D. W.; Soutschek, J.; Toudjarska, I.; Vornlocher, H. P.; Zimmermann, T. S.; Langer, R.; Anderson, D. G. A combinatorial library of lipid-like materials for delivery of RNAi therapeutics. *Nat Biotechnol* 2008, 26, 561-9.
286. Kim, H. R.; Kim, I. K.; Bae, K. H.; Lee, S. H.; Lee, Y.; Park, T. G. Cationic solid lipid nanoparticles reconstituted from low density lipoprotein components for delivery of siRNA. *Mol Pharm* 2008, 5, 622-31.
287. Davis, M. E.; Pun, S. H.; Bellocq, N. C.; Reineke, T. M.; Popielarski, S. R.; Mishra, S.; Heidel, J. D. Self-assembling nucleic acid delivery vehicles via linear, water-soluble, cyclodextrin-containing polymers. *Curr Med Chem* 2004, 11, 179-97.
288. Schiffelers, R. M.; Ansari, A.; Xu, J.; Zhou, Q.; Tang, Q.; Storm, G.; Molema, G.; Lu, P. Y.; Scaria, P. V.; Woodle, M. C. Cancer siRNA therapy by tumor selective delivery with ligand-targeted sterically stabilized nanoparticle. *Nucleic Acids Res* 2004, 32, e149.
289. Kim, S. H.; Jeong, J. H.; Lee, S. H.; Kim, S. W.; Park, T. G. PEG conjugated VEGF siRNA for anti-angiogenic gene therapy. *J Control Release* 2006, 116, 123-9.
290. Kim, S. H.; Jeong, J. H.; Lee, S. H.; Kim, S. W.; Park, T. G. Local and systemic delivery of VEGF siRNA using polyelectrolyte complex micelles for effective treatment of cancer. *J Control Release* 2008, 129, 107-16.
291. Kim, S. H.; Jeong, J. H.; Lee, S. H.; Kim, S. W.; Park, T. G. LHRH receptor-mediated delivery of siRNA using polyelectrolyte complex micelles self-assembled from siRNA-PEG-LHRH conjugate and PEI. *Bioconjug Chem* 2008, 19, 2156-62.
292. Sutton, D.; Kim, S.; Shuai, X.; Leskov, K.; Marques, J. T.; Williams, B. R.; Boothman, D. A.; Gao, J. Efficient suppression of secretory clusterin levels by polymer-siRNA nanocomplexes enhances ionizing radiation lethality in human MCF-7 breast cancer cells in vitro. *Int J Nanomedicine* 2006, 1, 155-62.
293. Sato, A.; Choi, S. W.; Hirai, M.; Yamayoshi, A.; Moriyama, R.; Yamano, T.; Takagi, M.; Kano, A.; Shimamoto, A.; Maruyama, A. Polymer brush-stabilized polyplex for a siRNA carrier with long circulatory half-life. *J Control Release* 2007, 122, 209-16.
294. Musacchio, T.; Vaze, O.; D'Souza, G.; Torchilin, V. P. Effective stabilization and delivery of siRNA: reversible siRNA-phospholipid conjugate in nanosized mixed polymeric micelles. *Bioconjug Chem* 2010, 21, 1530-6.
295. Salzano, G.; Riehle, R.; Navarro, G.; Perche, F.; De Rosa, G.; Torchilin, V. P. Polymeric micelles containing reversibly phospholipid-modified anti-survivin siRNA: a promising strategy to overcome drug resistance in cancer. *Cancer Lett* 2014, 343, 224-31.
296. Salzano, G.; Navarro, G.; Trivedi, M. S.; De Rosa, G.; Torchilin, V. P. Multifunctional Polymeric Micelles Co-loaded with Anti-Survivin siRNA and Paclitaxel Overcome Drug Resistance in an Animal Model of Ovarian Cancer. *Mol Cancer Ther* 2015, 14, 1075-84.
297. Navarro, G.; Essex, S.; Sawant, R. R.; Biswas, S.; Nagesha, D.; Sridhar, S.; de, I. C. T.; Torchilin, V. P. Phospholipid-modified polyethylenimine-based nanopreparations for siRNA-mediated gene silencing: implications for transfection and the role of lipid components. *Nanomedicine* 2014, 10, 411-9.
298. Aliabadi, H. M.; Landry, B.; Bahadur, R. K.; Neamark, A.; Suwantong, O.; Uludag, H. Impact of lipid substitution on assembly and delivery of siRNA by cationic polymers. *Macromol Biosci* 2011, 11, 662-72.

299. Yu, Y. H.; Kim, E.; Park, D. E.; Shim, G.; Lee, S.; Kim, Y. B.; Kim, C. W.; Oh, Y. K. Cationic solid lipid nanoparticles for co-delivery of paclitaxel and siRNA. *Eur J Pharm Biopharm* 2012, 80, 268-73.
300. Chang, R. S.; Suh, M. S.; Kim, S.; Shim, G.; Lee, S.; Han, S. S.; Lee, K. E.; Jeon, H.; Choi, H. G.; Choi, Y.; Kim, C. W.; Oh, Y. K. Cationic drug-derived nanoparticles for multifunctional delivery of anticancer siRNA. *Biomaterials* 2011, 32, 9785-95.
301. Mahmud, A.; Patel, S.; Molavi, O.; Choi, P.; Samuel, J.; Lavasanifar, A. Self-associating poly(ethylene oxide)-b-poly(α -cholesteryl carboxylate- ϵ -caprolactone) block copolymer for the solubilization of stat-3 inhibitor cucurbitacin I. *Biomacromolecules* 2009, 10, 471-478.
302. Falamarzian, A.; Lavasanifar, A. Chemical modification of hydrophobic block in poly(ethylene oxide) poly(caprolactone) based nanocarriers: Effect on the solubilization and hemolytic activity of Amphotericin B. *Macromolecular Bioscience* 2010, 10, 648-656.
303. Falamarzian, A.; Lavasanifar, A. Optimization of the hydrophobic domain in poly(ethylene oxide)-poly(varepsilon-caprolactone) based nano-carriers for the solubilization and delivery of Amphotericin B. *Colloids Surf. B Biointerfaces* 2010, 81, 313-20.
304. Safaei Nikouei, N.; Lavasanifar, A. Characterization of the thermo- and pH-responsive assembly of triblock copolymers based on poly(ethylene glycol) and functionalized poly(epsilon-caprolactone). *Acta Biomater.* 2011, 7, 3708-18.
305. Shahin, M.; Safaei-Nikouei, N.; Lavasanifar, A. Polymeric micelles for pH-responsive delivery of cisplatin. *J Drug Target* 2014, 22, 629-37.
306. Zhang, Q.; Vakili, M. R.; Li, X. F.; Lavasanifar, A.; Le, X. C. Polymeric micelles for GSH-triggered delivery of arsenic species to cancer cells. *Biomaterials* 2014, 35, 7088-100.
307. Garg, S. M.; Vakili, M. R.; Lavasanifar, A. Polymeric micelles based on poly(ethylene oxide) and α -carbon substituted poly(ϵ -caprolactone): An in vitro study on the effect of core forming block on polymeric micellar stability, biocompatibility, and immunogenicity. *Colloids and Surfaces B: Biointerfaces* 2015, 132, 161-170.
308. Aliabadi, H. M.; Mahmud, A.; Sharifabadi, A. D.; Lavasanifar, A. Micelles of methoxy poly(ethylene oxide)-b-poly(epsilon-caprolactone) as vehicles for the solubilization and controlled delivery of cyclosporine A. *J. Control. Release* 2005, 104, 301-11.
309. Diao, Y. Y.; Li, H. Y.; Fu, Y. H.; Han, M.; Hu, Y. L.; Jiang, H. L.; Tsutsumi, Y.; Wei, Q. C.; Chen, D. W.; Gao, J. Q. Doxorubicin-loaded PEG-PCL copolymer micelles enhance cytotoxicity and intracellular accumulation of doxorubicin in adriamycin-resistant tumor cells. *Int. J. Nanomedicine* 2011, 6, 1955-62.
310. Meier, M. A. R.; Aerts, S. N. H.; Staal, B. B. P.; Rasa, M.; Schubert, U. S. PEO-b-PCL Block Copolymers: Synthesis, Detailed Characterization, and Selected Micellar Drug Encapsulation Behavior. *Macromolecular Rapid Communications* 2005, 26, 1918-1924.
311. Qi, W.; Ghoroghchian, P. P.; Li, G.; Hammer, D. A.; Therien, M. J. Aqueous self-assembly of poly(ethylene oxide)-block-poly(epsilon-caprolactone) (PEO-b-PCL) copolymers: disparate diblock copolymer compositions give rise to nano- and meso-scale bilayered vesicles. *Nanoscale* 2013, 5, 10908-15.
312. Liggins, R. T.; Burt, H. M. Polyether-polyester diblock copolymers for the preparation of paclitaxel loaded polymeric micelle formulations. *Adv. Drug Deliv. Rev.* 2002, 54, 191-202.

313. Zhang, X. C.; Jackson, J. K.; Burt, H. M. Development of amphiphilic diblock copolymers as micellar carriers of taxol. *International Journal of Pharmaceutics* 1996, 132, 195-206.
314. Jeong, B.; Han Bae, Y.; Wan Kim, S. Biodegradable thermosensitive micelles of PEG-PLGA-PEG triblock copolymers. *Colloids and Surfaces B: Biointerfaces* 1999, 16, 185-193.
315. Rameez, S.; Alost, H.; Palmer, A. F. Biocompatible and biodegradable polymersome encapsulated hemoglobin: a potential oxygen carrier. *Bioconjug. Chem.* 2008, 19, 1025-32.
316. Garg, S. M.; Xiong, X. B.; Lu, C.; Lavasanifar, A. Application of click chemistry in the preparation of poly(ethylene oxide)-block-poly(ϵ -caprolactone) with hydrolyzable cross-links in the micellar core. *Macromolecules* 2011, 44, 2058-2066.
317. Toncheva, V.; Schacht, E.; Ng, S. Y.; Barr, J.; Heller, J. Use of Block Copolymers of Poly(Ortho Esters) and Poly (Ethylene Glycol) Micellar Carriers as Potential Tumour Targeting Systems. *Journal of Drug Targeting* 2003, 11, 345-353.
318. Wang, J.; Sun, R. H.; Zhang, N.; Nie, H.; Liu, J. H.; Wang, J. N.; Wang, H.; Liu, Y. Multi-walled carbon nanotubes do not impair immune functions of dendritic cells. *Carbon* 2009, 47, 1752-1760.
319. Elamanchili, P.; Lutsiak, C. M.; Hamdy, S.; Diwan, M.; Samuel, J. "Pathogen-mimicking" nanoparticles for vaccine delivery to dendritic cells. *J. Immunother.* 2007, 30, 378-95.
320. Mahmud, A.; Lavasanifar, A. The effect of block copolymer structure on the internalization of polymeric micelles by human breast cancer cells. *Colloids Surf. B Biointerfaces* 2005, 45, 82-9.
321. Topel, Ö.; Çakır, B. A.; Budama, L.; Hoda, N. Determination of critical micelle concentration of polybutadiene-block-poly(ethyleneoxide) diblock copolymer by fluorescence spectroscopy and dynamic light scattering. *Journal of Molecular Liquids* 2013, 177, 40-43.
322. Kang, N.; Perron, M. E.; Prud'homme, R. E.; Zhang, Y.; Gaucher, G.; Leroux, J. C. Stereocomplex block copolymer micelles: core-shell nanostructures with enhanced stability. *Nano Lett.* 2005, 5, 315-9.
323. Lutz, M. B.; Kukutsch, N.; Ogilvie, A. L.; Rossner, S.; Koch, F.; Romani, N.; Schuler, G. An advanced culture method for generating large quantities of highly pure dendritic cells from mouse bone marrow. *J. Immunol. Methods* 1999, 223, 77-92.
324. Ukawala, M.; Rajyaguru, T.; Chaudhari, K.; Manjappa, A. S.; Pimple, S.; Babbar, A. K.; Mathur, R.; Mishra, A. K.; Murthy, R. S. Investigation on design of stable etoposide-loaded PEG-PCL micelles: effect of molecular weight of PEG-PCL diblock copolymer on the in vitro and in vivo performance of micelles. *Drug Deliv.* 2012, 19, 155-67.
325. Tanaka, H.; Matsushima, H.; Mizumoto, N.; Takashima, A. Classification of chemotherapeutic agents based on their differential in vitro effects on dendritic cells. *Cancer Res.* 2009, 69, 6978-86.
326. Gou, M.; Wei, X.; Men, K.; Wang, B.; Luo, F.; Zhao, X.; Wei, Y.; Qian, Z. PCL/PEG copolymeric nanoparticles: potential nanoplatfoms for anticancer agent delivery. *Curr. Drug Targets* 2011, 12, 1131-50.

327. Ma, Z.; Haddadi, A.; Molavi, O.; Lavasanifar, A.; Lai, R.; Samuel, J. Micelles of poly(ethylene oxide)-b-poly(epsilon-caprolactone) as vehicles for the solubilization, stabilization, and controlled delivery of curcumin. *J. Biomed. Mater. Res. A* 2008, 86, 300-10.
328. Kelarakis, A.; Chaibundit, C.; Krysmann, M. J.; Havredaki, V.; Viras, K.; Hamley, I. W. Interactions of an anionic surfactant with poly(oxyalkylene) copolymers in aqueous solution. *J. Colloid Interface Sci.* 2009, 330, 67-72.
329. Punjabi, S. H.; Sastry, N. V.; Aswal, V. K.; Goyal, P. S. Effect of Surfactants on Association Characteristics of Di- and Triblock Copolymers of Oxyethylene and Oxybutylene in Aqueous Solutions: Dilute Solution Phase Diagrams, SANS, and Viscosity Measurements at Different Temperatures. *International Journal of Polymer Science* 2011, 2011.
330. Zhu, X.; Fryd, M.; Tran, B. D.; Ilies, M. A.; Wayland, B. B. Modifying the Hydrophilic-Hydrophobic Interface of PEG-b-PCL To Increase Micelle Stability: Preparation of PEG-b-PBO-b-PCL Triblock Copolymers, Micelle Formation, and Hydrolysis Kinetics. *Macromolecules* 2012, 45, 660-665.
331. Moghimi, S. M.; Pavey, K. D.; Hunter, A. C. Real-time evidence of surface modification at polystyrene lattices by poloxamine 908 in the presence of serum: In vivo conversion of macrophage-prone nanoparticles to stealth entities by poloxamine 908. *FEBS Letters* 2003, 547, 177-182.
332. D'Addio, S. M.; Saad, W.; Ansell, S. M.; Squiers, J. J.; Adamson, D. H.; Herrera-Alonso, M.; Wohl, A. R.; Hoye, T. R.; Macosko, C. W.; Mayer, L. D.; Vauthier, C.; Prud'homme, R. K. Effects of block copolymer properties on nanocarrier protection from in vivo clearance. *J Control Release* 2012, 162, 208-17.
333. Granucci, F.; Ferrero, E.; Foti, M.; Aggujaro, D.; Vettoretto, K.; Ricciardi-Castagnoli, P. Early events in dendritic cell maturation induced by LPS. *Microbes Infect.* 1999, 1, 1079-84.
334. Ferlay, J.; Soerjomataram, I.; Ervik, M.; Dikshit, R.; Eser, S.; Mathers, C.; Rebelo, M.; Parkin, D.; Forman, D.; Bray, F. GLOBOCAN 2012 v1.0 *Cancer Incidence and Mortality Worldwide: IARC CancerBase No. 11* [Online], 2013. (accessed 11/07/2015).
335. Chidambaram, M.; Manavalan, R.; Kathiresan, K. Nanotherapeutics to overcome conventional cancer chemotherapy limitations. *J Pharm Pharm Sci* 2011, 14, 67-77.
336. Perez-Herrero, E.; Fernandez-Medarde, A. Advanced targeted therapies in cancer: Drug nanocarriers, the future of chemotherapy. *Eur J Pharm Biopharm* 2015, 93, 52-79.
337. Brigger, I.; Dubernet, C.; Couvreur, P. Nanoparticles in cancer therapy and diagnosis. *Adv Drug Deliv Rev* 2002, 54, 631-51.
338. Iyer, A. K.; Khaled, G.; Fang, J.; Maeda, H. Exploiting the enhanced permeability and retention effect for tumor targeting. *Drug Discov Today* 2006, 11, 812-8.
339. Langer, R. Drug delivery and targeting. *Nature* 1998, 392, 5-10.
340. Na, J. H.; Koo, H.; Lee, S.; Min, K. H.; Park, K.; Yoo, H.; Lee, S. H.; Park, J. H.; Kwon, I. C.; Jeong, S. Y.; Kim, K. Real-time and non-invasive optical imaging of tumor-targeting glycol chitosan nanoparticles in various tumor models. *Biomaterials* 2011, 32, 5252-61.

341. Oerlemans, C.; Bult, W.; Bos, M.; Storm, G.; Nijssen, J. F.; Hennink, W. E. Polymeric micelles in anticancer therapy: targeting, imaging and triggered release. *Pharm. Res.* 2010, 27, 2569-89.
342. Lee, H.; Hoang, B.; Fonge, H.; Reilly, R. M.; Allen, C. In vivo distribution of polymeric nanoparticles at the whole-body, tumor, and cellular levels. *Pharmaceutical Research* 2010, 27, 2343-55.
343. Hu, Z.; Luo, F.; Pan, Y.; Hou, C.; Ren, L.; Chen, J.; Wang, J.; Zhang, Y. Arg-Gly-Asp (RGD) peptide conjugated poly(lactic acid)-poly(ethylene oxide) micelle for targeted drug delivery. *J Biomed Mater Res A* 2008, 85, 797-807.
344. Irwin, C. R.; Favis, N. A.; Agopsowicz, K. C.; Hitt, M. M.; Evans, D. H. Myxoma virus oncolytic efficiency can be enhanced through chemical or genetic disruption of the actin cytoskeleton. *PLoS One* 2013, 8, e84134.
345. Hue, J. J.; Lee, H. J.; Jon, S.; Nam, S. Y.; Yun, Y. W.; Kim, J. S.; Lee, B. J. Distribution and accumulation of Cy5.5-labeled thermally cross-linked superparamagnetic iron oxide nanoparticles in the tissues of ICR mice. *J Vet Sci* 2013, 14, 473-9.
346. Liu, Y.; Tseng, Y. C.; Huang, L. Biodistribution studies of nanoparticles using fluorescence imaging: a qualitative or quantitative method? *Pharmaceutical Research* 2012, 29, 3273-7.
347. Adams, D. J.; Kitchen, C.; Adams, S.; Furzeland, S.; Atkins, D.; Schuetz, P.; Fernyhough, C. M.; Tzokova, N.; Ryan, A. J.; Butler, M. F. On the mechanism of formation of vesicles from poly(ethylene oxide)-block-poly(caprolactone) copolymers. *Soft Matter* 2009, 5, 3086-3096.
348. Du, Z.-X.; Xu, J.-T.; Fan, Z.-Q. Micellar Morphologies of Poly(ϵ -caprolactone)-b-poly(ethylene oxide) Block Copolymers in Water with a Crystalline Core. *Macromolecules* 2007, 40, 7633-7637.
349. Askoxylakis, V.; Zitzmann, S.; Mier, W.; Graham, K.; Kramer, S.; von Wegner, F.; Fink, R. H.; Schwab, M.; Eisenhut, M.; Haberkorn, U. Preclinical evaluation of the breast cancer cell-binding peptide, p160. *Clin. Cancer Res.* 2005, 11, 6705-12.
350. Shahin, M.; Ahmed, S.; Kaur, K.; Lavasanifar, A. Decoration of polymeric micelles with cancer-specific peptide ligands for active targeting of paclitaxel. *Biomaterials* 2011, 32, 5123-33.
351. Alexis, F.; Pridgen, E.; Molnar, L. K.; Farokhzad, O. C. Factors affecting the clearance and biodistribution of polymeric nanoparticles. *Mol Pharm* 2008, 5, 505-15.
352. Talmadge, J. E.; Singh, R. K.; Fidler, I. J.; Raz, A. Murine models to evaluate novel and conventional therapeutic strategies for cancer. *Am J Pathol* 2007, 170, 793-804.
353. Wilmanns, C.; Fan, D.; O'Brien, C.; Radinsky, R.; Bucana, C.; Tsan, R.; Fidler, I. Modulation of Doxorubicin sensitivity and level of p-glycoprotein expression in human colon-carcinoma cells by ectopic and orthotopic environments in nude-mice. *Int J Oncol* 1993, 3, 413-22.
354. Chung, E. J.; Mlinar, L. B.; Sugimoto, M. J.; Nord, K.; Roman, B. B.; Tirrell, M. In vivo biodistribution and clearance of peptide amphiphile micelles. *Nanomedicine* 2015, 11, 479-87.
355. Perrault, S. D.; Walkey, C.; Jennings, T.; Fischer, H. C.; Chan, W. C. W. Mediating Tumor Targeting Efficiency of Nanoparticles Through Design. *Nano Letters* 2009, 9, 1909-1915.

356. Kunjachan, S.; Pola, R.; Gremse, F.; Theek, B.; Ehling, J.; Moeckel, D.; Hermanns-Sachweh, B.; Pechar, M.; Ulbrich, K.; Hennink, W. E.; Storm, G.; Lederle, W.; Kiessling, F.; Lammers, T. Passive versus Active Tumor Targeting Using RGD- and NGR-Modified Polymeric Nanomedicines. *Nano Letters* 2014, 14, 972-981.
357. Shokeen, M.; Pressly, E. D.; Hagooley, A.; Zheleznyak, A.; Ramos, N.; Fiamengo, A. L.; Welch, M. J.; Hawker, C. J.; Anderson, C. J. Evaluation of multivalent, functional polymeric nanoparticles for imaging applications. *ACS Nano* 2011, 5, 738-47.
358. Rangger, C.; Helbok, A.; von Guggenberg, E.; Sosabowski, J.; Radolf, T.; Prassl, R.; Andrae, F.; Thurner, G. C.; Haubner, R.; Decristoforo, C. Influence of PEGylation and RGD loading on the targeting properties of radiolabeled liposomal nanoparticles. *Int J Nanomedicine* 2012, 7, 5889-900.
359. Gaucher, G.; Dufresne, M. H.; Sant, V. P.; Kang, N.; Maysinger, D.; Leroux, J. C. Block copolymer micelles: preparation, characterization and application in drug delivery. *Journal of Controlled Release* 2005, 109, 169-88.
360. Letchford, K.; Zastre, J.; Liggins, R.; Burt, H. Synthesis and micellar characterization of short block length methoxy poly(ethylene glycol)-block-poly(caprolactone) diblock copolymers. *Colloids Surf. B Biointerfaces* 2004, 35, 81-91.
361. Zhang, J.; Wang, L. Q.; Wang, H.; Tu, K. Micellization phenomena of amphiphilic block copolymers based on methoxy poly(ethylene glycol) and either crystalline or amorphous poly(caprolactone-b-lactide). *Biomacromolecules* 2006, 7, 2492-2500.
362. Bae, Y.; Kataoka, K. Intelligent polymeric micelles from functional poly(ethylene glycol)-poly(amino acid) block copolymers. *Adv Drug Deliv Rev* 2009, 61, 768-84.
363. Yokoyama, M.; Fukushima, S.; Uehara, R.; Okamoto, K.; Kataoka, K.; Sakurai, Y.; Okano, T. Characterization of physical entrapment and chemical conjugation of adriamycin in polymeric micelles and their design for in vivo delivery to a solid tumor. *Journal of Controlled Release* 1998, 50, 79-92.
364. Sun, X.; Rossin, R.; Turner, J. L.; Becker, M. L.; Joralemon, M. J.; Welch, M. J.; Wooley, K. L. An assessment of the effects of shell cross-linked nanoparticle size, core composition, and surface PEGylation on in vivo biodistribution. *Biomacromolecules* 2005, 6, 2541-2554.
365. Yoshida, E.; Tanaka, M.; Takata, T. Direct preparation of core cross-linked micelles in a nonselective solvent. *Colloid Polym Sci* 2005, 284, 51-57.
366. Harada, A.; Kataoka, K. Supramolecular assemblies of block copolymers in aqueous media as nanocontainers relevant to biological applications. *Prog Polym Sci* 2006, 31, 949-982.
367. Riess, G. Micellization of block copolymers. *Prog Polym Sci* 2003, 28, 1107-1170.
368. Murthy, K. S.; Ma, Q. G.; Clark, C. G.; Remsen, E. E.; Wooley, K. L. Fundamental design aspects of amphiphilic shell-crosslinked nanoparticles for controlled release applications. *Chem Commun* 2001, 773-774.
369. Wooley, K. L.; Zhang, Q. Synthesis and characterization of shell cross-linked nanoparticles containing a degradable core domain. *Abstr Pap Am Chem S* 1999, 218, U488-U488.
370. Yang, T. F.; Chen, C. N.; Chen, M. C.; Lai, C. H.; Liang, H. F.; Sung, H. W. Shell-crosslinked Pluronic L121 micelles as a drug delivery vehicle. *Biomaterials* 2007, 28, 725-34.

371. Rijcken, C. J.; Snel, C. J.; Schiffelers, R. M.; van Nostrum, C. F.; Hennink, W. E. Hydrolysable core-crosslinked thermosensitive polymeric micelles: Synthesis, characterisation and in vivo studies. *Biomaterials* 2007, 28, 5581-5593.
372. Jamroz-Piegza, M.; Walach, W.; Dworak, A.; Trzebicka, B. Polyether nanoparticles from covalently crosslinked copolymer micelles. *J Colloid Interf Sci* 2008, 325, 141-148.
373. Talelli, M.; Iman, M.; Varkouhi, A. K.; Rijcken, C. J.; Schiffelers, R. M.; Etrych, T.; Ulbrich, K.; van Nostrum, C. F.; Lammers, T.; Storm, G.; Hennink, W. E. Core-crosslinked polymeric micelles with controlled release of covalently entrapped doxorubicin. *Biomaterials* 2010, 31, 7797-7804.
374. Narita, T.; Terao, K.; Dobashi, T.; Nagasawa, N.; Yoshii, F. Preparation and characterization of core-shell nanoparticles hardened by gamma-ray. *Colloid Surface B* 2004, 38, 187-190.
375. Susumu, K.; Uyeda, H. T.; Medintz, I. L.; Pons, T.; Delehanty, J. B.; Mattoussi, H. Enhancing the stability and biological functionalities of quantum dots via compact multifunctional ligands. *J Am Chem Soc* 2007, 129, 13987-96.
376. Zhao, C. L.; Winnik, M. A.; Riess, G.; Croucher, M. D. Fluorescence Probe Techniques Used to Study Micelle Formation in Water-Soluble Block Copolymers. *Langmuir* 1990, 6, 514-516.
377. Letchford, K.; Liggins, R.; Wasan, K. M.; Burt, H. In vitro human plasma distribution of nanoparticulate paclitaxel is dependent on the physicochemical properties of poly(ethylene glycol)-block-poly(caprolactone) nanoparticles. *Eur. J. Pharm. Biopharm.* 2009, 71, 196-206.
378. Forrest, M. L.; Yanez, J. A.; Remsberg, C. M.; Ohgami, Y.; Kwon, G. S.; Davies, N. M. Paclitaxel prodrugs with sustained release and high solubility in poly(ethylene glycol)-b-poly(epsilon-caprolactone) micelle nanocarriers: Pharmacokinetic disposition, tolerability, and cytotoxicity. *Pharmaceutical Research* 2008, 25, 194-206.
379. Cho, Y. W.; Lee, J.; Lee, S. C.; Huh, K. M.; Park, K. Hydrotropic agents for study of in vitro paclitaxel release from polymeric micelles. *Journal of Controlled Release* 2004, 97, 249-57.
380. Hu, F. Q.; Ren, G. F.; Yuan, H.; Du, Y. Z.; Zeng, S. Shell cross-linked stearic acid grafted chitosan oligosaccharide self-aggregated micelles for controlled release of paclitaxel. *Colloids Surf. B Biointerfaces* 2006, 50, 97-103.
381. Costa, P.; Sousa Lobo, J. M. Modeling and comparison of dissolution profiles. *Eur J Pharm Sci* 2001, 13, 123-33.
382. Parrish, B.; Breitenkamp, R. B.; Emrick, T. PEG- and peptide-grafted aliphatic polyesters by click chemistry. *J Am Chem Soc* 2005, 127, 7404-10.
383. Parrish, B.; Quansah, J. K.; Emrick, T. Functional polyesters prepared by polymerization of α -allyl(valerolactone) and its copolymerization with ϵ -caprolactone and δ -valerolactone. *Journal of Polymer Science, Part A: Polymer Chemistry* 2002, 40, 1983-1990.
384. Darcos, V.; El Habnoui, S.; Nottelet, B.; El Ghzaoui, A.; Coudane, J. Well-defined PCL-graft-PDMAEMA prepared by ring-opening polymerisation and click chemistry. *Polym Chem-Uk* 2010, 1, 280-282.
385. Darcos, V.; Tabchi, H. A.; Coudane, J. Synthesis of PCL-graft-PS by combination of ROP, ATRP, and click chemistry. *European Polymer Journal* 2011, 47, 187-195.

386. Habnoui, S. E.; Darcos, V.; Coudane, J. Synthesis and Ring Opening Polymerization of a New Functional Lactone, α -Iodo- ϵ -caprolactone: A Novel Route to Functionalized Aliphatic Polyesters. *Macromolecular Rapid Communications* 2009, 30, 165-169.
387. Ponsart, S.; Coudane, J.; Vert, M. A novel route to poly(epsilon-caprolactone)-based copolymers via anionic derivatization. *Biomacromolecules* 2000, 1, 275-81.
388. Binder, W. H.; Sachsenhofer, R. 'Click' Chemistry in Polymer and Materials Science. *Macromolecular Rapid Communications* 2007, 28, 15-54.
389. Lecomte, P.; Riva, R.; Jérôme, C.; Jérôme, R. Macromolecular Engineering of Biodegradable Polyesters by Ring-Opening Polymerization and 'Click' Chemistry. *Macromolecular Rapid Communications* 2008, 29, 982-997.
390. Hans, M.; Shimoni, K.; Danino, D.; Siegel, S. J.; Lowman, A. Synthesis and characterization of mPEG-PLA prodrug micelles. *Biomacromolecules* 2005, 6, 2708-17.
391. Yao, J. H.; Mya, K. Y.; Li, X.; Parameswaran, M.; Xu, Q. H.; Loh, K. P.; Chen, Z. K. Light scattering and luminescence studies on self-aggregation behavior of amphiphilic copolymer micelles. *J Phys Chem B* 2008, 112, 749-55.
392. Hu, X.; Chen, X.; Wei, J.; Liu, S.; Jing, X. Core crosslinking of biodegradable block copolymer micelles based on poly(ester carbonate). *Macromol Biosci* 2009, 9, 456-63.
393. Tang, Y.; Liu, G.; Yu, C.; Wei, X.; Zhang, G. Chemical oscillation induced periodic swelling and shrinking of a polymeric multilayer investigated with a quartz crystal microbalance. *Langmuir* 2008, 24, 8929-33.
394. Devadoss, A.; Chidsey, C. E. Azide-modified graphitic surfaces for covalent attachment of alkyne-terminated molecules by "click" chemistry. *J Am Chem Soc* 2007, 129, 5370-1.
395. Vestberg, R.; Malkoch, M.; Kade, M.; Wu, P.; Fokin, V. V.; Sharpless, K. B.; Drockenmuller, E.; Hawker, C. J. Role of architecture and molecular weight in the formation of tailor-made ultrathin multilayers using dendritic macromolecules and click chemistry. *Journal of Polymer Science, Part A: Polymer Chemistry* 2007, 45, 2835-2846.
396. Bromberg, J.; Darnell, J. E. The role of STATs in transcriptional control and their impact on cellular function. *Oncogene* 2000, 19, 2468-2473.
397. Kamran, M. Z.; Patil, P.; Gude, R. P. Role of STAT3 in cancer metastasis and translational advances. *Biomed Res Int* 2013, 2013, 421821.
398. Xiong, H.; Zhang, Z. G.; Tian, X. Q.; Sun, D. F.; Liang, Q. C.; Zhang, Y. J.; Lu, R.; Chen, Y. X.; Fang, J. Y. Inhibition of JAK1, 2/STAT3 signaling induces apoptosis, cell cycle arrest, and reduces tumor cell invasion in colorectal cancer cells. *Neoplasia* 2008, 10, 287-97.
399. Yang, C. H.; Fan, M.; Slominski, A. T.; Yue, J.; Pfeffer, L. M. The role of constitutively activated STAT3 in B16 melanoma cells. *Int J Inference Cytokine Mediator Res* 2010, 2010, 1-7.
400. Kortylewski, M.; Yu, H. Stat3 as a potential target for cancer immunotherapy. *J Immunother* 2007, 30, 131-9.
401. Lee, H.; Pal, S. K.; Reckamp, K.; Figlin, R. A.; Yu, H. STAT3: a target to enhance antitumor immune response. *Curr Top Microbiol Immunol* 2011, 344, 41-59.
402. Yuan, G.; Yan, S.; Xue, H.; Zhang, P.; Sun, J.; Li, G. JSI-124 suppresses invasion and angiogenesis of glioblastoma cells in vitro. *PLoS One* 2015, 10, e0118894.

403. Afifi, M. S.; Ross, S. A.; elSohly, M. A.; Naeem, Z. E.; Halaweish, F. T. Cucurbitacins of *Cucumis prophetarum* and *Cucumis prophetarum*. *J Chem Ecol* 1999, 25, 847-859.
404. Kaya, G. I.; Melzig, M. F. Quantitative determination of cucurbitacin E and cucurbitacin I in homoeopathic mother tincture of *Gratiola officinalis* L. by HPLC. *Pharmazie* 2008, 63, 851-3.
405. Molavi, O.; Shayeganpour, A.; Somayaji, V.; Hamdy, S.; Brocks, D. R.; Lavasanifar, A.; Kwon, G. S.; Samuel, J. Development of a sensitive and specific liquid chromatography/mass spectrometry method for the quantification of cucurbitacin I (JSI-124) in rat plasma. *J Pharm Pharm Sci* 2006, 9, 158-64.
406. Mosmann, T. Rapid colorimetric assay for cellular growth and survival: application to proliferation and cytotoxicity assays. *J Immunol Methods* 1983, 65, 55-63.
407. Hirano, T.; Ishihara, K.; Hibi, M. Roles of STAT3 in mediating the cell growth, differentiation and survival signals relayed through the IL-6 family of cytokine receptors. *Oncogene* 2000, 19, 2548-2556.
408. Ishdorj, G.; Johnston, J. B.; Gibson, S. B. Cucurbitacin-I (JSI-124) activates the JNK/c-Jun signaling pathway independent of apoptosis and cell cycle arrest in B leukemic cells. *BMC Cancer* 2011, 11, 268.
409. Ishdorj, G.; Johnston, J. B.; Gibson, S. B. Inhibition of constitutive activation of STAT3 by curcurbitacin-I (JSI-124) sensitized human B-leukemia cells to apoptosis. *Mol Cancer Ther* 2010, 9, 3302-14.
410. Su, Y.; Li, G.; Zhang, X.; Gu, J.; Zhang, C.; Tian, Z.; Zhang, J. JSI-124 inhibits glioblastoma multiforme cell proliferation through G2/M cell cycle arrest and apoptosis augmentation. *Cancer Biology & Therapy* 2008, 7, 1243-1249.
411. Henry, C. J.; Ornelles, D. A.; Mitchell, L. M.; Brzoza-Lewis, K. L.; Hiltbold, E. M. IL-12 produced by dendritic cells augments CD8+ T cell activation through the production of the chemokines CCL1 and CCL17. *J Immunol* 2008, 181, 8576-84.
412. Lee, S.; Margolin, K. Cytokines in cancer immunotherapy. *Cancers (Basel)* 2011, 3, 3856-93.
413. Hwang, E. S.; Hong, J.-H.; Glimcher, L. H. IL-2 production in developing Th1 cells is regulated by heterodimerization of RelA and T-bet and requires T-bet serine residue 508. *The Journal of Experimental Medicine* 2005, 202, 1289-1300.
414. Alshaker, H. A.; Matalka, K. Z. IFN-gamma, IL-17 and TGF-beta involvement in shaping the tumor microenvironment: The significance of modulating such cytokines in treating malignant solid tumors. *Cancer Cell Int* 2011, 11, 33.
415. Yu, H.; Lee, H.; Herrmann, A.; Buettner, R.; Jove, R. Revisiting STAT3 signalling in cancer: new and unexpected biological functions. *Nat Rev Cancer* 2014, 14, 736-46.
416. Levy, D. E.; Lee, C. K. What does Stat3 do? *J Clin Invest* 2002, 109, 1143-8.
417. Akira, S. Roles of STAT3 defined by tissue-specific gene targeting. *Oncogene* 2000, 19, 2607-11.
418. Desrivieres, S.; Kunz, C.; Barash, I.; Vafaizadeh, V.; Borghouts, C.; Groner, B. The biological functions of the versatile transcription factors STAT3 and STAT5 and new strategies for their targeted inhibition. *J Mammary Gland Biol Neoplasia* 2006, 11, 75-87.

419. Cui, Y.; Huang, L.; Elefteriou, F.; Yang, G.; Shelton, J. M.; Giles, J. E.; Oz, O. K.; Pourbahrami, T.; Lu, C. Y.; Richardson, J. A.; Karsenty, G.; Li, C. Essential role of STAT3 in body weight and glucose homeostasis. *Mol Cell Biol* 2004, 24, 258-69.
420. Foged, C.; Sundblad, A.; Hovgaard, L. Targeting vaccines to dendritic cells. *Pharmaceutical Research* 2002, 19, 229-38.
421. Tan, C.; Wang, Y.; Fan, W. Exploring polymeric micelles for improved delivery of anticancer agents: recent developments in preclinical studies. *Pharmaceutics* 2013, 5, 201-19.
422. Patrick Lim, S.; Jubo, L.; Christine, A.; Helen, L.; Mark, B. Polymeric Micelles for Formulation of Anti-Cancer Drugs. In *Nanotechnology for Cancer Therapy*, CRC Press: 2006; pp 317-355.
423. Lazarovits, J.; Chen, Y. Y.; Sykes, E. A.; Chan, W. C. W. Nanoparticle-blood interactions: the implications on solid tumour targeting. *Chem Commun* 2015, 51, 2756-2767.
424. Leaman, D. W.; Pisharody, S.; Flickinger, T. W.; Commane, M. A.; Schlessinger, J.; Kerr, I. M.; Levy, D. E.; Stark, G. R. Roles of JAKs in activation of STATs and stimulation of c-fos gene expression by epidermal growth factor. *Mol Cell Biol* 1996, 16, 369-75.
425. Liu, W. H.; Liu, J. J.; Wu, J.; Zhang, L. L.; Liu, F.; Yin, L.; Zhang, M. M.; Yu, B. Novel mechanism of inhibition of dendritic cells maturation by mesenchymal stem cells via interleukin-10 and the JAK1/STAT3 signaling pathway. *PLoS One* 2013, 8, e55487.
426. Lewko, W.; Oldham, R. Cytokines. In *Principles of Cancer Biotherapy*, Oldham, R.; Dillman, R., Eds. Springer Netherlands: 2009; pp 155-276.
427. Wallet, M. A.; Sen, P.; Tisch, R. Immunoregulation of dendritic cells. *Clin Med Res* 2005, 3, 166-75.
428. Song, S.; Yuan, P.; Wu, H.; Chen, J.; Fu, J.; Li, P.; Lu, J.; Wei, W. Dendritic cells with an increased PD-L1 by TGF-beta induce T cell anergy for the cytotoxicity of hepatocellular carcinoma cells. *Int Immunopharmacol* 2014, 20, 117-23.
429. Liu, R. Y.; Zeng, Y.; Lei, Z.; Wang, L.; Yang, H.; Liu, Z.; Zhao, J.; Zhang, H. T. JAK/STAT3 signaling is required for TGF-beta-induced epithelial-mesenchymal transition in lung cancer cells. *Int J Oncol* 2014, 44, 1643-51.
430. Starsichova, A.; Lincova, E.; Pernicova, Z.; Kozubik, A.; Soucek, K. TGF-beta1 suppresses IL-6-induced STAT3 activation through regulation of Jak2 expression in prostate epithelial cells. *Cell Signal* 2010, 22, 1734-44.
431. Park, S. J.; Nakagawa, T.; Kitamura, H.; Atsumi, T.; Kamon, H.; Sawa, S.; Kamimura, D.; Ueda, N.; Iwakura, Y.; Ishihara, K.; Murakami, M.; Hirano, T. IL-6 regulates in vivo dendritic cell differentiation through STAT3 activation. *J Immunol* 2004, 173, 3844-54.
432. Haabeth, O. A.; Lorvik, K. B.; Hammarstrom, C.; Donaldson, I. M.; Haraldsen, G.; Bogen, B.; Corthay, A. Inflammation driven by tumour-specific Th1 cells protects against B-cell cancer. *Nat Commun* 2011, 2, 240.
433. Hsu, C. Y.; Uludag, H. Cellular uptake pathways of lipid-modified cationic polymers in gene delivery to primary cells. *Biomaterials* 2012, 33, 7834-48.
434. Furgeson, D. Y.; Chan, W. S.; Yockman, J. W.; Kim, S. W. Modified linear polyethylenimine-cholesterol conjugates for DNA complexation. *Bioconjug Chem* 2003, 14, 840-7.

435. Gusachenko Simonova, O.; Kravchuk, Y.; Konevets, D.; Silnikov, V.; Vlassov, V. V.; Zenkova, M. A. Transfection efficiency of 25-kDa PEI-cholesterol conjugates with different levels of modification. *J Biomater Sci Polym Ed* 2009, 20, 1091-110.
436. Furgeson, D. Y.; Yockman, J. W.; Janat, M. M.; Kim, S. W. Tumor efficacy and biodistribution of linear polyethylenimine-cholesterol/DNA complexes. *Mol Ther* 2004, 9, 837-45.
437. Wang, Y.; Gao, S.; Ye, W. H.; Yoon, H. S.; Yang, Y. Y. Co-delivery of drugs and DNA from cationic core-shell nanoparticles self-assembled from a biodegradable copolymer. *Nat Mater* 2006, 5, 791-6.
438. Aichberger, K. J.; Mayerhofer, M.; Gleixner, K. V.; Krauth, M. T.; Gruze, A.; Pickl, W. F.; Wacheck, V.; Selzer, E.; Mullauer, L.; Agis, H.; Sillaber, C.; Valent, P. Identification of MCL1 as a novel target in neoplastic mast cells in systemic mastocytosis: inhibition of mast cell survival by MCL1 antisense oligonucleotides and synergism with PKC412. *Blood* 2007, 109, 3031-41.
439. Chetoui, N.; Sylla, K.; Gagnon-Houde, J. V.; Alcaide-Loridan, C.; Charron, D.; Al-Daccak, R.; Aoudjit, F. Down-regulation of mcl-1 by small interfering RNA sensitizes resistant melanoma cells to fas-mediated apoptosis. *Mol Cancer Res* 2008, 6, 42-52.
440. Schulze-Bergkamen, H.; Fleischer, B.; Schuchmann, M.; Weber, A.; Weinmann, A.; Krammer, P. H.; Galle, P. R. Suppression of Mcl-1 via RNA interference sensitizes human hepatocellular carcinoma cells towards apoptosis induction. *BMC Cancer* 2006, 6, 232.
441. Aliabadi, H. M.; Maranchuk, R.; Kucharski, C.; Mahdipoor, P.; Hugh, J.; Uludag, H. Effective response of doxorubicin-sensitive and -resistant breast cancer cells to combinational siRNA therapy. *J Control Release* 2013, 172, 219-28.
442. Akhtar, S.; Benter, I. Toxicogenomics of non-viral drug delivery systems for RNAi: potential impact on siRNA-mediated gene silencing activity and specificity. *Adv Drug Deliv Rev* 2007, 59, 164-82.
443. Chen, K.; Chen, X. Integrin targeted delivery of chemotherapeutics. *Theranostics* 2011, 1, 189-200.
444. Arap, W.; Pasqualini, R.; Ruoslahti, E. Cancer treatment by targeted drug delivery to tumor vasculature in a mouse model. *Science* 1998, 279, 377-80.
445. Wang, H.; Chen, K.; Cai, W.; Li, Z.; He, L.; Kashefi, A.; Chen, X. Integrin-targeted imaging and therapy with RGD4C-TNF fusion protein. *Mol Cancer Ther* 2008, 7, 1044-53.
446. Torchilin, V. P. Recent advances with liposomes as pharmaceutical carriers. *Nat Rev Drug Discov* 2005, 4, 145-60.
447. You Han, B.; Eun Seong, L. Polymeric Micelles Targeting Tumor pH. In *Nanotechnology for Cancer Therapy*, CRC Press: 2006; pp 443-464.

APPENDIX A

Development of other Formulations for Release of JSI-124

A.1. Experimental Methods

A.1.1. Preparation of JSI-124-loaded polymeric micelles based on PEO-*b*-PCL

Block copolymers of PEO₁₁₄-*b*-PBCL₃₁, PEO₁₁₄-*b*-PBCL₅₈, and PEO₁₁₄-*b*-PCCL₁₉ were synthesized according to Section 2.2.3. For physical encapsulation of JSI-124, 20 mg PEO₁₁₄-*b*-PBCL₃₁, PEO₁₁₄-*b*-PBCL₅₈, or PEO₁₁₄-*b*-PCCL₁₉ was dissolved with 1 mg of JSI-124 into 1 mL acetone. This solution was added to 5 mL of deionized water in a drop-wise manner under moderate stirring at room temperature, followed by the evaporation of acetone under vacuum. The prepared micellar solution was then centrifuged to remove any aggregates.

Block copolymer of PEO-*b*-PPCL was synthesized according to Section 4.2.3. For physical encapsulation of JSI-124 into crosslinked micelles, 1 mg JSI-124, 20 mg PEO-*b*-PPCL, and 5.1 mg crosslinking agent (tetraethylene glycol (bis)azide) were all added to 1 mL acetone and this solution was added to 5 mL deionized water containing 1.0 mg sodium ascorbate and 0.1 mg copper sulphate, in a drop-wise manner under moderate stirring at room temperature, followed by the evaporation of acetone under vacuum. The prepared micellar solution was then centrifuged to remove any aggregates.

A.1.2. Release of JSI-124 from block copolymer micelles

Release of free JSI-124 or JSI-124 physically encapsulated into PEO-*b*-PCCL micelles was assessed in deionized water at 37 °C according to a previous method with slight modification.¹ Free or micellar JSI-124 (5 mL solution containing 1 mg JSI-124) was prepared and transferred to a dialysis bag (MWCO - 3.5 kDa). The dialysis bag was placed in 500 mL of deionized water and release study was performed in a shaking water bath at 37

°C. At selected time intervals, the release media was replaced, and aliquots of 200 uL were withdrawn from the inside of the dialysis bag and analyzed by LC-MS.

A.2. Results

A.2.1. Encapsulation and release of JSI-124 from PEO-*b*-PCL based micelles

The encapsulation efficiency of JSI-124 in PEO-*b*-PCL based micelles is given in Table A.1. All the micelles show an encapsulation efficiency of 100 % indicating complete solubilization of JSI-124 into the micelles. The release profile of JSI-124 is given in Figure A.1. The release profile indicates that a relatively rapid release of JSI-124 from all the PEO-*b*-PCL based formulations similar to free JSI-124, with ~100 % drug release within 8 h of incubation.

Table A.3 Drug loading and encapsulation of JSI-124 in PEO-*b*-PCL based micelles

Block copolymer micelles	Drug Loading (%)	Encapsulation Efficiency (%)
PEO ₁₁₄ - <i>b</i> -PBCL ₃₁	7.5 ± 0.7	150.8 ± 13.6
PEO ₁₁₄ - <i>b</i> -PBCL ₅₈	6.0 ± 0.2	119.4 ± 3.0
PEO ₁₁₄ - <i>b</i> -PCCL ₁₉	5.5 ± 0.3	109.8 ± 5.6
Crosslinked micelles	5.1 ± 0.1	102.9 ± 2.0

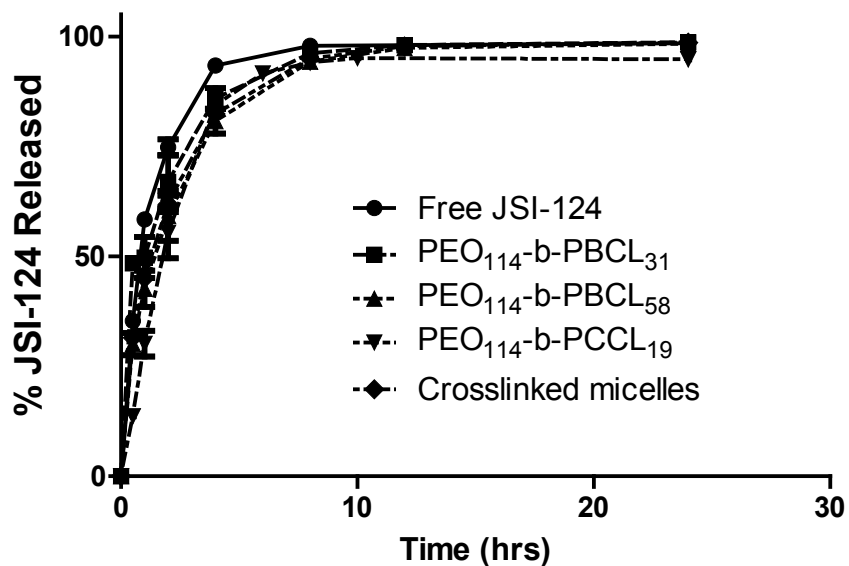


Figure A.3 *In vitro* release profile of JSI-124 from PEO-*b*-PCL based micelles in deionized water at 37 °C. Each point represents mean \pm SD ($n = 3$).

A.3. References

1. Garg, S. M.; Xiong, X. B.; Lu, C.; Lavasanifar, A. Application of click chemistry in the preparation of poly(ethylene oxide)-block-poly(ϵ -caprolactone) with hydrolyzable cross-links in the micellar core. *Macromolecules* 2011, 44, 2058-2066.

APPENDIX B

Preparation of PLGA Nanoparticles containing Ovalbumin

B.1. Method A

B.1.1. Preparation of PLGA nanoparticles

PLGA nanoparticles were prepared according to a previously published method.¹ Briefly, 20 mg/mL PLGA (poly(lactic-*co*-glycolic acid)) (50:50) was dissolved in 2 mL of acetone: dichloromethane (1:1 v/v) mixture to form the organic phase. The aqueous phase consisted of 8 mL of 5% polyvinyl alcohol (PVA). The organic and aqueous phases were sonicated for 30 s (level 4) in ice bath using a probe sonicator. The organic phase was removed by evaporation under pressure while the solution was constantly stirring.

B.1.2. Results

The PLGA nanoparticles formed aggregates after evaporation of organic solvent with a size > 1 μ M.

B.2. Method B

B.2.1. Preparation of PLGA nanoparticles

PLGA nanoparticles were prepared according to a previously published method with slight modification.² Briefly, PLGA (poly(lactic-*co*-glycolic acid)) (50:50) was dissolved in 1 mL of ethyl acetate and added to 2 mL of aqueous solution containing PVA. After mutual saturation of both the phases, the mixture was sonicated for 1.5 min in ice bath (level 4) using a probe sonicator. This solution was added dropwise to 50 mL of deionized water under constant stirring to allow for nanoprecipitation. Ethyl acetate was removed by overnight stirring. Aggregates were removed by centrifugation. The solution was then washed twice by ultracentrifugation (20000 rpm for 30 m) and then freeze-dried.

B.2.2. Results

Table B.1 gives the characterization of the various PLGA nanoparticles that were prepared. NP1, NP5, and NP6 had trouble in reconstitution of the sample in deionized water after freeze-drying whereas NP2, NP3, and NP4 did not reconstitute after freeze-drying. As seen in Table B.1, as the concentration of PVA was increased, the size of the nanoparticles decreased. Also, as the concentration of PLGA was increased, the size of the nanoparticles also increased.

Table B.4 Synthesis and characterization of PLGA nanoparticles

Name	Polymer conc. (mg/mL)	Emulsion ratio (org:aq)	PVA conc. (%)	Sonication time (min)	Size of NP pre-washing (nm)	Recovery after FD
NP1	20	1:2	1%	1.5	186.3	15%
NP2	20	1:2	2.5%	1.5	139.9	ND
NP3	20	1:2	5%	1.5	100.8	ND
NP4	20	1:2	5%	1.5	106.1	ND
NP5	40	1:2	5%	1.5	114.1	<2%
NP6	80	1:2	5%	1.5	140.6	<2%

ND - not detected

B.3. Method C

B.3.1. Preparation of PLGA nanoparticles

PLGA nanoparticles were prepared according to a previously published method.³ Briefly, 100 mg PLGA (poly(lactic-*co*-glycolic acid)) (50:50) was dissolved in 5 mL of acetone. A solution of 1:1 v/v ethanol/water was added dropwise (2 mL/min) into the PLGA solution under constant stirring until the solution became turbid. After 5 m of stirring, the suspension was transferred to 20 mL of deionized water in a glass beaker and stirred for another 20 m. Organic solvent was then removed under pressure while stirring. Solution was centrifuged to remove aggregates. The solution was then washed twice by ultracentrifugation (20000 rpm for 30 m).

B.3.2. Results

The PLGA nanoparticles formed aggregates after evaporation of organic solvent with a size > 1 μ M. On ultracentrifugation, the nanoparticles precipitated to form a hard cake which was resuspending in solution. This was expected as there was no stabilizer. On adding 5% PVA to the 20 mL deionized water, the nanoparticle solution did not form a cake during ultracentrifugation and the size was 250 nm. However, the nanoparticles formed aggregates after evaporation of organic solvent.

B.4. Method D

B.4.1. Preparation of PLGA nanoparticles

PLGA nanoparticles were prepared according to a previously published method.⁴ Briefly, 25 mg PLGA (50:50) was dissolved in 4 mL of chloroform. Aqueous phase consisted of 1 mL mixture of deionized water: methanol (7:3 v/v). The organic phase was added to the aqueous phase with constant stirring. The mixture was stirred for 30 m. The

mixture was then added dropwise to 10 mL deionized water containing 0.5% pluronic F-68 or 5% PVA. Organic solvent was removed by overnight stirring. The solution was then washed twice by ultracentrifugation (20000 rpm for 30 m) and then freeze-dried.

B.4.2. Results

No primary emulsion was formed as the chloroform and aqueous phase would separate before adding the two phases to 10 mL of water. Sonication was tried for 30 s at level 4, however, that lead to separation of the phases as well. The PLGA nanoparticles exhibited a size of 240 nm with pluronic F-68 whereas with PVA, the size was 450 nm. resuspending after ultracentrifugation was difficult with this method.

B.5. Method E

B.5.1. Preparation of ovalbumin loaded PLGA nanoparticles

PLGA nanoparticles were prepared according to a previously published method with slight modification.⁵ Briefly, 100 mg PLGA (50:50) was dissolved in 5 mL of propylene carbonate (PC). 0.5 mL of deionized water was added and the two phases were sonicated for 30 s (level 4) in an ice-bath to get primary emulsion using a probe sonicator. The primary emulsion was added into 10 mL of aqueous phase containing 4% w/v didodecyl dimethyl ammonium bromide (DMAB). The mixture was emulsified for 7 m using a high speed homogenizer (16000 rpm). In order to allow for diffusion of PC into water, 40 mL of deionized water was subsequently added under moderate stirring , leading to nanoprecipitation of the PLGA nanoparticles. The nanoparticle solution was then washed twice by ultracentrifugation (20000 rpm for 30 m) to remove PC and excess DMAB, and

then freeze-dried. For ovalbumin loaded nanoparticles 2 mg ovalbumin was dissolved in the initial 0.5 mL water used to prepare the primary emulsion.

B.5.2. Results

The size of empty nanoparticles was 91.1 nm. The size of ovalbumin loaded PLGA nanoparticles was 115.5 nm. However, no reconstitution took place after freeze-drying the sample even after adding sucrose as a cryoprotectant.

B.6. Method F

B.6.1. Preparation of ovalbumin loaded PLGA nanoparticles

Since ovalbumin is a hydrophilic protein, PLGA nanoparticles were prepared by modifying method B in section B.2 to prepare an w/o/w emulsion.⁵ Briefly, 50 mg PLGA (50:50) was dissolved in 1 mL of ethyl acetate and 100 μ L of deionized water was added to this. After mutual saturation of both the phases, the solution was sonicated for 30 s (level 4) in an ice bath to obtain the primary emulsion. This solution was added to 2 mL of aqueous solution containing 5% w/v PVA under constant stirring. The mixture was sonicated for 1.5 min in ice bath (level 3) using a probe sonicator to form the secondary emulsion. This solution was added dropwise to 50 mL of deionized water under constant stirring to allow for nanoprecipitation. Ethyl acetate was removed by overnight stirring. Aggregates were removed by centrifugation. The solution was then washed twice by ultracentrifugation (20000 rpm for 30 m) and then freeze-dried. Half of the solution was freeze-dried without cryoprotectant whereas the other half was freeze-dried after adding 10 % w/w sucrose. For

ovalbumin loaded PLGA nanoparticles, 5 mg ovalbumin was dissolved in 100 μ L deionized water which was added to ethyl acetate to form the primary emulsion.

B.6.2. Results

The size of ovalbumin loaded nanoparticles was 142.6 nm before ultracentrifugation. The size of nanoparticles was 151.9 nm after ultracentrifugation. The freeze-dried sample with sucrose resuspended easily with a size of 165.7 nm. The recovery after freeze-drying 5 mg ovalbumin loaded nanoparticles was 15.2 %. The drug loading was 0.79 ± 0.11 % whereas the encapsulation efficiency was 7.94 ± 1.11 %.

B.7. Method G

B.7.1. Preparation of ovalbumin loaded PLGA nanoparticles

Since method F in section B.6 gave size around 150 nm, and good redispersion and protein encapsulation, we further modified method F in order to increase recovery and protein encapsulation. The procedure is given in Table B.2. Briefly, 5 mg ovalbumin was dissolved in deionized water and added to 1 mL ethyl acetate in which 50 mg PLGA was previously dissolved. After mutual saturation of both the phases, the solution was sonicated for 30 s (level 4) in an ice bath to obtain the primary emulsion. This solution was added to 2 mL of aqueous solution containing 5% w/v PVA under constant stirring. The mixture was sonicated for 1.5 min in ice bath (level 3) using a probe sonicator to form the secondary emulsion. This solution was added dropwise to 50 mL of deionized water under constant stirring to allow for nanoprecipitation. Ethyl acetate was removed by overnight stirring.

Aggregates were removed by centrifugation. The solution was then washed twice by ultracentrifugation (20000 rpm for 30 m) and then freeze-dried.

Table B.5 Preparation of ovalbumin loaded PLGA nanoparticles

Name	OVA conc. (mg)	PLGA conc. (mg/ml)	Org:aq phase ratio (ml/ml)	PVA conc. (% w/v) (2 ml)	Sonication time (min)
NP7	5	50	1/0.1	5%	1.5
NP8	5	50	1/0.25	5%	1.5
NP9	5	50	1/0.5	5%	1.5
NP10	5	50	1/0.75	5%	1.5
NP11	5	50	1/1	5%	1.5

OVA - ovalbumin

B.7.2. Estimation of encapsulated ovalbumin

The amount of ovalbumin encapsulated in the PLGA nanoparticles was determined as follows. Briefly, 5 mg of freeze-dried nanoparticles were resuspended in 3 mL of 0.01N sodium hydroxide solution containing 5 % sodium dodecyl sulphate (SDS) and stirred continuously for 24 h. Solution was then centrifuged and the supernatant collected. The supernatant was analyzed for ovalbumin using BCA Protein assay kit.

B.7.3. Results

Table B.3 gives the characteristics of the ovalbumin loaded PLGA nanoparticles. NP7 showed the smallest average size of 137.2 nm however, the encapsulation of ovalbumin

was also the lowest with an encapsulation efficiency of only 7.42 %. NP10 and NP11 showed size above 300 nm with an encapsulation efficiency above 100 %. The size of the nanoparticles significantly increased as the concentration of aqueous phase increased. NP8 gave the best results with a smaller size of ~150 nm and an encapsulation efficiency of ~48 %.

Table B.6 Characteristics of ovalbumin loaded PLGA nanoparticles.

Name	Size (nm)	% Recovery (%)	% Loading (%)	Encapsulation Efficiency (%)
NP7	137.2 ± 1.4	16.2	0.74 ± 0.13	7.42 ± 1.26
NP8	148.9 ± 1.0	9.8	4.79 ± 0.27	47.91 ± 2.69
NP9	172.6 ± 2.4	5	0.94 ± 0.52	9.40 ± 5.21
NP10	342.9 ± 4.3	10.2	12.23 ± 0.36	122.34 ± 3.58
NP11	337.6 ± 2.6	6.2	10.68 ± 0.54	106.77 ± 5.42

B.8. References

1. Song, X.; Zhao, Y.; Hou, S.; Xu, F.; Zhao, R.; He, J.; Cai, Z.; Li, Y.; Chen, Q. Dual agents loaded PLGA nanoparticles: systematic study of particle size and drug entrapment efficiency. *Eur J Pharm Biopharm* 2008, 69, 445-53.
2. Choi, S.-W.; Kwon, H.-Y.; Kim, W.-S.; Kim, J.-H. Thermodynamic parameters on poly(d,l-lactide-co-glycolide) particle size in emulsification–diffusion process. *Colloids and Surfaces A: Physicochemical and Engineering Aspects* 2002, 201, 283-289.
3. Cheng, F. Y.; Wang, S. P.; Su, C. H.; Tsai, T. L.; Wu, P. C.; Shieh, D. B.; Chen, J. H.; Hsieh, P. C.; Yeh, C. S. Stabilizer-free poly(lactide-co-glycolide) nanoparticles for multimodal biomedical probes. *Biomaterials* 2008, 29, 2104-12.
4. Yadav, K. S.; Sawant, K. K. Modified nanoprecipitation method for preparation of cytarabine-loaded PLGA nanoparticles. *AAPS PharmSciTech* 2010, 11, 1456-65.
5. Kwon, H.-Y.; Lee, J.-Y.; Choi, S.-W.; Jang, Y.; Kim, J.-H. Preparation of PLGA nanoparticles containing estrogen by emulsification–diffusion method. *Colloids and Surfaces A: Physicochemical and Engineering Aspects* 2001, 182, 123-130.

APPENDIX C

Uptake of Polymeric Micelles by Dendritic Cells

C.1. Experimental Methods

C.1.1. *In vitro* cell uptake of DiI loaded PEO-*b*-PBCL micelles by BMDCs using flow cytometry

Cell uptake studies were carried out using the hydrophobic fluorescent probe DiI according to a method described previously.¹ Briefly, 30 μg DiI and 30 mg of PEO₁₁₄-*b*-PBCL₁₉ (synthesized according to Section 2.2.3) were dissolved in acetone (0.5 mL). This solution was added to 3 mL of water in a drop-wise manner followed by evaporation of the organic solvent under vacuum. The micellar solution was then centrifuged at $11,600 \times g$ to remove the un-encapsulated DiI. An aliquot of the micellar solution was diluted with an equal volume of DMSO and used to quantify the level of encapsulated DiI by Varian Cary Eclipse fluorescence spectrophotometer (Victoria, Australia), with an excitation wavelength of 550 nm and emission wavelength of 565 nm. Cell uptake was measured using flow cytometry.

BMDCs (generated from section 5.2.8) were seeded into a 12-well plate (2×10^5 cells/well) containing 1 mL of media on day 7. Free DiI or DiI loaded polymeric micelles were added and incubated for 4 h and 24 h at 37 °C. The final DiI concentration in each well was 0.5 $\mu\text{g}/\text{mL}$. Cells incubated with the medium were used as negative control. Following the incubation period, cells were removed and centrifuged at $500 \times g$ for 5 min and washed with cold PBS two times and then re-suspended in 0.5 mL FACS buffer (2% FBS in PBS). The resulting cell suspension was finally acquired on a Cell Lab Quanta SC flow cytometer (Beckman Coulter, Brea, CA) and analyzed using Beckman Coulter Quanta Analysis software. Ten thousand cells were counted with logarithmic settings. The cells associated

with DiI were excited with an argon laser (488 nm) and fluorescence was detected at 560 nm (FL2).

C.1.2. *In vitro* cell uptake of DiI loaded PEO-*b*-PBCL micelles by BMDCs using confocal microscopy

Confocal microscopy was used to compare the intracellular distribution of DiI loaded PEO-*b*-PBCL micelles according to a previous procedure with modification.² For this, on day 6 of BMDCs culture, cells were centrifuged and 5×10^4 BMDCs were cultured in 12-well plates on top of sterile cover slips previously coated with poly-L-lysine at 37 °C. On day 7, the media was removed and replaced with 1 mL media containing free DiI or DiI loaded PEO-*b*-PBCL micelles at a concentration of 0.5 µg/mL. The cells were incubated with the formulations for 24 h at 37 °C. After incubation, the media was removed and the cells were washed with serum free media (3×2 mL). The cells were fixed on ice with 2% formaldehyde for 20 min. The formaldehyde was removed by washing with media (3×2 mL). The cover slips were put on slides containing one drop of antifade (Molecular Probes, Invitrogen Co., OR). Cells were imaged using a Leica SP2 confocal microscope (Heidelberg, Germany) at 40x magnification. DiI was detected using an excitation of 543 nm and emission of 565 nm.

C.2. Results

C.2.1. *In vitro* cell uptake of DiI loaded PEO-*b*-PBCL micelles by BMDCs using flow cytometry and confocal microscopy

Flow cytometry and confocal microscopy were used to monitor the uptake of PEO-*b*-PBCL micelles in BMDCs. Figure C.1 shows the % uptake and mean fluorescence intensity (MFI) of DiI encapsulated PEO-*b*-PBCL micelles by BMDCs. Based on the flow cytometry results, it can be seen that BMDCs show uptake of DiI encapsulated PEO-*b*-PBCL micelles with an increase in the % DiI positive cells and MFI from 30.8 % and 17.5 at 4 h, to 82.7 % and 44.7 at 24 h, respectively.

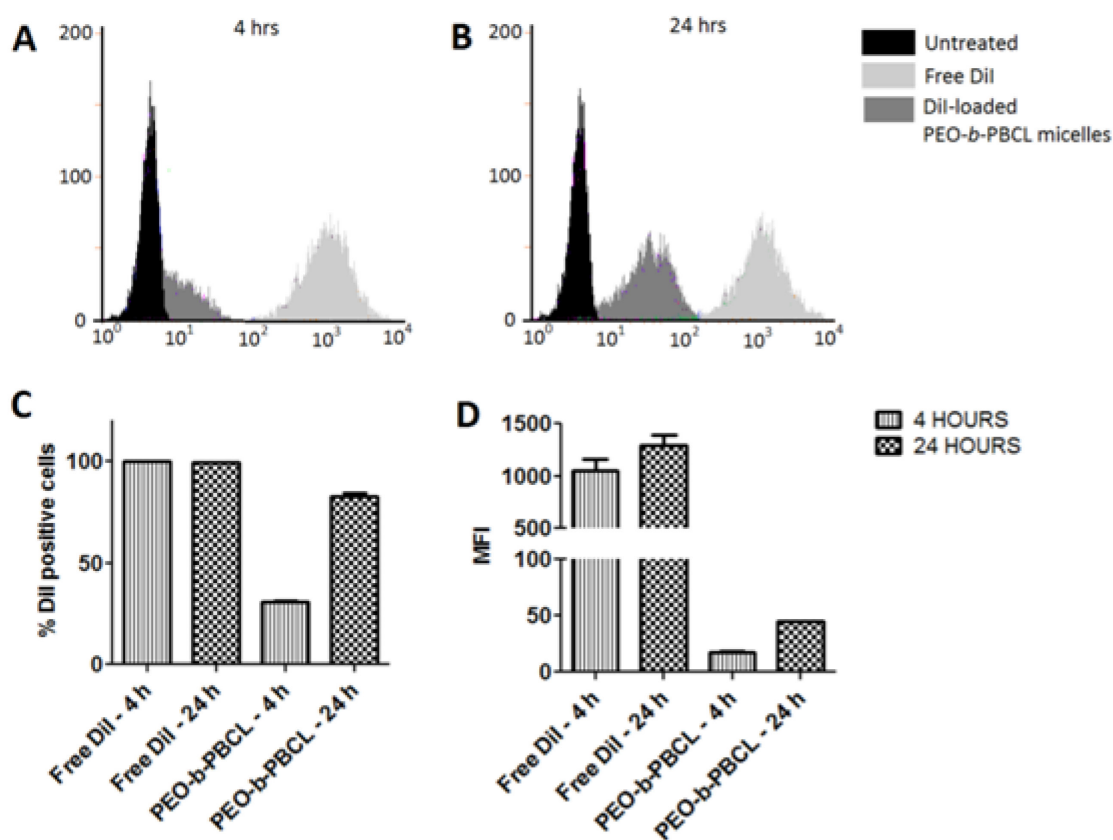


Figure C.4 Assessment of the uptake of DiI encapsulated PEO-*b*-PBCL by BMDCs as measured by flow cytometry at A) 4 h and B) 24 h. The data represents one out of three independent experiments which showed similar results. Uptake of DiI by BMDCs reported as C) % DiI positive BMDCs and D) MFI after treatment for 4 h and 24 h. Each bar represents mean \pm SD ($n = 3$)

Confocal microscopy images displaying BMDCs cells incubated with DiI-loaded PEO-*b*-PBCL micelles confirmed uptake of micelles by BMDCs (Figure C.2). After 24 h incubation, the BMDCs show that the DiI fluorescence is localized in the cytoplasmic compartment.

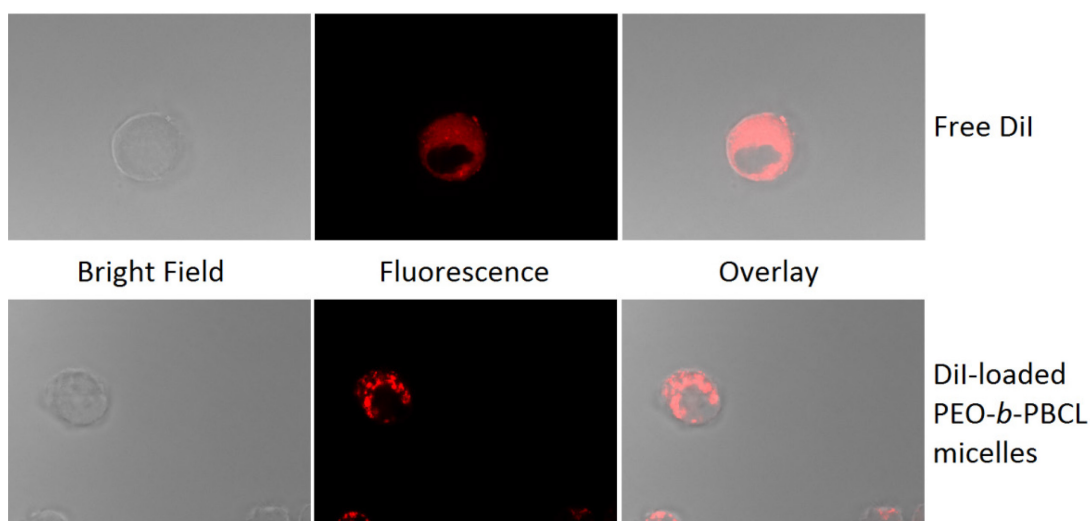


Figure C.5 Cellular uptake of DiI encapsulated in PEO-*b*-PBCL micelles by BMDCs using confocal microscopy after 24 h. Images represent bright field, DiI fluorescence (red), and merged (overlay) images.

C.3. References

1. Shahin, M.; Ahmed, S.; Kaur, K.; Lavasanifar, A. Decoration of polymeric micelles with cancer-specific peptide ligands for active targeting of paclitaxel. *Biomaterials* 2011, 32, 5123-33.
2. Wang, Y.; Yang, T.; Wang, X.; Wang, J.; Zhang, X.; Zhang, Q. Targeted polymeric micelle system for delivery of combretastatin A4 to tumor vasculature in vitro. *Pharmaceutical Research* 2010, 27, 1861-8.